Using spectral signatures as a toolbox for determining crop health status

John D. Stamford

A thesis submitted for the degree of Doctor of Philosophy

School of Life Sciences

University of Essex

June 2020

Acknowledgements

I would like to acknowledge the invaluable help and advice of Prof. Tracy Lawson, for providing the highest quality guidance, supervision and opportunity.

Secondly, I wish to acknowledge Dr. Iain Cameron for fantastic co-supervision, and invaluable advice regarding the technical aspects of imaging and remote sensing.

Finally, all member of the Plant Physiology Laboratory; Dr. Phil Davey, Dr. Silvere Vialet-Chabrand, Dr. Jack Matthews, Shellie Wall, and Jim Stevens, for continuous help and support and without whom the PhD would not have been as successful, and everyone else in the plant productivity group.

Duncan Sweeney for great friendship over the years.

Friends and family for continued support.

Georgia and Eden.

Summary

Spectral based techniques allow for rapid, non-invasive probing of plant and crop performance, and have potential to overcome current phenotyping bottlenecks for breeders and researchers while enabling farmers to optimise the inputs of fertilizer, irrigation and pesticides on their crops to maximise yields and reduce expenditure.

The Normalised Difference Vegetation Index (NDVI), uses the reflectance of near infra-red and visible red light to assess the performance and greenness of plants due to variation in chlorophyll content. Increasing the accessibility of NDVI imaging systems through the development of a small, low cost, and easy to use imaging system has potential to increase the uptake of NDVI imaging systems, especially amongst farmers and breeders. We first described a method for using a dual camera system based on the widely available Raspberry Pi platform to produce calibrated NDVI imagery, generating more robust estimates of NDVI than other low cost systems.

Then, we developed novel reflectance based spectral indices to assess plant water status, exploiting water content induced changes in leaf internal structure and subsequent variation in the reflectance of NIR. These indices used visible and NIR wavelengths to allow for a reflectance based assessment of leaf water status with standard VIS-NIR spectrometry and imaging systems, which are widely available and already is use by farmers and researchers over other systems that measure water content via short wave infra-red wavelengths, expanding the availability of accessible tools that can be used to assess leaf water status .

Finally, we developed a toolbox of spectral techniques can be used to track water and nitrogen of plants, as well as overall plant performance. The index of stomatal conductance (I_g), a thermographic technique, can be used to assess water content, predominantly soil relative water content (RWC). Chlorophyll fluorescence can be used to indicate overall plant performance and changes in soil RWC, and spectral reflectance indices can be used to measure both water and nitrogen content. To date, this is the first spectral toolbox developed utilizing these techniques that has been used to assess

water and nitrogen content, demonstrating the potential of a multi-technique spectral toolbox to monitor plant performance. The advantage of a spectral toolbox is primarily through the remote, non-invasive and rapid measurement compared to other techniques, which allows for a higher throughput of measurements, benefiting farmers and crop breeders who need to monitor crops grown over a large area of land, and reduced labour requirements over conventional leaf level technique.

The spectral toolbox serves as a foundation for future work using the combination of these techniques, intending to proliferate precision agriculture as a method to apply precise, site-specific applications of agricultural inputs such as fertilizer and irrigation based on crop requirements rather than blanket application, reducing costs to farmers through reduced inventory, fuel and labour. The rapid assessment of plant performance afforded by spectral techniques can additionally improve the phenotyping of future crop varieties for improved yields and growth, a necessary step in mitigating the effects of a changing climate and global population growth.

Table of Contents

Chapter 3 - Development of a novel spectral index to assess plant water status

Chapter 1 - Introduction

1.1 Overview

Photosynthesis is the most fundamental process for life on earth, converting light energy into chemical energy through the synthesis of carbohydrates. Photosynthetic organisms form the basis of the majority of the planet's ecosystems, providing a source of food and fuel as well as the generation of atmospheric oxygen.

However, global food security is at risk. It is estimated that food production will have to double to meet the requirements of a growing global population by 2050, and current efforts to increase crop yields are insufficient (Ray et al., 2013). Efforts to overcome food security threats are limited by a number of factors, such as the effects of a changing climate (Schmidhuber & Tubiello, 2007; Wheeler & Von Braun, 2013). Crops are likely to experience greater extreme weather events, higher temperatures and less rainfall for most places on Earth, and potentially greater vulnerability to pests and disease (Rosenzweig et al., 2001). These changes to the climate can have severe negative effects on crop yields (Schlenker & Roberts, 2009).

However, there are efforts to mitigate the effects of climate change and the growing food demand of a growing global population. There are breeding efforts to genetically increase yields and increase crop performance (Araus & Cairns, 2014; Simkin et al., 2019) under the predicted future climate of higher temperatures and less rainfall. Screening plants for traits such as higher yields under these conditions or better drought tolerance is crucial to identify and assess plant populations and cultivars for these desired traits (Chaerle & Van Der Straeten, 2001; Li et al., 2014; Pieruschka & Schurr, 2019), yet with the relative speed of crop breeding programmes and genetic modification, there is a bottleneck regarding the throughput of plant screening to identify these traits (Furbank & Tester, 2011).

'Plant health' is a term that is not well defined despite thorough discussion (Döring et al., 2012). It has been described by some as the combination of biotic and abiotic factors that influence whether that plant achieves its full genetic potential as a crop (Cook, 2000), such as the effect on plant performance due to the availability of key resources such as light, nutrients and water, as well as environmental factors such as soil type and climate. This has significant overlap with the definition of 'plant stress', a term which specifically refers to plants growing in non-ideal growth conditions (Mosa et al., 2017). When the demands applied upon a plant, for instance due to a lack of key resources, are in excess of the plant's ability to minimise these demands, this results in reversible sub-optimal growth which if sustained, of if the demand on the plant increases beyond what the plant can tolerate, can lead to permanent damage and possibly death. Consequently, the effect of both abiotic and biotic stresses on crops can severely impact yield and overall growth and performance.

Drought, for instance, is an abiotic stress that results in reduced yields. Drought induced low water content gives rise to osmotic change that leads to a loss of leaf turgor and stomatal closure, which has the effect of decreasing the uptake of CO_2 through the stomata, limiting the rate of photosynthesis (Farquhar & Sharkey, 1982).

Many environmental stresses, including drought, extreme temperatures, salinity, nutrient stress and pathogen infection, result in an increase in the production of Reactive Oxygen Species (ROS). Continuing to use drought as an example, stomatal closure in response to low water content also decreases the uptake of CO_2 and subsequently decreases the rate of CO_2 fixation, decreasing $NADP^+$ regeneration in the Calvin cycle (Sharma et al., 2012). As a result, there is insufficient electron acceptors resulting in an over-reduction of the electron transport chain, leading to an increased rate of electrons preferentially used for the reduction of oxygen through the Mehler reaction (Biehler & Fock, 1996). The generation of ROS are also generated as part of ordinary plant cellular metabolism, however ROS generation will lead to cellular damage if generated in excess of plant ROS dissipating mechanisms, and reduce yield and crop quality (Sharma et al., 2017; Sharma et al., 2012). The

prevention and dissipation of ROS is carried out by plant antioxidant systems. For example, the protonation of the thylakoid lumen in response to high light intensity induces a conformational change in the PSII antennae, promoting the dissipation of excess excitation energy and preventing the generation of ROS (Demmig-Adams & Adams, 2006; Ruban et al., 2012).

Plant phenotype, the anatomical, physiological and biochemical properties of a plant, is determined by both genetics and the influence of the environment (Walter et al., 2015). Phenotyping refers to the characterization of these properties of a plant, and to the measurement of any morphological, physiological, or biochemical process. Crop yield and water use efficiency, for instance, are key phenotypes that are target of many phenotyping efforts (Araus & Cairns, 2014; Munns et al., 2010). In the context of plant health, the response of a plant to biotic and abiotic stress is also an element of that plant's phenotype.

Phenotyping can therefore be used to identify key traits such as improved water use efficiency, higher yields, improved tolerance to salinity, and so on, allowing researchers to assess the impact of experimental treatments on crop performance and yield, and compare new and current crop varieties (Araus & Cairns, 2014; Awlia et al., 2016; Gonzalez-Dugo et al., 2015; Virlet et al., 2015).

In addition to using phenotyping techniques for plant breeding, the same phenotyping tools can also be used to monitor crop performance and health, generating crop data that can feed into a data-driven management approach by farmers (Balafoutis et al., 2017; van Evert et al., 2017). This approach enables farmers to make better decisions regarding water, fertilizer and pesticide inputs to mitigate the effects of abiotic and biotic stress, especially those that are a result of climate change (Liew et al., 2008). Phenotyping can use spectral techniques which measure the optical properties of leaves, over conventional techniques such as gas exchange. Spectral techniques enable researchers and farmers to probe the status of plant pigments, structure, and photosynthetic efficiency remotely and non-invasively.

1.1.1 Spectral Properties of Plants

1.1.1.1 Light absorption in photosynthesis

The absorption of light by plants is essential for photosynthesis. Incoming light is captured in the light-harvesting complex (LHC) antenna of plant photosystems (Photosystem II, PSII; or Photosystem I, PSI) (Horton et al., 1996; Nelson & Yocum, 2006) (Fig. 1.1). The LHC is responsible for light harvesting and energy transfer to photosystem reaction centres. The antenna of the LHC consists predominantly of chlorophyll molecules, with approximately half of all chlorophyll within a chloroplast bound in LHCs (Peterman et al., 1997). Absorption of irradiating light by chlorophyll results in an excitation of chlorophyll molecules. The excited chlorophyll is quenched by the photosystem reaction centres (Baker, 2008), by the transfer of excitation energy from the LHC antenna to the P_{680} chlorophyll in the reaction centre of PSII, or P_{700} chlorophyll in PSI. However, under excess light the excited state of chlorophyll in the antenna is not efficiently quenched by the reaction centre. When this occurs, there is a higher chance of chlorophylls in the excited state decaying to lower energy levels, leading to the production of chlorophyll triplets (Peterman et al., 1997). Chlorophyll triplets, which have a relatively long life in this form before further decay, react with molecular oxygen to produce singlet oxygen (Krieger-Liszkay, 2005). The generation of singlet oxygen, a radical oxygen species (ROS), which due its highly reactive nature can cause significant damage to proteins and pigments of the cell, leads to a reduction of photosynthetic efficiency known as photoinhibition.

The LHC antenna also consists of xanthophyll carotenoids, which serve multiple purposes. Firstly, the xanthophylls act to assist in light harvesting (Peterman et al., 1997). The absorption spectra for carotenoids differs to that of chlorophyll (Fig. 1.2), so that the composite spectra of chlorophyll and carotenoid pigments covers a broader range of wavelengths. Secondly, xanthophylls play a key role

in protecting against photoinhibition as a result of oxidative stress (Latowski et al., 2011; Mozzo, et al., 2008; Peterman et al., 1997). As mentioned, singlet oxygen is produced when the plant is experiencing light levels in excess of that which can be efficiency quenched. Xanthophylls prevent photodamage by quenching chlorophyll triplets, reducing the lifespan of the chlorophyll triplets and subsequent singlet oxygen formation (Peterman et al., 1995). Finally, xanthophyll carotenoids also serve to stabilise the structure of the LHCII complex (Lokstein et al., 2002; Pogson et al., 1998).

1.1.1.2 Electron transport chain

Once excitation energy is transferred to the P_{680} of the reaction centre, P_{680} transfers an electron to the electron acceptor Q_A via the initial electron acceptor pheophytin (Govindje et al., 2017; Rochaix, 2011). Oxidised P_{680} obtains its electron from the splitting of water in the oxygen evolving complex (Fig. 1.1). While Q_A is reduced, it is unable to accept any further electrons from P_{680}, so the reaction centre is considered "closed". When the reaction centre is "closed", excitation energy from P_{680} is unable to transfer to Q_a, and excitation energy from absorbed light in the LHCII antenna is unable to transfer to P_{680}.

From Q_A, electron transport continues across the thylakoid membrane, from PSII to PSI via cytochrome b_6f, before transfer to the electron carrier ferrodoxin and utilized by enzymes in the generation of NADPH from $NADP^+$ Further details on electron transport can be found at Govindjee et al. (2017) and Rochaix (2011).

The products of electron transport. NADPH and ATP, are used in the reduction and regeneration phases of the Calvin cycle (Fig. 1.1), where in the carbon fixation phase of the Calvin cycle the enzyme Ribulose 1,5-bisphosphate carboxylase/oxygenase (Rubisco) catalyzes the assimilation of CO_2 with ribulose 1,5-bisphosphate (RuBP) (Heldt & Piechulla, 2011). The product of the Calvin cycle, the sugar glyceraldehyde 3-phosphate, is exported from the chloroplast into the cytosol, and is used synthesise sugars such as glucose and starch.
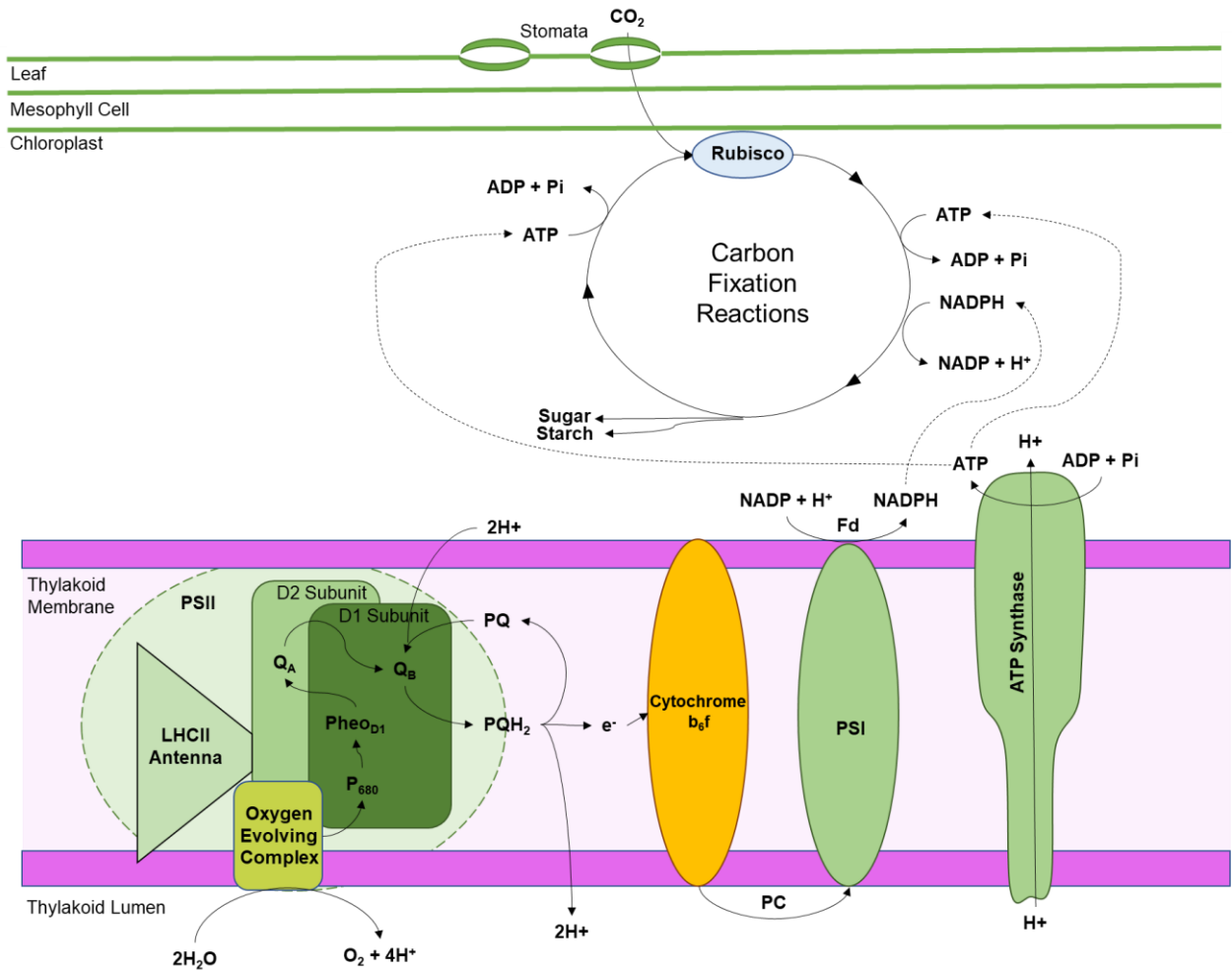
Figure 1.1 A simplified diagram demonstrating key steps of photosynthesis, with additional steps shown for electron transfer within PSII, with electron transfer starting at the oxygen evolving complex, to P_{680} and continuing to PSI and ferrodoxin. Abbreviations: Fd, ferrodoxin; LHCII, light harvesting complex II; Pheo, pheophytin; PSII, photosystem II; PSI, photosystem I; PC, plastocyanin; PQ, plastoquinone; PQH_2, plastoquinol; Adapted from Baker, 2008; Govindjee et al., 2017; Murchie & Lawson, 2013.
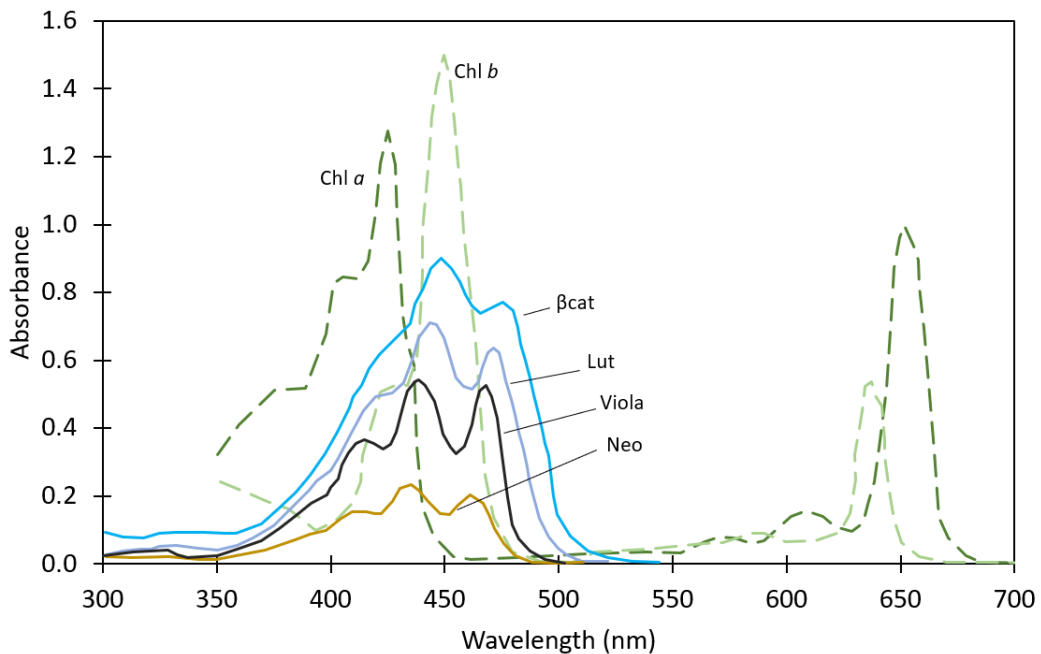
Figure 1.2 Absorption spectra of selected plant pigments of Chlorophylls (dashed lines) and four ubiquitous carotenoids, in diethyl ether solvent *Ch*l *a*; Chlorophyll *a*; *Chl b*, Chlorophyll *b*; *β-C*, β-carotene; *Lut*, lutein; *Neo*, neoxanthin; *Viola*, violaxanthin. Image adapted from Lichtenthaler & Buschmann (2001)

Nitrogen is essential for much of the photosynthetic apparatus, with proteins of the thylakoid membrane and Calvin cycle constituting the majority of a plant's nitrogen (Evans, 1989). Under low nitrogen availability, these key components are affected the most, decreasing the plant's capacity for photosynthesis. A large amount of nitrogen is utilized for Calvin cycle enzyme, with plants allocating anywhere from 20%-30% of leaf nitrogen to Rubisco (Makino, 2011). Limited nitrogen supply will also reduce carbon assimilation in C4 plants by reducing PEP carboxylase and Rubisco content (von Caemmerer, 2000). Nitrogen is also an important constituent in chlorophyll, with chlorophyll content decreasing under nitrogen deficiency and increasing when nitrogen availability increases (Ding et al., 2005; Hokmalipour & Darbandi, 2011; Tóth et al., 2002).

1.1.1.3 Spectral properties of plants; absorption, transmittance, and reflectance

Absorption of light by plant pigments is predominantly focused on a spectral region from 400nm to 700nm, the typical spectrum ranging from blue to red. This region is referred to as Photosynthetically Active Radiation (PAR) due to this region of light corresponded to the absorption spectra of pigments for the purposes of photosynthesis (Fig. 1.2). Light above 700nm, ranging up to approximately 1350nm, is referred to as Near Infra-red (NIR). As the wavelength progressed towards the NIR region, there is a rapid increase in reflectance due to less absorbance of NIR light by plant pigments (Fig. 1.3). This rapid increase, typically occurring near or just after the 700nm wavelength, is typically referred to as the 'red' edge (Filella & Penuelas, 1994).

From the end of NIR at 1350nm to 2400nm is another spectral region that is termed Shortwave Infra-Red (SWIR). Absorption of SWIR is associated with molecular water, which absorbs light in the NIR and SWIR regions. In fact, water absorption of SWIR is so strong that it is visible as two large decreases in reflectance at approximately 1400-1500nm and 1900-2000nm regions (Fig. 1.3).

Ultraviolet (UV) light refers to light from 10nm up to 400nm, although the majority of this is absorbed by the Earth's atmosphere, and so in the context of irradiating light UV wavelengths are generally considered as ranging from 280nm up to 380nm. While not associated with photosynthesis, UV absorbing plant pigments and other chemicals exist to prevent the highly energetic photons of UV wavelengths from causing damage to DNA and other molecules (Kiefer, 2007).

Irradiating light on a leaf is either absorbed by pigments of the leaf, reflected away from the leaf, or transmitted through the leaf. Reflectance is the measurement of light that is reflected away from the surface of the leaf. Reflectance can consist of factors such as light that has undergone internal scattering in the mesophyll due to refraction across air/cell interfaces, as is the case with reflected NIR light (Asner, 1998). Light that is not reflected continues through the leaf, with the majority of

visible light absorbed by plant pigments in a healthy plant. Finally, any light that has not been absorbed exits on the other side of the leaf, which is termed transmittance.

Transmittance, absorbance and reflectance are linked (Fig. 1.3), as light undergoes one of these three fates once in contact with a material such as a plant leaf, and a decrease in one will result in an increase in both of the others. This relationship between reflectance, transmittance and absorption can be expressed with the formula R + T + A = 1, with R being Reflectance; T, Transmittance; A, Absorption, and 1 the sum of light which reaches the leaf (Jacquemoud & Ustin, 2008). Reflectance can be separated into two components, R_s, the reflectance of light at the surface of the leaf and R_d, reflectance as a result of scattering and internal refraction between leaf tissues (Jacquemoud & Ustin, 2008).

This relationship between reflectance, absorption and transmittance therefore allows for the measurement of two to indicate the status of the other one. However, changes in absorption result in changes to both reflectance and transmission, and therefore does not require a measurement of both unless the exact amount of absorbed light is desired. Thus, the measurement of reflected light allows for the quantity and status of pigments within the plant to be measured. For instance, reflectance is routinely used to measure the nitrogen content of field crops (Schepers, et al., 1996; Schlemmer et al., 2013). Higher reflectance values, especially in the red wavelengths where pigment absorption of light is less saturated, indicated a lower quantity of chlorophyll pigments. Lower chlorophyll is an indicator of lower nitrogen availability as nitrogen is a component of the molecular structure of chlorophyll (Wang et al., 2014). Measuring changes in the reflectance of one spectral region against another unchanging spectral region, forms the basis of a spectral index.
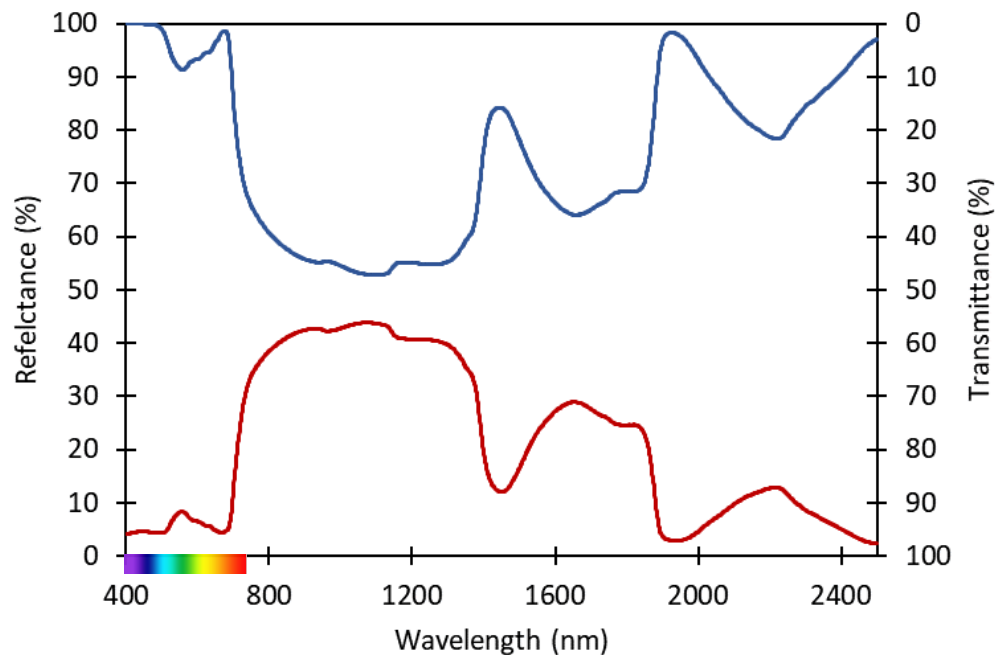
Figure 1.3 A example spectrum of a typical leaf*,* demonstrating the relationship between reflectance (red; lower) and transmittance (blue; upper). The space in the middle represents the amount of light for each wavelength which is absorbed. Colours for visible shown are shown between 400nm and 700nm. Ultraviolet (UV) light is not shown on this figure

1.1.2 Spectral Indices and how to measure them

A spectral index is a calculation or transformation of two or more spectral bands, although indices do exist that involve the transformation of only one spectral band (Gitelson et al., 2003), and can be calculated from any sensor capable of measuring reflected light (Fig. 1.4). Such sensors include spectrometers, which separates light and measures the intensity of light per wavelength. Cameras function similarly, except a camera sensor measures any light that reaches the sensor itself. Consumer cameras are fitted with an array of optical filters, to capture red, green and blue light. However, a camera can be installed with any optical filter, to capture individual wavelengths or bands, allowing for spatial measurement of spectral indices. Hyperspectral cameras perform a similar function, however these cameras are capable of capturing images consisting of reflectance for individual wavelengths ranging from across the visible, NIR and SWIR spectra.

Satellites, such as NASA's Landsat or ESA's Sentinel, orbit the earth capturing images of reflectance across the surface of the planet. The Sentinel satellites for instance, complete their imagery of the Earth in under a week, allowing for weekly updated reflectance imagery for researchers or agronomists. However, satellite imagery is very low resolution. The best reflectance imagery, as provided by the Sentinel satellites, has a resolution in which one square "pixel" of a satellite image typically representing a 10 x 10 metre area, although this is typically larger for most wavelengths, ranging from 20 x 20 metres to 60 x 60 metres (Drusch et al., 2012; ESA, 2020). Satellite imagery is therefore more suited for ecological monitoring, monitoring huge swathes of forests or other natural environments for seasonal and yearly changes in vegetation. For agriculture, if detailed information on crops in the field is needed, such as information regarding which areas need more fertilizer or are experiencing drought conditions, alternative imagery platforms such as UAV imagery may be more ideal (Fig. 1.4).

Imagery from unmanned aerial vehicles (UAV) or other aerial vehicles, is routinely used both in research and commercially for the imaging of crops in the field. UAVs can be employed with both cameras and small portable spectrometers, depending on the requirements of the flight. Hyperspectral cameras can also be utilized on UAVs, allowing for huge amounts of wavelengths to be measured. UAVs have the advantage of allowing a larger area of measurement, with entire fields capable of being measured within hours rather than days, effectively shifting the phenotyping bottleneck from data collection to data processing (Kefauver et al., 2017). Despite being further away from the canopy, there is not much difference between ground based and UAV based canopy level measurements (Gracia-Romero et al., 2019).

Another approach is the use of phenotyping platforms such as the Field Scanalyzer (Virlet et al., 2017). These platforms are equipped with an array of cameras and sensors, more than a UAV payload would allow, and are capable of collecting large amounts of data. These platforms however,

can only measure crops grown within their area of operation, and are predominantly utilised for research or as a tool for breeding programmes (Sadeghi-Tehran et al., 2017; Virlet et al., 2017)

Finally, the most common approach to phenotyping is through the use of hand held devices and leaf clips for leaf level measurements. Leaf level measurements are routine in laboratory and greenhouse measurement, and very common in the field. Leaf level measurements are less reliant on spectral techniques with infra-red gas exchange (IRGA), one of the most common techniques used, measuring the uptake of CO_2 and addition of water to the air as a result of CO_2 assimilation and stomatal conductance. However, chlorophyll fluorescence, spectrometry and thermography are still routinely used at the leaf level.

Many tools have also been devised to allow for plant phenotyping using spectral imaging, without requiring significant expertise. For instance, the MultispeQ, a handheld leaf clip developed by Kuhlgert et al (2016) has been developed to enable farmers and growers to collect key physiological measurements, such as chlorophyll measurements of photosynthetic performance and chlorophyll content, while additionally measuring environment variables such a PAR, atmospheric CO_2, and relative humidity. Leaf level measurements can also be developed using consumer hardware, such as a device developed to assess fruit ripeness (Das et al., 2016) or assess chlorophyll content using a smart phone adaptor (Friedrichs et al., 2017)

Thus, spectral techniques can be used across scales (Fig. 1.40, with advantages and costs at each level. However, the basics of the techniques used remains relatively constant regardless of scale. Two of the most common spectral indices across scales are the Normalized Difference Vegetation Index (NDVI) and the Photochemical Reflectance Index (PRI).
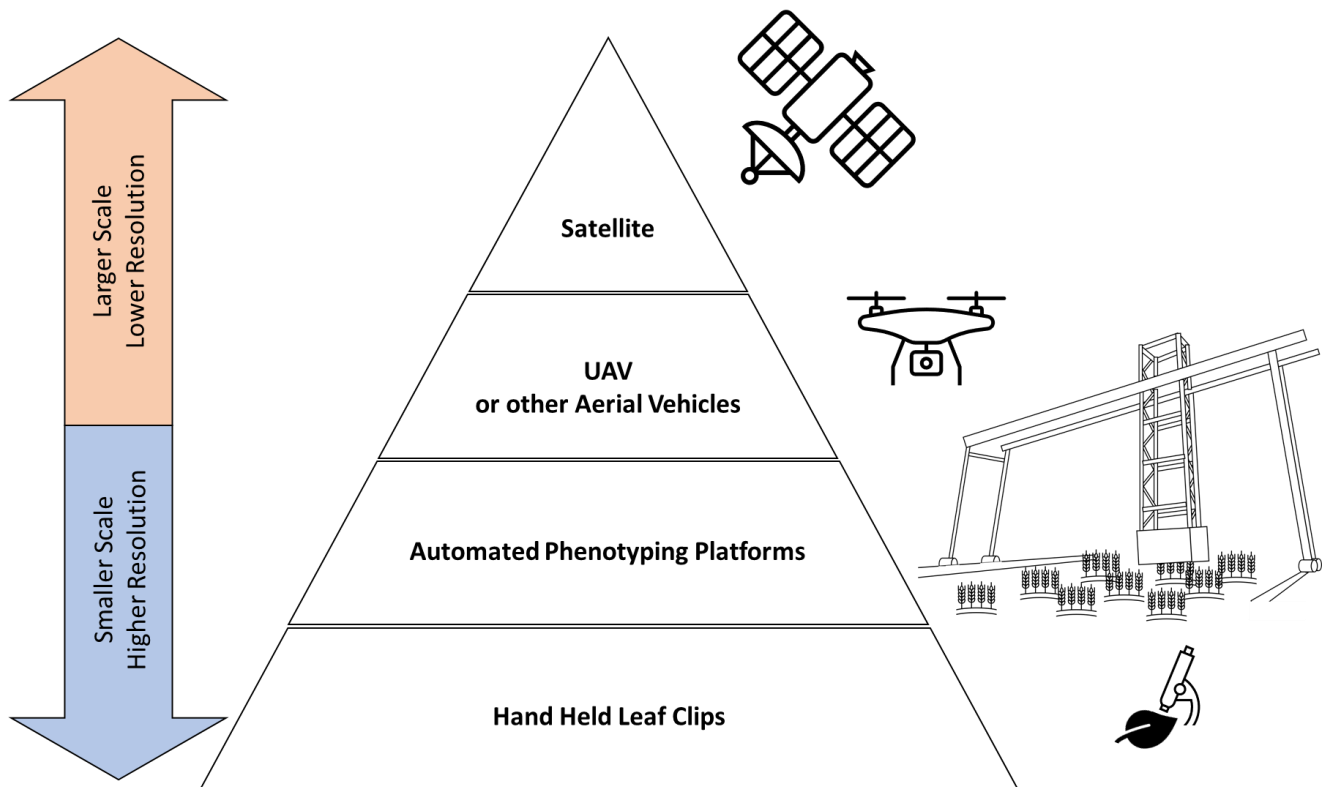
Figure 1.4 The various scales in which reflectance measurements can be collected. At the smallest scale are leaf clip measurements, with a typical setup consisting of fibre optics which illuminate an area of the leaf and collect reflected light for measurement in portable spectrometer. Automated phenotyping platforms consist of a measurement "head" consisting of an array of cameras and sensors. The measurement head can be raised/lowered and moved across a field automatically, quickly collecting canopy level measurement at a higher resolution. An unmanned aerial vehicle (UAV) can be equipped with cameras and sensors and flown over fields, capturing many images over a short time but at a lower resolution than phenotyping platforms or leaf clips. Satellites are equipped with narrow band spectrometers, and capable of measuring reflectance for huge swathes of land. While satellites clearly have the largest scale, capable of capture an entire field, this comes at a huge cost to resolution, with one square "pixel" of a satellite image typically representing a 20 metre by 20 metre area depending on the satellite and wavelength used.

.

1.1.2.1 The Normalized Difference Vegetation Index (NDVI)

The Normalized Difference Vegetation Index (NDVI) (Rouse & Space, 1978) is one of the most popular and oldest spectral indices, from widespread use in agriculture, up to satellite based imagery with NASA's Landsat and ESA's Sentinel multispectral imaging satellites. The NDVI is a structural index, in that it is a combined measure of both "greenness", measuring the degree of chlorophyll absorption of the red wavelengths, and of the structural properties of a leaf. Stressed and damaged plants exhibit greater reflection of NIR light due both to the effects of less red

absorption due to lower chlorophyll content, and to changes in the internal scattering of NIR as a direct result of a shift in the structural properties of a leaf, predominantly through the air/cell interfaces of the spongy mesophyll (Carter & Knapp, 2001; Liew et al., 2008).

It is calculated as Eq.1.1;

$$NDVI = \frac{(NIR - VIS)}{(NIR + VIS)} \qquad (1.1)$$

With NIR for the reflectance (%) of near infra-red, and VIS for the reflectance (%) of visible red light. An NDVI above zero has more NIR than VIS, whereas an NDVI below zero has more VIS than NIR. Decreases in the chlorophyll content, and thus less absorption (more reflectance) of red light, decreases the NDVI value towards a more negative value. A change in the structural properties of a leaf, such as through changes in the intracellular spaces of cells through water deficit, results in an increase in the reflectance of NIR, and thus also decreases the NDVI value towards a negative value.

Zhao et al. (2005) noted that when using NDVI, the bandwidth and central wavelengths of the red and NIR regions should be considered carefully. However, there is no standardised wavelength or spectral region for NDVI and it is common to see literature regularly citing different wavelengths (Magney et al., 2016; Suárez et al., 2008; Thenkabail et al., 2000). This often depends on the technical ability of equipment, for example the number of specific bands available on satellite imaging platforms and their bandwidth (Bannari et al., 1995; Clevers & Gitelson, 2013). As a good illustration of differing opinion in wavelength choice, Thenkabail et al. (2002) compiled a list of spectral regions and their associated relationship to physiology, suggesting red regions centred at either 660nm or 675nm as ideal for detecting differences due to stress and nitrogen content. However, Zhao et al. (2005) argue that using a red region between 680nm and 730nm is better for NDVI detection of nitrogen stress.

A larger spectral bandwidth (e.g. the distance between the lowest and highest wavelength of each red and NIR region) is reported to have no effect on NDVI values (Zhao et al., 2005). However, this is wavelength dependant, for example using 700nm as a red wavelength, which overlaps with the red edge itself, and a NIR wavelength of 850m have been reported as having a decreasing predicting power in the assessment of nitrogen content as the bandwidth for these two regions widens (Zhao et al., 2005).

NDVI is predominantly associated as an indicator of general plant health. While it is strongly linked to chlorophyll content, other stress factors will also play in a role in the 'greenness' of a plant (Fanizza et al. , 1991; Sanchez et al., 1983; Thenkabail et al., 2002). In one study, various macronutrient deficiencies all showed increased reflectance in VIS and NIR regions (Ayala-Silva & Beyl, 2005). However, magnesium and nitrogen deficiencies demonstrated larger increases than other macronutrient. Therefore, although a relatively simple index, the NDVI can have varying degrees of response and sensitivity.

1.1.2.2 The Photochemical Reflectance Index (PRI)

Another common narrowband spectral index is the Photochemical Reflection Index (PRI) (Gamon et al., 1992), measuring reflectance at wavelengths in the yellow-green spectrum. PRI traditionally uses wavelengths at 531nm and 570nm (Gamon et al., 1990a; Wong & Gamon, 2015), although variations do exist, such as the PRI_{515} index (Clemente et al., 2011).

The PRI can be measured as a leaf level measurement via leaf clips, or at a canopy level through mounting on UAVs or other platforms. However, at the canopy level PRI is sensitive to leaf angle, geometry of solar illumination, and the angle of the detector itself (Malenovsky et al., 2009), which can make the remote measurement of PRI challenging.

The development of PRI started with identifying absorbance changes in the green-yellow region alongside de-epoxidation of the xanthophyll cycle, built upon work demonstrating a relationship

between non-photochemical quenching and zeaxanthin content (Demmig et al., 1988), and changes in absorbance of light arising from the de-epoxidation of violaxanthin to zeaxanthin. Bilger et al. (1989) expanded upon this, investigating the effect of the xanthophyll cycle on the absorbance of healthy green plants. They identified changes in absorbance, from 465nm up to around 520nm, with a peak at 505nm and encompassing most of the 500-530nm range. The addition of DDT, an reducing agent which acts as an inhibitor of photosynthesis and known to affect non-photochemical quenching through inhibition of violaxanthin de-epoxidase (Jiang et al., 2004; Neubauer, 1993), lead to an inhibition of this absorbance change, linking this spectral response to the xanthophyll cycle.

Gamon et al., (1990) used this knowledge to scale up the measurement from leaf level based absorbance to a canopy level based reflectance measurement, by experimenting with dark adapted plants exposed to solar noon PPFD (Photosynthetic Photon Flux Density; a measurement of the flux of light in the spectrum of light that can be used in photosynthesis). Upon exposure to noon PPFD, decreases in reflectance could be seen at a peak from 500 up to 550nm, centred at 531nm. A good relationship between this change in reflectance at 531nm and the epoxidation state (EPS) of the leaves was observed for all measurements except for those that were collected 19 minutes or longer after exposure to solar PPFD. The addition of DDT, inhibiting de-epoxidation of the violaxanthin, again showed no change in reflectance.

One method to assess the relationship between reflection at the 531nm wavelength and the xanthophyll cycle was to use the herbicide DCMU. DCMU blocks electron transport from photosystem II to plastoquinone, preventing the reduction of plastoquinone (Metz et al., 1986), which has the effect of limiting the protonation of the thylakoid. As part of linear electron transport (Fig. 1.1), plastoquinone accepts elections from Photosystem II and two protons from the stroma of the chloroplast (Järvi et al., 2013; Mühlbauer & Eichacker, 1998). The electrons are passed to plastocyanin, further along the electron transport chain, while the two protons are passed into the lumen of the thylakoid (Tikhonov, 2014). As thylakoid lumen pH is key in the activation of

violaxanthin de-epoxidase (Fernández-Marín et al., 2011) this both inhibits the formation of zeaxanthin, and the higher pH facilitates the reverse process of zeaxanthin epoxidation forming violaxanthin (Jahns et al., 2009)

In the context of spectral reflectance, the addition of DCMU reduced the change in reflectance seen at 531nm when a plant is exposed to high light, which was what was seen by Gamon et al. (1992), thereby demonstrating the link between reflection at these wavelengths and the epoxidation state of the xanthophyll cycle. However, a weak relationship between reflectance and NPQ has been seen after prolonged measurement, attributed to changes to leaf shape and orientation, consistent with reports regarding the variability of PRI due to changes in leaf structure and angle, etc. (Rossini et al., 2013; Wong & Gamon, 2015). Yet despite this, PRI has been used as an indicator of long term diurnal NPQ (Gamon & Bond, 2013)

A spectral index could therefore be used, using wavelengths in the region sensitive to the xanthophyll cycle (i.e. 531nm) and a wavelength which was insensitive (i.e. 570nm), which would correspond directly to the epoxidation state of xanthophylls.

$$PRI = \frac{(R531 - R570)}{(531 + R570)} \qquad (1.2)$$

PRI is thus calculated as in Eq. 1.2, using reflectance at 531nm (R531) and reflectance at 570nm (R570).

As the xanthophyll cycle plays a major role in the non-photochemical quenching of excess light energy (Gilmore, 1997; Latowski et al., 2011), it could also be used to measure and track changes in NPQ. When there is excess absorbed light than can be used in photochemistry, absorbed light will increasingly be dissipated as heat through NPQ. During electron transport, there is accumulation of protons (protonation) and subsequent acidification of the thylakoid lumen. This change in pH leads to conformational change of the PSII antenna which facilitates the dissipation of energy from excited chlorophyll molecules, protonation of the PsbS protein, and the de-epoxidation of the pigment

violaxanthin to zeaxanthin in what is known as the xanthophyll cycle (Ballottari et al., 2012; Latowski et al., 2011), each operating to differing timescales (Müller et al., 2001).

The epoxidation of the xanthophyll can be slow enough to significantly impact photosynthesis and subsequent yield of crops. Kromdijk et al. (2016) modified Tobacco plants to overexpress enzymes related to NPQ such as violaxanthin de-epoxidase and zeaxanthin epoxidase (ZED), and the PsbS protein. Overexpression of ZED accelerates the epoxidation of zeaxanthin into violaxanthin, which plays a role in increasing the rate of NPQ relaxation. This had the result of increasing the kinetics of NPQ in response to fluctuating light, allowing for an increase in overall carbon assimilation throughout the course of a typical day. NPQ dissipates excited chlorophyll to prevent the generation of ROS, and slower relaxation results in a continued quenching of excited chlorophyll when ambient light levels return to optimal, limiting the efficiency of PSII and subsequent carbon fixation. This modification to NPQ resulted in an increase of around 15% plant dry matter due to quicker NPQ relaxation and thus higher carbon fixation.

1.1.3 Canopy level Spectral Indices

Indices such as NDVI and PRI were developed to allow for remote, canopy level measurements of vegetative health and indicators of photosynthetic performance (Gamon et al., 1995; Gamon et al., 2015; Guo & Trotter, 2004). However, there are still challenges associated with canopy level remote sensing measurements, such as the effects of soil reflection on apparent reflectance, ratio of stem to leaves, variation in leaf angle, and other technical challenges such as anisotropy, which can affect NDVI, PRI and any other spectral reflectance measurement (Asner, 1998; Steven, 1998).

As the ability to track canopy chlorophyll content is important for environmental monitoring and estimations of productivity (Gitelson et al., 2015), indices have been developed to improve upon NDVI for this purpose, increasing sensitivity to chlorophyll content while decreasing the effect of other factors such as soil and background reflectance.

Developed for canopy remote sensing applications, the Chlorophyll Absorption Reflectance Index (CARI) and modified CARI (MCARI) (Datt, 1999; Daughtry et al., 2000) use a wavelength of maximal chlorophyll absorption (e.g. 670nm) and spectral bands of minimal chlorophyll absorption (Datt, 1999; Haboudane et al., 2002). The derivation of a spectral ratio by dividing a wavelength that is sensitive to chlorophyll content by one that is insensitive, leads to a spectral index that is quantitatively related to chlorophyll content. The index is thus very sensitive to chlorophyll content, while reportedly less sensitive to the effects of lighting conditions, soil and other background reflectance common to canopy level measurements (Haboudane et al., 2002).

The Transformed Chlorophyll Absorption Reflectance Index (TCARI) is a modified MCARI that was developed to overcome the effects of leaf area, background reflectance and other non-photosynthetic components (Haboudane et al., 2002). This is done by compensating for these effects on the ratio by artificially increasing the ratio of reflectance at 700nm-670nm to the reflectance at 700nm-550nm, which is the region affected most by these effects. All of these indices (CARI, MCARI and TCARI) have been developed for the purpose of improving the remote measurement of chlorophyll content. Indices which track canopy chlorophyll content and green leaf area index can be used to estimate crop productivity (Peng & Gitelson, 2011), and thus TCARI has been used to remotely estimate Gross Primary Production (Zarco-Tejada et al., 2013). The Optimized Soil-Adjusted Vegetation Index (OSAVI), is another variation of NDVI which reduces the effects of soil background variation (Steven, 1998), reported to have a moderate performance in tracking yield (Gonzalez-Dugo et al., 2015).

Indices which are composed of two or more indices are referred to as "combined" indices. Indices based on the ones mentioned previously, MCARI/OSVAI and TCARI/OSAVI are two very similar "combined" indices; the TCARI and MCARI can be combined with OSAVI, an index based on a modified NDVI (Huete, 1988), which involves applying a correction factor, dependant on vegetation density, which shifts the values of the NDVI. The index has been able to successfully measure crop canopy

cover with around 5% error (Steven, 1998). TCARI/OSAVI was highlighted as having greater insensitivity to leaf area and soil reflectance, while still retaining sensitive measurements of chlorophyll content (Haboudane et al., 2002), although other work suggests both have similar sensitivity (Wu et al., 2008). Wu et al. also demonstrated the effectiveness of both TCARI/OSAVI and MCARI/OSAVI in estimating chlorophyll concentrations for different species of wheat, suggesting the indices will perform independent of species. Overall, combined indices such as MCARI/OSAVI and TCARI/OSAVI, have a strong correlation to chlorophyll content at the canopy level (Zarco-Tejada et al., 2004), and thus correlated to plant nitrogen content (Clevers & Gitelson, 2013).

The index of TCARI/OSAVI, along with many of the other previously discussed indices (Baluja et al., 2012), have also been shown to correlate to stem water potential and stomatal conductance in some species (Ballester et al., 2017; Baluja et al., 2012), while this relationship has not been seen in other species (Ballester et al., 2017). It is worth remembering that these indices are concerned with detecting pigment concentration, not water content, and therefore are likely to be affected by concurrent decreases in chlorophyll content that occur during water stress, rather than water status itself (Chutia & Borah, 2012; Sanchez et al., 1983).

Finally, Gitelson et al. (2003) investigated a range of leaves with differing pigment content and were able to identify regions of reflectance which correlated strongly with chlorophyll content. Using the reciprocal of reflectance, they identified a region from 520nm to 550nm, and a region from 695nm to 705nm. From this they developed indices based on these regions, in particular a red-edge chlorophyll index ($CI_{red-edge}$), based on the reciprocal of the ratio of reflectance at 783nm to reflectance at 705nm. On a leaf level, the indices worked very well with leaf level measurements (Schlemmer et al., 2013), tracking leaf nitrogen and chlorophyll. These regions also corresponded to bands on the MODIS satellite, and although the location of spectral bands between satellites varies, the index did not significantly differ between various central bands. Measurements based on bands

available to the Sentinel-2 satellite maintained a good correlation to canopy chlorophyll and nitrogen content (Clevers & Gitelson, 2013).

1.1.4 Ongoing developments in spectral techniques

Spectral vegetation indices are being developed and improved continuously, for use at both the leaf or canopy level and for a wide array of applications. Select examples of some spectral indices in use in both research and industry and be seen in Table 1.1, however while no exhaustive list of vegetation indices exists, the actual number of spectral indices is significantly higher, estimated to be at least between 300 and 500 indices (Henrich et al., 2011). More comprehensive lists can be found within the literature and databases (Bannari et al., 1995; Henrich et al., 2011; Xue & Su, 2017; Zarco-Tejada et al., 2004)

Many indices arrive from tailoring a pre-existing spectral index to the desired species and/or physiology. A good example is the multiple variations of vegetation indices (VI) e.g. NDVI, that exist, such as the Red Edge Normalised Vegetation Index (RENVI), which directly uses bands on the red edge (750nm and 705nm), increasing the sensitivity of the index to changes in vegetation (Gitelson & Merzlyak, 1994).

A fundamental aspect of spectral signatures is understanding which wavelengths are most relevant to the physiological property of interest. One common approach is to develop a spectral index specifically for a species and physiological trait or stressor of interest. Such an approach would have greater predictive power, and be indicative of the physiology of that species. In many cases, most spectral indices could benefit from "spectral fine-tuning" (Rapaport et al., 2015), however finding the right spectral index for the intended measurement can ultimately be a trial and error approach. However, with increasing powerful computing abilities, newer modelling based approached are having greater success at developing novel spectral signatures, especially ones that can be related to aspects of physiology that had not previously possible to measure spectrally, such as the maximum rate of rubisco carboxylation (V_{cmax}) (Ainsworth et al., 2014; Serbin et al., 2012; Silva-Perez et al.,

2018; Yendrek et al., 2017). Using computational methods, many indices have been developed to identify specific combinations of disease and species. Examples include detecting wheat leaf rust in wheat (Ashourloo et al., 2014) yellow mosaic disease in soybean (Saad et al., 2013), and orange rust in sugarcane (Apan et al., 2002). In general, these specific indices correlate greater with diseases than other generalised indices such as NDVI.

Table 1.1 A small selection of spectral reflectance indices, demonstrating the breadth of available spectral indices. R[wavelength] denotes reflectance at a specific wavelength. Many indices serve a similar function to each other, while many use the same regions of wavelengths.

INDEX	NAME	CALCULATION	REFERENCE
NDVI	Normalised Difference Vegetation Index	$(R_{NIR} - R_{RED}) / (R_{NIR} + N_{RED})$	Rouse et al 1978
CI$_{RedEdge}$	Chlorophyll Index Red Edge	$(R_{NIR}/R_{RedEdge})-1$	Schlemmer et al. 2013
RVSI	Red-edge vegetation stress index	$(R714nm + R752nm) + 2-R733nm$	Ashourloo et al 2014
SAVI	Soil-adjusted vegetation index	$(R_{NIR}-R_{RED})(1+L) / (R_{NIR}+R_{RED})(1+L)$	Huete 1988
NDWI	Normalized difference water index	$(R860 - R1240)/(R860 + R1240)$	Gao 1996
TCARI	Transformed Chlorophyll Absorption Reflectance Index	*See: Reference*	Fitella and Penuelas 1994
MSI	Moisture Stress Index	*See: Reference*	Rock et al 1986
OSAVI	Optimised Soil Adjusted Vegetation Index	$(R800 - R670)/(R800 + R670 + 0.16)$	Steven 1998
TCARI/OSAVI	*See: TCARI and OSAVI*	See: OSAVI; TCARI	Haboudane et al. 2002
MSAVI	Modified Chlorophyll Absorption Reflectance Index	$(R800 - R670)/(R800 + R670 + 0.16)$	Haboudane et al. 2002
MCARI	Modified chlorophyl (*a* and *b*) absorption in reflectance index	$(R700nm - R670nm) - 0.2(R700nm - R550nm) * (R700nm / R670nm)$	Daughtry et al 2000
WI	Water Index	$R900/R970$	Penuelas et al 1993
SRPI	Simple Ratio Pigment Index	$R430/R680$	Penuelas et al 1994, 1995
VARI	Visible Atmospherically Resistant Index	$R_{GREEN} - R_{RED} / R_{GREEN} + R_{RED} - R_{BLUE}$	Gitelson et al 2002; Naidu et al 2009
PRI	Photochemical Reflectance Index	$(R531 - R570) / (R531 + R570)$	Gamon et al 1992
PRI$_{515}$	Photochemial Reflectance Index	$(R515 - R5310) / (R515 + R531)$	Zarco-Tejada et al 2013
WABI-1	Water Balance Index	$(R1490 - R531) / (R1490 + R531)$	Rapaport et al 2015
WABI-2	Water Balance Index	$(R1500 - R538) / (R1500 + R538)$	Rapaport et al 2015
WABI-3	Water Balance Index	$(R1500 - R538) / (R1500 + R538)$	Rapaport et al 2015
LRDSI_1	Red-edge Vegetation Stress Index	$6.9 \times (R605 / R455) - 1.2$	Ashourloo et al 2014
LRDSI_2	Leaf Rust Disease Index	$4.2 \times (R695 / R455) - 0.38$	Ashourloo et al 2014

1.1.4.1 Spectral regions and their applications

Knowledge of spectral regions that are applicable to a specific stress response that you wish to identify and track is key to using the correct spectral measurement (Thenkabail et al. 2002). In most cases, changes in reflectance can be very general, with similar changes in reflectance seen due to a wide range of factors, such as drought or low nitrogen availability, which can affect plant pigment content similarly. Increases in the green and red regions occur in response to almost all stresses regardless of stress agent or species (Carter, 1993), demonstrating the difficulty in identify specific causes of stress outside of general plant health. This is not strictly unique to visible wavelengths of light either. A study by Carter (1993) investigated the response of leaf spectral reflectance to plant stress on a small group of various plant species exposed to various stressors. Pathogen attack, soil condition, herbicides and low water content all had a significant effect on reflectance at wavelengths above 1000nm.

While the visible spectra is associated with changes in plant pigmentation, namely chlorophylls, the NIR and SWIR regions above 800nm are strongly associated with water content in plants. There are five main bands in the spectral response of a leaf that correspond with water absorption (Fig. 1.5). These are centred at 970nm, 1200nm, 1450nm, 1930nm and 2500nm (Seelig et al., 2008).
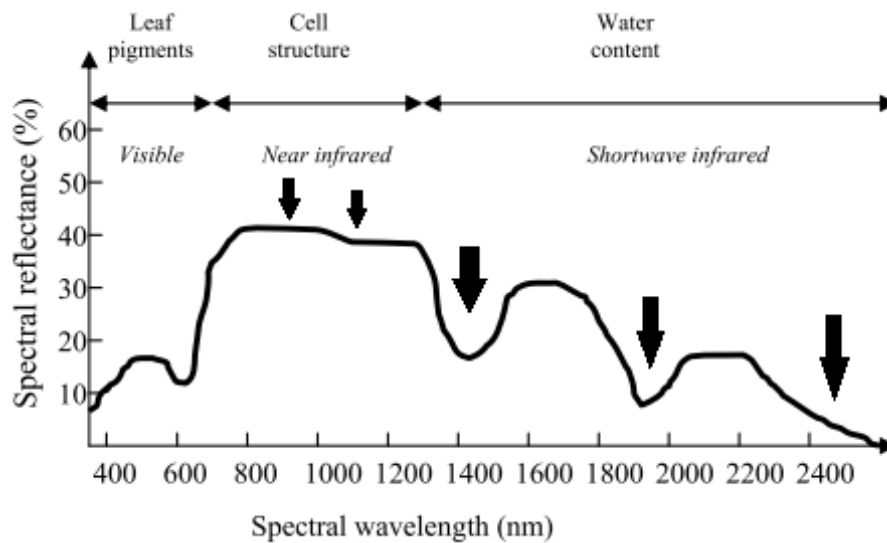
Figure 1.5 Typical relative reflectance response of a leaf, highlighting the predominant contributing factor to the spectral response of visible, near infrared and shortwave infrared wavelengths. Black arrows indicate water absorption bands. Adapted from (Govender et al., 2009; Seelig et al., 2008)

The Water Index, an index of ratio of reflectance at 900nm and 970nm, with 900nm being insensitive to water content, closely tracks changes in relative water content and leaf water potential in leaves (Peñuelas et al. 1993). Another common index, the Normalized Difference Water Index (NDWI) (Gao, 1996), uses the 860nm and the 1240nm wavelengths, to measure the water content in vegetation canopies. Although the two wavelengths used here have weak water absorption properties (Fig. 1.5), the indices have shown good results.

The ratio of 1300nm and 1450nm was identified by Seelig et al. (2008) as correlating strongly with the relative water content of leaves, exhibiting also a high sensitivity. However, while useful for laboratory and leaf level measurements, the water absorption bands at 1450nm and above are generally unsuitable for canopy measurements due to the strong absorption of light at these wavelengths by atmospheric water vapour (Seelig et al., 2008). When considering atmospheric effects on measured reflectance, the weaker absorbing bands in the NIR region (950-970nm) and

1150-1260 nm and 1520-1540nm of the SWIR region demonstrate the best overall correlation to leaf water content (Sims & Gamon, 2002).

The choice of wavelength for measuring water content also depends on the thickness of leaves for canopy measurements, as water content of thin leaves (<0.5cm thickness) is correlated strongest with indices in the NIR bands (Sims & Gamon, 2003). However, Ceccato et al. (2001) and Harris et al. (2006) demonstrated that a combination of NIR and SWIR provide the best results for estimating leaf water content, with the NIR concerned most with internal structure and thus is actually affected less by water content directly.

While the NIR and SWIR are strongly associated with water content, Rapaport et al (2015) analysed the spectral differences of grapevine grown under a water deficit and identified four key regions, which includes visible light in a green region at 530–550nm. However, the visible green wavelengths are identified as being sensitive by most types of stress (Carter, 1993), and thus not specific to water content.

1.1.4.2 Developing new spectral indices

A knowledge of spectral regions and how they are affected by the physical properties of a leaf is important in the development of spectral indices, yet it remains a challenge to develop new indices that target specific aspects of plant health. A commonly used method for the development of indices is to plot prospective wavelengths against ground truth measurements. The resulting co-efficient of determination (R^2) can thus also be plotted to generate a heat map, with wavelengths that resulted in a stronger relationship being "hotter" than others. This technique is employed routinely (Lu et al., 2015; Peñuelas et al., 1995; Shimada et al., 2012; Thenkabail et al., 2000; Thenkabail et al., 2002). An example of this technique was work by Lu et al (2015), who developed modified spectral indices which have a strong relationship to leaf chlorophyll content across species, and on both abaxial and adaxial sides of a leaf, by modifying the wavelengths used in a pre-existing spectral index by Datt

(1999). The spectral indices were developed by iterating through combinations of wavelengths, comparing the output against chlorophyll content, and using a heatmap to determine the ideal wavelengths.

Other methods for developing spectral indices is through computational methods. As had briefly been mentioned previously, Serbin et al (2012) set out to identify regions of plant reflectance which can be used to predict values of V_{cmax}, the rate of RuBP carboxylation, and J_{max}, RuBP regeneration, and analysed the hyperspectral reflectance of leaves from 450nm up to 2500nm. This is performed by using a partial least squares regression on a large dataset comprising of spectral measurements and ground truth measurements obtained through conventional techniques. This is used to develop a predictive model based on the full spectrum of hyperspectral measurements. This technique has allowed for hyperspectral reflectance measurements to predict photosynthetic capacity (Meacham-Hensold et al., 2019) and measure biochemical and physiological traits in wheat (Silva-Perez et al., 2018). This technique has also been used to detect the effects of ozone on plant photosynthesis (Ainsworth et al 2014). However, despite the promising results, a drawback so far to this method is the necessity of hyperspectral measurements, as hyperspectral cameras and leaf-clip based field spectrometers can be expensive. In some cases, they have the same price range as gas exchange systems such as those produced by Li-Cor, PP systems and ADC, but with less accuracy than these systems. Therefore, for now, this technique sits firmly in the world of research, with institutions performing significant amounts of high throughput phenotyping able to obtain a significant benefit.

This is only a small preview of the spectral indices available. Numerous reviews and papers list a significant breadth of indices (Zarco-Tejada et al. 2004; Sankaran et al. 2010; Bannari et al. 1995), with new indices continuously being developed. There is a vast array of options when it comes to spectral measurements, with many of the physical properties of a plant from pigment to water content that can be measured through changes in reflectance.

This also demonstrates that reflectance measurements can be a powerful tool in phenotyping and assessing plant performance. By understanding the relationship between reflectance and common stressors, a 'catalogue' defining changes in reflectance due to factors related to plant performance, such as chlorophyll and water content, or the status of the xanthophyll cycle, can be developed. However, reflectance is not the only spectral technique that is available.

1.2 Chlorophyll Fluorescence

1.2.1 Overview

Chlorophyll fluorescence is a powerful tool that provides information regarding the efficiency of photosynthesis, by measuring the re-emission of light from photosystem II (PSII). As this technique yields information regarding light use, some parameters therefore closely correlate with photosynthetic rates. When light energy is captured by chlorophyll in the light-harvesting complex (LHC) of plant photosystems (PSII and PSI), the capture of light by the LHC results in this light energy exciting an electron within the chlorophyll molecules of the photosystems. This excited electron has three fates; photochemistry, non-photochemical quenching, and fluorescence.

To recap from the earlier discussions of *Section 1.1.1* and *Section 1.1.2.2,* in photochemistry, excited chlorophyll is quenched by the reaction centre of PSII, through the transfer of excitation energy from the chlorophyll of the LHC antenna to the P_{680} chlorophyll in the reaction centre of PSII. Once the excitation energy is transferred to the reaction centre, an electron, derived from the splitting of water in the oxygen evolving complex, is transferred to the electron acceptor Q_A via the initial electron accepter pheophytin (Rochaix, 2011). The electron transport continues from Q_A across the thylakoid membrane, ultimately generating NADP and ATP in the process.

While Q_A is reduced, it is unable to accept any further electrons from P_{680}, so the reaction centre is considered "closed" (Murchie & Lawson, 2013). When the reaction centre is "closed", excitation

energy from P_{680} is unable to transfer to Q_A, and excitation energy from absorbed light in the LHCII antenna is unable to transfer to P_{680}. When there is excess absorbed light, more than can be used in photochemistry, absorbed light will increasingly be dissipated as heat through a mechanism called non-photochemical quenching (NPQ) (Baker, 2008). During both linear and cyclic electron transport, there is accumulation of protons (protonation) and subsequent acidification of the thylakoid lumen. This change in pH leads to conformation change of the PSII antenna, protonation of the PsbS protein, and the de-epoxidation of the pigment violaxanthin to zeaxanthin in what is known as the xanthophyll cycle (Jahns et al., 2009; Latowski et al., 2011). Xanthophylls such as zeaxanthin prevents oxidative damage by quenching chlorophyll triplets, which have a chance to form when chlorophyll decays to a lower energy state as a result of not being quenched by the reaction centre (Peterman et al., 1995; Ruban et al., 2012).

Lastly, there is a rate of decay of excited chlorophyll back down to its ground state. This results in the emission of energy, of a longer wavelength than the light causing initial excitation. For chlorophyll there are two fluorescent peaks at 690nm and 740nm (Meroni et al., 2009), and thus fluorescence can be measured using these wavelengths. The processes of photochemistry, NPQ and fluorescence are in competition – a decrease in one process will increase the other two.

1.2.2 Chlorophyll Fluorescence Measurements - PAM

Pulse Amplitude Modulated (PAM) fluorescence allows researchers to manipulate and probe inside the light harvesting complexes (LHC) of leaves, to reveal information about photosynthetic activity. The method works by applying a low intensity measuring beam, which induces fluorescence at a known frequency. The detector measures fluorescence yield at the same frequency as the measuring beam, thus recording fluorescence caused by the measuring beam (Bradbury & Baker, 1981; Schreiber et al., 1986), allowing for measurements under ambient light (Maxwell & Johnson, 2000). Fluorescence as a result of excitation by the measuring beam is termed F_o, and represents the minimum levels of fluorescence emitted when Q_A is fully oxidised ('open').

Saturation with a high intensity light pulse induces maximum fluorescence (F_m), the level of fluorescence when Q_A is fully reduced ('closed'). The difference between minimal (F_o) and maximum fluorescence is known as variable fluorescence (F_v). Measurements of these variables in dark adapted or light adapted leaves allows for a range of values to be derived (Maxwell & Johnson, 2000) which measurements can reveal information regarding photochemical and non-photochemical quenching.

There are numerous in depth reviews on the topic of chlorophyll fluorescence, that explain both the theoretical (Baker, 2008; Misra et al., 2012; Murchie & Lawson, 2013) and practical (Maxwell & Johnson, 2000; Ritchie, 2006; Roháček et al., 2008) aspects of the technique, including as a tool for stress detection (Sayed, 2003).

The maximum quantum efficiency of PSII (F_v/F_m; variable fluorescence divided by maximum fluorescence) is measured on a dark adapted leaf. A dark adapted leaf is used as this is when Q_A is fully oxidised and can accept an electron from P_{680}, and thus indicates the maximum efficiency in which Q_A is reduced by light absorbed by PSII. A dark adapted leaf also has minimal NPQ, which would otherwise compete with photochemistry, enabling for the theoretical maximum quantum efficiency of PSII to be measured.

Any impacts of stress which damage or cause photoinhibition of PSII, will decrease the value for this measurement. This measurement is routinely used in plant physiology (Maxwell & Johnson, 2000). Measurements of F_v/F_m can sometimes be used to measure the effects of nitrogen stress (Jin et al., 2015; Živčák et al., 2014), and has been used to phenotype plants for water use efficiency (McAusland et al., 2013).

Another key measurement of chlorophyll fluorescence includes the operating efficiency of PSII (F_q'/F_m'). This is a measurement taken in the light, which measures the fraction of absorbed light that is actually used in PSII photochemistry, and thus is also in competition with NPQ as a sink for absorbed light energy. Increases in PPFD correspond to a decrease in F_q'/F_m', as an increased

proportion of light is dissipated through NPQ or decays to the ground state, which has the effect of decreasing the efficiency of absorbed light which is utilised in photochemical quenching (Baker, 2008).

The maximum quantum efficiency in the light (F_v'/F_m'), is a measure of the maximum proportion of absorbed light that can be used in photosynthesis in the light when Q_A is maximally oxidised (Baker, 2008). Any decrease in $F_v/F_{m'}$ indicates an increase in NPQ, and thus this measurement can be used as an indicator of the contribution of NPQ to changes in the operating efficiency of PSII (F_q'/F_m') (Baker, 2008; Murchie & Lawson, 2013)

1.2.3 Chlorophyll Fluorescence Measurements - SIF

Chlorophyll fluorescence has seen developments as a tool for use in remote sensing applications. While typical chlorophyll fluorescence measurements are conducted using actively induced PAM techniques, which yields the parameters as described in *Section 1.2.2* and listed by Baker (2008), passive steady state fluorescence can also be detected under solar illumination, and thus fluorescence can be detected within the solar spectrum reflected from leaves (Meroni et al., 2009), known as solar-induced fluorescence. Fluorescent emission from chlorophyll has two peaks, at 690nm and 750nm. However, the emission is very weak when compared to irradiated light and subsequent reflection, causing a very weak increase in the recorded reflectance of leaves near the two peak wavelengths. However, the solar spectrum has narrow bands of reduced irradiance, known as Fraunhofer lines (Meroni et al., 2009; Zarco-Tejada et al., 2012). These lines are caused by absorbance of light by the most abundant elements. In the case of passive fluorescence, the absorbance of light by hydrogen in the solar atmosphere, and telluric oxygen from earth's atmosphere, correspond with the same wavelengths as chlorophyll fluorescence emissions. Thus, the reflected spectrum from a plant leaves will also contain narrow bands of reduced radiance – however, fluorescent emissions of chlorophyll will increase the radiance of these narrow bands. Other methods for remote fluorescence measurements include LiFT (Laser-Induced Fluorescence

Transient) (Kolber et al., 2005; Pieruschka et al., 2012). Unlike the short, but high intensity saturating light of PAM fluorescence, LiFT is based on fast repetition rate fluorescence (Kolber et al., 1998), in which short excitations of various intensity and duration are used to derive values of photochemical and non-photochemical quenching.

As chlorophyll fluorescence is an *in vivo* probe of photosynthesis, allowing for non-invasive measurements, it offers significant utility as a tool in assessing plant health, considering that photosynthesis is the primary component of plant health.

1.3 Thermography

1.3.1 Overview

Stomatal conductance to water vapour (g_s) is a key physiological measurement, measuring the rate of water loss through the stomata over a specific area per second, measured as mol m^{-2} s^{-1}. Stomatal conductance is a component of transpiration, the flow of water from the roots to evaporation by the leaves and stem. Stomatal conductance is a major limiting factor in the rate of photosynthesis, through reducing or increasing the intake of carbon dioxide while balancing water lost through the stomata through evapotranspiration.

Environmental conditions such as water availability affect the rate of stomatal opening through the release of Abscisic Acid (ABA) in the roots and shoots. Abscisic Acid is transported to guard cells where it induces stomatal closure through the activation of guard cell efflux ion channels, leading to water efflux and stomatal closure (Cotelle & Leonhardt, 2019). Alongside water availability, ABA is also produced to regulate stomatal response to other stressors such as light, humidity, temperature and CO_2 concentration (Assmann & Shimazaki, 1999; Radin, 1984; Tuteja, 2007).

Stomata are sensitive to fluctuations in vapour pressure deficit (VPD). Vapour pressure deficit is the difference between how much moisture is currently in the air, and how much moisture the air can hold at full saturation. The amount of moisture in the air is temperature dependant, with warmer air able to hold greater amounts of moisture than cooler air. When air is saturated, moisture will condense out. VPD is important for plants as saturated air (a low VPD) will reduce the rate of evaporation, and thus transpiration. However, a VPD that is too large will rapidly increase evaporation and transpiration. Synthesis of ABA in the guard cells has been shown as a mechanism to balance water loss during low atmospheric relative humidity, alongside a passive hydraulic to a decrease in leaf turgor (Bauer et al., 2013; Lange et al., 1971; Merilo et al., 2018)

Even after stomatal closure, foliar ABA concentration can increase, maintaining a reduced stomatal conductance even when water status recovers (Tombesi et al., 2015) as a mechanism to protect against fluctuating water availability. This highlights the strong relationship between stomatal conductance and water status, and the importance of optimum irrigation scheduling to prevent large fluctuations in water availability which can impact stomatal conductance and affect yield.

Thermal radiation is the emission of electromagnetic radiation from matter due to temperature. The wavelengths emitted are dependent on temperature, however wavelengths within the long-wavelength infrared range (LWIR) can be used to measure temperature, as all matter above absolute zero emits infrared radiation proportional to its intrinsic temperature (Shahsafi et al., 2019).

One of the main factors that can affect the temperature of a plant is the rate of transpiration, the rate of total water loss over a given time period, measured as mol m^{-2} s^{-1}. Water has a large specific heat capacity, meaning that water requires a large input of heat energy to produce a change in temperature (Cooper, 2005). When there is a transfer of heat energy from an object with a low specific heat capacity to water, the temperature of water will increase less than the temperature of the object will decrease.

Therefore, within a leaf a lot of thermal energy is transferred from the cells of the leaf to water. High transpiration rates lead to higher volumes of water leaving the leaf via the stomata, thus the thermal energy transferred to the water is effectively transported out of the leaf, cooling it (Fuchs, 1990; Goudriaan, 1977). Changes in stomatal opening alter the rate of transpiration, which leads to a similar change in evaporative cooling of the leaf. Thus, changes in temperature can be used to estimate stomatal conductance, and measurement of leaf temperature by infrared thermography can be used for non-invasive, rapid measurements of leaf temperature.

1.3.2 Thermography based indices

Initial work on relating leaf temperatures to plant water status involved stress indices, such as CWSI (Crop Water Stress Index) (Idso et al., 1981; Jackson et al., 1981); and the WDI (Water Deficit Index), which expanded upon the CWSI by including spectral reflectance measurements to differentiate between vegetation and soils (Moran et al., 1994)

The Crop Water Stress Index (CWSI) is expressed as such;

$$CWSI = (T_{PLANT} - T_{WET}) / (T_{DRY} - T_{WET})$$

With T_{PLANT} being the temperature of the sample, and T_{WET} and T_{DRY} as a wet reference and a dry reference. The Crop Water Stress Index (Idso et al., 1981; Jackson et al., 1981), uses the relationship between T_c (Canopy Temperature) minus T_a (Air Temperature) and VPD to quantify water stress, originally designed to assist with the scheduling of irrigation. However, such an index is empirical, designed to indicate the water status of a plant, and not directly related to stomatal conductance.

The Index of Stomatal Conductance (I_g) (Jones, 1999, 2002), is proportional to stomatal conductance.

$$I_g = (T_{DRY} - T_{PLANT}) / (T_{PLANT} - T_{WET})$$

With T_{PLANT} being the temperature of the sample, and T_{WET} and T_{DRY} as a wet reference and a dry reference. The wet references represent a leaf with zero resistance to water vapour. The dry

reference represents a leaf with infinite resistance to water vapour. The use of reference leaves

provides a range of temperatures as a result of varying stomatal conductance.

Stomatal conductance and temperature are linked via leaf energy balance. The leaf energy balance is

an equation linking environmental conditions with the properties of the leaf. Variables in the

equation include the leaf boundary layer resistance to water vapour, air density, heat capacity of the

air, air vapour deficit, and is described in numerous literature (Guilioni et al., 2008; Jackson et al.,

1981; Jones, 1999; Jones & Schofield, 2008; Leinonen et al., 2006; Moran et al., 1994). The use of

wet and dry references eliminates the need for environmental measurements, as the references,

with similar absorptive properties to a leaf (Jones et al., 2009), allows for the reference to act as

both the high and low expected values of temperature that a leaf will exhibit, and thus the high and

low values of stomatal conductance (Leinonen et al., 2006).

An accurate measurement of g_s can be made with knowledge of the leaf boundary layer (Guilioni et

al., 2008; Leinonen et al., 2006), however the Ig can be taken further, to measure the leaf

conductance to water vapour (g_{lw}). The g_{lw} can be used as an approximation for stomatal

conductance, although it also includes other conductances such as water loss through the cuticle

(Jones, 1999). g_{lw} is calculated as such;

$$g_{lw} = I_g \times G$$

in which;

$$G = g_{REF}(T_{REF} - T_{WET}) / (T_{DRY} - T_{REF})$$

g_{REF} is reference with a known conductance to water vapour, and T_{REF} is the temperature of the

reference. g_{REF} is calculated by recording the temperature over a range of stomatal conductances, in

the same environmental conditions as the intended sample. However, this is also a major drawback

of calculating actual conductance values.

The Index of Stomatal Conductance, I_g, has been used successfully in phenotyping drought tolerant and drought sensitive varieties (Zaman-Allah et al., 2011). The index has been proven in greenhouse conditions (Grant et al., 2006) to distinguish between irrigated and non-irrigated plants across a variety of species, with differences in g_s and Ig between watered and water deficit plants appearing at approximately the same time. I_g showed correlations to stomatal conductance in field conditions, and was able to distinguish between different irrigation treatments (Grant et al, 2007), however a modification to the method used non-irrigated and fully irrigated canopies as wet and dry references.

Maes et al. (2016) developed a new wet reference, made from green cotton over a steel wire frame. This new references was able act as a wick for water, staying wet as long as a pool of water was available, decreasing variability inherent in spraying wet references. From this, a stable wet reference could be obtained, and could be utilised in a model (Maes & Steppe, 2012; Maes et al., 2016), improving the relationship between Ig and conductance, while enabling for continuous remote measurement without requiring an operator. As I_g, and thermal imaging in general, is strongly linked with plant water status, these indices would be good potential targets for combining with other known spectral indices.

Thermal imaging remains a key technique in the remote measurement of stomatal conductance, a key physiological measurement. As well as an indicator for water status, of which thermal imaging and stomatal conductance remains the best indicator for, there are other aspects of plant health which relate to conductance. Plants produce salicylic acid in response to pests and other infections (Malamy et al., 1990), which elicits stomatal closure, and thus a reduction in stomatal conductance, as a response to prevent further infection through open stomata. Increases in plant temperature can be associated with infection (Chaerle et al., 1999) However, there are also plant pathogens which release a virulence factor to open stomata, increasing the rate of infection (Melotto et al., 2008).

Using thermography for phenotyping and screening cultivars and plants with greater water use efficiency is another key use for thermal imagery. While stomatal conductance may decrease in plants with improved water use efficiency, it is also important to also measure the rate of photosynthetic carbon assimilation to ensure decreased conductance does also limit assimilation (Lawson, 2009). As a result, thermography can be combined with chlorophyll fluorescence, which allows for calculations of carbon assimilation, enabling both conductance and assimilation to be measured simultaneously (Chaerle et al., 2007; McAusland et al., 2013). This underlines the necessity of a combined technique approach, as plant physiology and health, and the effect a change in one aspect of physiology has on other aspects, can only be fully understood when multiple measurements are collected.

1.4 Aims and Objectives

There is a wide array of tools and methodologies that can be employed to remotely assess plant performance. The difficulty that can arise when using only one spectral index or technique to accurately identify and assess causes of stress and sub-optimal plant performance suggests that a combined approach could yield a more powerful assessment. Previous work which has begun to combine spectral techniques has demonstrated this potential, allowing for both a greater insight and availability of measurements that were not previously possible to measure non-invasively or remotely.

The overall aim of this project is to identify and develop new techniques and spectral indices that can track plant performance. One of the most common spectral indices, NDVI, is routinely used in agriculture for monitoring crop performance. However, to date, there is no low cost imaging system that can be used for collecting NDVI imagery. This project aims to develop a low cost NDVI imaging system will allow for a greater uptake of NDVI imagery in agriculture and research, especially for those in developing countries or budget conscious. Such a system will allow for more farmers to have the ability to detect regions of their field that require inputs such as fertilizer and irrigation, as

opposed to costly blanket applications of these inputs. This decreases the associated costs of water, fertilizer, machinery and labour, increasing profits and also reducing the negative effects of fertilizer on the local environment (Balafoutis et al., 2017; Mulholland et al., 2008; Prasad, 1998).

Water status is a key factor affecting plant performance, especially through stomatal closure in response to low water content and subsequent decreases in carbon assimilation. Spectral indices exist for detecting leaf water content, however the equipment that measures reflectance above 900nm and in the SWIR wavelengths with sufficient sensitivity can be expensive. There are very few indices below the wavelength of 900nm that measure water status. An index that uses NIR and visible wavelengths however, can be measured by more common spectrometers that are already widely available. This project therefore aims to develop a spectral index using visible and NIR wavelengths that can measure leaf water status, exploiting the variation in internal refraction of NIR light within the leaf due to variation

Finally, this project aims to combine spectral reflectance indices, chlorophyll fluorescence and thermography into a 'spectral toolbox', and assess the ability of this spectral toolbox to assess crop water and nitrogen status. Combinations of techniques have been previously used, such as in the detection of water status, however the spectral toolbox here will be used to assess both water status and nitrogen status separately, and in combination. As far as is known, this is the first time a spectral toolbox will be developed for this purpose. This will form the foundation of a 'stress catalogue', which can be built upon by future work.

Chapter 2 - Development of a low cost NDVI imaging system using the Raspberry Pi

2.1 Introduction

To meet the demands of an increasing population and maintain food security, production of new crop varieties with increased yield and performance through crop breeding programmes and genetic modification is key. However, the rate at which new varieties can be screened is outpaced by the rate at which new varieties can be produced (Furbank & Tester, 2011). Spectral imaging, a technique using multiple bands across the electromagnetic spectrum has assisted in overcoming this bottleneck by providing a rapid, non-contact assessment of plant performance. However, issues such as the necessary expertise and technology to correctly collect and process images has limited its use outside of the agritech and academic world (Furbank & Tester, 2011; Minervini et al., 2015; Rahaman et al., 2015).

The Normalised Difference Vegetation Index (NDVI) is a measure of chlorophyll absorption in the red wavelengths (Rouse & Space, 1978) and is one of the most routinely used spectral indices, both in research and agriculture thanks to its ability to quickly assess overall plant health (Xue & Su, 2017). The NDVI is the ratio between near infra-red (NIR) and red (VIS) light, which are differentially absorbed by the chloroplast. An NDVI above zero has more NIR than VIS, and thus there is greater absorption of visible red light by chlorophyll, indicating a healthy plant. An NDVI below zero conversely has more VIS than NIR, due to less absorption of visible red light. Plants exhibit greater reflection of red light due to a decrease in chlorophyll content and a resulting reduction in the absorption of visible light, which is instead either reflected or transmitted through the plant.

The availability of NDVI imaging systems has increased alongside the increasing popularity of unmanned aerial vehicles (UAVs), and while easy to use and readily available, commercial systems can be expensive with prices typically from US$2000 to US$5000 per device. Many agricultural and

commercial applications involve the deployment of agricultural machinery or UAVs, all loaded with these costly but highly accurate narrowband multi-sensor cameras. For many growers, an alternative exists in satellite imagery, which is freely available and provides a better option for crop imaging, and is routinely used to measure NDVI for agriculture and environmental monitoring. However, satellite NDVI imagery has a low resolution, with the best available imagery representing a 10 metre area per pixel (Drusch et al., 2012), rendering it effective only for measuring overall growth or health on a large scale. More affordable imaging devices are available, for instance some systems priced at US$380 can capture NDVI imagery using NIR and blue wavelengths, however these come with drawbacks as blue wavelengths are less sensitive to chlorophyll content than red wavelengths (Sims & Gamon, 2002).

Consequently, there is a large market for low cost NDVI imaging systems that are capable of measuring with accuracy and precision. As a result, there are numerous methodologies for producing NDVI imaging systems, aimed at providing a low cost solution for research, environmental monitoring, and agriculture. One common approach is the use of two separate cameras, using almost the same methodology as higher-quality commercial imaging systems. In this dual camera approach, the first camera, a standard RGB camera with its infra-red (IR) blocking filter removed and replaced with a narrow band NIR filter, effectively replaces one of the colour channels (i.e. Red, Blue, or Green) into a NIR channel (Kaizu & Imou, 2008; Ritchie et al., 2008; Sakamoto et al., 2012; Shibayama et al., 2015), while the second camera is just a standard RGB camera used for measuring visible red light. The construction of many of these systems can require time and skill to setup, along with the cost of the digital cameras and optical filters themselves. However, these systems show good linear relationships to spectrometry and satellite NDVI measurements (Sakamoto et al., 2012).

Other designs include systems that have been designed to implement custom dual band pass optical filters, which allow narrow regions in desired red and NIR wavelengths to pass onto the sensor of a single camera (Dworak et al., 2013). This enables accurate measurements of both red and NIR

spectral regions by a single camera, and therefore allows for both sets of images to be accurately collected by a single device. This approach is used by many commercial systems, such as UAV based cameras built by Sentera (Minneapolis, MN, USA) and AgroCam (Debrecen, Hungary). More experimental methods include one creative approach of using a web cam based security camera to derive visible and NIR imagery, all from a single camera, through the use of the NIR night vision feature of such cameras (Anika et al. 2018). There are many more instances of NDVI systems designed for environmental monitoring, tracking relative changes in NDVI and greenness throughout the seasons (Anderson et al., 2016; Richardson et al., 2007; Ryu et al., 2014), although none of these options are generally accessible outside of academia as an easy to use and low-cost option for NDVI imagery.

Despite the various methods used in NDVI measurements, an important step true for all imaging systems is the requirement to calibrate images. Calibration standardises all collected images so that the same NDVI value is measured regardless of lighting conditions (e.g. light intensity and spectral quality). Primarily, calibration allows the conversion of pixel values (also referred to as *digital numbers*) as measured by a digital camera, into relative spectral reflectance (%). In most applications, reference samples of a known spectral reflectance are placed within the field of view of the camera, and from this the relationship between pixels values and spectral reflectance can be empirically calculated. This can be performed at a minimum using a reference with high reflection, and a reference with low reflectance (Baugh & Groeneveld, 2008). Known as the empirical line method (Smith & Milton, 1999), this technique is routinely used in commercial field imaging such as that using UAVs.

There is to date, no complete system using low cost devices that can produce calibrated NDVI images, or a system that lends itself to customisation and integration with other platforms and systems. All current systems require generally expensive optical filters (Dworak et al., 2013), or a lack a comprehensive method of calibration

The overall aim of this work is to develop a complete low cost, easy to assemble and use, imaging based technique for accurate and reliable imaging of NDVI by combining a method for calibrating captured images with low cost, off-the-shelf imaging made accessible with the Raspberry Pi platform. The objectives for this work are to i) Construct an imaging system that allows for capture of visible red and near-infra red (NIR) imagery, using the Raspberry Pi, ii) Calibrate red and NIR imagery to known spectral reflectance, iii) Assess the performance of a Raspberry Pi based NDVI imaging system against other NDVI capable devices. The Raspberry Pi based NDVI imaging system is intended to rival other systems through the lower cost of materials, ease of use in part due to the ease of use of the Raspberry Pi platform and the method of image calibration, and overall 'openness' of the system to allow users to customise to their requirements.

2.2 Materials and Methods

2.2.1 Camera Setup

The Raspberry Pi is a small single board computer, initially designed as an education tool, but has since found popularity from hobbyists to researchers across disciplines. The Raspberry Pi is a compact fully operational computer, similar to most laptops and desktop computers, yet priced affordably due its requirement as an educational tool. A major benefit is the 'stripped down' nature of the Raspberry Pi, consisting of the bare computer board, and thus is highly customisable both physically and in terms of software, with uses of the Raspberry Pi ranging from weather stations, to integration into industrial machinery. The Raspberry Pi has been used in plant imaging, such as for measuring leaf area (Boulord et al., 2000), and plant shape, height and other physical traits (Tovar et al., 2018), which can be used for phenotyping for high biomass crops.

To construct the *NDVIpi* system, the Raspberry Pi Compute Module was used in conjunction with the Raspberry Pi I/O Board (Raspberry Pi Foundation, Caldecote, UK). The I/O board has two individual camera ports (Fig. 2.1), which enables the attachment of two cameras to the Raspberry Pi via the Raspberry Pi CMDK Camera Adapter (Raspberry Pi Foundation, Caldecote, UK). Two cameras were

connected to the Raspberry Pi. The first was a standard RGB camera designed for the Raspberry Pi, known as the PiCamera (Raspberry Pi Foundation, Caldecote, UK). The other is a NoIR PiCamera (Raspberry Pi Foundation, Caldecote, UK), which was lacking an Infra-Red (IR) blocking filter on the lens (Fig. 2.1). Both cameras used an Omnivision OV5647 CCD sensor (Omnivision, California, USA). Images were captured in an unencoded RGB format. A blue filter made of PET plastic, of the type named "Alice Blue" (Alice Blue 197, Lee Filters, Hampshire, UK) was placed over the lens of the NoIR camera. The filter has a low transmittance of red wavelengths (Appendix 1, Fig. A1), while allowing infra-red light to pass. Both cameras measure light onto one of three channels; Red, Blue and Green (RGB). Due to the transmission spectrum of the Alice Blue filter, the red channel of the NoIR camera will actually allow a minimal amount of red light through the filter, but will have very high amounts of near infra-red (NIR) - the wavelengths above 700nm - due to the lack of the IR blocking filter. This replaces the red channel of the NoIR camera with NIR, and so the measured intensity on the red channel corresponds to the intensity of NIR light. An assessment of the effect of this filter on measured NIR light is described in Appendix 1.

A camera holder was constructed to allow side-by-side stereo placement of the cameras (Fig. 2.1), which assists in improving the accuracy of image alignment. Camera settings used for both cameras are listed in Table 2.1. The filterless RGB PiCamera, used in the collection of visible red images, was prone to saturation and thus the shutter speed is lower. It was essential that shutter speed and ISO were correctly configured to suit the light environment, as this ensures all images utilised the full range of the camera. Images which are saturated are unable to be accurately calibrated across the full range of 0% to 100% reflectance.

The Bayer filter response on most RGB cameras typically measure a red spectrum on their red channel from 580nm up to 700nm, with peak sensitivity typically at around 600nm (Deglint et al., 2016; Lebourgeois et al., 2007; Pagnutti et al., 2017). However, the PiCamera which is used here has not been officially characterised.

2.2.2 Normalised Difference Vegetation Index Measurements

The Normalised Difference Vegetation Index (NDVI) is calculated as;

$$NDVI = \frac{(NIR - RED)}{(NIR + RED)} \qquad 1.1$$

In which NIR is near infra-red reflectance, and VIS is reflected visible light in the red spectrum. The output of NDVI ranges from -1, in which there is more visible light than NIR, to +1, in which there is more NIR than visible light.

Based on the general broad spectrum of the red channel, the wavelengths selected for visible red reflectance was 620nm, while the NIR wavelengths were selected at 750nm. Thus, NDVI for the *NDVIpi* system can be calculated as;

$$NDVI_{RaspPi} = \frac{(R750 - R620)}{(R750 - R620)} \qquad 1.2$$

With *R* denoting reflectance at a specific wavelength (i.e. 750nm or 620nm). Despite the prevalence of NDVI as a measurement, there is no universally agreed-on standard for NDVI wavelengths. Key regions and wavelengths have been previously identified for optimal relationships to key characteristics (Thenkabail et al., 2002), but it is common to see literature regularly citing different wavelengths (Magney et al., 2016; Suárez et al., 2008). This often depends on the technical ability of equipment, for example the number of specific bands available on satellite imaging platforms or imaging cameras and their bandwidth (Bannari et al., 1995; Clevers & Gitelson, 2013).
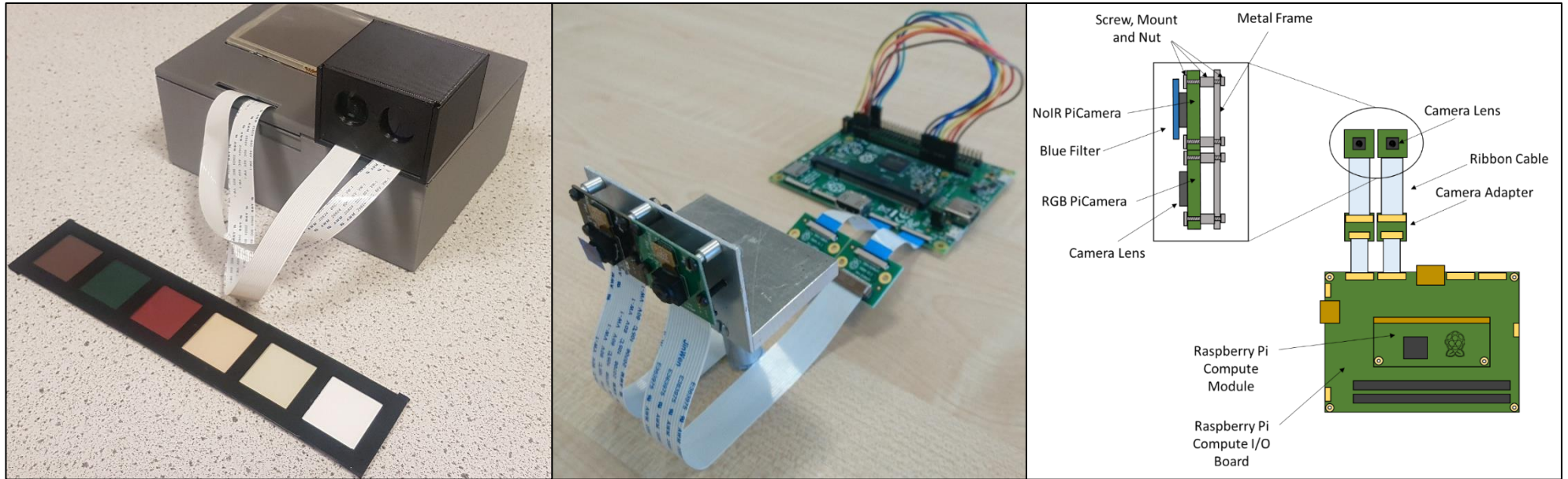
Figure 2.1 An image and schematic of the core setup for the Raspberry Pi Compute, PiCamera and NoIR PiCamera, and the metal camera holder. The camera holder keeps the two cameras at the same plane, allowing for good alignment of captured images.

Table 2.1 Camera settings for the two cameras used for the Raspberry Pi Imaging system.

Camera Setting	NoIR PiCamera	PiCamera (RGB)
ISO	400	400
Shutter Speed (µs)	2500	400

Figure 2.2 Raspberry Pi Calibration board, consisting of six diffuse reference materials with known relative reflectances (Fig. 2.3; Table 2.2), which are used to calibrate the digital number of images captured by the Raspberry Pi to actual measurements of relative reflectance.

Table 2.2 Measured relative reflectance of the six reference materials of the Raspberry Pi calibration board, of Red (620nm – 680nm) and NIR (720nm - 750nm) light, derived from *Appendix 1 Fig. A3*

# (Colour)	Red Reflectance (%)	NIR Reflectance (%)
1 (White)	91.13	88.15
2 (Sand)	62.36	61.05
3 (Brown)	16.07	16.10
4 (Indian Birch)	65.12	62.97
5 (Forest Green)	4.91	5.50
6 (Burgundy)	29.35	38.78

As an example of a commercial NDVI imaging system, a Micasense RedEdge camera (Micasense, Seattle, WA, USA) was setup to collect pictures alongside the *NDVIpi* system. The Micasense RedEdge ('Micasense') receives light for a narrow band of red and NIR, and the wavelengths used differ to those used by the *NDVIpi*. The Micasense is composed of five narrowband cameras, and an automatic gain/exposure feature to prevent saturation. The red camera, at a wavelength of 668nm had a full width at half maximum (FWHM) of 10nm. The "Red Edge" camera had a wavelength of 717nm with a FWHM of 10nm. The NIR camera was a wavelength of 840nm and a FWHM of 40nm. NDVI was calculated using the two NIR bands, with R denoting reflectance centred at a specific wavelength;

$$NDVI_{Micasense1} = \frac{(R717 - R668)}{(R717 - R668)} \qquad\qquad 1.3$$

$$NDVI_{Micasense2} = \frac{(R840 - R668)}{(R840 - R668)} \qquad\qquad 1.4$$

2.2.3 Image Processing

All *NDVIpi* code, image manipulation and image calibration was performed using the Python language (Python Software Foundation), OpenCV library (opencv.org) and NumPy (numpy.org). Image alignment and general image analysis was performed with the Fiji software (Schindelin et al., 2012). Image alignment, which aligns two image to overlap, was performed using the SIFT algorithm (Lowe, 2004) plugin for Fiji, which identifies similar features in the images and transforms one image to match the features of the other. Alignment worked by loading both NIR and visible red images into Fiji. The algorithm was run, which matched features present in both pictures and transformed the NIR image to fit over the visible image

2.2.4 Calibration of *NDVIpi* and Micasense RedEdge images

2.2.4.1 NDVIpi Calibration

Calibration of the *NDVIpi* was performed using a calibration board, consisting of six Kayospruce Odyssey (Kayospruce, Hampshire, UK) materials fixed to a flat hard backing (Fig. 2.2). The material chosen is tough, UV resistant, spectrally consistent with relatively good diffuse properties. A total of sixteen colours were initially available for selection. Reflectance was measured for all sixteen colours, identifying colours which demonstrated relative uniformity across the red and near infra-red spectrum, with six samples chosen from the original sixteen available colours (see Appendix 1, Fig. A3). The reflectance of the six samples all vary from each other (Table 2.2) to allow for a wide range of reflectances. These six samples were used to construct the calibration board, in which all six samples were placed together.

Images were calibrated using the empirical line method (Smith & Milton, 1999). The empirical line method is the use of two or more materials of known reflectance, to calibrate images from relative values of digital numbers as measured by a camera, into values of reflectance. Six references were used to ensure a good linear relationship. The six references were fixed onto a board, forming a calibration board, which was placed in every image taken with the *NDVIpi*.

To calibrate images into reflectance, captured images were transferred to a PC for processing. The first step was to convert images from digital numbers into reflectance (Fig. 2.3). For every image, the average digital number (ranging from 0 – 255) of the pixels for each of the six calibration materials was measured. This was performed for both the red channel from the RGB camera, and the red channel from the NoIR camera. The initial relationship between the measured digital number of each calibration material, and the known reflectance of each material as listed in Table 2.2, was calculated (Fig. 2.4A).

The resulting relationship was then be used to calibrate the entire image into values of reflectance.

After obtaining spectral reflectance values, the next step is to convert reflectance data back into an image, however the data is now normalized to the full range of digital numbers. In this example, for an 8 bit image this range would be from 0 to 255 (Fig. 2.4B), however 16 bit images were actually used to preserve the resolution of reflectance values (see below). As seen in Fig. 2.4C, the effect of calibration and utilization is the full range of the image is now in use, with the intensity of each pixel corresponding directly to a reflectance value. Thus, white pixels signify 100% reflectance, while black pixels represent zero reflectance. This is a crucial step, as the digital numbers of every pixel within every image are now a direct proxy for spectral reflectance.

A thresholding equation was applied to modify any out of bound values, setting values that have values below the 0% reflectance value to zero, and all values above the 100% reflectance back down to 100%. This step produces a clean image with minimal noise from background areas that have different lighting to the area of interest. Calibrated images were then saved as 16 bit PNG files, hence 0% reflectance was represented by a digital number of 0, and 100% reflectance represented by a digital number of 65536. Once saved as 16bit images, the calibrated images were loaded into the Fiji software for alignment with the SIFT algorithm.

The final step (Fig. 2.3) is to use the calibrated images, which are now a direct proxy for reflectance, to calculate NDVI. A python script utilising the OpenCV library was used to perform the NDVI calculation pixel by pixel. The output of the NDVI calculation was saved as a greyscale image, in which a digital number of 0 represent an NDVI of -1, and 255 represents an NDVI of +1.

NDVI values were extracted from the images using the Fiji software to select regions of interest from each image and obtain the mean digital number. To rescale a digital number (0 - 255) from these images back into NDVI (-1 to +1), the digital number can be converted back to NDVI via this equation, in which *Pixel* is the average digital number of each region of interest:

$$NDVI = \left(Pixel \times \left(\frac{2}{255} \right) \right) - 1 \qquad\qquad 1.5$$

2.2.4.2 Micasense RedEdge Calibration

The Micasense RedEdge was calibrated using the exact same process as the *NDVIpi*. The relationship between measured digital number and spectral reflectance of the calibration board was linear.
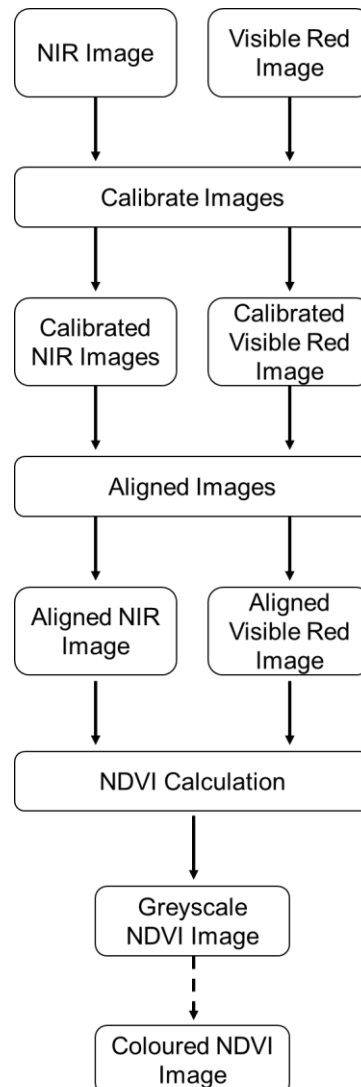
Figure 2.3 The process of calibration, showing each step from captured images to the generation of the output NDVI image. Dashed arrows show an optional step.

Figure 2.4 Example data showing calibration and normalization. **A)** Calibration of raw digital number, direct from images captured by a camera, using the known reflectances of the six calibration materials to find the relationship between digital number and reflectance. Once the relationship is established for an image, raw digital number for the en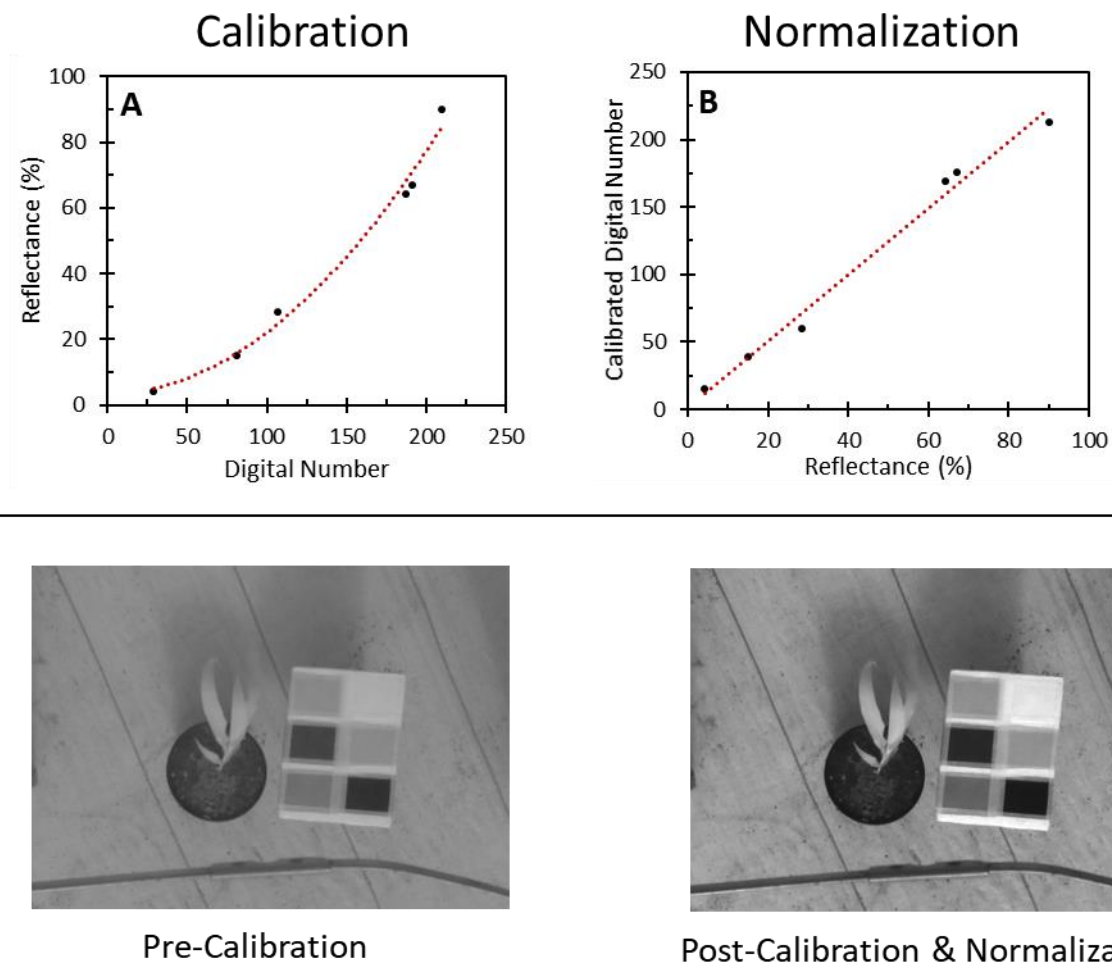tire image can be converted into values of reflectance **B)** Normalization of reflectance data, by re-scaling the converted reflectance values (from 0%-100%) to use the full 8 bit (0-255) range. The 8 bit range was used here for illustration purposes to match the 8 bit range of the raw images, however actual normalization used 16 bit (0-65535) to prevent loss of data when re-scaling reflectance to digital number **C)** A typical NIR image, demonstrating the visual difference between images before and after the calibration and normalization process, with the image on the right now using the full range of the image, with image colour (from white to black) corresponding to actual values of reflectance.

2.2.5 Plants and Growth Conditions

Dwarf French Bean *(P. vulgaris)* were grown in a growth cabinet under 200 µmol m^{-2}s^{-1} of light for 8 hours a day, at a temperature of approximately 21°C. Plants of Wheat (*T. aestivum*) and Barley (*H. vulgare*) were grown in pots with compost (Levingtons F2S, Ipswich, UK), in a greenhouse under ambient lighting during the months of February and March 2018, with a lighting system providing a minimum of 200 µmol m^{-2} s^{-1} supplementary lighting in case of cloudy or dim lighting conditions. French Bean were grown in pearlite growing medium (Pearlite Standard, Sinclair Pro, Cheshire, UK), with half of the plants supplemented with Hoaglands solution (Hoagland & Arnon, 1950).

2.2.6 Reflectance Measurements

Spectral reflectance measurements were collected with a FLAME-S Spectrometer (Ocean Optics, USA), and a Reflection Probe fibre optic (Ocean Optics, USA). This fibre optic provided illumination, and collected reflected light. A tungsten bulb provided illumination, with around 198 µmol m^{-2} s^{-1} of light reaching the sample through the fibre optics. The bulb was powered by a separate regulated power supply. A fan was fitted at the rear of the bulb to regulate generated heat. A leaf clip was constructed to enable a fixed geometry between the probe end of the fibre optic and the plane of the sample, which was sprayed with matt black paint to reduce reflection within the leaf clip. A Spectralon reflectance standard (WS-1, Ocean Optics, USA), which has 99% diffuse reflection across the 400nm to 1500nm wavelength range, was used as a reference for 100% reflection.

2.2.7 NDVI measurements under defined irradiance

Plants of French Bean, Wheat and Barley were measured under known irradiance of 800 µmol m^{-2} s^{-1} of light. For each measurement, a leaf of each plant was laid across a flat surface, approximately 60cm below an LED light source (Heliospectra AB, Göteborg, Sweden).

The calibration board was present in all images, on the same plane as each measured leaf. Directly after each image capture, spectral reflectance measurements were also taken from four quadrants

of each leaf of French Bean, or measured along the length of the leaf blade for wheat and barley. The two *NDVIpi* cameras were located above the leaves, next to the light source facing directly down towards the leaf samples.

To verify the calibration methodology, the NDVI values as measured by the *NDVIpi* camera were compared against values measured with the spectrometer, with the choice of wavelength used in the NDVI calculation by the spectrometer varied in order to identify which wavelengths best correspond to the NDVI values derived from *NDVIpi* images.

Using the NDVI values from the *NDVIpi* as a standard, NDVI was calculated from spectrometry data using a NIR wavelength of 750nm, while the choice of red wavelength was varied from 600nm up to 700nm. The same was repeated with a fixed visible red wavelength of 620nm, using NIR wavelengths from 700nm up to 800nm. The % difference between the *NDVIpi* NDVI values and the values calculated with each wavelength was recorded.

Using six references may be suitable in a laboratory or in low throughput phenotyping; however for taking multiple images in the field, such as with a UAV based setup for crop imaging, the use of six references can be unpractical. Therefore, NDVI images of wheat and barley were also calculated using only two references; the highest reflecting material (*White*), and the lowest reflecting material (*Forest Green*).

2.2.8 Comparison of NDVI from the *NDVIpi* and Micasense RedEdge, measuring plants under ambient lighting in a greenhouse environment

The performance of the *NDVIpi* Imaging system was compared to the Micasense RedEdge, a widely used commercial system. Measurements in a greenhouse were collected on French Bean. Plants were transferred to the greenhouse one hour before measurement began. Plants were setup near to the window of the greenhouse and arranged into a grid. Measurements were collected under ambient lighting conditions in the greenhouse, ranging from 200 μmol m^{-2} s^{-1} up to 900 μmol m^{-2} s^{-1} of light. The Raspberry Pi system and a Micasense RedEdge camera (Micasense, Seattle, WA, USA)

were elevated above the plants at a distance of 1 metre. Images were taken by the Micasense RedEdge approximately 30 seconds after Raspberry Pi images, to ensure the images by the two systems were taken within the same time period. The calibration targets were present in all images collected by both camera systems. Images from the Micasense RedEdge were calibrated using the same method as the *NDVIpi*. Both cameras were mounted on a retort stand, which was extended to allow heights of 1 metre.

2.3 Results

2.3.1 The effect of the blue filter on measured light intensity

It was seen on a simulation of the filter (Fig. 2.5; Appendix 1), that there is a red 'leak' through the Alice Blue filter allowing approximately 5% - 15% transmission of visible red light onto the NIR camera. This has an effect on NDVI measurements, primarily due to the affect of increased reflection of visible red light from stressed leaves. Therefore, increases in visible red light will also be measured by the NIR camera as an apparent increase in NIR light, due to transmission of red light through the filter. As a result, the difference between theoretical NIR images with no red transmission and NIR with the red transmission of the Alice Blue filter widens (Fig. 2.5A). Therefore, one unintended effect of the filter is an overestimation in NDVI at low values (Fig. 2.5B). It was calculated that there is a 0.92955% increase in NIR as measured by the camera as a direct result of red light transmission onto the red channel (Fig. 2.5A), and this value was used to factor out the presence of red light which is transmitted through the filter.

2.3.2 NDVI Measurements under defined irradiance

Images produced by the system (Fig. 2.6) demonstrate good results at both close and far distances. Images close to the leaves (Fig. 2.6D) maintain a good level of detail. A colour scheme for NDVI that is similar to the colours of a leaf, produces an image (Fig. 2.6D) that is visually comparable to the original RGB image, although a very small amount of mis-alignment can also be seen at the very

edge of the leaves. Imaging of NDVI with the *NDVIpi* system shows a good relationship in comparison to spectrometry derived measurements (Fig. 2.7), for all three plant species. However, higher NDVI values appeared to be underestimated (Fig. 2.7A).

The large bulk of French Bean data may be predominantly responsible for underestimating high (>0.6) NDVI values due to a cluster of high NDVI values that are lower than the rest of the data. Omission of French Bean (Fig. 2.7B) shows an improved relationship (R^2 = 0.95). Analysis of image histogram data, using 40 selected images of French Bean and wheat data, showed a greater skew towards a lower NDVI in NDVI images for the broad leaf French Bean (Skewness = 1.16, S.D. = 0.49) than the leaves of grasses (Skewness = 0.67, S.D. = 0.47).

Analysis of the wavelengths used to calculated NDVI from spectrometry data (Fig. 2.8) shows that the wavelengths which produces NDVI values closest to those obtained by the *NDVIpi* imagery is 620nm (Fig. 2.8A), the same red wavelength that the system was calibrated to. NIR wavelengths perform similarly from 740nm up to 800nm (Fig. 2.8B), verifying that the calibration process has correctly calibrated images to red wavelengths of 620nm and NIR wavelengths of 750nm.

Using two references produces NDVI measurements that are less precise, yielding a weaker relationship (R^2 = 0.96, Fig. 2.9A) to spectrometry data than six references (R^2 = 0.98, Fig. 2.9B). The range of values derived from using two references also showed a slightly higher overall NDVI values for all measurements, although this increase is systematic.

2.3.3 Comparison of NDVI from the *NDVIpi* and a commercial NDVI system, measuring greenhouse grown plants under ambient lighting

Comparison of the Raspberry Pi system against the MicaSense shows clear difference in NDVI values between the two systems (Fig. 2.10; Fig. 2.11), which can be attributed to the use of different wavelengths by the two systems in the NDVI calculation. Thus, the output of the two systems is not

directly comparable, although in general measured NDVI for vegetation saturates at values from 0.8 to 0.9 (Gu et al., 2013).

A comparison of the NDVI used by the two systems, by comparing the NDVI as measured by the spectrometer using the same wavelengths as each of the camera systems (Fig. 2.12), reveals a saturation of NDVI$_{Micasense}$ for much of the measured plants, while NDVI$_{RaspPi}$ has overall lower NDVI values that have not saturated. Calculating the co-efficient of variation (CV) shows a CV of 10.58 for *NDVIpi*, and 6.82 for Micasense. Therefore, the Micasense produces less variable measurements than Raspberry Pi measurements, however the *NDVIpi* system allows for the detection of smaller differences in NDVI and thus the 'greenness' of plants.
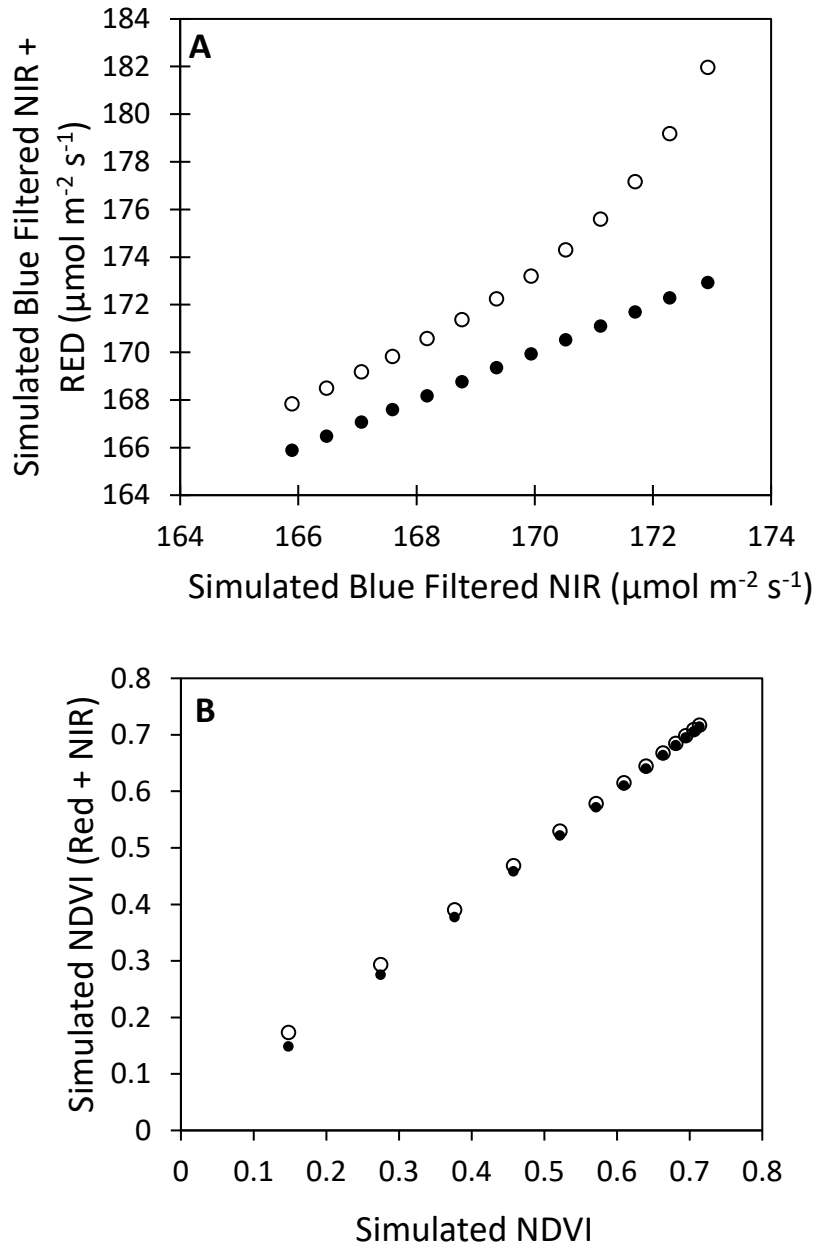
Figure 2.5 (A) Simulated light levels detected by a camera lens from an 800 μmol m^{-2} s^{-1} light source, reflected from modelled leaf reflectance for leaves with varying chlorophyll content, and measured after transmission through the Alice Blue filter. The measured NIR light, with added red light representing the 5%-15% transmission of red light through the Alice Blue filter, is compared to PPFD measured with a simulated camera lens that only receives NIR light, without the extra transmission of red light. ● represents the PPFD of measured NIR, if red light leaking onto the red channel was zero (1:1 relationship for NIR). ○ represents the PPFD of both NIR and additional red light, as transmitted through the filter. The distance between the two measurements is the amount of visible red light that is transmitted through the filter and is therefore measured as additional NIR light by the camera, which was calculated as 0.92955%

(B) Simulated NDVI calculated from same dataset, showing the NDVI for a camera with no red light transmission by the Alice Bue filter, and NDVI with some red light transmission. The increase in red light on the NIR channel is seen here by the overestimation of NDVI at low values.
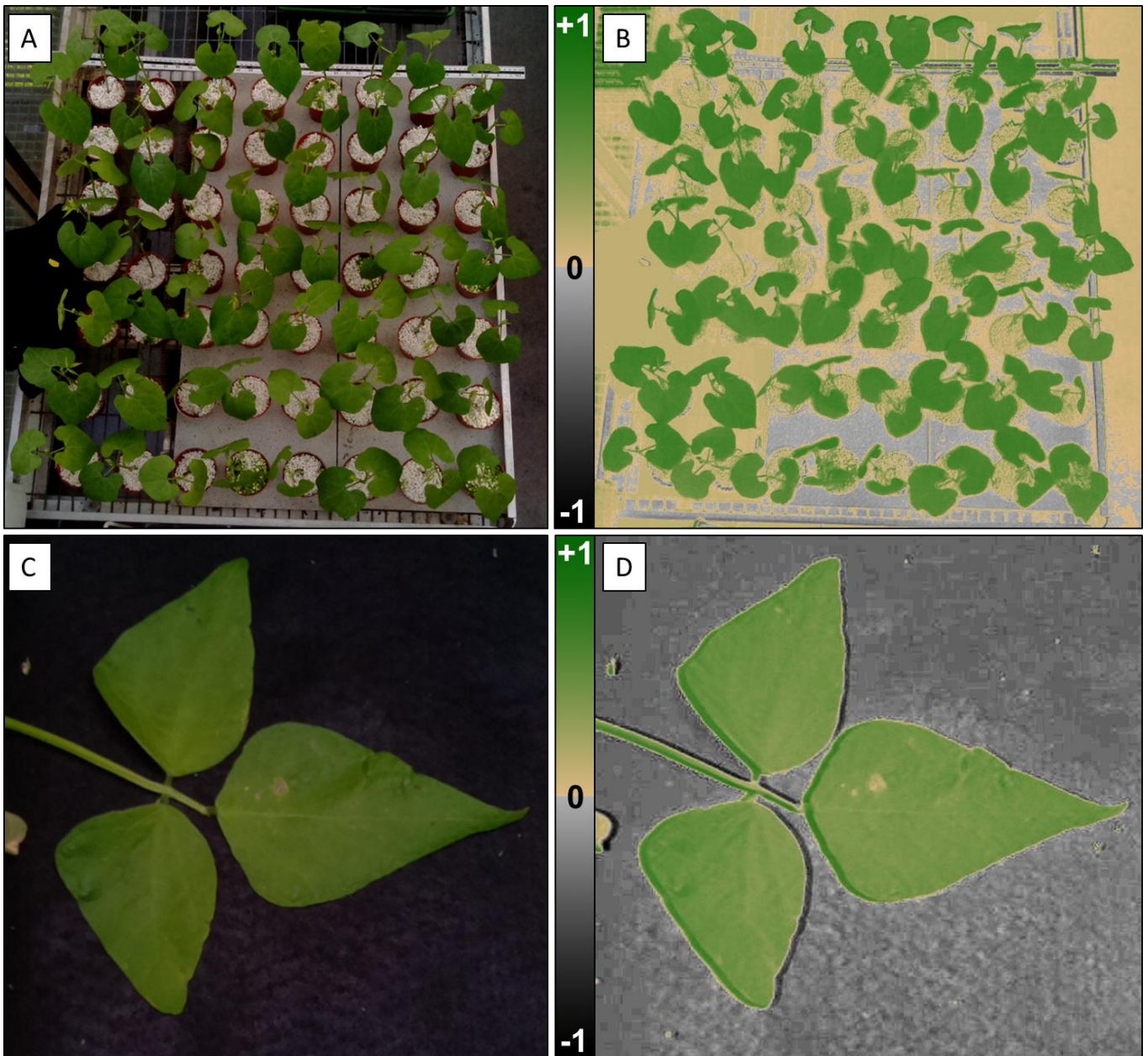
Figure 2.6 A) RGB image of French Bean plants inside of a greenhouse **B)** Resulting coloured NDVI image of these plants. **C)** RGB image of French Bean leaves taken under a controlled light source **D)** Resulting NDVI image. The colour scheme chosen produced an image that visually corresponds to the RGB image
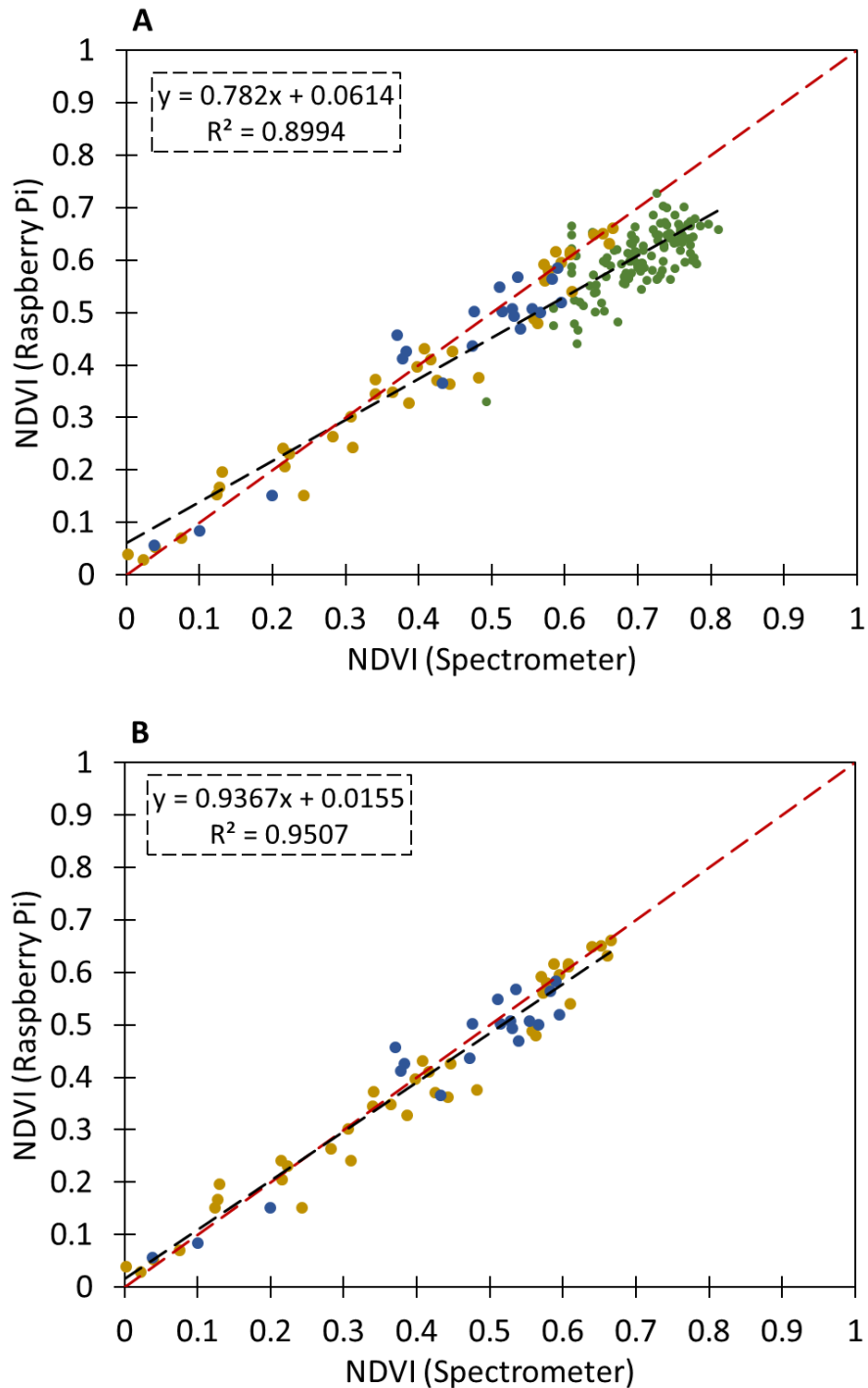
Figure 2.7 Comparison of NDVI imaging with the Raspberry Pi, and NDVI as measured with a spectrometer. Red dashed line represents a 1:1 relationship with NDVI calculated from the spectrometer. Wheat (●), Barley (●), and French Bean (●) **(A)** NDVI imaging compared to spectrometry NDVI (n=181) **(B)** Dataset with French Bean measurements omitted. In all instances, the Raspberry Pi images demonstrate a good relationship ($R^2 > 0.89$) with spectrometry derived NDVI, highlighting the robustness of the system.
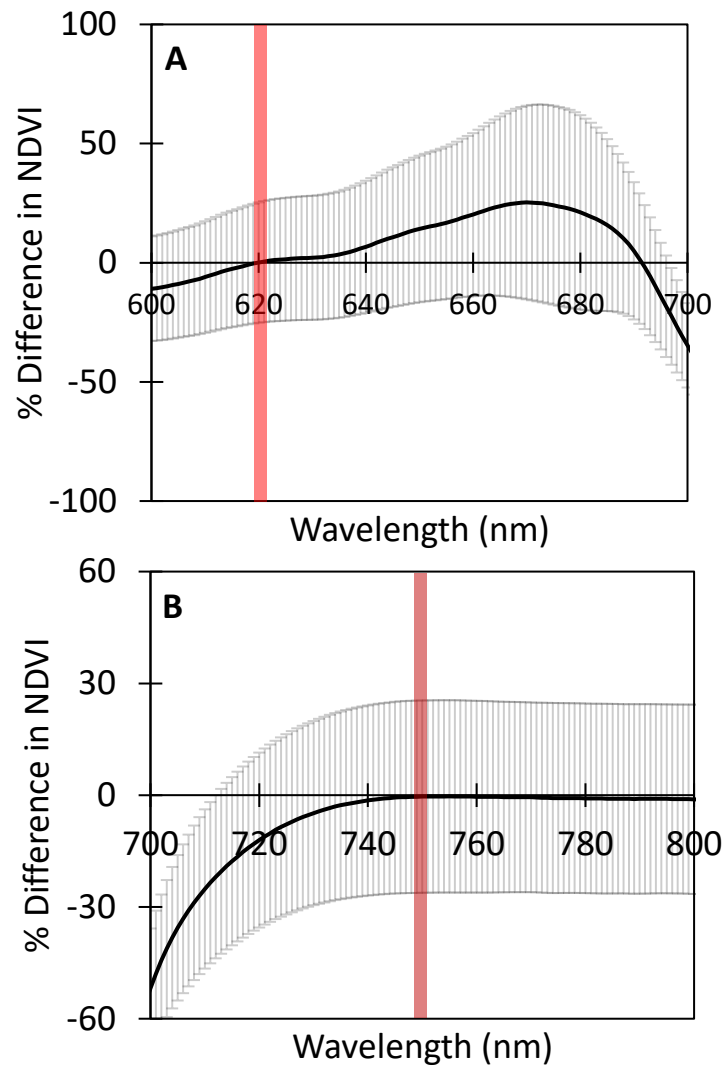
Figure 2.8 Analysis to identify the wavelengths, from spectrometry-derived NDVI calculations, that most closely correspond to the NDVI values as obtained from Raspberry Pi imagery. Measuring the percentage (%) difference between the NDVI from the Raspberry Pi camera, and spectrometry derived NDVI at each wavelength. **(A)** NDVI with the wavelength for visible red ranging from 600nm up to 700nm, with NIR wavelength fixed at 750nm **(B)** NDVI wavelength for NIR ranging from 700nm up to 800nm, with visible red fixed at 620nm. From this data, the wavelengths which produced an NDVI value that best matched the values as measured by the Raspberry Pi system, correspond to the wavelengths that the Raspberry Pi images were calibrated to; 620nm for red and 750nm for NIR, indicated by the red bars. Error ± standard deviation
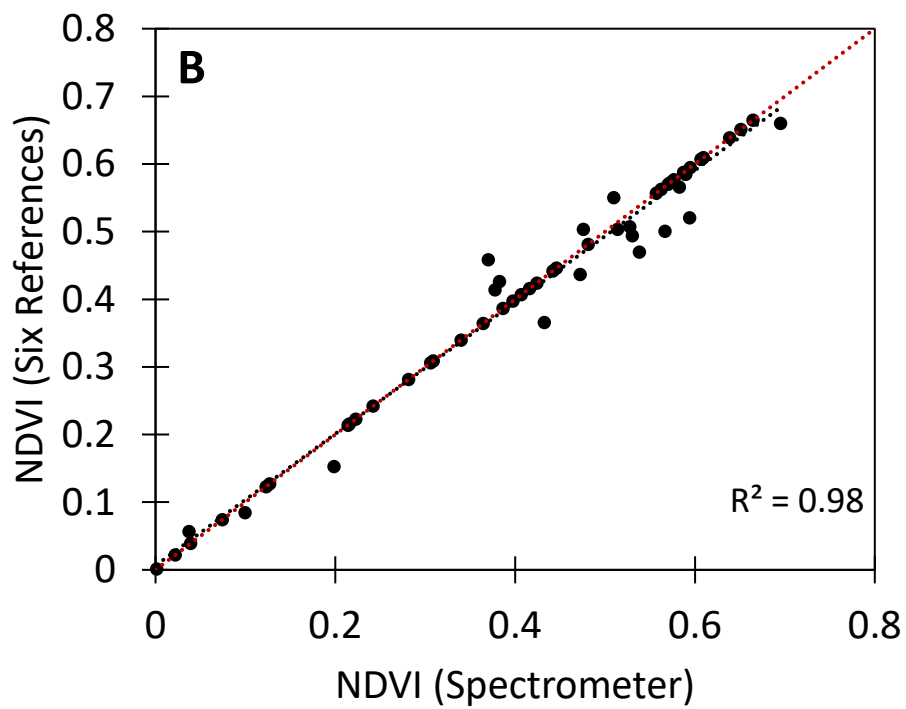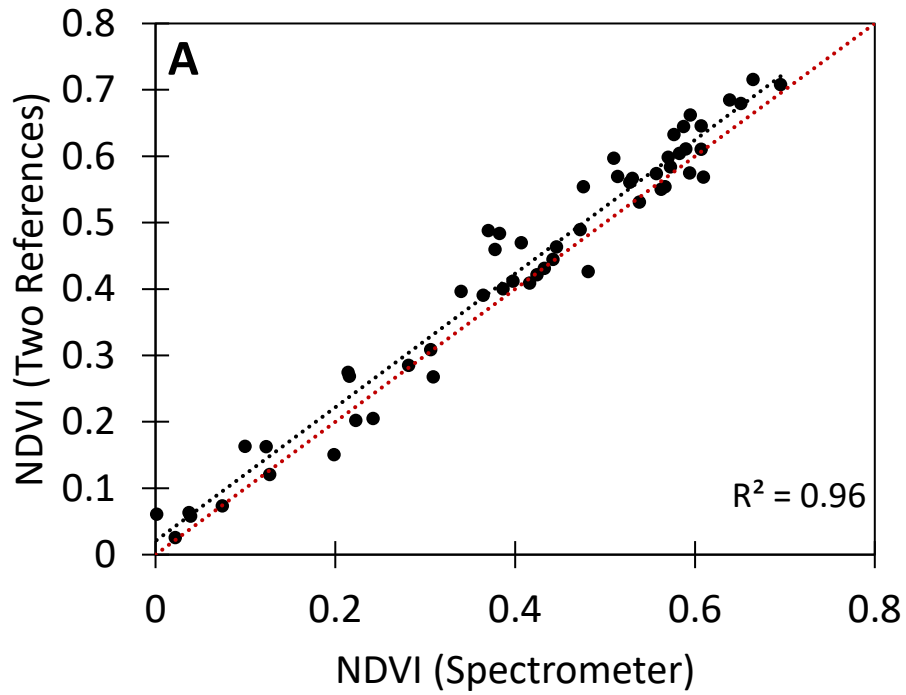
Figure 2.9 Comparison of images calibrated with either **(A)** Two or **(B)** Six references, against NDVI calculated using spectrometry data for wheat and barley.
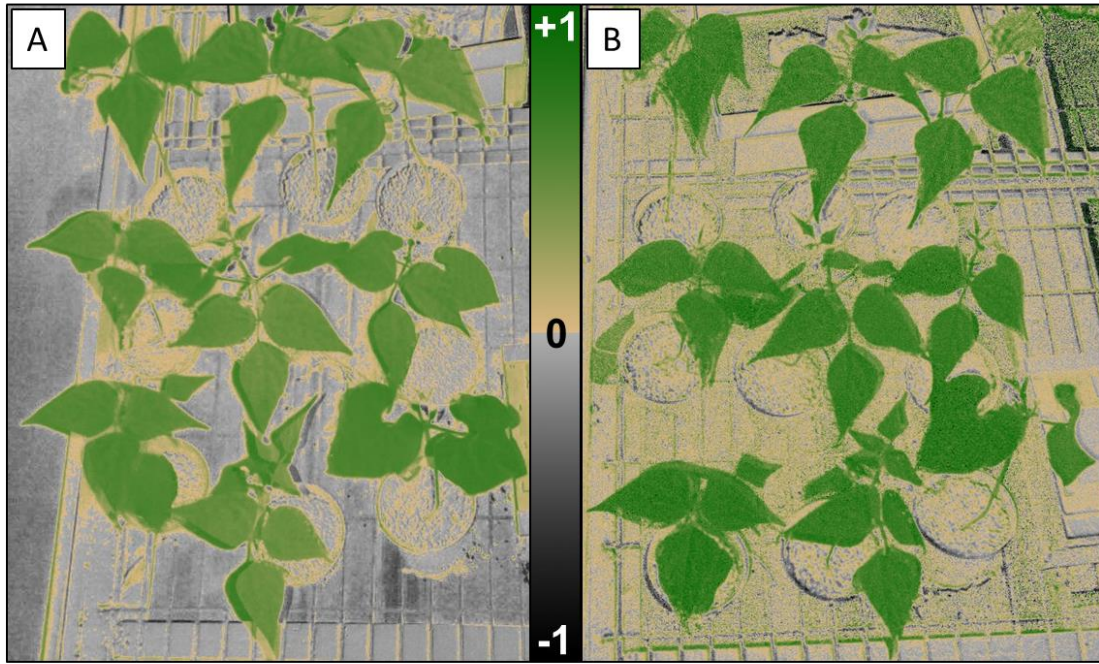
Figure 2.10 NDVI images of French Bean, taken in a greenhouse under ambient lighting. **A)** NDVI image from the NDVIpi system **B)** NDVI images from the Micasense RedEdge
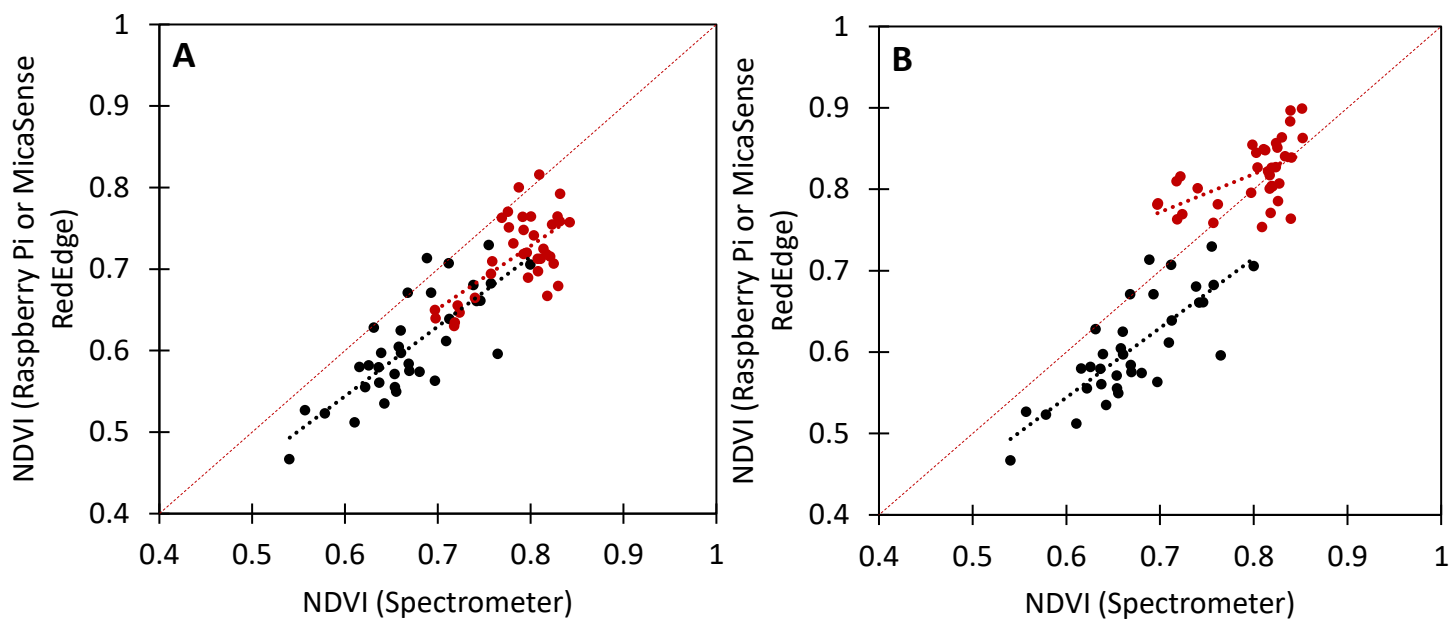
Figure 2.11 Greenhouse measurements of *French Bean* . Measurements were collected under ambient lighting conditions with nine plants per image. ● NDVI measured with the Raspberry Pi, compared to spectrometry NDVI calculated with wavelengths at 620nm for red and 750nm for NIR (R^2 = 0.62, y= 0.86x + 0.03) **(A)** ● NDVI measured by the Micasense RedEdge, compared to spectrometry NDVI calculated with wavelengths at 668nm for red and 717nm for NIR (R^2 = 0.41, y= 0.77x + 0.11). **(B)** ● NDVI measured by the Micasense RedEdge, compared to spectrometry NDVI calculated with wavelengths at 668nm for red and 840nm for NIR (R^2 = 0.30, y= 0.47x + 0.44).
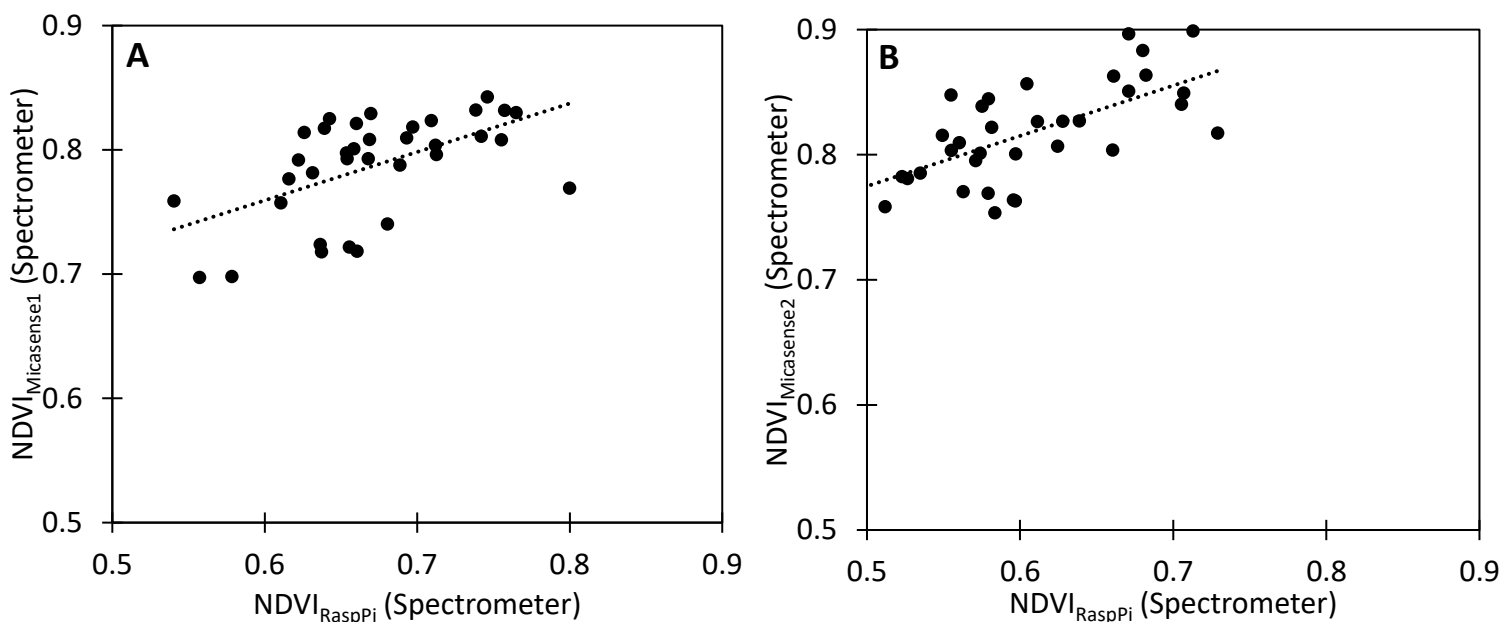
Figure 2.12 Relationship between NDVI$_{RaspPi}$ and NDVI$_{Micasense}$, as measured by spectrometry. **A)** NDVI$_{RaspPi}$ shows a larger range of values before saturation, whereas NDVI$_{Micasense}$ quickly saturates at 0.8. Thus, NDVI$_{RaspPi}$ demonstrates a higher sensitivity to chlorophyll content, and does not saturate easily at high chlorophyll contents. The R^2 is 0.30, therefore the relationship between the two is poor. Overall, the Raspberry Pi system shows promise as a robust NDVI imaging system, with higher sensitivity to plant health than common commercial NDVI imaging systems. **B)** NDVI$_{Micasense2}$ shows the same effect, however saturation has occurred for all measurements

2.4 Discussion

The *NDVIpi* imaging system has demonstrated comparable performance for the measurement of NDVI against standard spectrometry measurements. The use of the empirical line method with fabric based reflectance standards is successfully able to yield accurately calibrated NDVI images with off-the-shelf Raspberry Pi components, and an optical filter made from PET plastic. Thus, an accurate NDVI system can successfully be built from low cost, off-the-shelf components accessible to most consumers, effectively making it one of the few "out of the box" NDVI imaging platforms.

However, with all the benefits of the low cost system described here, there are some considerations that all users should be aware of. Firstly, it should be noted that the use of two references is less precise than using six (Fig. 2.9), although the loss of precision is small and differences in NDVI can still be detected accurately with a decrease in reliability. Should greater precision be required, such as for detecting smaller differences between plants or treatments, the full six references can be used. However, two references can be ideal for many situations in which greater precision is not required such as rapid phenotyping in both field and greenhouse environments, and imaging of field crops to assess health.

Secondly, using plastic optical filters does allow for NIR light to be measured on a IR-filter removed camera, although it is worth considering the need to account for the leakage of red light onto the NIR channel due to low amounts of transmission that may occur through these filters, depending on the transmission profile of the filter used. As demonstrated (Fig. 2.5), any leakage of light will result in an overestimated value for NDVI, especially at lower NDVI values, as it is predominantly the change in visible red wavelengths which alters for stressed plants. Any camera using a modified RGB camera in conjunction with a plastic optical filter for measuring NIR will have to account for this effect on all NIR imagery.

Thirdly, the methodology presented here did present some difficulties with image alignment. Alignment was better for images in which leaves were on a flat plane relative to the camera. Any variation in height resulted in poor performance of the alignment algorithm, due to the resulting parallax from using two off-set cameras which individually may see areas of the plant that are not visible to the other camera. For plants with a tall canopy, such as grasses, alignment can be expected to perform poorly. Remediation of this issue can be found by increasing the distance between plants and cameras, as this will reduce the parallax effect of using two cameras. Canopy-level UAV imagery, for instance, can be expected to produce better alignment than laboratory leaf-level imagery, due to a smaller parallax resulting from a longer distance to the camera. Commercial software is available which may perform better alignment, however there is a limit to the amount of improvements that can be found by software. Ultimately this is an issue that should be considered prior to imaging to ensure the best possible quality of image alignment, and is not unique to the *NDVIpi* imaging system.

Finally, an offset was seen for the relationship between spectrometer and the *NDVIpi* (Fig. 2.7A). Analysis of histogram data shows that French Bean NDVI imagery was underestimating NDVI. This variation may be due to the method of sampling with the spectrometer, which used a leaf clip to collect measurements from each quadrant of every leaf measured. The *NDVIpi* on the other hand, measured the entire leaf area present in the image. Therefore, structural areas such as veins, which have a lower NDVI value, will be under-represented in the spectrometry data collected here.

2.4.1 Greenhouse NDVI Imagery

Both *NDVIpi* and Micasense RedEdge demonstrated NDVI values lower than measurements collected by the spectrometer (Fig. 2.11). As previously mentioned, the use of a broad leaf plant species such as French Bean produced NDVI values that were lower than those collected by the spectrometer due to the use of a leaf clip, which only measured a small area of each leaf, and this was seen here with both camera devices as the *NDVIpi* data in Fig. 11 is also similar to that of Fig. 2.7A.

65

There is a clear difference in NDVI values between the two systems, as data collected with the Micasense RedEdge is higher (0.70 – 0.90) than the *NDVIpi* (0.54 - 0.80) (Fig. 2.11A, 2.12A). This can be attributed to the choice of wavelengths by the two systems. The wavelength of 665nm used by the Micasense is close to a spectral region near 680nm which corresponds to the peak red absorption spectrum for chlorophyll (Sims & Gamon, 2002), whereas the wavelength at 620nm as used by the *NDVIpi* is not. Red wavelengths further from this region (i.e. >600nm & <680nm), such as the 620nm wavelength used by the *NDVIpi,* are subject to greater changes in reflection as chlorophyll does not absorb light at those wavelengths as strongly as chlorophyll absorbs light near the 680nm region. This suggests $NDVI_{RaspPi}$ is able to measure changes in chlorophyll content for plants with higher chlorophyll content, whereas $NDVI_{Micaesense1}$ will show similar values for all plants above a certain chlorophyll content (Fig. 2.10) due to the saturation of absorbed red light. The same response is seen for $NDVI_{Micasense2}$ (Fig. 2.11B), with most NDVI values above 0.8. Therefore, the *NDVIpi* appears to be detecting changes in overall plant 'greenness' and possible chlorophyll content, that the Micasense system has lower sensitivity to. This was supported visually during data collection, as many of the leaves were showing visible differences in the level of greenness.

However, the co-efficient of variation (CV) values of 10.58 for *NDVIpi* and 6.82 for Micasense, demonstrates a better performance by the Micasense RedEdge in terms of reliability. This is a result of the narrowband filters employed by the Micasense system, whereas the broadband channels used by the *NDVIpi* are susceptible to changes in reflected light from other wavelengths, within both the red or NIR spectrum. The apparent relatively lower sensitivity to chlorophyll content of the NDVI from the Micasense RedEdge may be more desirable for most agricultural applications. For instance, NDVI images may be collected to measure crop cover, which is used to assess the performance of the crop in terms of growth and calculate yield. A system with a greater ability to differentiate between vegetation and non-vegetation would be desired over a system that has higher sensitivity

to chlorophyll, but overall lower NDVI values, which may result in misidentification and miscalculation.

Additionally, the Micasense RedEdge can be used to measure Normalised Difference Red Edge (NDRE), which uses wavelengths on the red edge (i.e. between 700nm and 720nm) and NIR. This index is associated with better performance than NDVI for measuring chlorophyll content in crops (Clevers & Gitelson, 2013; Eitel et al., 2010), as the red edge is not strongly absorbed by chlorophyll. While better performance can be gained with any red wavelength that is outside the main peak region of the absorption spectrum of chlorophyll (Sims & Gamon, 2002), the red edge will always perform better than other red wavelengths due to this region being at the very edge of chlorophyll absorption spectra. Further, the narrowband optical filter employed by the Micasense RedEdge will always provide accurate and reliable measurements of both NDVI and NDRE. Thus, NDRE measurements by the Micasense system will yield more accurate estimates of chlorophyll content than can be measured by the *NDVIpi* system, even if the *NDVIpi* were to be used to measure NDRE.

Overall, the *NDVIpi* system produces comparable NDVI measurements to 'gold-standard' spectrometry measurements and NDVI imagery with a popular commercial camera, the Micasense RedEdge. The *NDVIpi* also shows a potentially higher sensitivity to chlorophyll content than NDVI from the Micasense RedEdge, due to the choice of red wavelength, but at a cost of higher variation. The Micasense RedEdge is more beneficial for situations in which the price of the system is not a concern, higher accuracy is desired, and a system that offers flexibility between an index more sensitive to chlorophyll content (NDRE) or an index that is preferred for general crop greenness and crop cover is preferred (NDVI),

2.4.2 Comparison with other NDVI imaging systems

Using the *NDVIpi* imaging system has many advantages, such as ease of use and lower price point. In total, the system can be procured for approximately US$400-US$500. The *Micasense RedEdge* for instance, retails at approximately US$4500 - US$5000, but does have extra features such as

integrated GPS and built-in wireless control. Other systems include the customisable and module Tetracam *Macaw 6*, retailing at US$14,000 with the ability to swap optical filters, or the smaller *Tau2* for US$8000 per camera which measures green, red and NIR imagery, and down-welling irradiance for reflectance calibration which negates the need to use calibration targets inside of collected imagery. Other companies such as *Max Max*, modify commercial cameras specifically for NDVI imagery, with optical filters being added. The price range for these system can range from US$1600 up to US$6000. Imaging system for NDVI can also be built using consumer level camera equipment, through the removal of the IR filter (Ritchie et al., 2008) and in its place a new filter that blocks all light below NIR wavelengths (e.g. 710nm) can be installed.

In comparison to some of the systems described, the use of a Raspberry Pi enables the use of affordable, mass-produced, low-cost cameras to be used for accurate NDVI imagery. One of these cameras, which lacks an IR filter (The "NoIR PiCamera"), is one of the few mass produced and off-the-shelf NIR cameras available. The sibling of the NoIR camera, the standard RGB camera (The "PiCamera"), allows the NoIR camera to be paired with an almost identical camera. The Raspberry Pi itself is by design, easy to use and customisable, and can be integrated easily into any new or pre-existing applications – e.g. mounted in greenhouses, or on farm vehicles and UAVs to capture imagery of entire fields. The combination of this system with a method for accurate calibration of images, allows for imagery without necessarily requiring a detailed analysis of camera sensor design and operation, providing a suitable ISO and shutter speed is used, improving the system's ease of use.

For research applications this also allows the system to be integrated with other imaging based systems. For instance, thermography, another imaging based technique, is used to measure evapotranspiration and stomatal conductance of plants (Grant et al., 2016; Grant et al., 2006; Guilioni et al., 2008; Leinonen et al., 2006; Maes et al., 2016), and thus also used to indicate water status (Jones et al., 2009; Möller et al., 2007).

However, thermography enabled devices are rapidly decreasing in both size and price, and therefore would be a logical next step in integrating with NDVI imagery. NDVI imaging is regularly used agriculturally as an indicator of chlorophyll and nitrogen content to optimise fertilizer applications. A combined NDVI and thermal imaging system could give an overview of the two primary factors of crop performance, water status and nitrogen content, at an affordable price compared to many multispectral or multi-technique devices, while being more accessible.

2.5 Conclusion

A methodology for the measurement of NDVI, using two Raspberry Pi cameras, can be used to produce accurate NDVI imagery. This system utilizes low cost, off-the-shelf components for the Raspberry Pi system, and easy to obtain and use plastic optical filters, with a calibration method to convert collected images into images of spectral reflectance. There are two steps which are essentials for this system. The first is the calibration of red and near-infra red imagery with calibration targets of a known spectral reflectance. The second is the characterisation of the filter used to isolate near-infra red wavelengths, to accommodate for transmission of other wavelengths on the camera channel, which may result in an overestimation of NIR, and thus NDVI.

The *NDVIpi* imaging system is a robust tool for the measurement of NDVI, comparable to other commercial systems but for a fraction of the cost. The system also demonstrates good sensitivity to chlorophyll content, and thus the *NDVIpi* system can be used to reliably and accurately measure plant health.

Chapter 3 - Development of a novel spectral index to assess plant water status

3.1 Introduction

Water status is one of the primary aspects of plant health. Droughted crops perform poorly and produce significantly less biomass (Chaves et al., 2002; Tezara et al., 1999). Therefore, detection of water status and the onset of water stress is a key target of plant imaging and remote sensing (Grant et al., 2016; Jackson et al., 1981; Moller et al., 2006; Suárez et al., 2008). Water status is one of the primary factors that limits photosynthesis and depresses yield, thus it is essential that an affordable and easy method to rapidly assess water status of crops is made available for use in agriculture.

However, there are very few spectral indices that can be used for water status in the visible and near-infrared below 900nm range (Govender et al., 2009). This is an important consideration as equipment that measures reflectance above 900nm with sufficient sensitivity can be expensive, whereas there is an increasing amount of devices, from ever-smaller spectrometers to multi-spectral cameras, which can accurately measure reflectance of wavelengths below 900nm.

We theorise that a spectral index that may be able to track changes in internal structure, such as that due to variation in leaf turgidity, may be able to serve as an indicator of leaf water status. As leaf turgor relates directly to the water content of a plant, it may serve as a more useful indicator of water status than current indices such as the Water Index (Peñuelas et al., 1993). However, leaf turgor can be difficult to measure directly, especially dynamically. On the other hand, leaf thickness has been identified as a good indicator of water status, although the relationship has been described as discrete rather than continuous (Afzal et al., 2017; Seelig et al., 2015).

Changes in mesophyll structure, predominantly through the air-cell interface between mesophyll cells and mesophyll air spaces, are responsibly for internal refraction and scattering of near-infrared (NIR) light, and thus the high reflectance of NIR. Changes in water content, which affects both the

turgor of mesophyll cells and structure of air spaces, should result in detectable variation in reflected NIR due to alteration of the air-cell interface. Comparing variation in reflected NIR to wavelengths which are unaffected by changes in internal structure, in theory would allow for a measurement of leaf water status.

The wavelength 550nm for instance, is able to penetrate through the epidermal and palisade cells of a leaf with less absorbance by plant pigments, when compared to red and blue wavelengths which are strongly absorbed in the epidermis and palisade cells (Vogelmann et al., 1989). Therefore, a ratio of NIR to 550nm may partially cancel out reflectance from the upper surfaces of a leaf, as both NIR and 550nm are able to penetrate through these upper layers, in theory leaving only the fraction of NIR reflectance due to internal scattering in the spongy mesophyll.

Therefore, this work aims to investigate the ability of spectral indices to measure changes in water status, due to changes in spongy mesophyll structure as a result of variation in leaf water content. The first index to be investigated will be referred to as a '800/550 Index' and uses spectral reflectance at 800nm and 550nm.

A consideration for developing visible spectral indices is the influence of chlorophyll fluorescence emission spectra, corresponding to a region from 680nm to 800nm (Meroni et al., 2009). The effects of chlorophyll fluorescence can contribute to reflected light intensity (Zarco-Tejada et al., 2000) and obfuscate the effects of leaf water content on spectral reflectance. Likewise, the xanthophyll cycle, a component of non-photochemical quenching (Baker, 2008), is involved in the de-epoxidation of the pigment violaxanthin to zeaxanthin, which alters the pigment's ability to absorb light in a spectral region centred at 531nm. This has been previously exploited as an indicator of NPQ by the Photochemical Reflectance Index (PRI) (Gamon et al., 1992). The spectral region sensitive to the xanthophyll cycle includes the wavelength of 550nm, and thus the state of de-epoxidation of the xanthophyll cycle must also be considered for its effect on any index using the 550nm wavelength.

The overall aim of this work is to develop a spectral index which can be used to assess the water status of a leaf, sensitive to changes in leaf turgor. More immediate aims are to assess the response of the 800/550 index to changes in internal leaf water content, through stomatal kinetics and changes in the vapour pressure deficit (VPD) between the leaf and atmosphere.

Objectives:

i)   Assess the ability of a spectral index of 800nm/550nm to detect changes in leaf water relations, through changes in VPD

ii)   Analyse the response of the visible and NIR spectrum of reflected light to changes in leaf water content, to identify spectral regions and potential new indices that demonstrate a strong relationship to changes in leaf water relations

3.2 Methods

3.2.1 Growth Conditions

Plants of Basil (*O. basilicum*) and Dwarf French Bean *(P. vulgaris)* were grown in compost (Levingtons F2S, Ipswich, UK) in a greenhouse under ambient lighting during the months of October and November 2018, with a lighting system providing a minimum of 200 μmol m^{-2} s^{-1} supplementary lighting in case of cloudy or dim lighting conditions. Plants were grown for at least 14 days prior to any measurements.

3.2.2 Reflectance Modelling

Leaf reflectance was modelled using the PROSPECT radiative transfer model for simulating leaf reflectance (Feret et al., 2008; Jacquemoud et al., 1996; Jacquemoud & Baret, 1990; Jacquemoud et al., 2009) to assess the viability of spectral indices to assess water status. Using inputs of leaf anatomy such as leaf thickness, and pigment and water content, the model treats the leaf as consisting of multiple 'layers' (e.g layers for leaf thickness layers or water content). These layers are treated as semi-transparent plates, and total reflection, refraction and transmission for each plate is

calculated. Similarly, scattering and absorption of each plate are also calculated. The sum of all plates yields the total reflection and transmission of light through the modelled leaf. Increasing or decreasing the layers as defined by the input parameters affects the interaction between irradiance, the absorption of light by pigments, and refraction due to the physical structure of the leaf, thus simulating the total percentage of light which is reflected and transmitted. Further information and a detailed description can be found in the work of Jacquemoud & Baret (1990).

Modelling here was focused on two parameters, leaf structure and equivalent water thickness. The leaf structure parameter, which adds extra layers to the leaf, representing the number of air and cell wall interfaces within the mesophyll. Model settings were set at defaults values of 30 µg/cm² chlorophyll content, 10 µg/cm² carotenoid content, 1 a.u. brown pigments, which represents polyphenol pigments, and 0.009 g/cm² leaf mass per unit area. Water thickness ranged from 0 to 0.060 µg cm², at 0.005 µg cm² intervals.

The first index to be investigated will be referred to as a '800/550 Index', and is defined as

$$800/550 \ Index = \frac{R800}{R550}$$

where R800 and R550 are the spectral reflectance at 800nm and 550nm. Two other common indices include The NDVI (Normalised Difference Vegetation Index) (Rouse & Space, 1978), routinely used in agriculture but was selected here due the index also using wavelengths in the NIR, and the Water Index (WI) (Peñuelas et al., 1993), a spectral index that directly measures water content through absorption of light at 950nm by water.

$$NDVI = \frac{(R750 - R620)}{(R750 + R620)}$$

$$WI = \frac{R900}{R950}$$

with R750 for reflectance at the near infra-red wavelength of 750nm; R620 for reflectance at the visible red wavelength of 620nm; R900 for reflectance at 900nm, and R950 for reflectance at 950nm

3.2.3 Spectral measurements and Gas Exchange

An Li-6400 (LI-COR, Lincoln, Nebraska, USA) infra-red gas analyser (IRGA) was used to collect gas exchange data. Leaf temperature was maintained at 22°C ± 1.0°C. Flow rate was maintained at 500μms. Dew point was set to 12°C ± 0.1°C using a LI-610 Dew Point Generator (LI-COR, Lincoln, Nebraska, USA). Vapour Pressure Deficit (VPD) in the chamber, in the presence of a transpiring leaf, was maintained at 1 ± 0.05 kPa. Full H_2O scrub resulted in a VPD of 2.2 ± 1.0 kPa. A LiCor 6400-14 Opti-Sciences Fluorescence Probe Adapter (LI-COR, Lincoln, Nebraska, USA) was used that provided an access port for a fibre optic to be located directly inside of the chamber itself. Silicon tubing and paraffin wax strips were used to ensure an airtight seal between the interior of the chamber and the exterior, where the fibre optic is located. A halogen light provided illumination onto the chamber, providing 800 μmol m^{-2} s^{-1} PPFD.

Leaf reflected light was measured using a Flame-S spectrometer (Ocean Optics, USA). The box width of the spectrometer was set to six, so the values of six adjacent pixels above and below each pixel were averaged together, providing a cleaner signal at a very small reduction of spectral resolution. Integrating time and the number of scans to average was set so that each measurement utilized the full range of the spectrometer. For measurements occurring over a time period, the first measurement collected during the experiment, for each repetition, was set as the standard. All subsequent measurements were normalised to this initial measurement. Thus, resulting measurements will shows the relative change in reflected light from the initial measurement

3.2.4 Vapour Pressure Deficit Step Change

To measure the response of the spectral index to changes in VPD and stomatal conductance, gas exchange and spectral measurements were collected at 20 second intervals.

French Bean plants were taken directly from the greenhouse to the IRGA chamber inside the laboratory. The plants were left for 30 minutes to equilibrate to the chamber conditions, where

irradiance was higher than the greenhouse. Measurements were collected for 10 minutes, at steady state. After this period, the VPD of the chamber was increased to around 2.2 kPa, for a 15 minutes period. This was followed by a 15 minutes period of 1 kPa VPD. This cycle was repeated.

3.2.5 Light Induction of dark adapted French Bean (P. vulgaris)

To investigate the effect of chlorophyll fluorescence, PRI, and associated changes in reflectance of wavelengths on the 800/550 Index, French Bean plants were dark adapted for a 45 minute period. One of the two primary leaves of French Bean were then placed into the IRGA chamber, with leaf temperature maintained at $22°C \pm 1.0°C$. Flow rate was maintained at $500\mu ms$ and dew point was set to $12°C \pm 0.1°C$ using a LI-610 Dew Point Generator (LI-COR, Lincoln, Nebraska, USA)

An FMS-2 (Hansatech, Cambridge, UK) was used to collect fluorescence measurements for plants in the chamber. A dark adapted measurement was first performed to collect the measurement of F_m, which is required to calculate NPQ (Baker, 2008; Murchie & Lawson, 2013). The plant was then exposed to 800 μmol m^{-2} s^{-1} light. The FMS-2, providing a saturating pulse of 6000 μmol m^{-2} s^{-1} at 5 minutes intervals, was used to measure the operating efficiency of PSII (F_q'/F_m') and non-photochemical quenching (NPQ) at every 5 minutes for a total of 40 minutes.

3.2.6 Leaf Cutting and Thickness

To identify spectral regions that demonstrate a strong relationship to changes in leaf water relations, a leaf cutting protocol was performed to elicit a decrease in leaf water content. Leaves of *P. vulgaris* were used in the same chamber as described in section 3.2.3. Light was provided at 800 μmol m^{-2} s^{-1} PPFD. Leaf temperature was maintained at $22°C \pm 1.0°C$. Vapour Pressure Deficit (VPD) in the chamber was initially set to 1 ± 0.05 kPa. Leaves were given time to acclimate to the environment in the chamber, until a steady state was reached.

A MultispeQ v1.0 (Michigan State University, East Lansing, MI, USA), an updated version of the MultispeQ Beta (Kuhlgert et al., 2016), was used to measure leaf thickness. The device contains a

Hall Effect sensor, in which the variable magnetic strength between two magnets due to a difference in distance between them, generates a variable voltage. The device was calibrated to actual thickness by using multiple layers of Whatman 1001-110 filter paper (Whatman, Maidstone, Kent, UK), which has a thickness of 0.18mm per filter. The device was attached on the same anatomical region of the leaf as that inside the chamber, but on the half of the leaf that was not inside the chamber. Thickness measurements were recorded every 60 seconds for a period of 45 minutes, and the leaf was cut from the rest of plant immediately after the first measurement was recorded.

3.2.7 Analysis of Indices

To identify the optimum index to use to measure leaf thickness, a computer script was written using R (R Core Team, 2017). The script iterated through the reflectance of every wavelength from 400nm up to 900nm, and divided each of these wavelengths ($λ1$) by the reflectance of every wavelength from 400nm up to 900nm ($λ2$). This generated an array of every combination of $λ1/λ2$ using all wavelengths from 400nm to 900nm. Each generated $λ1/λ2$ index was correlated to leaf thickness data, producing an R^2 value describing the relationship between the two variables. A heatmap was generated that plotted the array of R^2 for every index. Each wavelength for $λ1$ was on the Y axis, and $λ2$ on the X axis, with the point in which every wavelength intersects representing the relationship with leaf thickness.

3.2.8 Leaf Water Potential

Leaf water potential was measured using a SKPM 1400 Plant Moisture Vessel (Skye Instruments, Powys, UK). Leaves were taken from plants between 12pm and 2pm. These leaves were placed in a plastic bag and cut from the stem, immediately after spectral measurements and placed into the moisture vessel. Basil plants were investigated alongside French Bean, to assess the relationship between water potential and spectral indices in more than one species.

3.3 Results

3.3.1 Reflectance Modelling

Modelled output of reflectance based on water content clearly demonstrates the lack of wavelengths in the visible spectrum which are directly affect by water content. Only wavelengths in the region of NIR associated with weak absorbance of light by water (>900nm) show any effect from the variation of water content (Fig. 3.1A), with a decrease in reflectance due to the associated increase in the absorbance by water of these wavelengths due to an increase in water content. Modelled leaf structure however (Fig. 3.1B), demonstrates two areas which are strongly affected by changes in leaf structure. The first are NIR wavelengths above 700nm, which are unaffected by plant pigments and subject to internal scattering, while the second in the green region from 500nm up to 660nm, with a peak at 550nm.

Calculated indices based on simulated water content and leaf thickness (Fig. 3.2) shows a strong relationship for each of the three indices with water content, however the range of values for all indices is negligible (Fig. 3.2A, B, C). The range for NDVI (Fig. 3.2A), from 0.737 to 0.736, is extremely small when compared to the usual range of NDVI for vegetation from 0.2 to 0.8. The 800/550 index (Fig. 3.2B) also shows a strong negative relationship with water content and ranges from 5.15 to 5.12. The water index (Fig. 3.2C), like the previous indices, shows a strong relationship with a range of values as expected (Penuelas et al., 1997).

However, for leaf structure, there is no significant relationship between NDVI and leaf structure (Fig. 3.2D). The 800/550 index shows again a strong negative relationship with a higher R^2 than the other indices, but has an increased range from a high of 5.50 to a low of 3.50, and the water index only has a total range of 0.01. Therefore, the 800/550 index based on modelled data, appears to be strongly affected by changes in mesophyll structure and leaf structure, and to an extent water absorption of NIR. However, leaf structure was used here as proxy for structural change as a result of leaf water

content or leaf turgor, as neither water content or leaf structure simulated changes in water turgor directly.
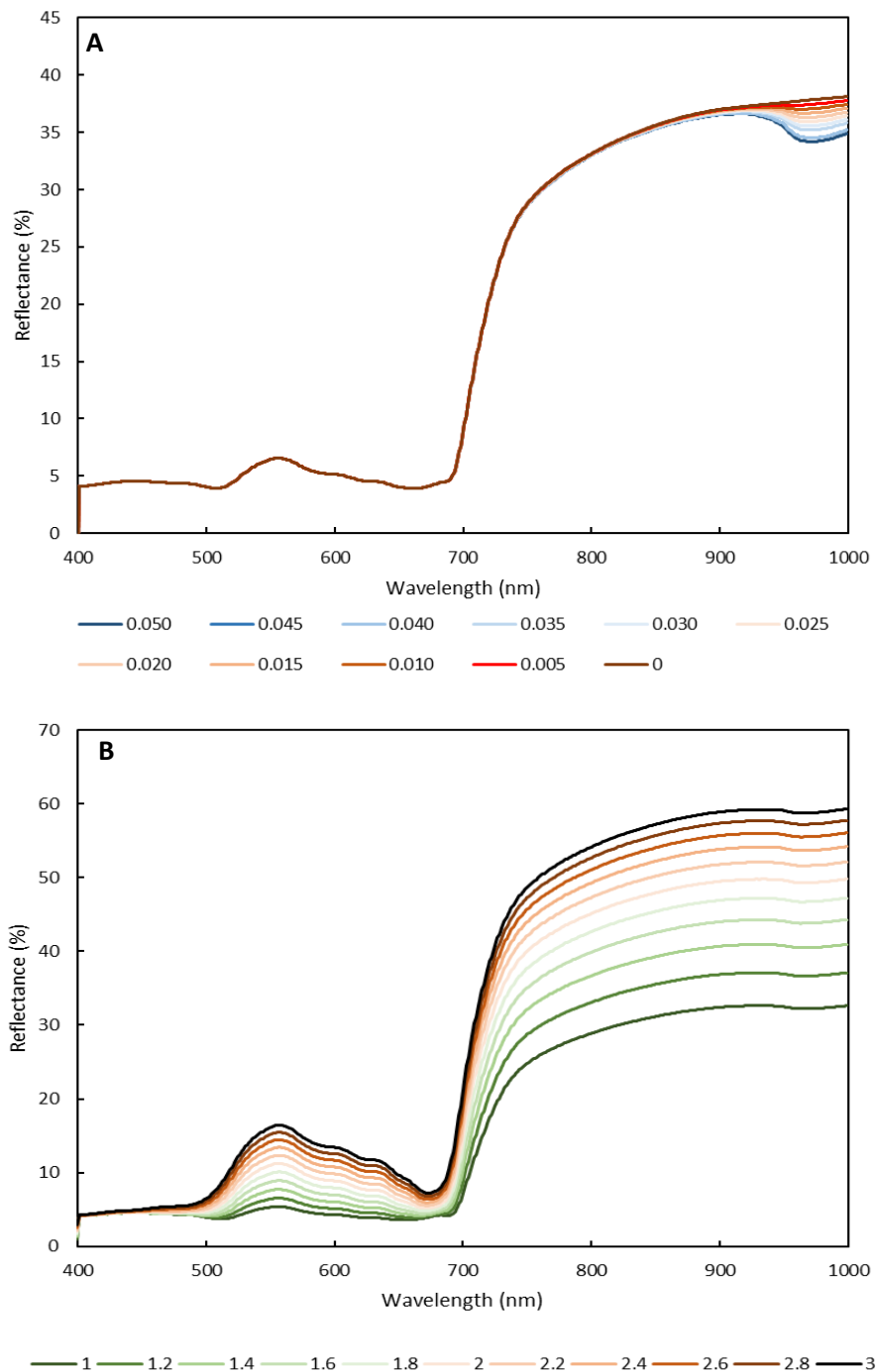
Figure 3.1 Modelled reflectance through PROSPECT. (**A**) Reflection for changes in the values of equivalent water thickness ($\mu g/cm^2$) (**B**) Reflection for changes in leaf structure, simulating increases in the thickness of a leaf, and an increase in intercellular space.
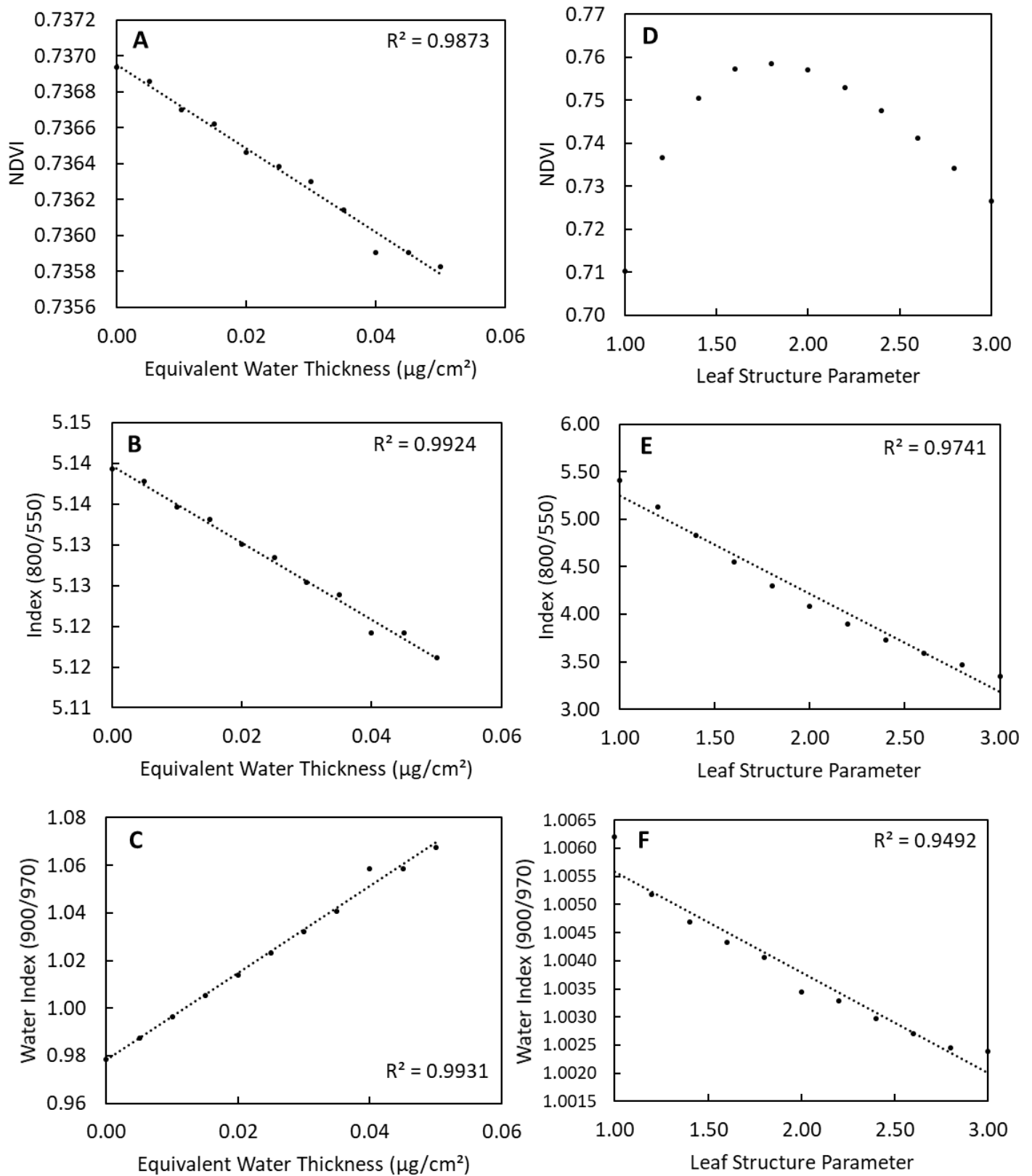
Figure 3.2 The response of the 800/550 index using reflectance at 800nm and 550nm, the Normalised Difference Vegetation Index (NDVI) and the Water Index against changes in modelled water thickness (**A,B,C**) and changes in leaf structure (**D,E,F**).

3.3.2 Vapour Pressure Deficit Step Change

The response of the 800/550 index in response to increased VPD to 2.2 kPa (Fig. 3.3A), as seen at the 10 minute time point, took approximately two minutes before the higher VPD had any affect on the index. At the halfway point of the first cycle of elevated VPD, at 17 minutes, the index begins to decrease, but does not return to original values until around ten minutes after VPD had returned back to its original value of 1 kPa. The second VPD increase, after 40 minutes, resulted in a similar response of the index. However, this response was dampened in comparison to the first change in VPD, with the index not reaching half the values of the response for the first VPD change.

Stomatal conductance initially increases (Fig. 3.3B) upon increasing VPD to 2 kPa, due to the Ivanoff effect – an increase in transpiration upon exposure to low humidity (Rufelt 1963) and the higher gradient between water in the leaf and in the air of chamber. However, after the initial increase stomatal conductance begins to decrease as stomata close in response to the higher VPD. Returning the chamber VPD back to 1 kPa results in stomatal re-opening, however the stomata opened at a much slower rate than they closed. Increasing VPD for a second time was again similar to the initial VPD response but with a smaller initial increase in stomatal conductance. The 800/550 index initially increases upon an increase to VPD, opposite to the decrease in stomatal conductance which decreases from the 10 min mark, but at 20 min the index decreases.

Assimilation rate decreases upon an increase in VPD. While stomatal conductance initially increases due to lower atmospheric humidity, this does not necessarily indicate an increase in the uptake of CO_2 if stomatal aperture is relatively unchanged. The subsequent decrease in stomatal conductance does however limit the uptake of CO_2, thus decreasing CO_2 availability for photosynthesis.

An analysis of changes in reflected light intensity across the entire measured spectrum (Fig. 3.4), showing the two halves of the first VPD response (10 to 30 min of Fig. 3.3A). The first half of the

response consists of an increase in reflected light due to high VPD (Fig. 3.4A), occurring between 10 and 19 min of Fig. 3.3, and the second half is the decrease between 19 and 30 min (Fig. 3.4B). Both demonstrate similar changes in reflected light across the spectrum, however the region from 580nm to 650nm was higher at 30 min, compared to other wavelengths, than it was when reflectance was increasing from 10 to 19 minutes. The initial peak of reflected light at 700nm appears to increasingly 'shift' towards lower wavelengths. The spectral regions at 550nm, 680nm and above 800nm appear to retain their characteristics across all time points.
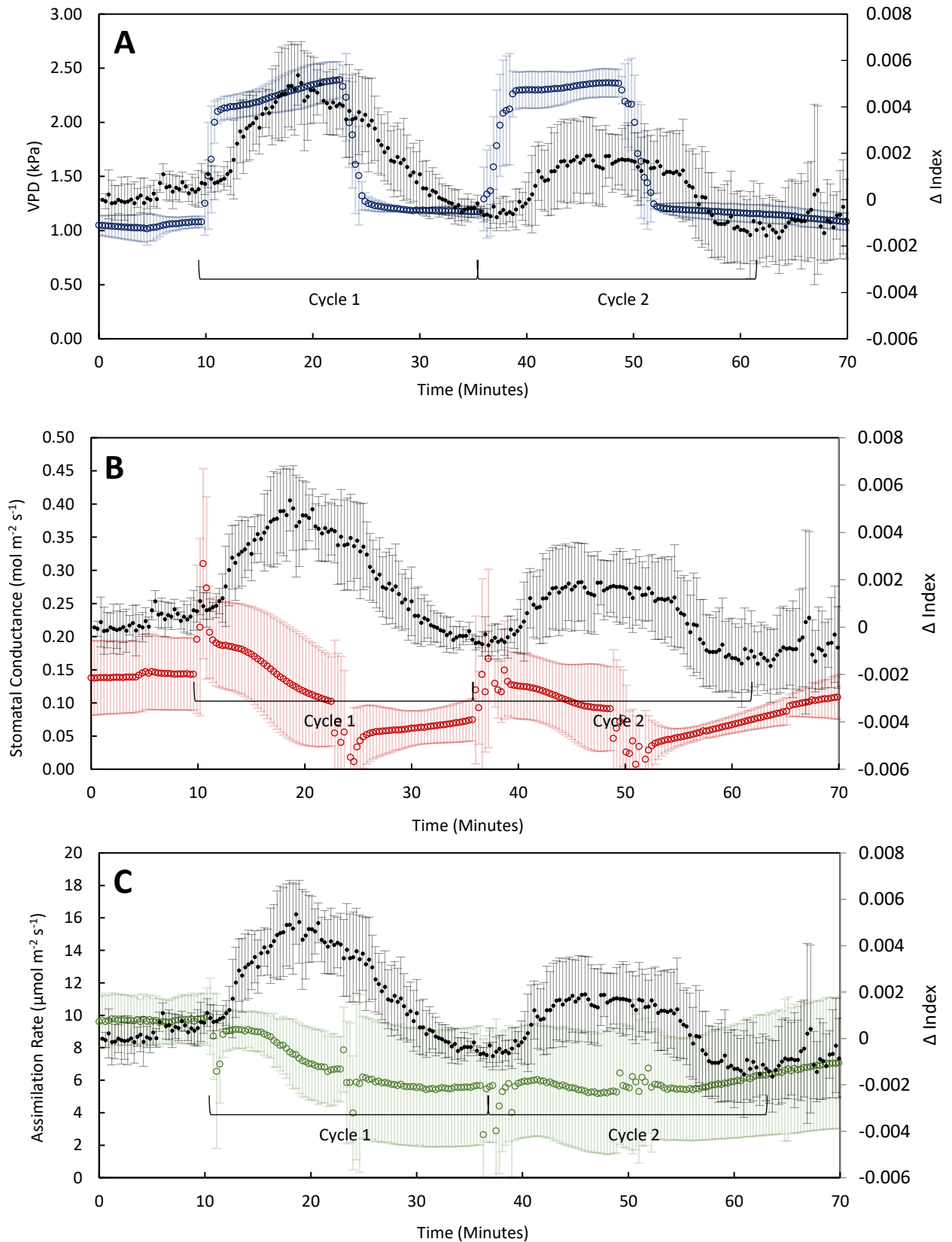
Figure 3.3 The response of the 800nm/500nm Index (●), stomatal conductance (○), and assimilation rate (○), to changes in VPD$_{Leaf}$ (○) from ~1kPa to ~2.2kPa for the primary leaves of *French Bean* under 800 µmol m^{-2} s^{-1}. VPD was increased at 10 minutes and decreased at 25 minutes (Cycle 1), increased again at 40 minutes, and decreased finally at 55 minutes (Cycle 2). (**A**) VPD$_{leaf}$ and 800nm/550nm index, indicating the two VPD cycles . The 800nm/550nm Index and (**B**) stomatal conductance, and (**C**) assimilation rate, with the VPD cycle of **A** indicated in both. Index values are normalised, with 0 being the initial value of the index at 0 minutes, showing difference in index values to this time point. Leaf temperature was maintained at 22°C ± 1.0°C, and dew point was set to 12°C ± 0.1°C. Data is mean with standard deviation (n=5).
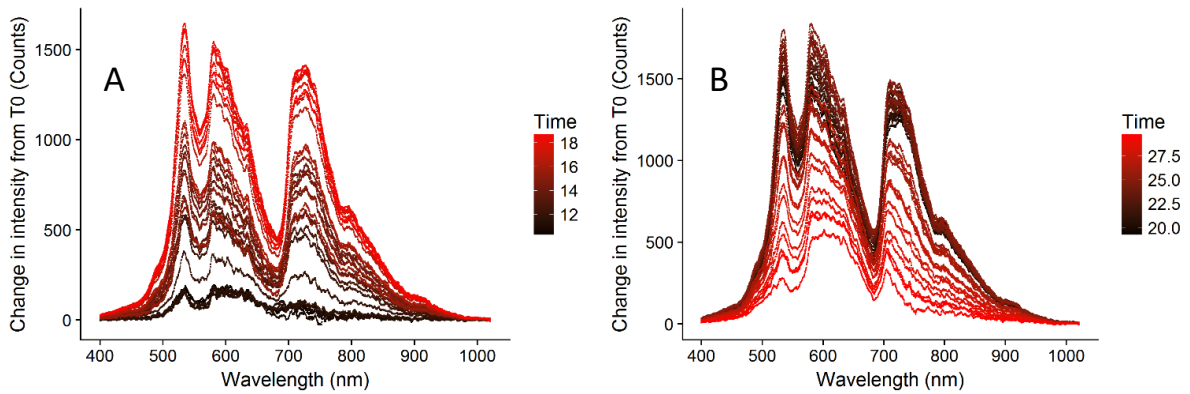
Figure 3.4 Changes in reflected spectrum of light for leaves of French Bean, during changes in VPD (Fig. 1). The time points were chosen for the increase and decrease of the first VPD cycle, from (**A**) 10 minutes to 19 minutes, and (**B**) 19 minutes to 30 minutes. The *change in intensity from T0* represents the different between light intensity measured at each time point to that measured at 0 minutes. (n=5)
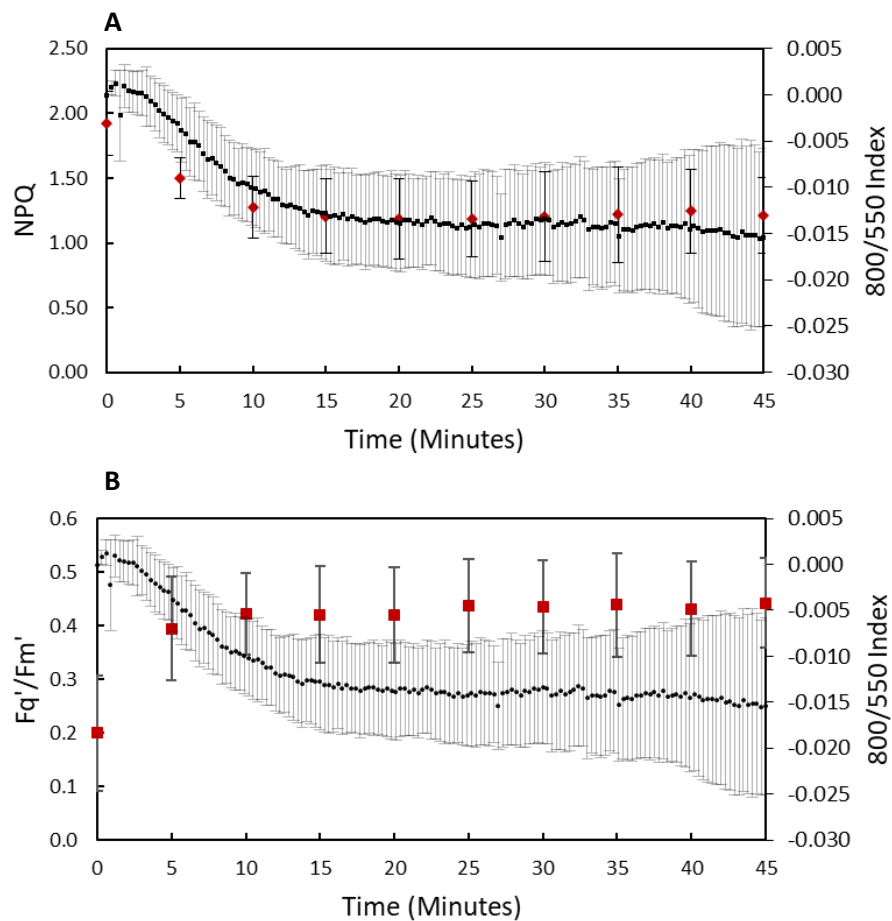
Figure 3.5 Changes in F_q'/F_m' (■), NPQ (◊) and the index (●) of dark adapted French Bean placed under 800 μmol m^{-2} s^{-1} light. Index values are normalised, with 0 being the initial value of the index at 0 minutes, showing difference in index values to this time point. Data is mean with standard deviation (n=5)
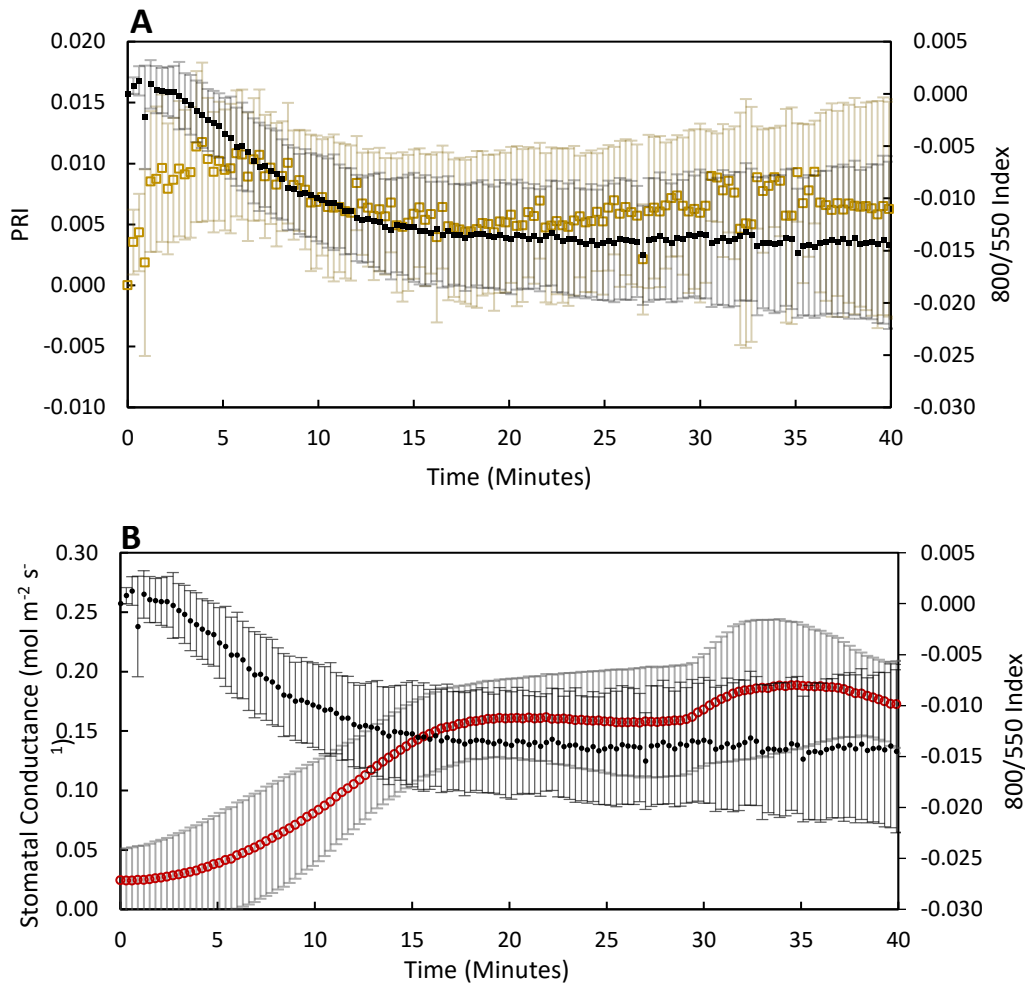
Figure 3.6 The response of the 800nm/500nm Index (●) and **A** the photochemical reflectance index (PRI) (○), **B** stomatal conductance (○) upon the light induction of dark adapted French Bean. Both the 800/550 index and PRI are normalized to 0, so that each data point is the difference between the measurement at each time point to that measured at 0 minutes. Data is mean with standard deviation (n=5)
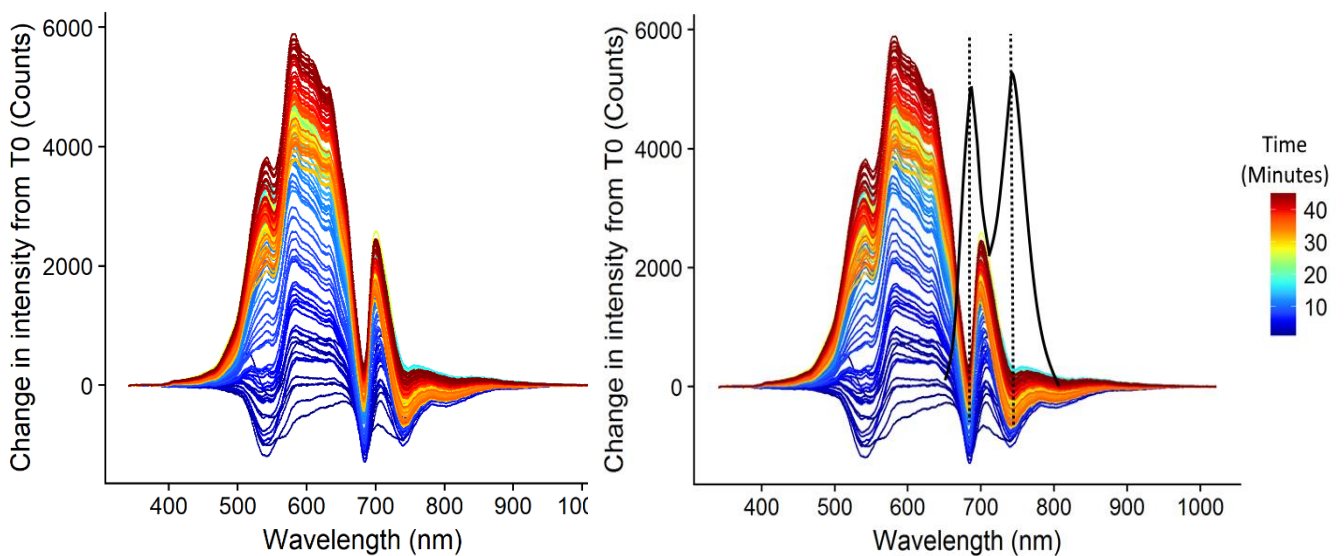
Figure 3.7 (A) Changes in reflected spectrum of light for leaves of dark adapted French Bean placed under 800 μmol m^{-2} s^{-1} light at 0 minutes. The *change in intensity from T0* represents the different between light intensity measured at each time point to that measured at 0 minutes (n=5) **(B)** Same graph but with fluorescence emission spectra overlaid, with the two emission peaks shown by black dashed lines. Emission spectra is not to scale with the rest of the graph. Data adapted from *Meroni et al* (2009).

3.3.3 Light Induction to assess the effects of chlorophyll fluorescence on spectral index

A light induction experiment was performed to investigate the effects of chlorophyll fluorescence on the change in reflected light intensity, due to possible overlap with chlorophyll fluorescence emission spectra and the 800nm wavelength, and NPQ related de-epoxidation of violaxanthin and the 550nm wavelength, which may obfuscate the effects of leaf water content on spectral reflectance. The light induction shows that the 800/550 index decreases alongside a decrease in NPQ (Fig. 3.5A) and increase in F_q'/F_m' (Fig. 3.5B), with all measurements reaching a steady state after a period of ten minutes. PRI initially increases while the 800/550 index decreases (Fig. 3.6A), before both indices decrease from the 6 minute time point and level off. Stomatal conductance concurrently increases alongside a decrease in the spectral index (Fig. 3.6B). Analysis of the spectrum (Fig. 3.7) shows an initial decrease in the overall light intensity of reflected light for the first few minutes, which quickly increases for the rest of the time period. The greatest change was in wavelengths 580nm to 660nm, with a small peak focussed around 550nm. Wavelengths in the near infra-red, above 730nm, do not increase back up to their initial intensity at 0 minutes, until around 30 to 40 minutes, and in comparison to Fig. 3.7 do not change intensity as strongly. The increase in the spectrum is more than double the variation seen in the VPD response (Fig. 3.4). There is a slight decrease in intensity between 10 and 30 minutes, before increasing again.

3.3.4 Leaf Cutting and Thickness

Incision of the leaf resulted in a decrease in leaf thickness (Fig. 3.8). There was a larger decrease in thickness in the first ten minutes, with the rate of decrease gradually falling and steadying off by the end of the 50 minutes (Fig. 3.8A). Concurrently, the index increases during the first ten minutes, before levelling off in similarly (Fig. 3.8A). When comparing both thickness and the index (Fig. 3.8C) to assess how the index responds to changes in thickness, there is a good relationship between the

two measurements (R^2 = .96, p < 0.001). However, plotting each replicate individually shows a variable response to a decrease in leaf thickness, with some individuals demonstrating an increase in the index, while other individuals decrease (Fig. 3.8D), likely due to the rapid loss of water content also resulting in extreme structural change, and thus an extreme change in internal scattering of NIR.

Plotting each individual replicate instead of the mean (Fig. 3.8D) shows that the high variation seen is also attributed to the lack of a physical relationship between the Index and leaf thickness, as in relative terms there is clearly a good relationship (Fig. 3.8C). However, one sample may have a value from the index of 2.57 for a leaf thickness of 0.34mm, but another sample with the same leaf thickness of 0.34mm will have an index value of 2.35.

3.3.5 Analysis of Spectral Indices

Analysis of potential indices shows three clear areas which show good sensitivity to leaf thickness (Fig. 3.9). The first is the blue region from 400nm up to 480nm, the second is a very small region at 550nm, and the final region is from 660nm to 680nm. All these regions perform well when NIR (>700nm) is divided by these regions, which act as a relatively stable reference to compare variation in NIR against.

Based on this data, alternative indices were derived and plotted against thickness (Fig. 3.10). Here, all three alternative indices demonstrated a consistent positive relationship with leaf thickness. The index $\frac{(800nm/665nm)}{440nm}$ (Fig. 3.10D) had the highest R^2 of 0.37. A completely flaccid, desiccated leaf was associated with a value between 0.6 and 0.7 while a leaf at full thickness was associated with a value above 0.9.
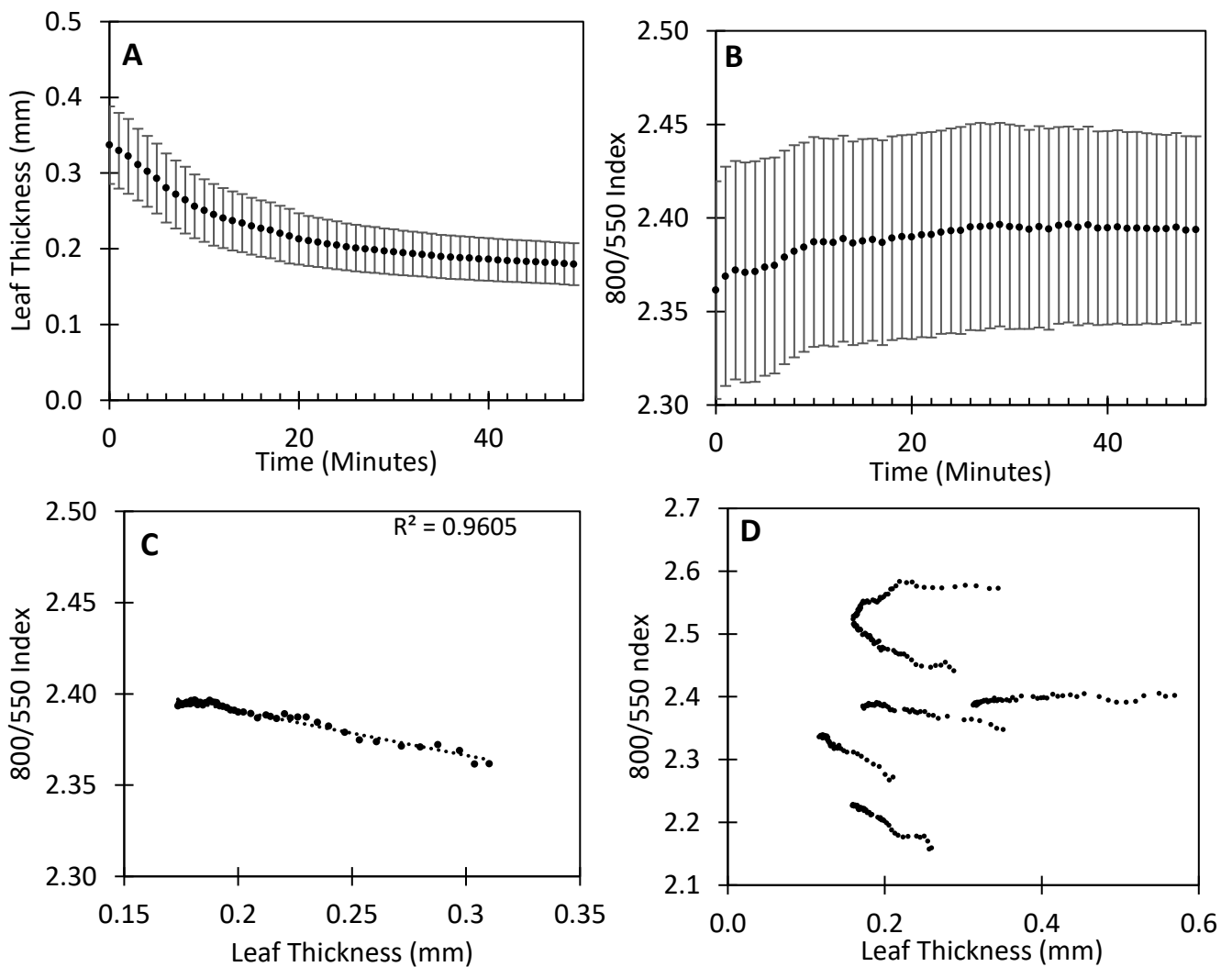
Figure 3.8 Leaf thickness and Index for French Bean leaves after separation from main plant, using leaf thickness as a proxy for leaf turgor. **(A)** The change in leaf thickness over a 50 minute time window. Error ± S.E (n=6) **(B)** Index calculated from reflectance at 800nm and 550nm Error ± S.E (n=6) **(C)** Relationship between the 800nm/550nm index and leaf thickness. Error bars not shown but are present in **A** & **B**. (n=6) R^2 = .96, p < 0.0001 **(D)** Individual repetitions plotted separately, demonstrating the high variability between leaf thickness and the index
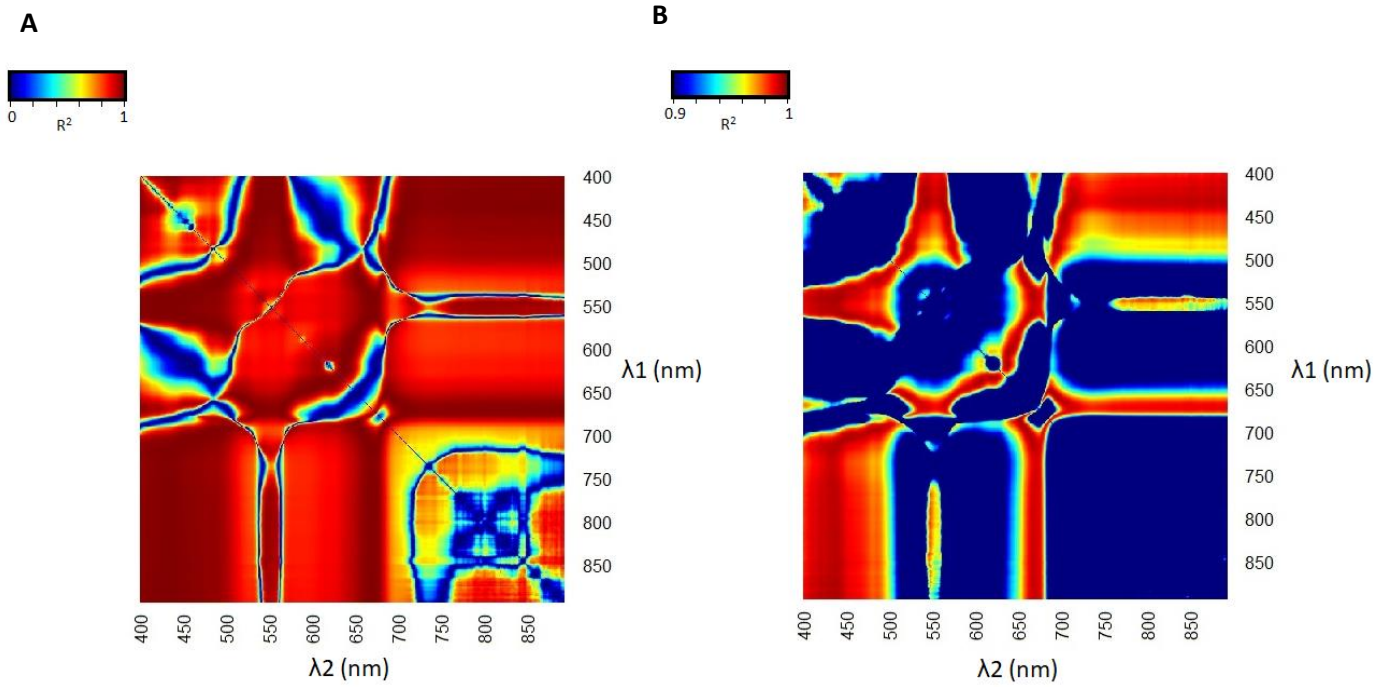
Figure 3.9 Relationship between indices calculated as λ1/λ2, and leaf thickness after cutting leaves from the main plant (**A**) Heatmap showing the R^2 value between indices calculated at λ1/λ2, and leaf thickness as measured in Fig. 3.9, with $R^2 = 0$ being blue and $R^2 = 1$ being dark red (**B**) Same data, but all R^2 below 0.9 is coloured blue as per key
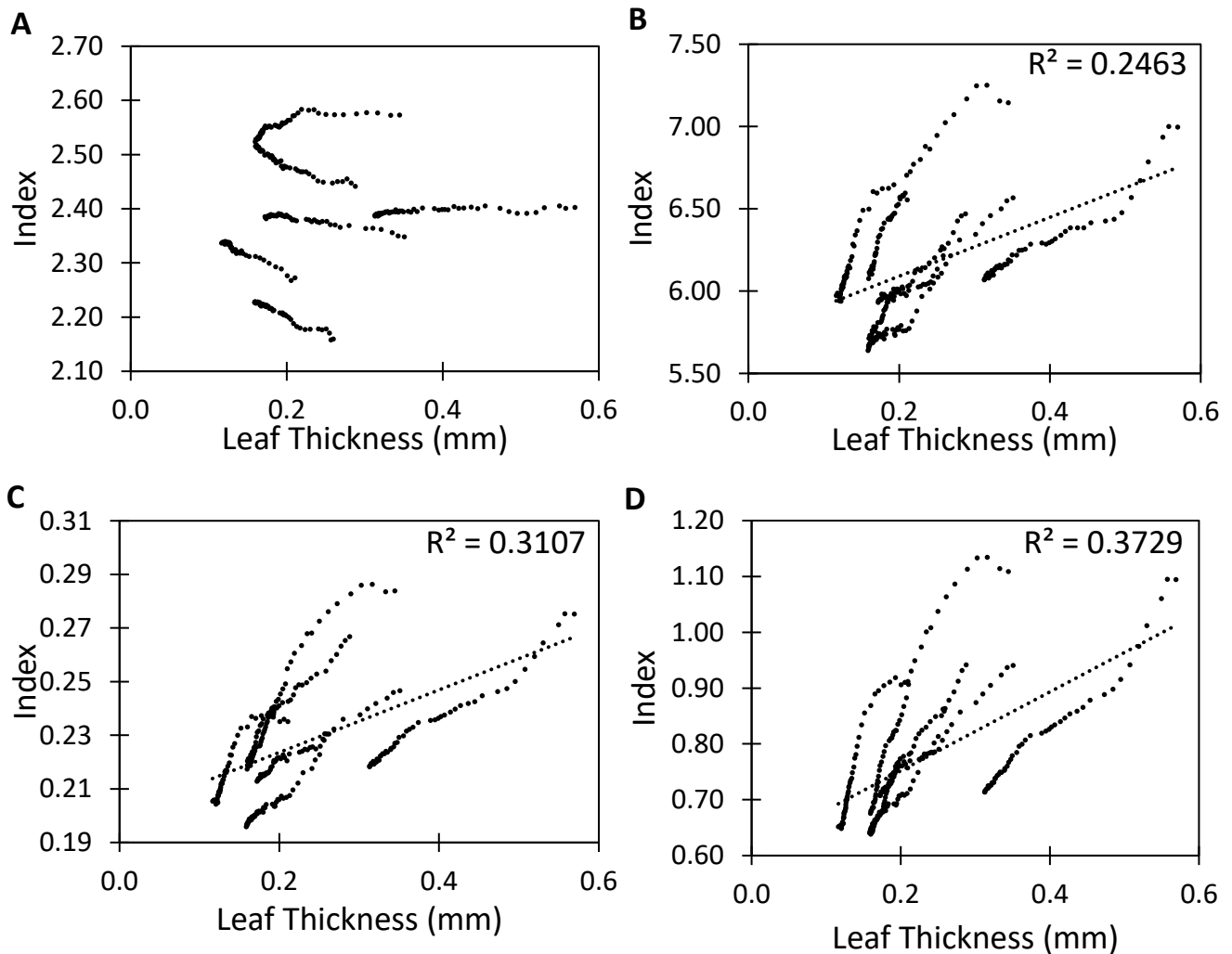
Figure 3.10 Individual repetitions of data from Fig. 3.9, plotted separately and re-calculated with alternative indices derived from the optimal wavelength selection from Fig. 3.11, calculated as (**A**) 800nm/550nm (**B**) 800nm/440nm (**C**) (800nm/550nm)/440nm (**D**) (800nm/665nm)/440nm

3.3.6 Leaf Water Potential

For both species and indices, there was an overall weak relationship between indices and water potential. However, there was a relationship between leaf water potential and all indices until -0.4 MPa (Fig. 3.11), with the strongest relationship seen between French Bean and the index of $\frac{(800nm/665nm)}{440nm}$ (Fig 3.11 E), with an R^2 of 0.59, followed by the 800nm/440nm index. Below -0.4 MPa, the relationship between spectral indices and water potential decouples. For Basil, (Fig. 3.11 A,B,C) all indices decrease alongside a decreasing water potential before decoupling at a water potential of -0.4 MPa. In *French Bean* (Fig. 3.11 D,E,F) the indices increase before also decoupling at 0.4 MPa.
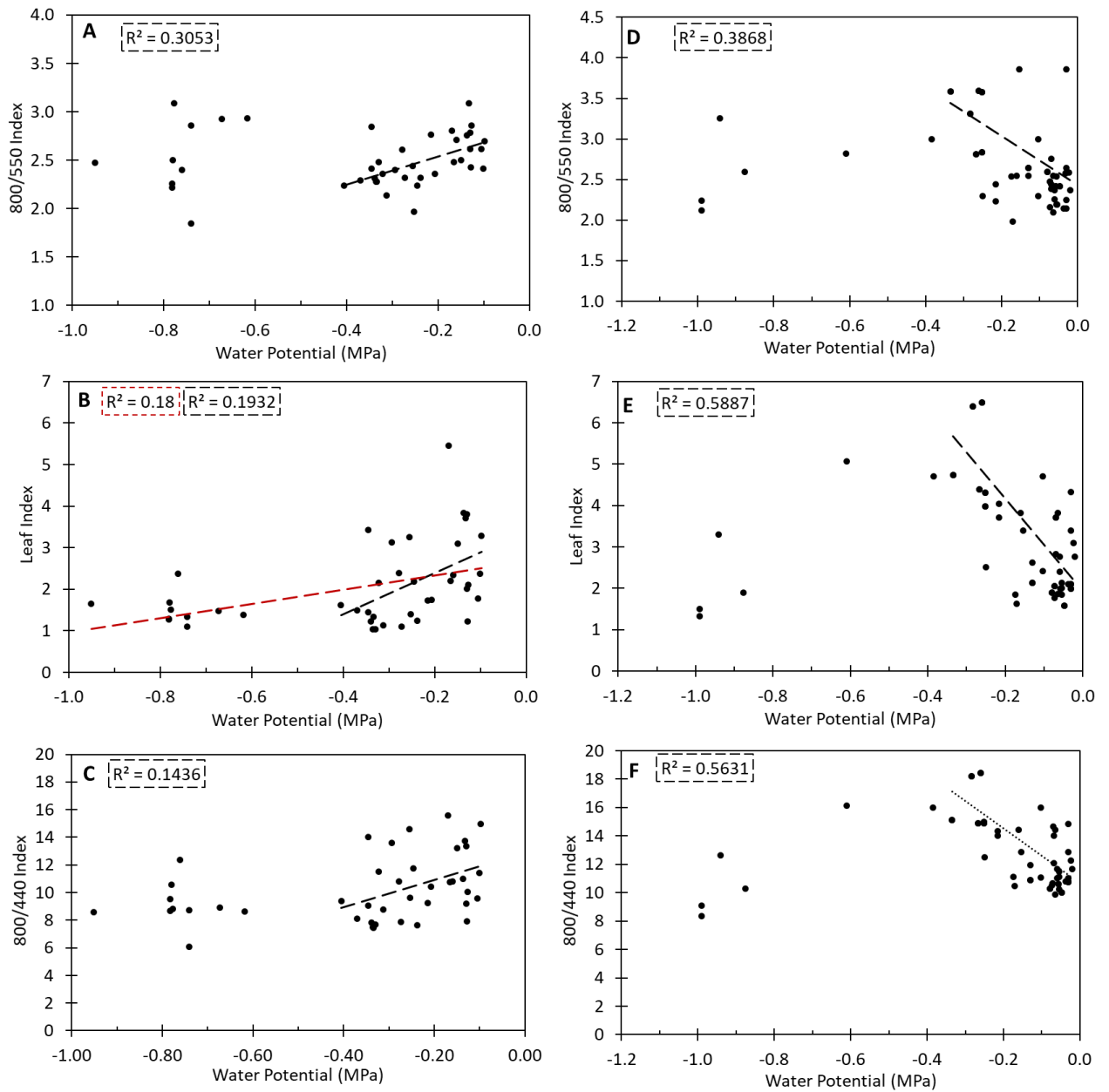
Figure 3.11 Measurements of the 800nm/550nm index, the 800nm/440nm index, and the Leaf Index, against leaf water potential for Basil **(A, B, C)** and French Bean **(D, E, F)**. As leaf water potential decreases from a state of high water content and full turgor, the indices here decrease for Basil and increase for French Bean until both species reach approximately -0.4 MPa, in which there is a decoupling between all indices and leaf water potential. This decoupling is likely a result of plasmolysis, which will significantly alter the structure of a leaf and affect the internal refraction and scattering of light. Trendline and coefficient of determination is shown for values that are greater than -0.4 MPa, except for the red dashed lined in **B**, which consists of all data points.

3.4 Discussion

3.4.1 Vapour Pressure Deficit Step Change

The response of the index appears to be affected by both VPD and stomatal conductance, with the index seeming to 'lag' being VPD. This could be explained by the leaf acting as a buffer for water vapour, requiring time for the leaf to lose its water pressure sufficiently to affect the physical properties of the leaf, as well as time for a 're-pressurisation' of the leaf with water vapour from the rest of the plant, replenishing the water lost from the leaf. The results also appear consistent with literature demonstrating that step changes in VPD result in changes in leaf turgor (Shackel & Brinckmann, 1985), supporting the idea that the index is measuring changes in the physical structure due to changes in leaf turgor. The decrease of the index at the 20 minute time point appears to be when the closure of the stomata allows for water transported from the xylem to replenish lost water at a greater rate than water is lost through transpiration, shown most clearly by the reduced reaction of the index to the second VPD increase near the 40 minutes time point. Despite the high VPD of 2.3 kPa, stomatal conductance is maintained at a rate below initial values, and therefore the loss of turgor pressure will also be reduced.

The analysis of the spectrum of the leaf for the VPD response (Fig. 3.4) shows a large range in light intensity for wavelengths at 530nm and a region around 600nm. There is also a high range for wavelengths above 700nm, wavelengths more associated with the physical structure of the leaf due to low absorption of light by plant pigments at these wavelengths, and an increase in internal scattering across air/cell interfaces (Gates et al., 1965). The relative conservation of the 'troughs' at 550nm and 680nm, and the 'step' at 800nm, suggest that these regions are relatively stable, present also in the light induction (Fig. 3.7). There does appear to be a 'red shift' of high reflectance near 700nm shifting towards lower wavelength, and an increase of the region between 600nm and 660nm, in comparison to other wavelengths, which is known to increase alongside the red shift in stressed plants due to decreases in chlorophyll (Carter & Knapp, 2001).

However, due to the sensitivity of the spectrometer in the setup used for this experiment, this may actually be an indication of a reduction of carbon assimilation due to stomatal closure, with carbon assimilation decreasing as soon as VPD was increased and remaining low for the duration of the experiment (Fig. 3.3D). Therefore less absorbed light is being used in photochemistry, and a greater fraction of absorbed light is dissipated as heat via NPQ, or remitted as fluorescence at wavelengths between 650nm and 800nm (Meroni et al., 2009). The effect of reduced photosynthesis is suggested due to the changes in the intensity of reflected light in wavelengths that are associated with chlorophyll absorption (Gitelson et al., 2003). Another possibility, for a response over a relatively short timescale, could be the effect of chloroplast movement (Kasahara et al., 2002). In the presence of high light, chloroplast have been shown to move into stacks, reducing the amount of incident radiation, although this would only account for some of the response seen.

3.4.2 Light Induction

Dark adapted leaves have minimal stomatal conductance, and therefore it is assumed that leaf turgor and water content will be at its maximal. Therefore, the light induction (Fig. 3.6Bs) should show a decrease in leaf turgor while stomata open and gradually decrease from maximal turgor. However, the response of the index is instead in the opposite the one seen in Fig. 3.3, in which an increase in the index corresponds to an assumed decrease in leaf turgor. It can therefore be assumed that other factors are involved that are affecting the index. Chlorophyll fluorescence measurements (Fig. 3.5) suggest that apparent changes in reflected light due to changes in the intensity of fluorescence and absorption of light due to changes in pigments might be one of those factors.

Chlorophyll fluorescence emission spectra corresponds to wavelengths from 680nm up to 800nm (Campbell et al., 2008; Meroni et al., 2009) (Fig. 3.7B), which would be a factor when less absorbed light is used in photochemistry due to a lowered assimilation of carbon and thus increased non-photochemical quenching and fluorescence emission. For the light induction (Fig. 3.6, Fig. 3.7), in

which changes due to chlorophyll fluorescence parameters would be greatest, the region from 680nm up to 800nm has a much smaller change in intensity overall, with the initial decrease in reflectance most likely due to an increase in photochemical quenching, and thus a reduction in chlorophyll fluorescence emission. Thus, the operating efficiency of PSII influences reflected wavelengths in this region, which includes NIR up to 800nm. This could explain the increase in reflectance at 700nm after the VPD response, which may be the result of a decrease in the operating efficiency of PSII and subsequent increase in fluorescence emission (Fig. 3.4) (Zarco-Tejada et al., 2000). Data from the light induction shows NPQ and F_q'/F_m' (Fig. 3.5) changing over a similar timescale as the index, however stomatal conductance also increases over the time period (Fig. 3.6B), which would affect the turgor pressure of the leaf and therefore also have an effect on the index. Again, it should also be noted that here the index decreases upon stomatal opening, whereas for the previous work on VPD response (*Section 3.4.1*) it increased. This is attributed to a lower change of intensity at 800nm for the light induction experiment than for the VPD response experiment, whereas 550nm exhibits a greater response for the light induction experiment than for the VPD response experiment. Increased reflection at wavelengths between 500nm and 560nm therefore suggests other effects. PRI, which is an indicator of the epoxidation state of the xanthophyll cycle, measures reflectance at a peak between 515nm and 530nm due to de-epoxidation of the pigment violaxanthin in response to excess absorbed light as part of NPQ, which modifies the absorption spectra of the pigment and therefore affecting reflectance. Here, PRI initially increases alongside NPQ (Fig. 3.6A), before decreasing after 6 minutes alongside the 800nm/550nm index. This suggests that the spectral region between 500nm and 560nm is likely affected by the change in reflectance due to the xanthophyll cycle which can mask or interfere with the ability of the 800nm/550nm index to track leaf water content.

Finally, for both VPD response (Section 3.4.1) and light induction experiments, stomatal conductance was relatively low for what can be expected from French Bean. This is likely due to the lower light available to the plants while growing as a result of the season and cloud cover. The index would

ideally be used on crops under the much higher light of late spring and summer. Therefore, the VPD response would be much greater than observed here, as the higher stomatal conductance would allow for a higher rate of transpiration under a high VPD, resulting in a larger change in leaf turgidity.

3.4.3 Analysis of Indices

The blue spectrum is generally unaffected by changes in pigment content unless under severe stress due to very strong absorbance by chlorophyll and other pigments (Sims & Gamon, 2002), and therefore is relatively stable, making the blue region an ideal candidate as a reference wavelength to measure changes in NIR light against. Similarly, the region from 660nm up to 680nm corresponds to an area of chlorophyll absorbance of red light. However, chlorophyll absorbance of blue is very strong and saturated, whereas variation in chlorophyll content will correspond to changes in reflected red light (Sims & Gamon, 2002). Therefore, using red wavelengths for the leaf turgor index will expose the index to variation linked with chlorophyll content. Another area that showed good relationship to leaf thickness was a small region centred around 550nm. This might be explained by the ability of 550nm to pass through the upper layers of the leaf, thus while red and blue act as a stable reference for measuring changes in NIR, 550nm may instead cancel out reflectance of NIR from the upper stages, isolating reflected NIR from the spongy mesophyll. However, the region centred on 550nm may not be suitable due to previously discussed sensitivity to the de-epoxidation of the xanthophyll cycle, which can affect the ability of the index to measure leaf water content. For this reason, the 800nm/550nm does not appear to be the optimal index for measuring leaf water status. However, the alternative indices that were investigated (Fig. 3.10) show promise in developing a reliable indicator of water status.

The index $\frac{(800nm/665nm)}{440nm}$ (Fig. 3.11D), based on data with leaf thickness, in which a desiccated leaf was associated with a value between 0.6 and 0.7, and a leaf at full turgor with a value above 0.9, may have potential as a crop monitoring tool for water status. For instance, greenhouse irrigation systems could track plants and when the index value drop below 0.85, and apply an irrigation

treatment. The index 800nm/440nm also shows potential as an index for monitoring crop water status, and there was little effect of chlorophyll fluorescence on the reflection of 440nm (Fig. 3.7), which indicates minimal influence of chlorophyll fluorescence emission spectra on this index. Since it is the internal scattering of NIR that is the main factor that is affected by water content due to changes in the internal structure of the mesophyll, the selection of a stable wavelength that does not change with water content may be a better candidate, effectively acting as a reference against which variation in NIR can be compared against. In the visible spectrum, the most stable region of reflectance is blue (400nm – 500nm), which is unaffected by water content.

3.4.4 Leaf Thickness

However, while these alternative indices show a good relationship with leaf thickness, that does not necessarily indicate they have a relationship with leaf water content, despite using leaf thickness as a direct proxy for leaf turgor. Likewise, while the original 800/550 index may have a relatively poor relationship with leaf thickness, this does not preclude the possibility that it has a strong relationship with actual leaf turgor. However, actual leaf turgor was not measured as part of this work.

Slaton et al. (2001) looked at leaf anatomical characteristics in an attempt to estimate reflected NIR, looking at key structural component, which would be expected to be a large influence on structural scattering of NIR, such as leaf trichrome density, and leaf cuticle thickness. Mesophyll related parameters such as the proportion of the mesophyll occupied by intercellular air spaces (%IAS) and the ratio of mesophyll cell surface exposed to intracellular air spaces per unit leaf surface area (A_{mes}/A) were also investigated. While leaf thickness and %IAS were correlated, albeit weakly, to changes in reflected NIR, A_{mes}/A was strongly correlated to reflected NIR. This highlights the relationship between leaf structure and reflectance of NIR due to internal scattering.

Plants can maintain leaf turgor despite a loss in water content through solute accumulation and osmotic adjustment (Turner, 2018), thus leaf turgor does not necessarily directly relate to actual water content. Leaf thickness has been identified as a good proxy for leaf water content (Afzal et al.,

2017; Seelig et al., 2015). However, the link between leaf thickness and leaf turgor is not necessarily strong (Seelig et al., 2015), which suggests the possibility that leaf thickness could a better indicator of leaf water status. However, while Slaton et al. indicates that reflected NIR is strongly affected by leaf structure, this may also suggest that a combination of these factors are at play with regards to reflection of NIR light. However, leaf turgor measurements would be required to fully establish the relationship between leaf turgor and NIR reflection.

3.4.5 Leaf Water Potential

While leaf turgor was not measured in this experiment, leaf water potential for French Bean and Basil was measured in order to determine a relationship between the indices discussed here and a wide range of leaf water status measurements. The discontinuation of the relationship of Fig. 3.12 may be due to changes in internal structure severely affecting the refraction and reflection of both visible and near infra-red light. Thus, there is a possibility that as the leaves approach wilting, the structure of the leaf varies sufficiently to result in a major change in refractive properties. This effect may be specific to the species used, as both Basil and French Bean have very large, thick leaves that are not as woody or as tough as other species such as wheat. This can be observed in work by Foley et al. (2006), with the spectral region between 700nm and 900nm showing in some cases non-continuous variation in reflectance with progressive wilting. In French Bean, the $\frac{(800nm/665nm)}{440nm}$ index and the 800nm/440nm index showed best relationship with water potential in French Bean, however in Basil only the 800nm/550nm index performed best, and that's still relatively poor compared to the performance of these indices when used on French Bean. Therefore, it may be the case that some species may not be suitable for monitoring by these spectral indices due to decreased sensitivity to the effects of decreased water content on internal scattering of near infra-red light. Future work will be required to fully assess these indices on a wider range of plant species.

Additionally, it would be hugely beneficial to separate out the components of leaf water potential in order to determine leaf turgor. The main components of leaf water potential are (Jones, 2013);

$$\Psi = \Psi_P + \Psi_\pi$$

In which Ψ is leaf water potential, Ψ_π is the osmotic component and Ψ_p is the pressure component. The osmotic component is determined by solutes in the plant cell, while the pressure component represents the internal hydrostatic pressure of high volumes of water inside of rigid plant cell walls. It is this pressure component that maintains turgor. The pressure component can be determined by measuring leaf water potential, and then disrupting the cells of the leaf such as by freezing the leaf with liquid nitrogen and grinding the leaf with a pestle and mortar. This removes the pressure component (i.e. cell walls). Water potential can be measured again, however without the pressure component the water potential of the solutes will be measured. From these two measurements, the pressure component, and therefore leaf turgor, can be determined.

The three indices used show potential as indicators of water status, although based on measurements of leaf water potential are not able to clearly distinguish between severe water stress and well-watered plants. However, these indices have potential to be used in combination with other spectral tools, and may improve the measurement of water status, especially for low to moderate water stress.

3.5 Conclusion

As an indicator of leaf water status, the 800/550 index is sensitive to changes in water content due to changes to NIR reflection due to changes in the structural properties of a leaf. However, the 550nm wavelength is susceptible to variation from variation in reflection due to the effects of chlorophyll fluorescence and xanthophyll pigments associated with non-photochemical quenching, and in work here had a poor relationship with leaf thickness, although leaf thickness is not an absolute proxy for water content.

An analysis of the visible and NIR spectrum, to identify spectral regions sensitive to changes in leaf water content and to develop new spectral indices, identified two new indices: i) 800nm/440nm,

and ii) the index of $\frac{(800nm/665nm)}{440nm}$. These two indices are also based on the changes in the internal scattering of NIR due to leaf structural variation as a result of decreasing water content, however the reference wavelength has been modified to 440nm from 550nm. The 440nm is known within literature to be a relatively stable wavelength, with changes in reflectance at 440nm occurring when there is a severe decrease in chlorophyll content.

These indices show an ability to measure leaf water content, as a result of changes to leaf structure and the internal refraction of NIR light due to decreasing water content. All indices had a moderate relationship with leaf water potential, until leaves reached water potentials in which the leaves began to severely wilt. Further work is needed to fully establish the relationship between these indices and leaf turgor, and validate these indices as useful spectral signatures for monitoring of plant water status. This includes assessing the performance of the indices across plant species, and to present greater variation in water content and water stress, to fully assess the performance of these indices. However, the work here suggests that the indices proposed have good potential as a tool for indicating leaf water status using visible and NIR wavelengths.

Chapter 4 - Spectral toolbox to assess crop water status

4.1 Introduction

The global population is expected to increase significantly by 2050, increasing to a projected 9.6 billion from a current population of 7.2 billion, with a simultaneous increase in the number of people who are considered undernourished (FAO, 2012). To meet the increased demand for food, it is estimated that crop yields have to double by 2050, and based on current yield increases is a target that is unlikely to be met (Ray et al., 2013). Improvement in crop yields are obtained through breeding (Araus & Cairns, 2014; Faralli et al., 2019) and more recently bioengineering efforts (Kromdijk et al., 2016; Simkin et al., 2019). However, yield improvements are reliant on phenotyping for desired traits or performance, and in the case of breeding programs this involves analysing large numbers of cultivars or lines simultaneously over the course of a growing season.

Another approach to increasing crop yield is through improvements in the management of crops, such as through the optimisation of irrigation protocols and fertilizer inputs, both of which can result in large increases in crop yield (Mueller et al., 2012). Abiotic stress, such as temperature, water (Lamaoui et al., 2018) nutrient deficiency (Fageria et al., 2008), and especially nitrogen deficiency (Evans, 1989; Jin et al., 2015), can significantly affect crop yields, and management of stress conditions is an important target for improving crop yield (Fageria et al., 2008). Management of stress can also involve improving crop use of available resources, while maintaining high yields. For instance, crop nitrogen use efficiency can be optimised, allowing for improved growth in low nitrogen conditions (Ding et al., 2005; Schluter et al., 2012), but again this is also dependent on phenotyping for these desired traits.

Therefore, the ability to non-invasively measure crop water status, nitrogen content, and other factors relating to crop health and performance, is essential to improving crop yields. However,

conventional techniques can be destructive or slow, limiting the ability to measure entire crops across multiple fields. Imaging and optical based techniques, however, can perform many of these measurement rapidly and non-destructively, enabling for continuous measurement of crop health for a large number of plants or crop fields (Araus & Cairns, 2014; Liew et al., 2008; Munns et al., 2010) and key measurements of photosynthesis (Meacham-Hensold et al., 2019)

The primary focus of this work is to use optical and imaging based techniques to identify spectral signatures. Spectral signatures refer to the variation in reflected or emitted wavelengths of vegetation. Here, spectral signatures can be used to assess crop health status, through the development of a 'toolbox' of spectral techniques and measurements, that can identify not only the status of plant health but determine which stress factors, such as low water or nitrogen content, high temperatures, and any combination of factors, is effecting plant health and performance.

The work presented here will form the foundation of this spectral toolbox, focusing primarily on monitoring the spectral response to water content, upon which further work can be built upon. Techniques that can be employed in such a spectral toolbox include thermography, which has been demonstrated to have a strong relationship with stomatal conductance (Grant et al., 2006; Maes et al., 2016), chlorophyll fluorescence to provide insight into photosynthetic efficiency, and spectral reflectance to measure changes in leaf structure and pigment content.

Water status is one of the primary factors affecting plant performance (Lawlor, 2002). Stomatal conductance is a strong indicator of water status, with drought leading to ABA synthesis in roots and affecting ABA synthesis in guard cells (Bauer et al., 2013; McAdam & Brodribb, 2015), which acts as a signal for stomatal closure in leaves (Kollist et al., 2014), as well as passive hydraulic response of stomata, such as through changes in guard cell turgor (Merilo et al., 2018; Mott & Peak, 2013). However, this decrease in conductance limits gas exchange and CO_2 diffusion into the mesophyll and thus decreases intracellular CO_2 concentration, limiting the rate of carbon assimilation (Farquhar &

Sharkey, 1982). Thus, it is crucial to monitor water content to minimise the response to low water content, which will negatively affect plant growth.

Thermography is a technique that allows for remote, non-destructive measurements of stomatal conductance through the measurement of leaf temperature, from which stomatal conductance can be determined. Cooler leavers are associated with greater transpiration and stomatal conductance, due to the cooling effect of water due to water's high specific heat capacity, meaning that molecules of water can absorb large amounts of heat energy before there is a change in temperature of the water. Thus, water is capable of removing large amounts of heat energy from the environment around the molecules of water. Higher stomatal conductance means more water is transpired, and thus more heat is removed from the leaf (Jones, 2013). Due to this relationship between stomatal conductance and leaf temperature, if the highest and lowest temperatures associated with minimum and maximum stomatal conductance were known, an index can be calculated to that is proportional to stomatal conductance. Such a method has been proposed (Jones, 1999), using two reference leaves along with the leaves of interest. References covered in grease or sprayed with water represent leaves with the temperature of a leaf with theoretical minimum or maximum conductance, with grease preventing any transpiration by blocking the flow of water from the leave surface, and the spraying of water covers the leaf in a layer of water that will evaporate as if conductance was at maximum (Jones, 1999). These references allow for a value to be calculated that is proportional to stomatal conductance (Jones, 1999). This index has been shown to be a good indicator of stomatal conductance (Grant et al., 2006), although the technique is sensitive to non-ideal environmental variables such as low light or temperature (Grant et al., 2016), and further steps can be applied to the technique to obtain an estimate of actual stomatal conductance (Leinonen et al., 2006)

Another common technique for remote measurements is spectral reflectance, measuring the amount of light which is reflected from a leaf. Many wavelengths are associated with aspects of

plant physiology such as leaf structure and pigment content, and spectral indices can be derived which relate to many key measurements (Liew et al., 2008). Many indices have previously been used to assess water status, such as NDVI, PRI (Rossini et al., 2013; Suárez et al., 2008), and others (Ballester et al., 2017; Shimada et al., 2012). Some of the most commonly cited indices seen in literature are listed in Table. 4.1 in addition to other less common indices, along with indices proposed in previous chapters, that have all shown potential as indicators of water stress (Dobrowski et al., 2005; Elvanidi et al., 2017; Hernandez Clemente, et al., 2011; Shimada et al., 2012).

A common index is the water index (Peñuelas et al., 1993), exploiting the weak absorption of light near 970nm by water. Numerous indices exist for wavelengths above 900nm (Rapaport et al, 2015), which all exploit regions of strong light absorption by water. However, devices which measure above 900nm are generally more expensive than devices which only measure the visible and NIR spectrum, while visible and NIR devices are rapidly decreasing in size and cost. In addition to the practical aspects, the wavelengths above 900nm may not be required when using spectral reflectance as part of a 'toolbox' of techniques, due to the overlap between other techniques in their ability to detect water stress.

Finally, chlorophyll fluorescence is a routine technique allowing for measurements of photosynthesis through photochemical quenching, and measurements of non-photochemical quenching (NPQ) (Baker, 2008; Maxwell & Johnson, 2000; Murchie & Lawson, 2013). Photosynthetic performance is an obvious key measurement of plant health, however NPQ is also an indicator of plant stress (Ravazi et al. 2008; Sarlikioti et al., 2010; Souza, Machado et al., 2004)

The combination of imaging and optical techniques could allow for improvements over existing methodologies, for measuring and assessing plant health and the detection of plant stress (Chaerle et al., 2009). Common approaches involve the combination of spectral reflectance and chlorophyll fluorescence, for measuring water status (Schickling et al., 2016; Shrestha, Brueck, & Asch, 2012).

Adding thermography with this combination is also used (Panigada et al., 2014), as well as just chlorophyll fluorescence and thermography (Ni et al., 2015). However, in general such studies have been limited in the actual techniques used, such as; not exploring the full spectral range, using reflectance based fluorescence measurements, which while benefit remote sensing applications yields less information on photosynthetic performance compared to other chlorophyll fluorescence parameters (Baker, 2008). Away from the field, techniques have been combined together to provide a new, powerful tool for measurements in a laboratory setting, such as the combined imager developed by McAusland et al. (2013), which brings together thermography and fluorescence to image water use efficiency.

The aim of the work presented in this chapter are to assess the ability of a theoretical spectral 'toolbox', consisting of chlorophyll fluorescence, thermography and spectral reflectance, to measure the water status of two Arabidopsis ecotypes, to form the foundation of a spectral toolbox for assessing plant health. This initial work aims to use this spectral toolbox to assess plant water status. Using two ecotypes, one of which is known to be drought resistance, will help evaluate the performance and robustness of a spectral toolbox to measure the health of plants with differing physiological characteristics.

Objectives:

i) Assess the ability of a theoretical spectral 'toolbox', consisting of chlorophyll fluorescence, thermography and spectral reflectance, to measure the water status of two Arabidopsis ecotypes

ii) Identify novel spectral responses to decreases in water status

4.2 Methods

4.2.1 Growth Conditions

Two ecotypes of *Arabidopsis thaliana,* the Col-0 ecotype and the C24 ecotype, were grown. C24 was chosen due to its improved water use under droughted conditions due to a lower overall stomatal conductance (Bechtold et al., 2018; Bechtold et al., 2010), and differing leaf structure and anatomy such as a lack of visible trichromes. Pots were filled with compost (Levingtons F2S, Ipswich, UK) and the surface of pots was covered in a layer of clear plastic balls at the surface to reduce loss of soil water content through evaporation. The bottom of the pots also contained a layer of the same clear plastic balls, to reduce the amount of water and soil that was present in each pot. Plant pots were prepared to ensure the exact same weight of materials was used.

Both ecotypes were grown in a PlantScreen (PSI, Drasov, Czech Republic) automated phenotyping platform. The platform consists of a growth chamber and a measuring chamber. A conveyor system in the platform allows for trays of plants to be transported between chambers. The conveyor system also transports the trays to scales that are used to automatically weigh each pot, calculate how much water is required and water each pot from above until the desired weight is reached. The weight of the pots at 0% soil relative water content (RWC) was determined by taking a sample of prepared pots, and drying them in an oven at 80 °C. The average dry weight of these pots was used as the weight for 0% soil RWC. The weight for pots at 100% soil RWC was determined by watering plants to saturation, ensuring there were no water drops falling from the base of the pots.

Light levels were set to 200 µmol m^{-2} s^{-1}, and controlled automatically to provide nine hours of light each day. Automated watering occurred before the lights were turned on, and after they were switched off. Once the plants had reached a sufficient size, with at least three leaf layers, each ecotype was separated into three different watering regimes over a period of 18 days. One regime would be watered to 80% soil relative water content (RWC), the second to 50% soil RWC, and the

final group 20% soil RWC. Due to the improved performance under drought conditions of C24, 80% soil RWC was not used for C24.

Temperature of the growth environment was set to 21 °C, with humidity regulated to maintain 60% relative humidity.

4.2.2 Chlorophyll Fluorescence

Chlorophyll fluorescence was measured using a Hansatech FMS-2 (Hansatech, Cambridge, UK), which was setup immediately beside the phenotyping platform. The fibre optic and leaf clip of the FMS-2 was attached to a leaf and measurements were taken for each plant. For light adapted measurements, the FMS-2 provided 200 μmol m^{-2} s^{-1} of actinic light.

In the morning, prior to the turning of lights in the growth chamber, dark adapted fluorescence parameters of F_v/F_m were measured. The parameter of F_m was recorded, which is required to calculate NPQ (Baker, 2008; Murchie & Lawson, 2013). Light adapted measurements of F_q'/F_m' and NPQ were collected one hour after chamber lights were turned on. The FMS-2, providing a saturating pulse of 6000 μmol m^{-2} s^{-1} was used to measure the operating efficiency of PSII (F_q'/F_m') and non-photochemical quenching (NPQ).

4.2.3 Thermography

The index of stomatal conductance (I_g) (Jones, 1999) was calculated from thermal imagery. This index uses a wet and dry reference to calculate the temperature of references with theoretical minimal and maximal stomatal conductance.

A FLIR A655SC (FLIR Systems, Oregon, USA) was integrated into the phenotyping platform, located within the measuring chamber. Measurements were performed at the same time window each day, three hours after lights were turned on. Prior to measurements, two Arabidopsis plants that were not used in the experiment were placed among measured plants, to be uses as wet and dry references. For the wet reference, one plant had its leaves sprayed with water. For the dry

reference, the other plant had leaves that were covered in Vaseline. All measurements were taken under an ambient light of 200 μmol m^{-2} s^{-1}. Upon the spraying of the wet leaf, one minute was allowed to pass to allow temperatures to equilibrate to the environment, and thermal images were captured. Temperature data was extracted from thermal images using the *FLIR Tools* software package (FLIR Systems, Oregon, USA), and I$_g$ calculated as per Eqn. 4.1, as defined by Jones (1999).

$$I_g = \frac{(T_{leaf} - T_{wet})}{(T_{dry} - T_{leaf})}$$

4.1

With T$_{leaf}$ being leaf temperature, T$_{wet}$ the temperature of the wet reference leaf, and T$_{dry}$ the temperature of the dry reference leaf.

4.2.4 Reflectance

Spectral reflectance measurements were collected *in situ* with a FLAME-S Spectrometer (Ocean Optics, USA), and a Reflection Probe fibre optic (Ocean Optics, USA). This fibre optic provided illumination and collected reflected light. Reflectance was measured from 400nm up to 850nm. A tungsten bulb provided illumination, with around 198 μmol m^{-2} s^{-1} of light reaching the sample through the fibre optics. The bulb was powered by a separate regulated power supply. A fan was fitted at the rear of the bulb to regulate generated heat. A leaf clip was constructed to enable a fixed geometry between the probe end of the fibre optic and the plane of the sample, which was sprayed with matt black paint to reduce reflection within the leaf clip. A Spectralon reflectance standard (WS-1, Ocean Optics, USA), which has 99% diffuse reflectance. OceanView software (Ocean Optics, USA) was used to calculate % reflectance based on the reflectance of the spectralon reflectance standard under darkness and full light. Integrating time was set to ensure that peak intensity was at approximately 80% of the maximum intensity measurable by the spectrometer, as recommended by the manufacturer. Bin width on the OceanView software was set to a value of 6 to reduce noise, which averages the intensity over six pixels of the spectrometer. Spectral indices were calculated as

per Table 4.1, listing indices which have been described in literature as suitable for measuring water content, and are calculated using only visible and near-infrared light.

Table 4.1 Spectral Indices for assessing leaf water status, and their formulation. R[Wavelength] denotes reflectance at that wavelength (nm).

Index	Formula	Reference
NDVI	(R720-R620)/(R720+R620)	*See: Chapter 2*
mrNDVI	(R750-R705)/(R750+R705-2*R445)	(Sims & Gamon, 2002)
ND$_{Shimada}$	(R490-R620)/(R490+R620)	Shimada et al., 2012
NDWI$_{Green}$	(R800-R550)/(R800+R550)	*Chapter 3*
PRI	(R531-R570)/(R531+R570)	(Gamon, Peñuelas, & Field, 1992)
PRI$_{570-515}$	(R570-R515)/(R570+R515)	(Hernandez Clemente et al., 2011)
PRI$_{560-610}$	(R560-R610)/(R560+R610)	(Elvanidi et al., 2017)
800/550	R800/R550	*Chapter 3*
800/440	R800/R440	*Chapter 3*
(800/665)/440	(R800/R665)/R440	*Chapter 3*
740/800	R740/R800	(Dobrowski et al., 2005)
690/600	R690/R600	(Dobrowski et al., 2005)

A computer script was written using R (R Core Team, 2017) to iterate through the reflectance of every wavelength from 400nm up to 900nm, and divided each of these wavelengths (*Wavelength X*) by the reflectance of every wavelength from 400nm up to 900nm (*Wavelength Y*). This generated an array of every combination of *X/Y* using all wavelengths from 400nm to 900nm. Each generated *X/Y* index was correlated to either soil RWC or leaf RWC, producing an R^2 value describing the relationship between the two variables. A heatmap was generated that plotted the array of R^2 for every index, for both soil RWC and leaf RWC.

4.2.5 Gas Exchange and Physical Measurements

An CIRAS-2 (PP Systems, Amesbury, MA, USA) infra-red gas analyser (IRGA) was used to collect gas exchange data under ambient conditions of 21°C and 60% relative humidity. The CIRAS-2 CO_2 inlet was connected to a carboy via a bung. The bung also contained an air inlet into the carboy. The carboy acts to buffer CO_2 concentration, preventing large spikes or drops in CO_2 concentration. Leaf angle when in the CIRAS-2 chamber was maintained to be horizontal to above lights. Leaf area was calculated by imaging plants in the CIRAS-2 chamber and measuring in Fiji (Schindelin et al., 2012).
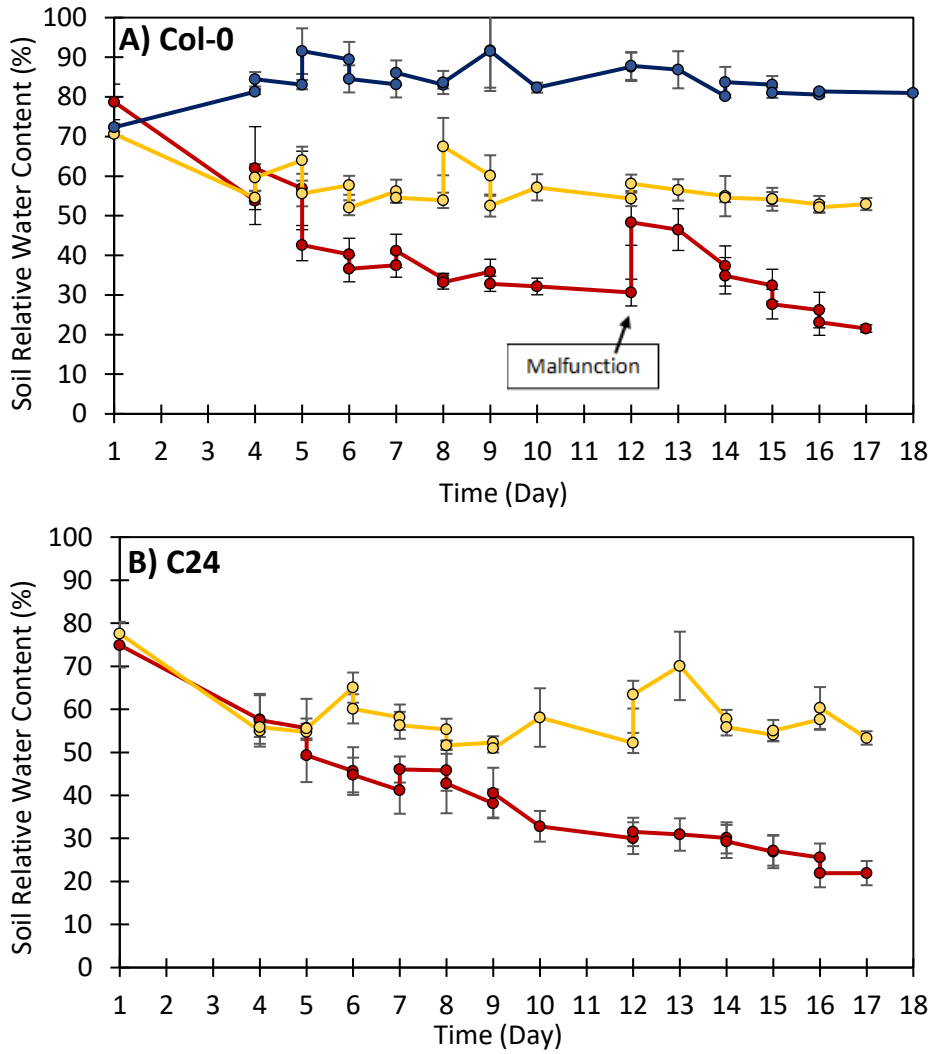
Leaf relative water content (RWC) was measured by collecting leaves at midday and weighing the fresh weight. Leaves were then placed into a universal tube, with the water covering approximately 1cm of the base of the leaf. Leaves were left for 4 hours, before weighing again. After weighing, leaves were placed in an oven (80°C) overnight.

4.3 Results

4.3.1 Plant Water Status

The soil RWC for Col-0 can be seen Fig. 4.1 A. The length of time required for soil RWC to reach 50% was five days (Fig. 4.1 A), while it took seventeen days to reach 20%. The 20% soil RWC treatment for Col-0 was unfortunately affected by a malfunction of the phenotyping platform, which overwatered the plants on day 12, from 30% up to around 50% soil RWC (Fig. 4.1 A), before taking 5 days to drop down to 20%. The soil RWC for C24 can be seen Fig. 4.1 A, and a similar length of time was required to reach 50% and 20% soil RWC, of five and seventeen days respectively.

Leaf RWC taken at the end of the experiment showed no significant difference between 80% and 50% RWC for Col-0, however the Col-0 20% treatment was significantly lower with a leaf RWC of just under 77% (Fig. 4.2) (P < 0.001). The C24 ecotype shower a trend of a lower leaf RWC for the 20% treatment, but this was not significant.

Figure 4.1 Daily relative water content (RWC) of the soil, as measured gravimetrically by the conveyor system, showing the actual soil RWC experienced by *Arabidopsis thaliana* under 200 μmol m^{-2} s^{-1}. Days with two measurements show the RWC for plant pots weighed in the morning and in the evening, with the higher values of the two being the evening weight. A watering malfunction is shown that overwatered the Col-0 20% RWC treatment. **(A)** The RWC for three treatments of Col-0. **(B)** The RWC for two treatments of Col-0. Blue (•) is 80% target RWC, Yellow (•) is 50% target RWC, and Red (•) is 20% target. n=10, error ± S.E.
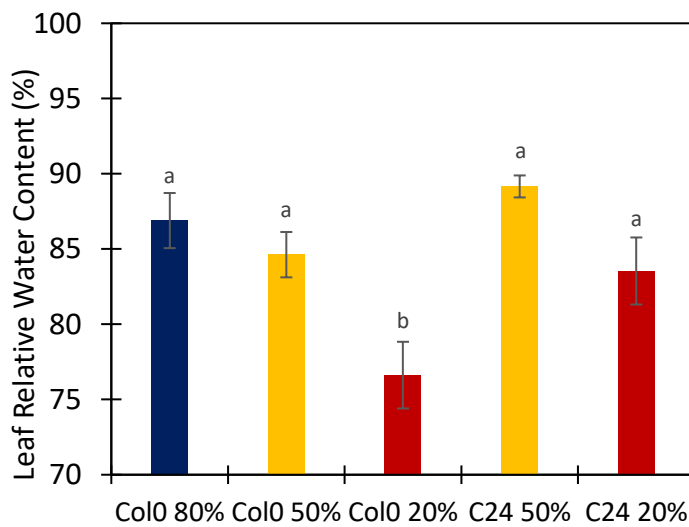
Figure 4.2 Leaf RWC measured at the very end of the experiment on day 18 (•) 80% Soil RWC, (•) 50% Soil RWC, (•) is 20% Soil RWC. (n=5) Error ± S.E
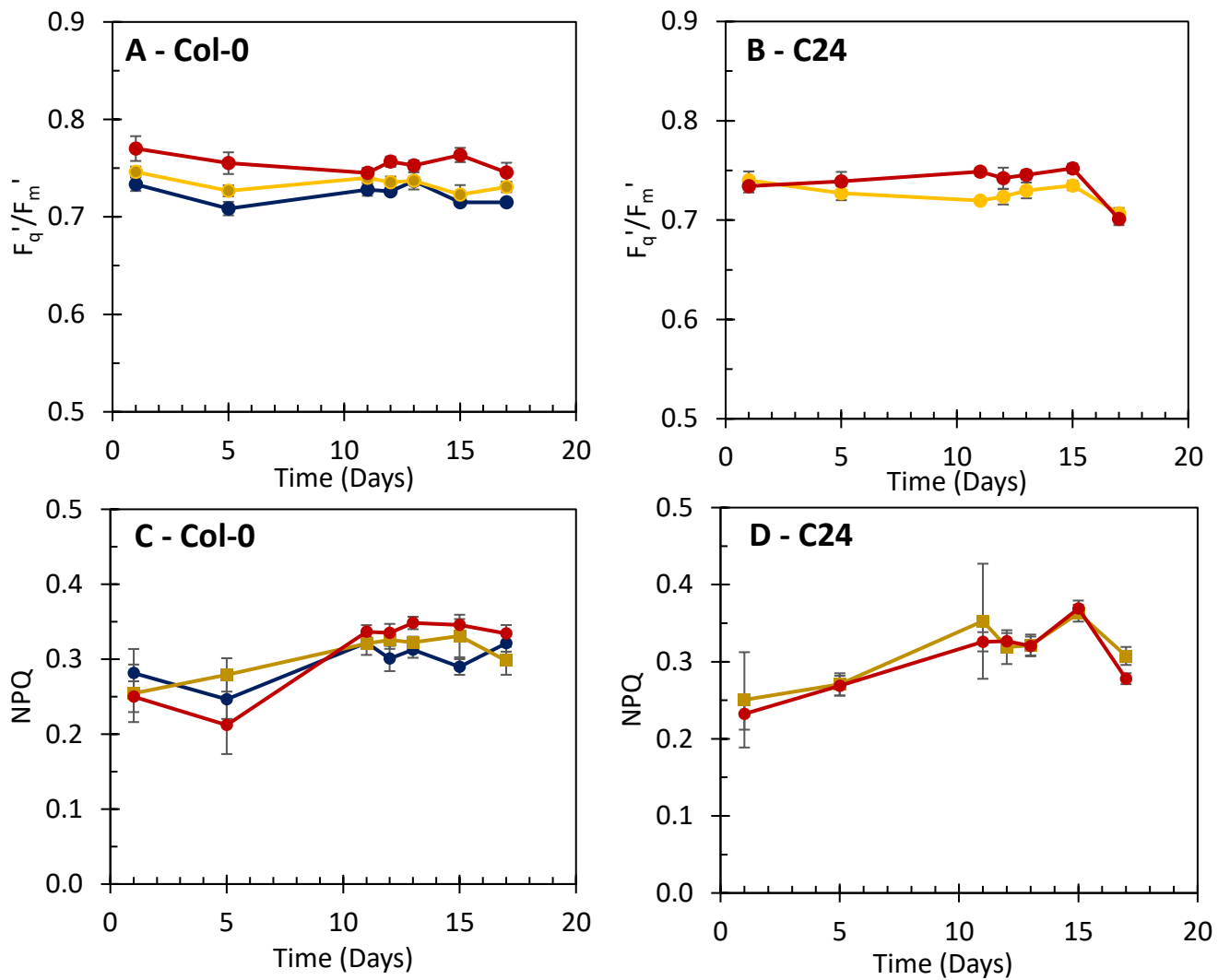
4.3.2 Chlorophyll Fluorescence

There was no effect of water treatment on measurements of chlorophyll fluorescence in either Col-0 or C24 (Fig. 4.3), with values for F_q'/F_m' between 0.72 to 0.76 in all plants measured (Fig. 4.3 A & B). Likewise, the same was observed for NPQ with values remaining at around 0.3 for all treatments and both ecotypes (Fig. 4.3 C & D). However, a negative relationship ($R^2 = 0.4$) between NPQ and soil RWC (Fig. 4.4 A) was observed, although no relationship between soil RWC and F_q'/F_m' was found (Fig. 4.4 B).

4.3.3 Thermography

The index of stomatal conductance (I_g) showed a strong positive relationship with stomatal conductance (Fig. 4.5). As a tool for assessing plant health, I_g demonstrated sensitivity to water status in Col-0, showing significant differences between treatments (Fig. 4.6 A). As mentioned previously, the water content for the 20% RWC treatment on Day 12 for Col-0, temporarily increased up to 48% (Fig. 4.1 A) due to a malfunction of the automated watering system. This increase in water content was mirrored by measurements of I_g, with I_g for the 20% Col-0 treatment increasing from 0.5 up to 1.15 immediately after the increase in RWC from 30% up to 50% between Day 13 and Day 16 (Fig. 4.6A). Plotting the relationship between soil RWC and I_g for Col-0 shows a positive relationship ($R^2 = 0.49$).

C24 showed an overall lower I_g than Col-0, with an I_g between 0.2 and 0.6 for C24 compared to values from 0.4 up to 1.8 for Col-0. However, overall there was no difference in I_g between water treatments for the C24 ecotype (Fig 4.6B) except for final day, although there was a trend for higher conductance for the 50% treatment towards the end of the experiment. There was a poor correlation between I_g and RWC for C24 due to an overall lower and consistent range of I_g values (Fig. 4.7B)

Figure 4.3 Chlorophyll fluorescence parameters for the operating efficieny of PSII (F_q'/F_m'), a measure of the actual fraction of light being used for photosynthesis, and non-photochemical quenching (NPQ) For all figures, Blue is 80% target RWC, Yellow is 50% target RWC, and Red is 20% target **(A)** F_q'/F_m' of the Col-0 ecotype. **(B)** F_q'/F_m' of the C24ecotype **(C)** NPQ of the Col-0 ecotype **(D)** NPQ of the C24 ecotype. (●) 80% Soil RWC, (●) 50% Soil RWC, (●) is 20% Soil RWC. n=10, error ± S.E.
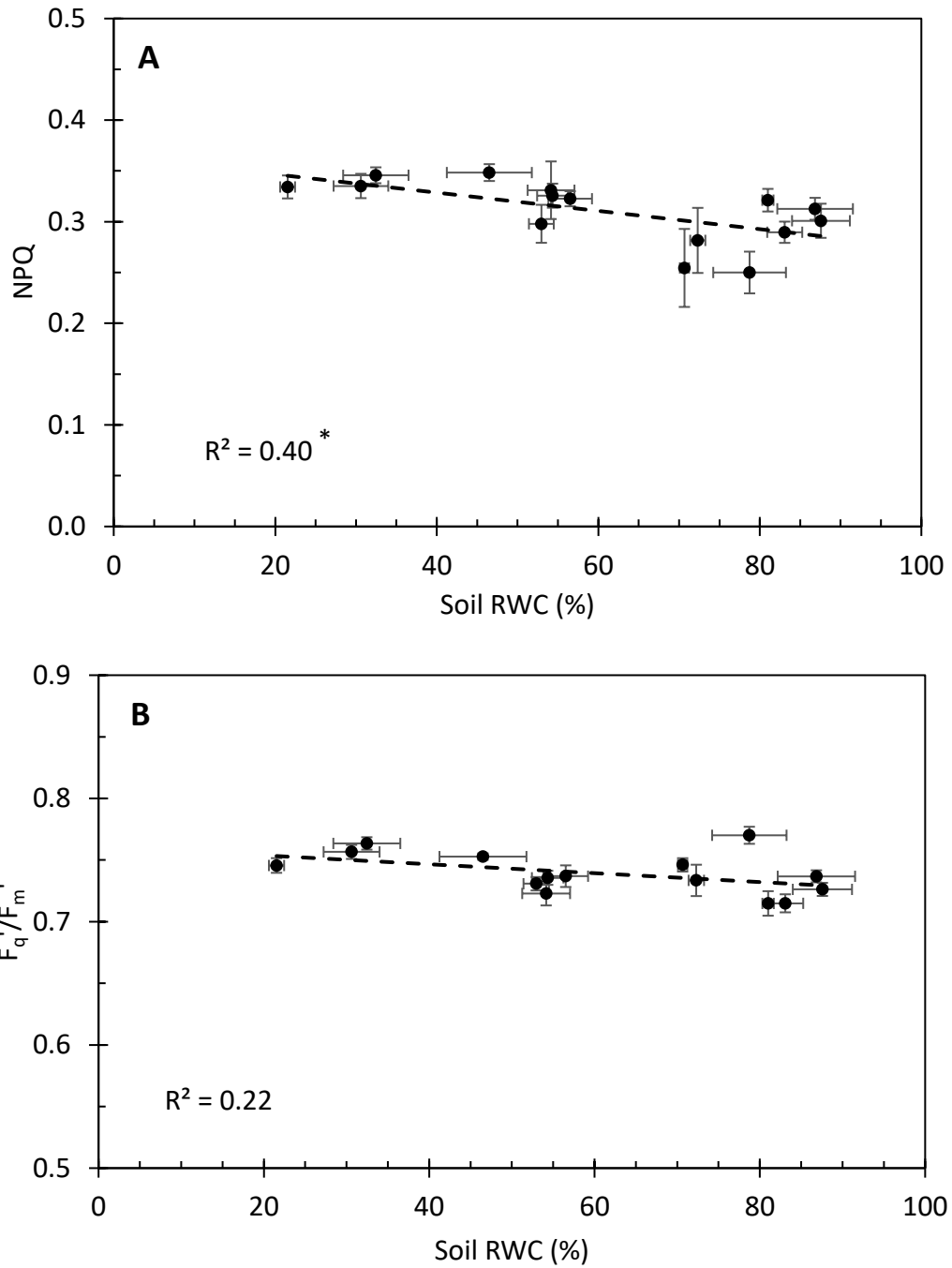
Figure **4.4** Relationship between soil relative water content (RWC) and chlorophyll fluorescence parameters of **A)** Non-photochemical Quenching (NPQ) and **B)** PSII operating efficiency (F_q'/F_m') , for *Arabidopsis* Col-0 ecotypes. n=10, error ± S.E. * = p < 0.05

$R^2 = 0.85*$
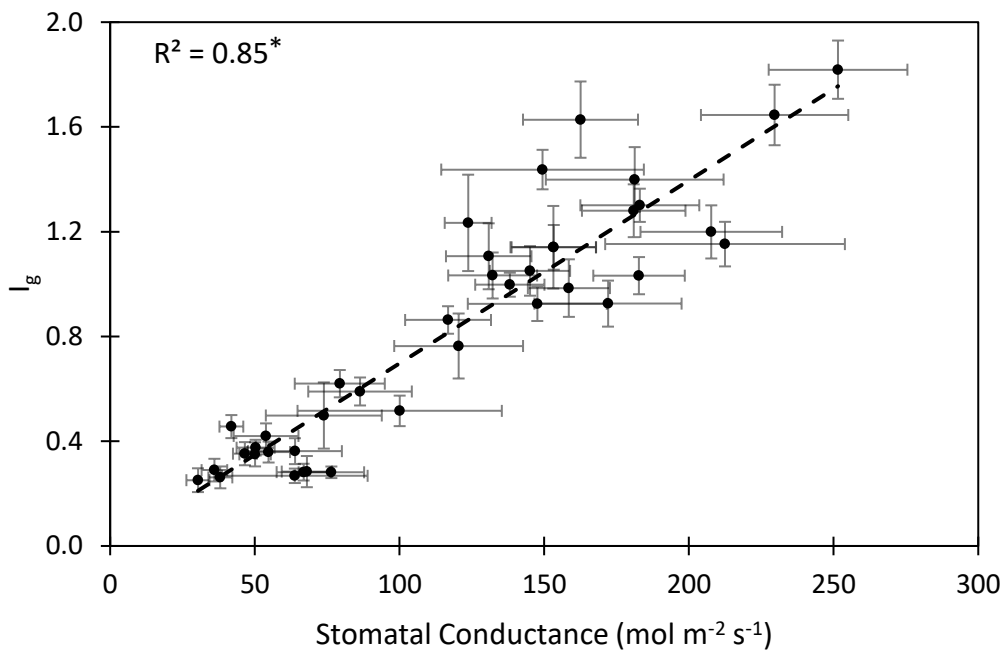
Figure 4.5 Average stomatal conductance and the index of stomatal conductance (I_g) for all treatment and ecotypes, demonstrating the strong relationship between I_g, a proxy for stomatal conductance, and measured using thermography with wet and dry reference leaves and actual stomatal conductance. n=10, error ± S.E.
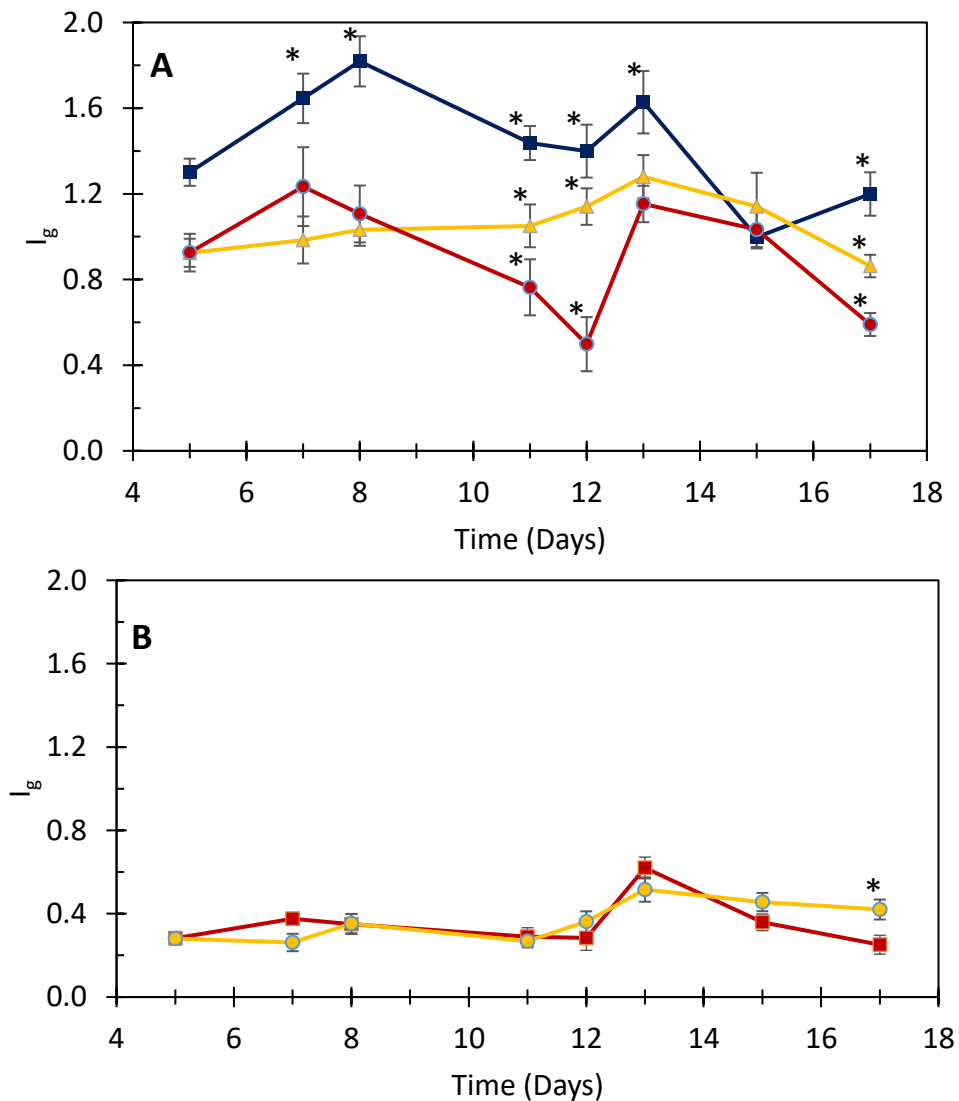
Figure 4.6 Index of Stomatal Conductance (I_g), a proxy for stomatal conductance. Blue is 80% target RWC, Yellow is 50% target RWC, and Red is 20% target RWC. **(A)** I_g for the Col-0 ecotype **(B)** I_g for the C24 ecotype. (●) 80% Soil RWC, (●) 50% Soil RWC, (●) is 20% Soil RWC. n=10, error ± S.E. * = $p < 0.05$, significantly different to other treatments on the same day

Figure 4.7 Index of Stomatal Conductance (I_g), a proxy for stomatal conductance. **(A)** I_g for the Col-0 ecotype **(B)** I_g for the C24 ecotype. (●) 80% Soil RWC, (●) 50% Soil RWC, (●) is 20% Soil RWC. n=10, error ± S.E.

4.3.4 Reflectance
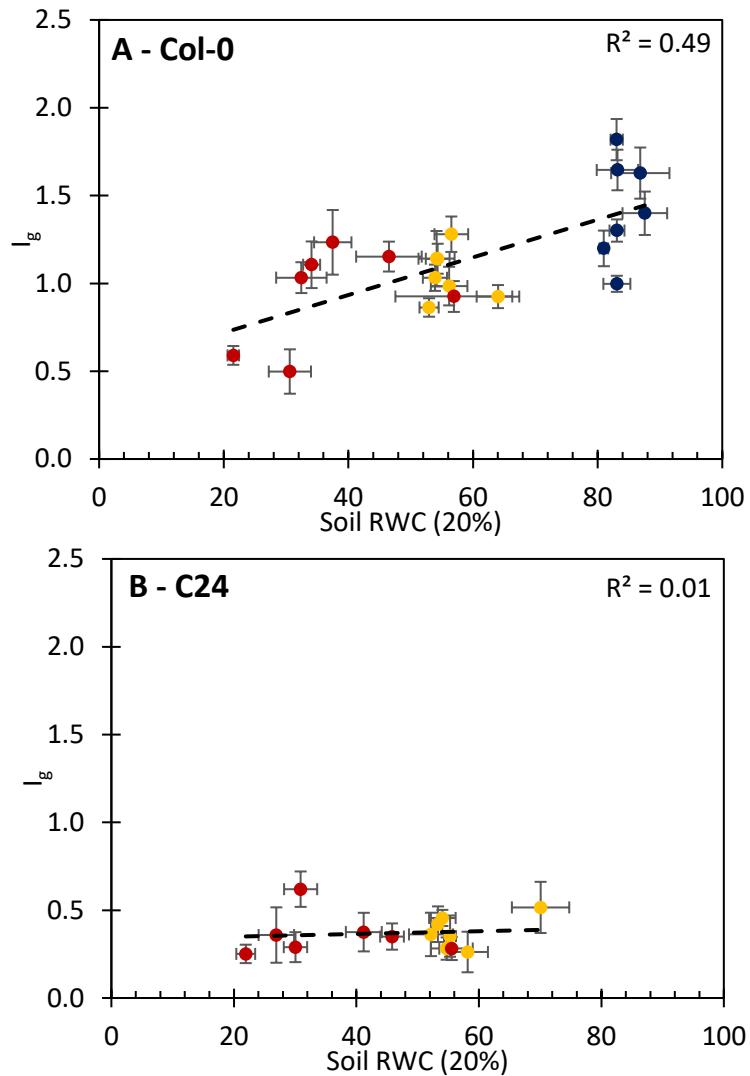
There was in general a poor correlation found between all investigated spectral indices and both leaf and soil RWC (Table 4.2). Some indices (e.g. mrNDVI) did demonstrate a weak relationship to leaf RWC, or soil RWC (e.g. $PRI_{560-510}$) (Fig. 4.8), however overall a good relationship between leaf and soil RWC and spectral indices was not found.

An assessment to identify spectral regions sensitive to water status through the calculation of a simple ratio, showed only poor correlations between calculated spectral measurements and soil RWC (Fig. 4.9 A), and leaf RWC (Fig. 4.9 B), with the best correlation between calculated indices and soil RWC being wavelengths from 612nm up to 617nm (e.g. 617nm/614nm, R^2 = 0.395). With regards to leaf RWC, it appears as though NIR wavelengths are more sensitive to leaf water content, with the highest R^2 seen for leaf RWC being 0.78 for the ratio of 831nm/814nm, demonstrating the sensitivity of NIR to leaf water content.

Table 4.2 Coefficient of determination (R^2) for the relationship between calculated spectral indices, and RWC for Col-0 *Arabidopsis.* * = $p < 0.05$

Index	Soil RWC	Leaf RWC
NDVI	0.04	0.05
mrNDVI	0.01	0.27*
ND$_{Shimada}$	0.18	0.08
NDWI$_{Green}$	0.16	0.16
PRI	0.01	0.08
PRI$_{570-515}$	0.14	0.01
PRI$_{560-510}$	0.22*	0.02
740/800	0.22*	0.19
690/600	0.13	0.01
800/550	0.18	0.16
800/440	0.05	0.00
$\frac{(800/665)}{440}$	0.02	0.00
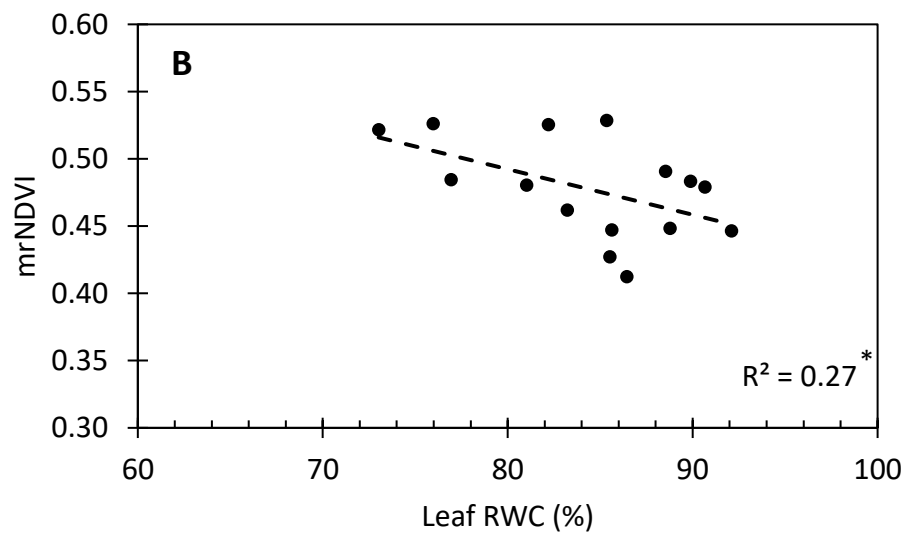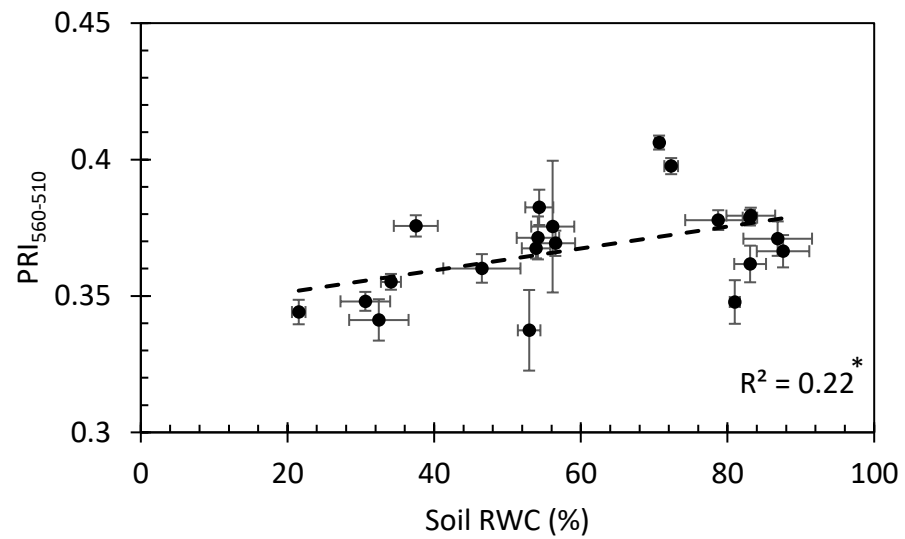
Figure **4.8** Relationship between **A)** the spectral reflectance based index of PRI$_{560\text{-}510}$ and soil relative water content (RWC) for Col-0 *Arabidopsis*, n=10, error ± S.E **B)** Individual measurements of mrNDVI and Leaf RWC, for the individuals in which leaf RWC measurements were collected. * = p < 0.05
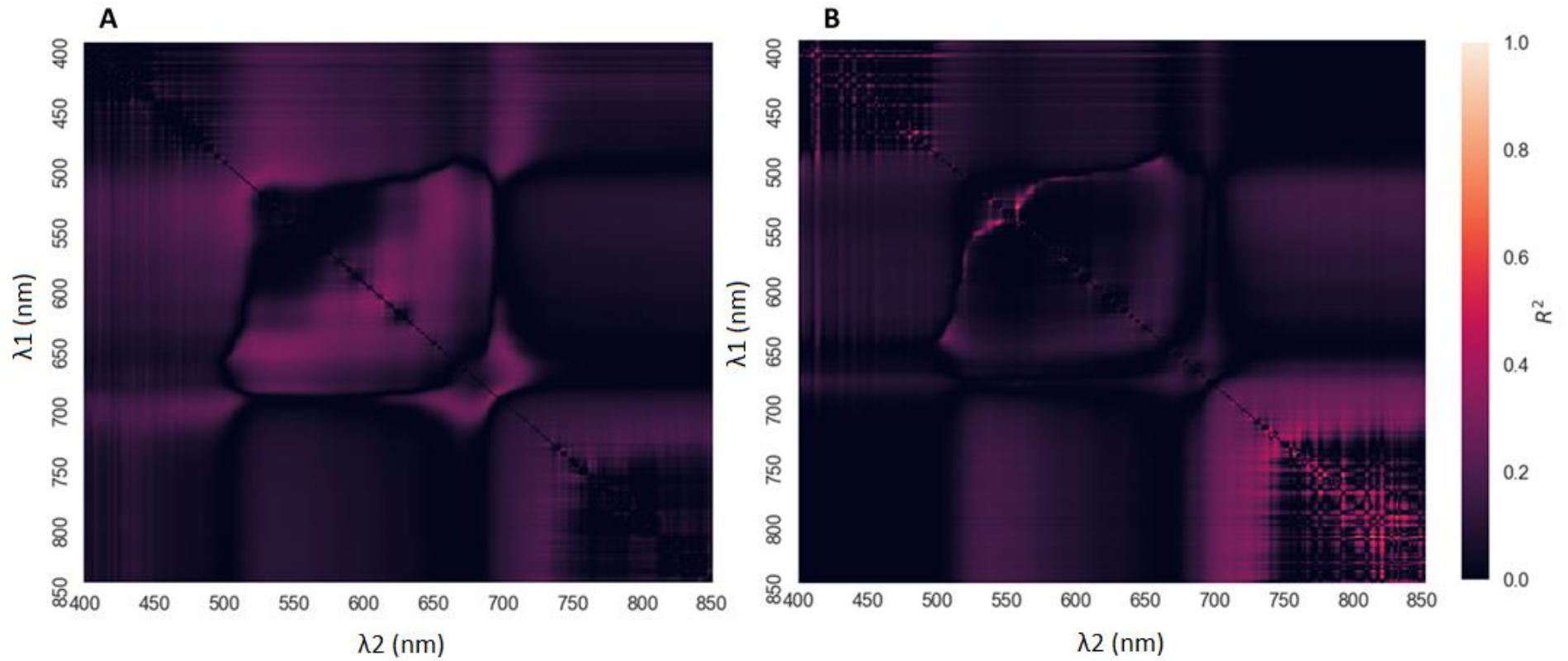
Figure 4.9 A heatmap for every variation of a simple ratio vegetation index, calculated as λ1 divided by λ2. Each combination shows a colour corresponding to the coefficient of determination (R^2) between each index and either **(A)** soil relative water content, or **(B)** leaf relative water content.
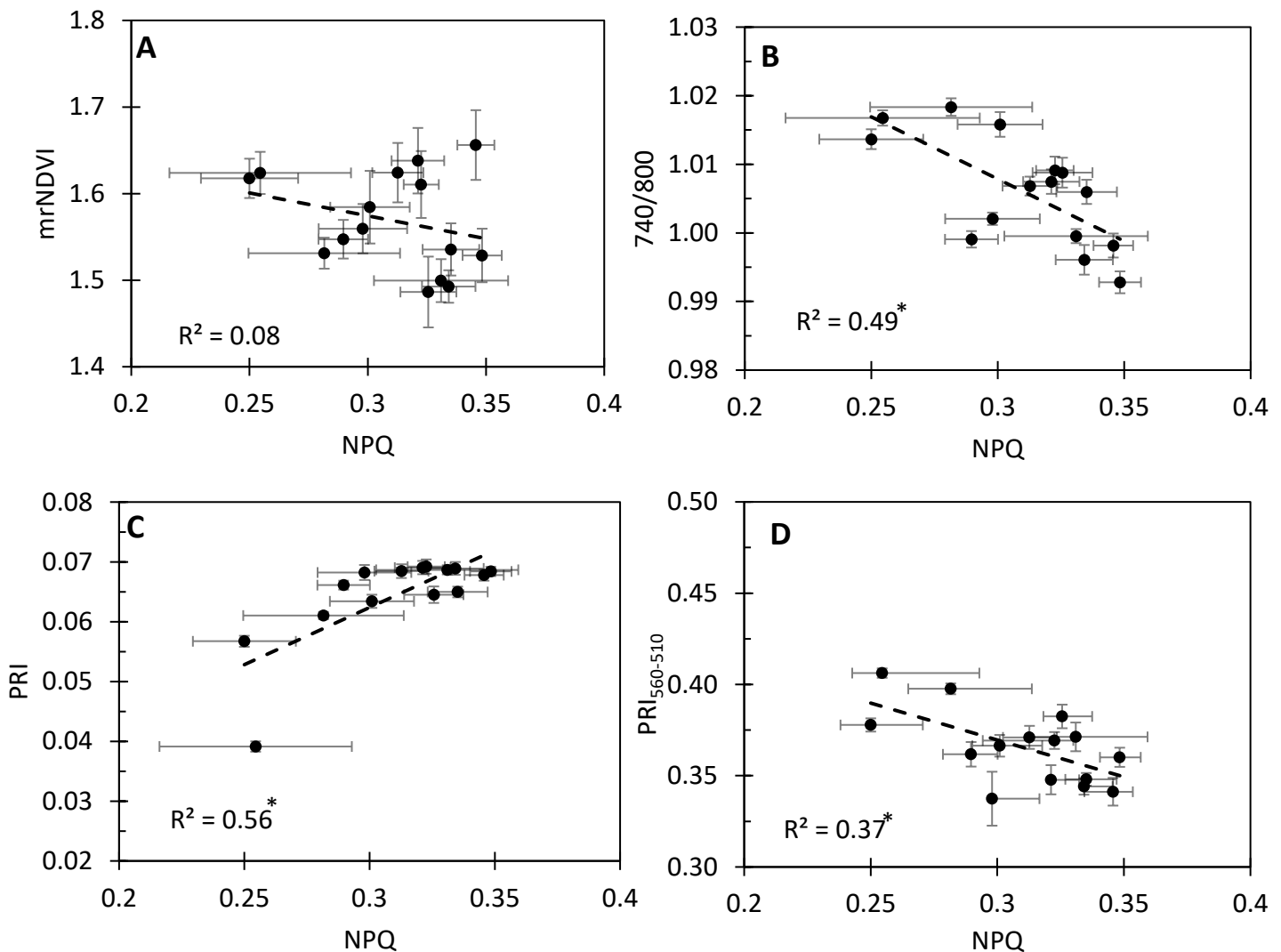
Figure 4.10 Relationship between non-photochemical quenching (NPQ) and spectral reflectance indices of **A)** mrNDVI **B)** the simple ration of 740nm/800nm **C)** the photochemical reflectance index (PRI) **D)** PRI using wavelengths of 560nm and 510nm. n=10, error ± S.E. * = $p < 0.05$

4.3.5 Relationship between spectral measurements

Both NPQ and the spectral indices of mrNDVI, $PRI_{560-510}$ and 740/800 showed some sensitivity to changes in water content. Therefore, the relationship between NPQ and these indices was investigated (Fig. 4.10). The indices of PRI, $PRI_{560-510}$ and 740/800 all demonstrated some degree of a relationship to NPQ, with PRI showing the best relationship ($R^2 = 0.56$). The index mrNDVI, which demonstrated the best relationship to leaf RWC, here was poorly related to NPQ ($R^2 = 0.08$).

4.4 Discussion

The malfunction resulting in accidental watering of the 20% soil RWC treatment provided a good opportunity to observe the sensitivity of thermography to soil water content. As the I_g index is proportional to stomatal conductance, as seen both here and in literature (García-Tejero et al., 2016; Pou et al., 2014), I_g can be used to monitor the response of stomatal to water content, and the recovery of stomata in response to re-watering (Miyashita et al., 2005). As stomatal conductance is a major factor affecting carbon assimilation, and environmental factors such as low water content can desynchronise the relationship between carbon assimilation and stomatal conductance (Lawson & Vialet-Chabrand, 2019), the monitoring of stomatal conductance to minimise the risk of low water content and subsequent remedial treatment to ensure stomatal recovery by re-watering crops in the field, will be beneficial as a tool for precision agriculture and improving crop management.

Thermography measurements here were conducted in a relatively stable environment, namely with light levels remaining constant. However, in the field, environmental factors will be highly variable, and thus thermography measurements will be hugely affected (Grant et al., 2016; Jones, 2002). For instance, plants will exhibit lower conductance values on cloudy days regardless of water status due to lower solar radiation (Maes & Steppe, 2012; Prashar & Jones, 2014), and the difference between plants with differing water status may be minimal or in some cases non-existent. Therefore, under some circumstances it can be difficult to assess water status through thermography alone, unless environmental factors such as temperature, humidity, and lighting conditions, which all affect stomatal response, are also taken into account. The index of stomatal conductance, which uses wet and dry references, inherently accounts for some of the effect of variable environment on the technique itself (Prashar & Jones, 2014), so it is predominantly the stomatal response to environment that affects resulting measurements. These variables are not only factors to consider on a day-by-day basis, but diurnally throughout the course of a day as the time of day plays a key

role in thermography derived measurements, and should be factored into any data collection to ensure comparable measurements are obtained. Midday measurements generally prove to be optimal, as evaporative demand is at its greatest (García-Tejero et al., 2016; Grant et al., 2016).

Chlorophyll fluorescence measurements of F_q'/F_m' and NPQ have been linked to water status (Sarlikioti et al., 2010; Souza et al., 2004). Stomatal closure due to reduced water content can limit CO_2 availability for carbon assimilation, and thus lower consumption of ATP and NADPH, reducing the sink for end products of electron transport, resulting in a decrease in electron transport rate and a build up of potentially damaging excitation energy in photosystems that needs to be dissipated through NPQ processes to prevent the generation of radical oxygen species (Baker & Rosenqvist, 2004; Flexas et al., 1999; Gollan et al., 2017; Murchie & Lawson, 2013). However, photorespiration, which occurs when the availability of O_2 becomes increasingly greater than available CO_2, can also act as a sink for electron transport (Peterhansel et al., 2010). As a result, most effects due to water status on chlorophyll fluorescence are experienced when leaf water stress is below 80% (Sarlikioti et al., 2010).

Yet only one treatment in this experiment (Col-0 20% Soil RWC) reached a leaf RWC below this value. Decreases in F_q'/F_m' are associated with the onset of more severe drought (Baker & Rosenqvist, 2004; Hazrati et al., 2016). For instance, despite seeing stomatal closure (Fig. 4.6), there was no major effect on chlorophyll fluorescence parameters as there was no significant difference between treatments (Fig. 4.3), consistent with what is seen in literature showing little change in F_q'/F_m' due to mild drought stress, as a result of photorespiration maintaining electron transport rates despite decreases in CO_2 assimilation (Baker & Rosenqvist, 2004; Flexas et al., 2002). Thus, the relationship between F_q'/F_m' and soil RWC was poor (Fig. 4.4 B).

There was however, a trend for NPQ to increase as soil RWC decreased (Fig. 4.4 A). Interestingly, the spectral indices of PRI$_{560-510}$ and PRI$_{570-515}$, showed a weaker relationship to soil RWC than NPQ (Table 4.2), even though PRI indices are associated with NPQ through the xanthophyll cycle, a component

of NPQ. De-epoxidation of the pigment violaxanthin to zeaxanthin, which alters the absorption of light at specific wavelengths by the pigment, increases under increased protonation of the thylakoid membrane, which occurs when water content decreases (Baker, 2008; Gamon et al., 1992). However, as the PRI is a measurement of the epoxidation state of the xanthophyll cycle, other NPQ components which also contribute to dissipation of excitation energy, such as the conformation change of PSII and the PsbS protein, will affect the relationship between PRI and NPQ measurements (Sukhova & Sukhov, 2018)

Visible and NIR wavelengths up to 900nm are generally considered a poor indicator of water status, although spectral indices such as PRI are associated with water status (Ballester et al., 2017; Sarlikioti et al., 2010; Suárez et al., 2008), and was one of the better performing indices here. Initially it appears as though the better performing spectral indices are predominantly related to NPQ (Fig. 4.10), which is unsurprising as many of these indices (e.g. PRI) are designed to relate to NPQ (Dobrowski et al., 2005). However, PRI had a very poor relationship to leaf (R^2 = .08) and soil RWC (R^2 = .01, Table 4.2) but the strongest relationship with NPQ, which suggests that it is not solely the relationship with NPQ that is driving these spectral indices. Although, Sarlikioti et al., (2010) note that PRI is poorly correlated with RWC when PPFD is below 700 μmol m^{-2} s^{-1}, as was the case in this experiment, in addition to other factors that affect PRI such as plant structure and other optical properties. The index of mrNDVI showed no relationship to NPQ, and thus this index appears to be sensitive to other aspects of physiology, most likely leaf structure due to the use of NIR wavelengths in the calculation of the index. The sensitivity of NIR to leaf RWC (Fig. 4.7B) out of all the spectral regions investigated is consistent with what is seen in the literature due to the effects of water content on leaf structure (Lisar et al., 2012), and the sensitivity of NIR wavelengths to leaf structure (Slaton et al., 2001). However, the overall poor performance of spectral indices seen in this experiment is likely due to the lack of sufficient water deficit experienced (Fig. 4.1, 4.2), due to factors such as the water retaining properties of the soil, volume of soil used, and the system error resulting in the re-watering of the 20% Col-0 treatment.

Other spectral indices using wavelengths above 900nm (Peñuelas et al., 1993), are associated with good performance in measuring leaf water content. However, these techniques are limited by the high price of equipment due to the need for additional sensors on the spectrometer. The ability of thermography to measure stomatal conductance, and increasingly more indices in the visible-NIR spectrum that can assess water status (e.g. Shimada et al., 2012), diminishes the need for these indices.

The overall insensitivity of spectral reflectance in the visible and NIR regions seen here due to insufficient water stress, may actually be beneficial for the development of a spectral toolbox. For instance, a measurement using a toolbox of chlorophyll fluorescence, thermography and spectral reflectance on a plant with sub-optimal water availability, may demonstrate only a negligible response in spectral reflectance indices, while other techniques that are more sensitive to water status may respond accordingly, such as the decline in stomatal conductance as measured by thermography (Fig. 4.7). Thus, the overall response of all techniques will indicate that there is sub-optimal water availability but not yet any onset of water stress, with the negligible change in the values of the spectral indices or chlorophyll fluorescence parameters indicating no effect on plant pigment content or photosynthetic performance.

Other stressors, for example nutrient limitation, may also affect certain spectral reflectance indices and chlorophyll fluorescence in addition to stomatal conductance (Chappelle et al., 1984; Davenport et al., 2005), which is a spectral signature different to the one described for sub-optimal water availability, which only affects stomatal conductance.

Spectral techniques have clear benefits over alternative techniques for assessing water status. Conventional techniques such as soil water measurement, destructive sampling of leaf RWC, or the use of infra-red gas analysis (IRGA) for measurements for stomatal conductance and photosynthesis, are limited by a bottleneck of speed for measurement and throughput. The use of spectral techniques as a tool to decrease this bottleneck includes the considerable effort in obtaining key

photosynthetic measurements, such as the maximum rate of carboxylation (VC_{max}), through spectral techniques in place of conventional IRGA devices (Ainsworth et al., 2014; Meacham-Hensold et al., 2019; Serbin et al., 2012), which can rapidly speed up the daily throughput of photosynthetic measurements.

Spectral techniques are a crucial component of precision agriculture (Zhang & Kovacs, 2012), allowing farmer to optimise growth conditions for their crops, identify the onset of biotic and abiotic stress sooner, and enable precise remedial action with variable inputs over blanket treatments of water, fertilizer or pesticides and herbicides (Chang et al., 2005; Shanahan, 2001). This can reduce the costs of growing crops, while maximising yields.

Thus, the spectral characteristic of an initial decline in water content, can be defined by a decrease in stomatal conductance, and an increase in NPQ. Spectrally, the indices of $PRI_{560\text{-}510}$ and 740/800 will begin to trend towards a decrease in measured values, and mrNDVI will trend towards an increase, as soil and leaf RWC decreases. More prolonged periods of low water availability may elicit further physiological responses that will affect both spectral reflectance and chlorophyll fluorescence, such as a decrease in the operating efficiency of PSII and further increases in non-photochemical quenching

4.4.1 Development of a Spectral Toolbox for assessing plant health

The results of this experiment can be used to begin building a spectral toolbox, for assessing plant health (Fig. 4.11).

While the results of the experiment here show no effect on F_q'/F_m and a small increase NPQ due to soil RWC, generally decreases in F_q'/F_m', increase in NPQ, and subsequent decrease in PRI, are associated with moderate to severe water stress (Sarlikioti et al., 2010; Shahenshah & Isoda, 2010). However, information beyond what has been seen in this experiment has not been included in the spectral toolbox or Fig. 4.11 at this stage.

A factor to consider regarding the use of a spectral toolbox, are the range of values that are expected. For instance, here Col-0 and C24 had vastly different stomatal conductances under normal well-watered conditions (Fig. 4.6, 4.7), with the values for healthy C24 at a similar range as Col-0 with low soil RWC. If this was a crop in the field for instance, and ecotype or variety was not accounted for, this would falsely lead to the assumption that the crops were experiencing low water content, when in fact they were not, and therefore would be at risk of being over watered.

As further experimental work is performed with the spectral toolbox, the results from that work can be added to expand the library of spectral responses (Fig. 4.11).

Chlorophyll Fluorescence

F_q'/F_m' : No change
NPQ : Small increase

Decreasing water availability

Spectral Reflectance

➢ No significant change in indices
➢ Decrease $PRI_{560-510}$ and 740/800
➢ Increase mrNDVI

Decrease in I_g

Thermography
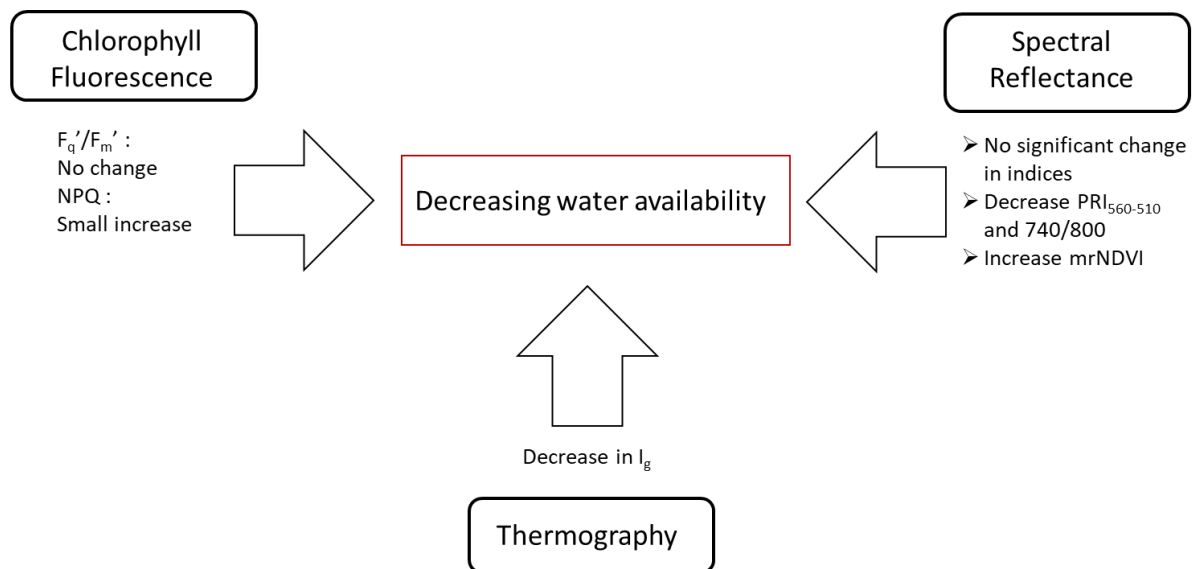
Figure 4.11 A diagram of the spectral toolbox, based on the results of experimental work as descried here, demonstrating an initial version of a spectral toolbox. Black box represents each technique of the toolbox; Arrow represents the output of measurements using these techniques; Red box represents the expected status of plant performance.

4.5 Conclusion

A spectral toolbox combining well established spectral techniques can be used to identify spectral signatures relating to plant health. Here, the foundation for this spectral toolbox was developed through the assessment of water status. Thermography based techniques demonstrate good sensitivity to changes in water content as consistent with literature. The drought resistant ecotype C24 showed no effect of water treatment on measured spectral techniques. Spectral indices were not able to indicate a decrease in soil RWC, while NPQ began to increase as soil RWC decreased.

Novel spectral responses to decreases in water status, such as through the investigation of spectral reflectance indices in Fig. 4.9, and in combination with chlorophyll fluorescence and thermography, were not found due to the lack of sufficient water stress.

While the water deficit applied here was insufficient to elicit water stress and therefore unable to determine the spectral signature for water stress, a spectral toolbox consisting of chlorophyll fluorescence, thermography, and spectral reflectance, is able to indicate the initial onset of low water content. The onset of decreasing water availability is signified through a decrease of the I_g index and small increases in NPQ, and no response from the other spectral measurements of F_q'/F_m' and spectral reflectance, due to changes in soil RWC over the time period of the experiment. These responses, or lack thereof, constitute the spectral signature for decreasing water content, and in the context of a grower or farmer constitutes an indicator of when additional irrigation is required.

This result can therefore be used as a "signature" for a response to decreasing water availability as measured by a spectral toolbox. A key advantage of using a spectral toolbox is that a 'stress catalogue' can theoretically be constructed, defining the response of a spectral toolbox to a range of environmental stressors. A library of spectral "signatures" can allow growers and farmers to identify factors that are negatively affecting crop performance, and enable remedial action to be taken.

Chapter 5 – A spectral toolbox to assess plant water and nitrogen content

5.1. Introduction

In the previous chapter, *Chapter 4*, we investigated the use of optical and imaging based techniques to identify spectral signatures that can be used to assess crop health status, through the development of a theoretical 'toolbox' of spectral techniques and measurements. The ability to measure nitrogen content, crop water status, and environmental factors such as temperature and humidity, which all affect crop health and performance, is essential to improving crop yields. Conventional techniques can be destructive or slow, limiting the ability to measure entire crops across multiple fields. Imaging and optical based techniques, on the other hand, rapidly and non-destructively allow for the continuous measurement of crop health for large areas of crops. This is essential to meeting the expected population growth predicted for 2050, with the estimated need for current crop yields to double (Ray et al., 2013)

A 'catalogue' of stress has been proposed before, based on using multiple techniques to identify unique responses for each stress type (Chaerle et al., 2009). While such compilations of the response of spectral techniques to biotic and abiotic plant stress exist, there has not been many instances of a well-defined, universal 'spectral toolbox'. Such a toolbox should consist of a fixed methodology to allow for consistent measurements across growth conditions and environments, allow for spatial and temporal assessment of crop health. Such a toolbox would lend itself well to future utilization agriculturally and within industry, with a fixed methodology reducing the level of expertise needed to setup instruments, measure crops, and interpret results. There are certain combinations of techniques within the literature that are used and remain popular for assessing crop health (Calderón et al., 2013; Panigada et al., 2014; Suárez et al., 2008), although few investigate the effect of combined, multiple stressors, and those that do tend to only use one technique. That said, there has been some work on the use of combined spectral techniques for screening plant populations,

such as for overall plant performance and the effects of biotic stress (Chaerle et al., 2007). Work by Zarco-Tejada et al. (2012) is one of the first instances of a combined toolbox of spectral reflectance, thermography, and fluorescence, although this work was aimed primarily at UAV based measurements, and there were limitations such as the use of solar induced fluorescence instead of conventional actively induced chlorophyll fluorescence, which limits the parameters that can be measured, and the focus only on water stress detection.

As described in *Chapter 4*, a spectral toolbox consisting of chlorophyll fluorescence, thermography and spectral imaging can be used to identify spectral signatures that can be used to assess crop health status. Thermography has been demonstrated to strongly relate to stomatal conductance (g_s) (Grant et al., 2006; Maes et al., 2016), which can be used to indicate water status. Spectral reflectance indicates the content of pigments within a leaf such as chlorophyll (e.g. Gitelson et al., 2003), internal structure of leaves (Castro & Sanchez-Azofeifa, 2008; Slaton et al., 2001), and the state of xanthophyll de-epoxidation (Gamon et al., 1992). Chlorophyll fluorescence is a powerful technique for the assessment of photochemistry and non-photochemical quenching, and thus is a key indicator of plant performance and plant stress (Baker, 2008; Murchie & Lawson, 2013). Further discussion on these techniques and their application for the assessment of water status so far can be viewed in *Chapter 4*.

Low nitrogen (N) availability is a limiting factor on photosynthetic efficiency and carbon assimilation, as chlorophyll and Calvin cycle proteins constitute the majority of leaf nitrogen (Evans, 1983; Evans, 1989), and thus, photosynthetic efficiency is negatively affected by N limitation (Evans, 1989; Huang et al., 2004). Low N is also associated with lower conductance, due to an increased intracellular CO_2 concentration as a result of reduced carbon assimilation (Mott, 1988), although it has been suggested that under N-limiting conditions, g_s itself may be the greater limiting factor for carbon assimilation, rather than the effect of N availability itself (Broadley et al., 2010). The relationship

between chlorophyll content and nitrogen content is closely linked, and thus leaf chlorophyll can be used to indicate nitrogen content (Evans, 1989).

Under drought conditions, there was a lower photosynthetic rate for plants with low N availability, but lower g_s for plants with high N (Shangguan et al., 2000). Thus, the combined effect of drought and low nitrogen can cloud the assessment of plant health, making it difficult to comprehensively understand which stress factor is affecting plant performance.

The aim for this study is therefore to assess the ability of a theoretical spectral 'toolbox', consisting of chlorophyll fluorescence, thermography and spectral reflectance, to assess the water status and chlorophyll content of spring wheat.

The objectives are to apply four treatment, with either high or low soil water content, and either an additional or no additional application of nitrogen to soil. The ability of the spectral 'toolbox' to measure these factors will be assessed based on actual measurements of leaf water content and content. Finally, as the spectral toolbox is intended as a future field based measurement, meteorological factors will be considered for their effect on resulting spectral measurements.

5.2 Methods

5.2.1 Treatment and growth conditions

Spring wheat of the variety *Mulika* was grown. Seeds were germinated for a week, before being transferred to 24 x 8L pots, and placed outside on the roof of the University of Essex on the 5th April 2018, which was later than recommended due to significant, unseasonal snow during the month of March. Soil was clay based, and collected from a local agricultural field near to Colchester, Essex, UK.

Four treatments were applied (Table 5.1). Two groups were grown with added nitrogen, but one group was grown with a target soil relative water content (RWC) of 70% ("N"), and one with a soil RWC of 20% ("ND"). All Soil RWC was measured prior to re-watering. Two groups were grown with no added nitrogen, but also under 70% ("H") and 20% ("HD") soil RWC. Plants reached Growth Stage 31 (GS31) on the 5th June, and first nitrogen treatment was applied shortly after. Nitrogen treatment of NH_4^+ and NO^- was applied on three dates; 8th June, 22nd June, and the 2nd of July, corresponding to GS31, GS39 and GS64. Each application, individual pots received 0.2815g of elemental nitrogen. Meteorological measurements were collected by a weather station was that was constructed at the site of the experiment (Aercus WS2083, Aercus Instruments, New Zealand).

Table 5.1 List of treatment groups and applied soil RWC, and whether additional nitrogen was applied

Name	Target Soil RWC (%)	Nitrogen	No. of Plants
● N	70	+	6
● ND	20	+	6
● H	70	-	6
● HD	20	-	6

5.2.2 Physical Measurements

Leaf relative water content (RWC) was measured by collecting leaves between 12:00 and 14:00. Leaves were sampled on two dates towards the end of the experiment pre-flowering, on the 29th

June and 6th July, to reduce damage to plants as each plant had produced minimal tillers, in most cases just one primary tiller. Leaves of each plant were cut 1cm of the base of the leaf, and the ends of the leaves were cut 4cm further along the leaf, and fresh weight was measured. Leaves were then placed into a universal tube, with the water covering approximately 1cm of the base of each leaf. Leaves were left for 4 hours, before weighing again. After weighing, leaves were placed in an oven (80°C) overnight.

Samples for chlorophyll content measurements were collected by punching four 7mm holes from between the centre and base of the leaves, and immediately placing them in liquid nitrogen. In the laboratory, leaves were ground on ice with 80% acetone, centrifuged at high speed for 5 minutes, with the supernatant collected for measurement. Absorbance at 652nm (A_{652}) was measured against acetone blanks. Total chlorophyll was calculated as 27.8 multiplied by A_{652}, divided by total leaf area.

5.2.3 Chlorophyll Fluorescence

Chlorophyll fluorescence was measured using a PAM 2500 (Walz, Effeltrich, Germany). Dark adapted measurements of the maximum operating efficiency of photosystem II (PSII) (F_v/F_m) were performed by placing plants in the dark for 30 minutes prior to measurement. Plants were taken from outside between the hours of 8:00 and 8:45.

Light adapted measurements of the operating efficiency of photosystem II (PSII) (F_q'/F_m') and non-photochemical quenching (NPQ) were taken under an LED light source (Heliospectra AB, Göteborg Sweden) set to 600 µmol $m^{-2} s^{-1}$ of light. Plants were transferred to the light source from outside for 5 minutes prior to measurements. Measurements were performed between the hours of 11:00 and 13:00.

5.2.4 Reflectance

Reflectance measurements were the same as Section **4.2.4**, except that the indices measured calculated as per Table 5.2, and measurements were performed immediately after light adapted

chlorophyll fluorescence was measured for each plant. Spectral indices were chosen from literature that have been used either to assess water status, or to assess chlorophyll content. One index, the $CI_{800-720}$ is a variant of $CI_{RedEdge}$, but has been named differently to allow for easier discrimination.

5.2.5 Thermography

The index of stomatal conductance (I_g) (Jones, 1999) was calculated from thermal imagery, using a thermal camera (TH7100 Thermal Tracer, NEC Avio Infra-red Technologies Co. Ltd, Japan). This index uses a wet and dry reference to calculate the temperature of references with theoretical minimal and maximal g_s, as described in *Section 4.2.3.*

Individual plants were laid flat on a grid made from fishing wire to allow for air to continue to circulate around the leaves, minimising any change to transpiration or boundary layer. Prior to measurements, two wheat leaves that were not used in the experiment were also placed on the fishing wire grid, to be used as wet and dry references as per *Section 4.2.3*. Measurements were collected between the hours of 11:00 and 14:00.

Concurrently, immediately after imaging each plant, gas exchange measurements were taken using an LCpro-SD infrared gas analyser (ADC Bioscientific Ltd, Hoddesdon, UK), using ambient environmental conditions. Both thermography and gas exchange measurements took place on the roof, immediately in the vicinity of the growth area.

Table 5.2 Spectral indices and their formulation, with R denoting reflectance at that wavelength (nm) e.g. R620 is reflectance at 620nm

Index	Formula	Reference
NDVI	(R720-R620)/(R720+R620)	(Li et al., 2014; Rouse et al. 1974)
mrNDVI	(R750-R705)/(R750+R705-2*R445)	(Sims & Gamon, 2002)
NDRE	(R800-R717)/(R800+R717)	(Li et al., 2014)
$ND_{Shimada}$	(R490-R620)/(R490+R620)	Shimada et al., 2012
$NDWI_{Green}$	(R800-R550)/(R800+R550)	*Chapter 3*
PRI	(R531-R570)/(R531+R570)	(Gamon, Peñuelas, & Field, 1992)
$PRI_{570-515}$	(R570-R515)/(R570+R515)	(Hernandez Clemente et al., 2011)
$PRI_{560-610}$	(R560-R610)/(R560+R610)	(Elvanidi et al., 2017)
$CI_{RedEdge}$	(R783/R705)-1	(Clevers & Gitelson, 2013; Gitelson et al., 2005)
$CI_{800-720}$	(R800/R720)-1	(Gitelson et al., 2005; Schlemmer et al., 2013)
Datt	(R850-R710)/(R850-R680)	(Datt, 1999)
mDatt	(R719-R726)/(R719-R743)	(Lu et al., 2015)
740/800	R740/R800	(Dobrowski et al., 2005)
690/600	R690/R600	(Dobrowski et al., 2005)
800/550	R800/R550	*Chapter 3*
800/440	R800/R440	*Chapter 3*
(800/665)/440	(R800/R665)/R440	*Chapter 3*
617/614	R617/R614	*Chapter 4*

5.3 Results

5.3.1 Meteorological Conditions

Temperature and relative humidity across the time period of the experiment is shown in Fig. 5.1. There was an overall trend of increasing temperature and decreasing relative humidity from the start of the experiment to the end, with highest daytime temperature increasing from around 20°C at the start of the experiment near the 4th and 5th of June 2018, up to 27°C by the end of the experiment on 29th June 2018. Likewise, lowest relative humidity decreases from 60 to 70%, down to 30%, at the same time period.

5.3.2 Physiological measurements

The soil RWC can be seen in Fig. 5.2. Plants in the treatment group *H* demonstrate higher soil RWC throughout the experiment, followed by *N* and *HD. ND* had lowest soil RWC of all the treatments. Additionally, all treatment groups show a decrease in measured soil RWC prior to re-watering, likely as a result of higher temperatures and humidity.

Leaf RWC, which was measured on two days at the end of the experiment, shows a clear clustering of treatment groups (Fig. 5.3), although there was no statistically significant difference between treatments. The water groups of *N* and *H* have consistently higher leaf RWC (85-90% on June 29th, 70-75% July 6th) than the drought groups of *ND* and *HD* (75% on June 29th, 55-65% July 6th). As was seen with soil RWC, there is an overall trend for leaf RWC to decrease towards the end of the experiment.

Chlorophyll content shows the groups with added nitrogen (*N* and *ND*) had higher chlorophyll content than the groups that did not (*H* and *HD*) (Fig. 5.4). There is higher chlorophyll for *N* and *ND* treatments on July 4th than June 29th, which corresponds to the application of nitrogen on July 2nd.
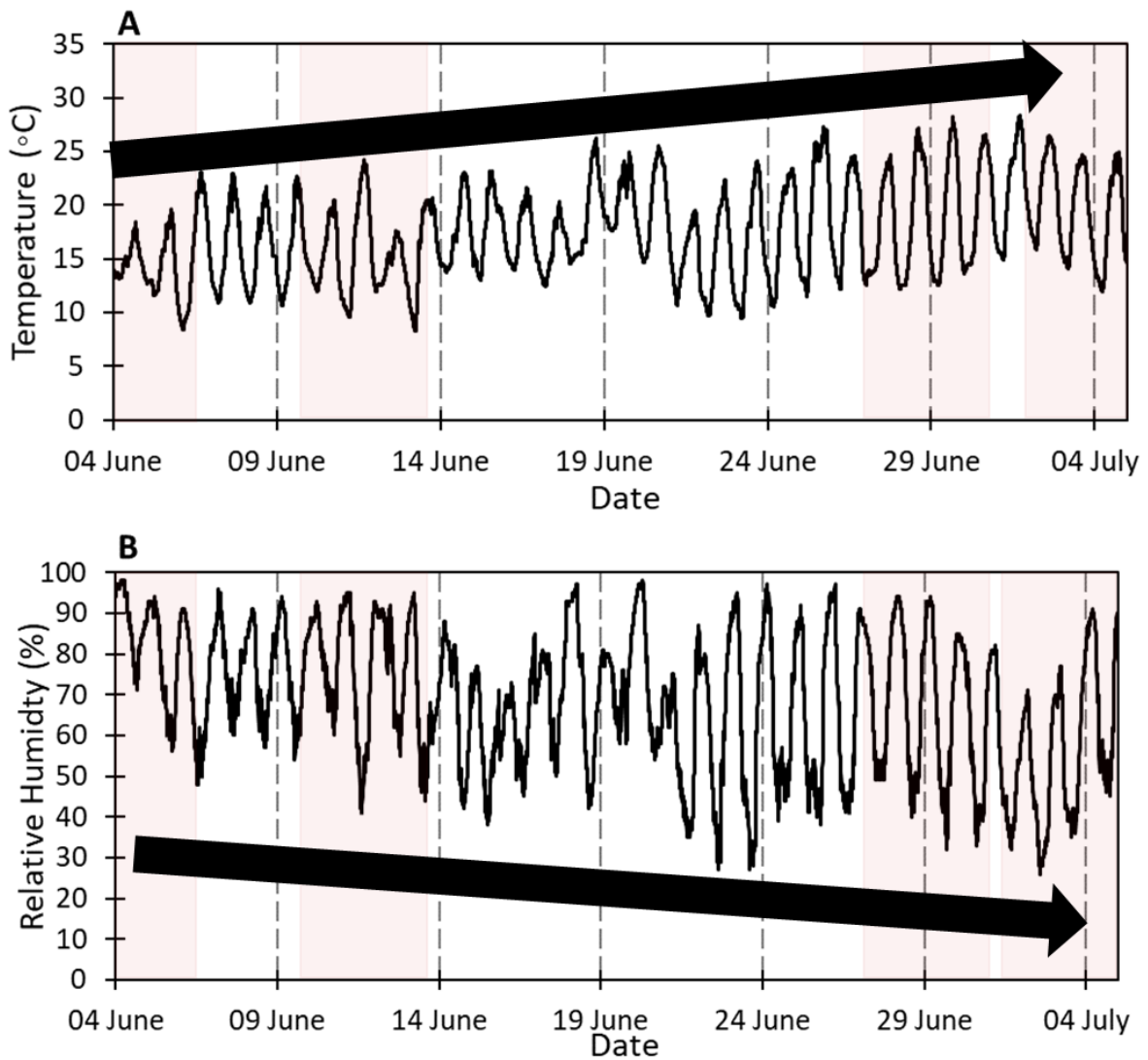
Figure 5.1 Meteorological data during the course of the experiment **A)** Temperature recorded at 5 minute intervals **B)** Relative humidity recorded at 5 minute intervals. Red highlight indicates periods of measurement. Arrow shows overall trend in maximum temperature or minimum relative humidity

Table 5.3 Measured PPFD (μmol m^{-2} s^{-1}) of PAR on dates in which measurements were collected.

Date	PPFD
June 5th	*1027*
June 12th	*307*
June 29th	*2112*
July 4th	*1911*
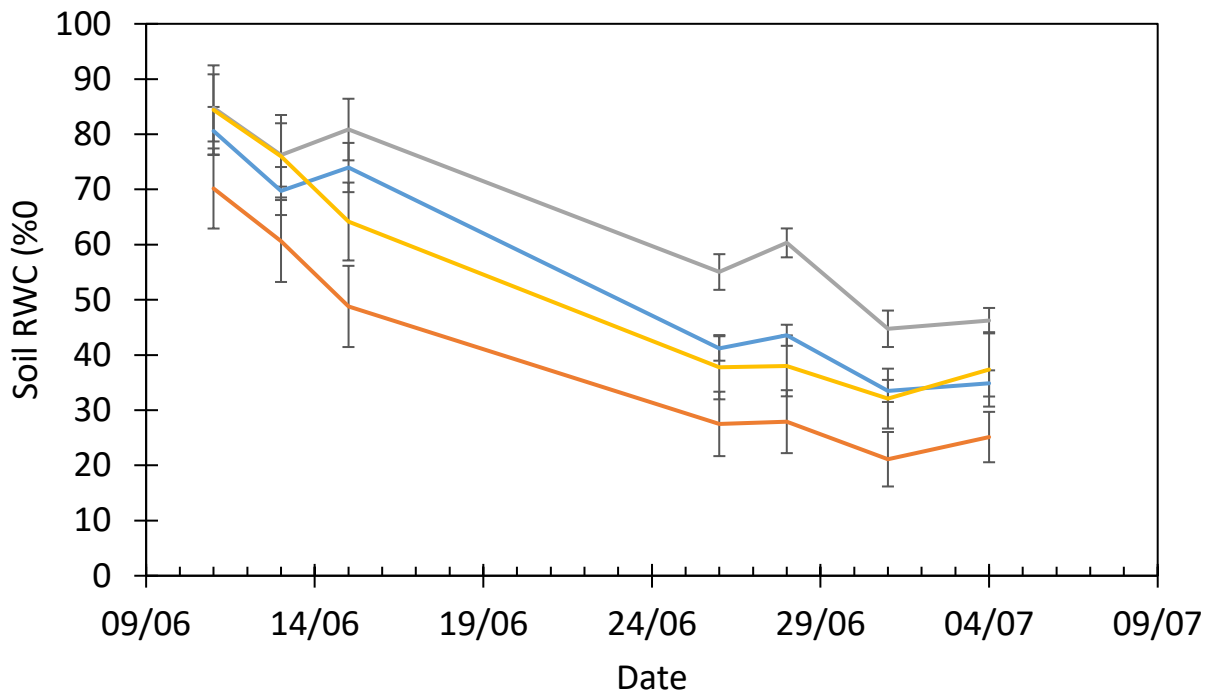
Figure 5.2 Gravimetric soil relative water content (RWC), measured in the morning prior to addition of water. Re-watering was back up to target soil RWC of Table 5.1. ● N ● ND ●H ● HD. Error ± S.E, n=6

5.3.3 Thermography

The index of stomatal conductance (I_g) shows a strong relationship with g_s (R^2 = 0.63, Fig. 5.5 A), demonstrating good performance of the index as a proxy for g_s. Using I_g to monitor g_s of each treatment groups (Fig. 5.5 B), shows an overall trend of a rapidly decreasing I_g over the course of the experiment. The watered groups (*N* and *H*) had a higher I_g than the drought groups (*H* and *HD*) (Fig. 5.5 B), but there was no significant difference between treatments.

There was a strong relationship between I_g and soil RWC (R^2 = 0.70, Fig. 5.6 A), however the relationship between I_g and leaf RWC was very weak (R^2 = 0.17, Fig. 5.6 B), although this may be due to leaf RWC data only being collected near the end of the experiment.
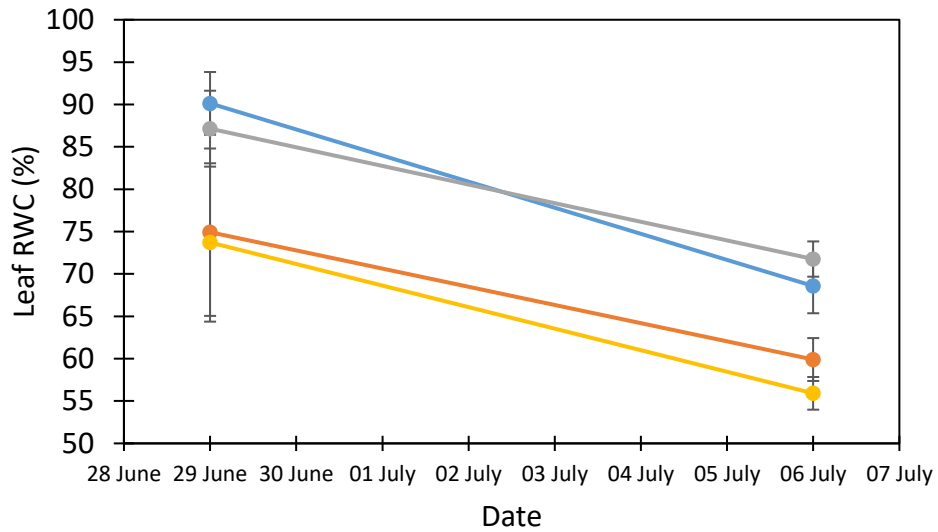
Figure 5.3 Leaf relative water content (RWC) of destructively sampled leaves from youngest fully mature leaves. ● N ● ND ●H ● HD. Error ± S.E, n=6
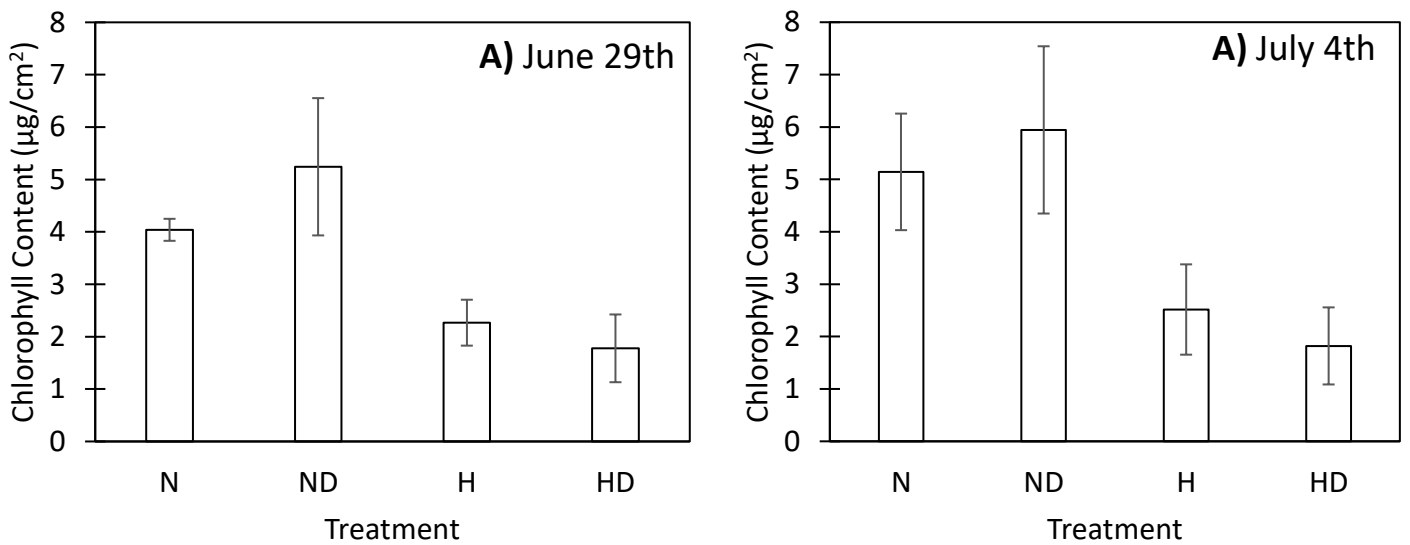
Figure 5.4 Chlorophyll content of destructively sampled leaves from youngest fully mature leaves on **A**) June 29th (n= 4-5), and **B**) July 4th (n= 2-5). ● N ● ND ●H ● HD. Error ± S.E
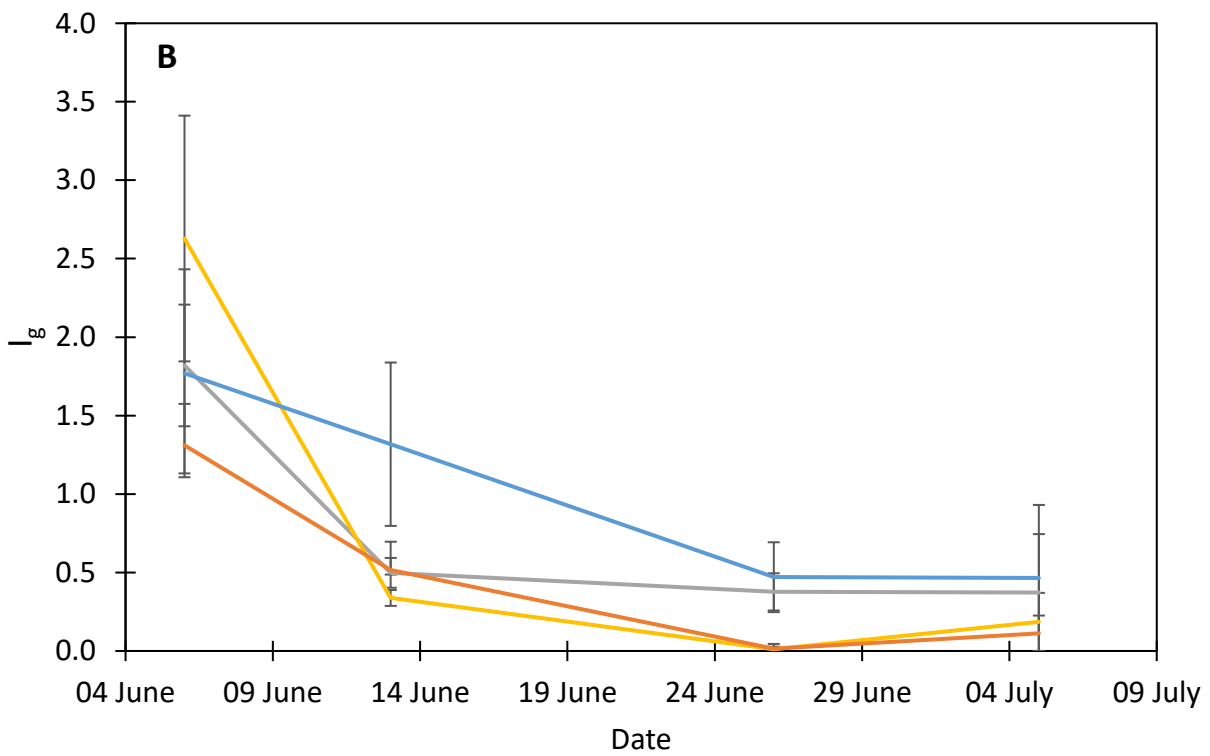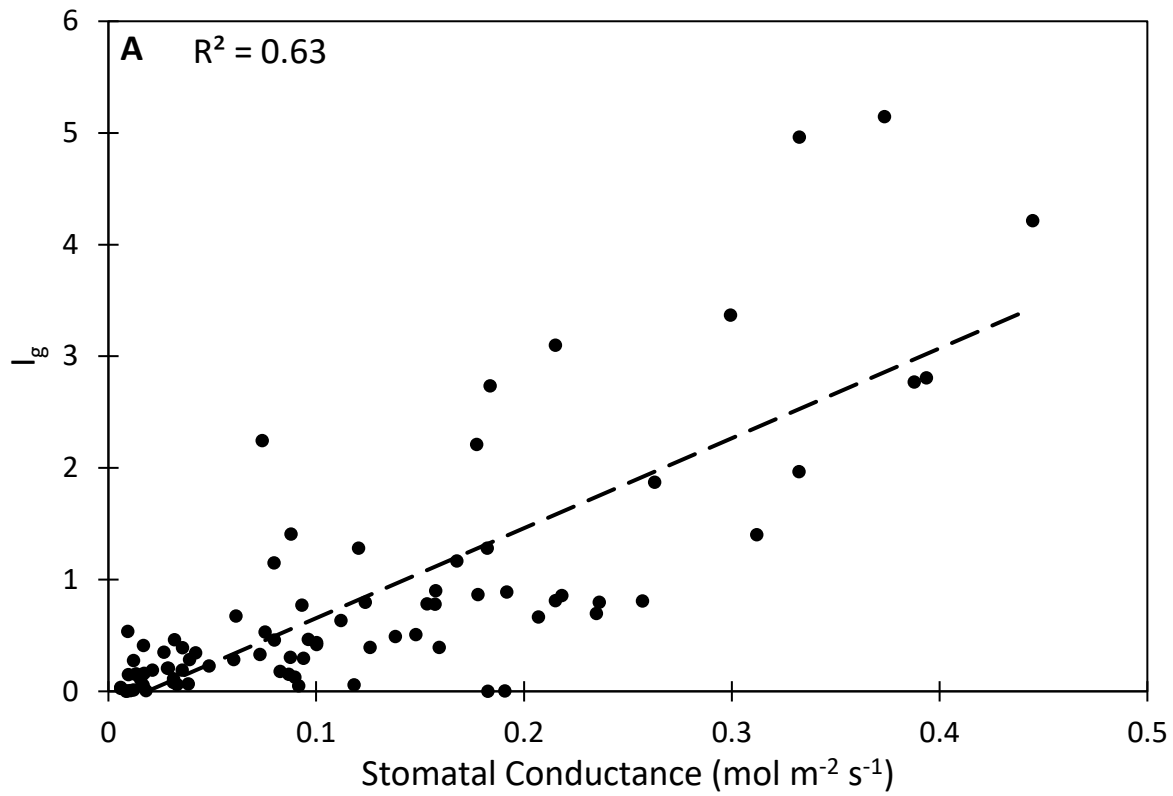
Figure 5.5 A) Relationship between measured stomatal conductance, and thermography derived measurements of the index of stomatal conductance (I_g) of all treatments (p<0.001) **B)** Measurements of the index of stomatal conductance for treatment groups across the timeframe of the experiment. ● N ● ND ● H ● HD. Error ± S.E, n=6
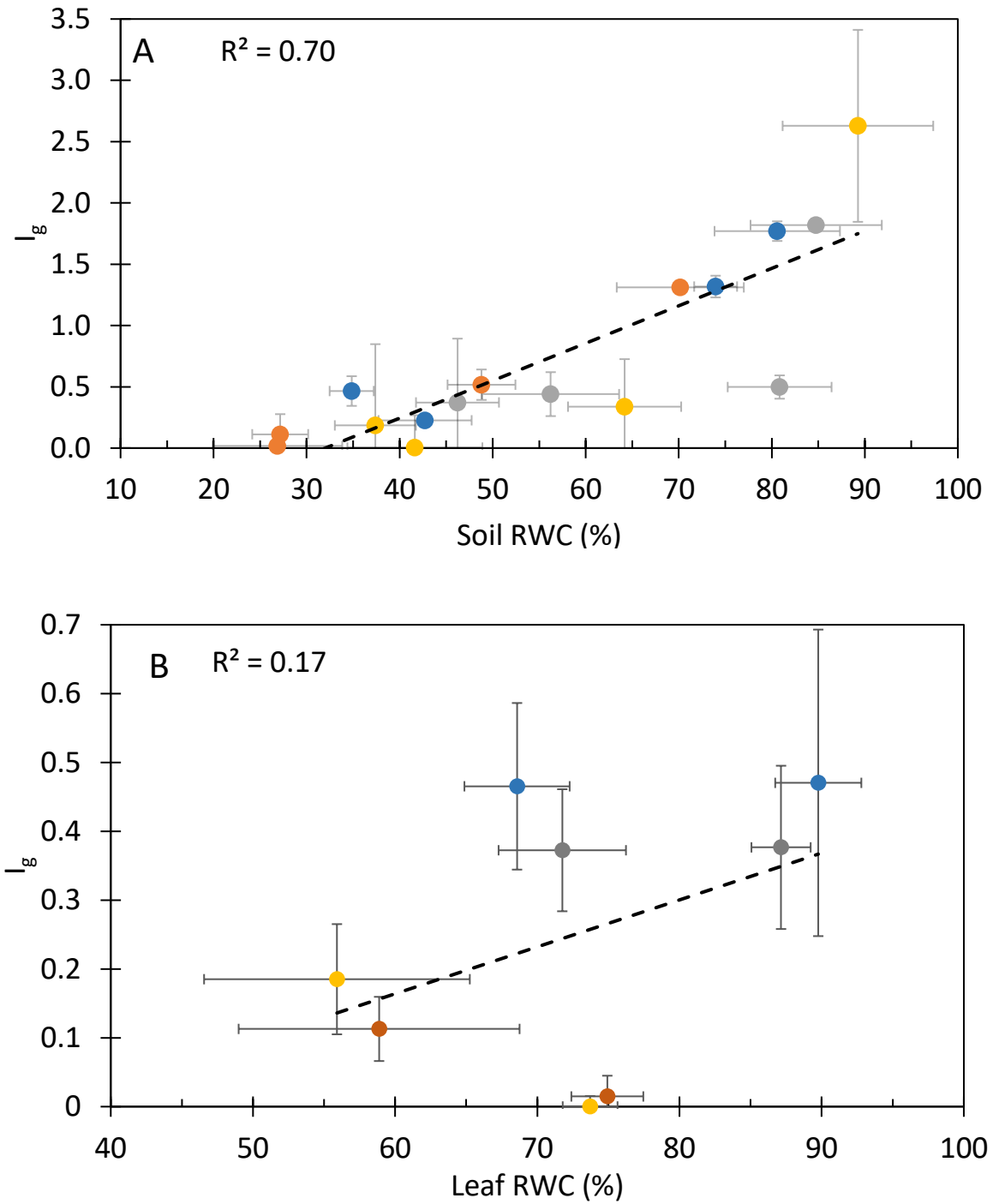
Figure 5.6 Relationship between measured thermography derived measurements of the index of stomatal conductance (I_g) and **A)** soil relative water content (RWC) p<0.001 **B)** leaf relative water content (RWC). ● N ● ND ●H ● HD. Error ± S.E, n=6

5.3.4 Reflectance

5.3.4.1 Chlorophyll Content

The relationship between spectral indices and chlorophyll content (Table 5.4, Fig. 5.7) shows good performance for most indices. The best performing index for measuring chlorophyll content was 800/550 (Table 5.4), with an R^2 of .59 and an RMSE of 2.37. Indices with a similar R^2, but a much larger RMSE, include $CI_{RedEdge}$ (R^2 =.59, RMSE = 3.29), $CI_{800-720}$ (R^2 =.60, RMSE = 3.85), Datt (R^2 =.60, RMSE = 3.72) and NDRE (R^2 =.61, RMSE = 4.00). The mDatt index, previously proposed as a improved index that is insensitive to the structure of leaf surfaces on, is outperformed by the original Datt index. Many of the indices that have been used in literature to assess water status show also show a relationship to chlorophyll content (mrNDVI, R^2 = 0.55; PRI, R^2 = 0.34; $ND_{Shimada}$, R^2 = 0.51), except for the 800/440 index which has one of the lowest relationships to chlorophyll content (R^2 = 0.16, Fig. 5.7). Thus, the index of 800/550 can be used as a proxy for chlorophyll content over the entire timeframe of the experiment (Fig. 5.8). There was a clear trend for groups with a nitrogen treatment (*N* and *ND*) to have higher chlorophyll content than those without (*H* and *HD*), with significant differences between the *HD* group and the *N* + *ND* groups on 29th June. On the final day of measurement, on the 4th July, after the final application of the nitrogen treatment, the chlorophyll content of *ND* dropped below *N*, while *N* maintained, with significant differences between *N* and the *H* + *HD* groups.

5.3.4.2 Soil and Leaf Relative Water Content

The relationship between spectral indices and soil and leaf RWC (Table 5.5) shows poor performance for almost all indices. Indices which performed well for measuring leaf RWC include the indices of 800/440 (R^2=0.61, Fig. 5.9 A) and (800/665)/440 (R^2=0.61), which were proposed in *Chapter 3*, and PRI (R^2=0.52) and 617/614 (R^2=0.55). However, despite the high relationship with leaf RWC for the 800/440 index, the index only showed an R^2 of 0.25 against soil RWC. Only two indices demonstrated any relationship to soil RWC; PRI (R^2=0.47) and 617/614 (R^2=0.35, Fig. 5.9 B).

Due to the good performance of 800/440 with relative leaf RWC (Fig. 5.9 A) and 617/614 with relative soil RWC (Fig. 5.9 B), these two indices were selected as potential indicators of water status.

5.3.4.3 Combination of spectral reflectance based indices to assess water and nitrogen status

Plotting just two indices together, it may be possible to determine the combined chlorophyll and water status of a plant. Using the 800/550 index as a representative of chlorophyll content, three potential water indices of 800/440 (Fig. 5.10 A,B), 617/614 (Fig 5.10 C,D) and PRI (Fig. 5.10 E,F) can be plotted against the index. All three water indices show a similar starting region for all treatments at the start of the experiment (Fig. 5.10 A, C, E), except for PRI (Fig 5.12 E), which shows a much lower starting PRI value for the H group. As the experiment progresses, the treatments of *ND*, *H* and *HD* move away from the *N* group in all cases, ending up with each treatment occupying, approximately, its own quadrant (Fig. 5.10 B, D, F). This quadrant represents the range of values for each combination of high or low nitrogen and water content, when using two indices with one measuring water status, and one measuring chlorophyll content.

Table 5.4 Spectral indices and coefficient of determination (R^2) to chlorophyll content ($\mu g/cm^2$), and Root Mean Square Error (RMSE). * = p<0.05, ** = p <0.01, *** = p<0.001

Index	Chlorophyll Content	RMSE
NDVI	.53***	3.71
mrNDVI	.59***	3.76
NDRE	.61***	4.00
$ND_{Shimada}$	.55***	4.27
$NDWI_{Green}$	.60***	3.82
PRI	.41***	4.17
$PRI_{570-515}$	.35***	4.02
$PRI_{560-510}$	.19*	3.95
$CI_{RedEdge}$	.59***	3.29
$CI_{800-720}$	.60***	3.85
Datt	.60***	3.72
mDatt	.49***	3.83
740/800	.15***	3.41
690/600	.00	3.52
800/550	.59***	2.37
800/440	.16*	2.38
$\frac{(800/665)}{440}$	.26*	3.85
617/614	.00	3.38
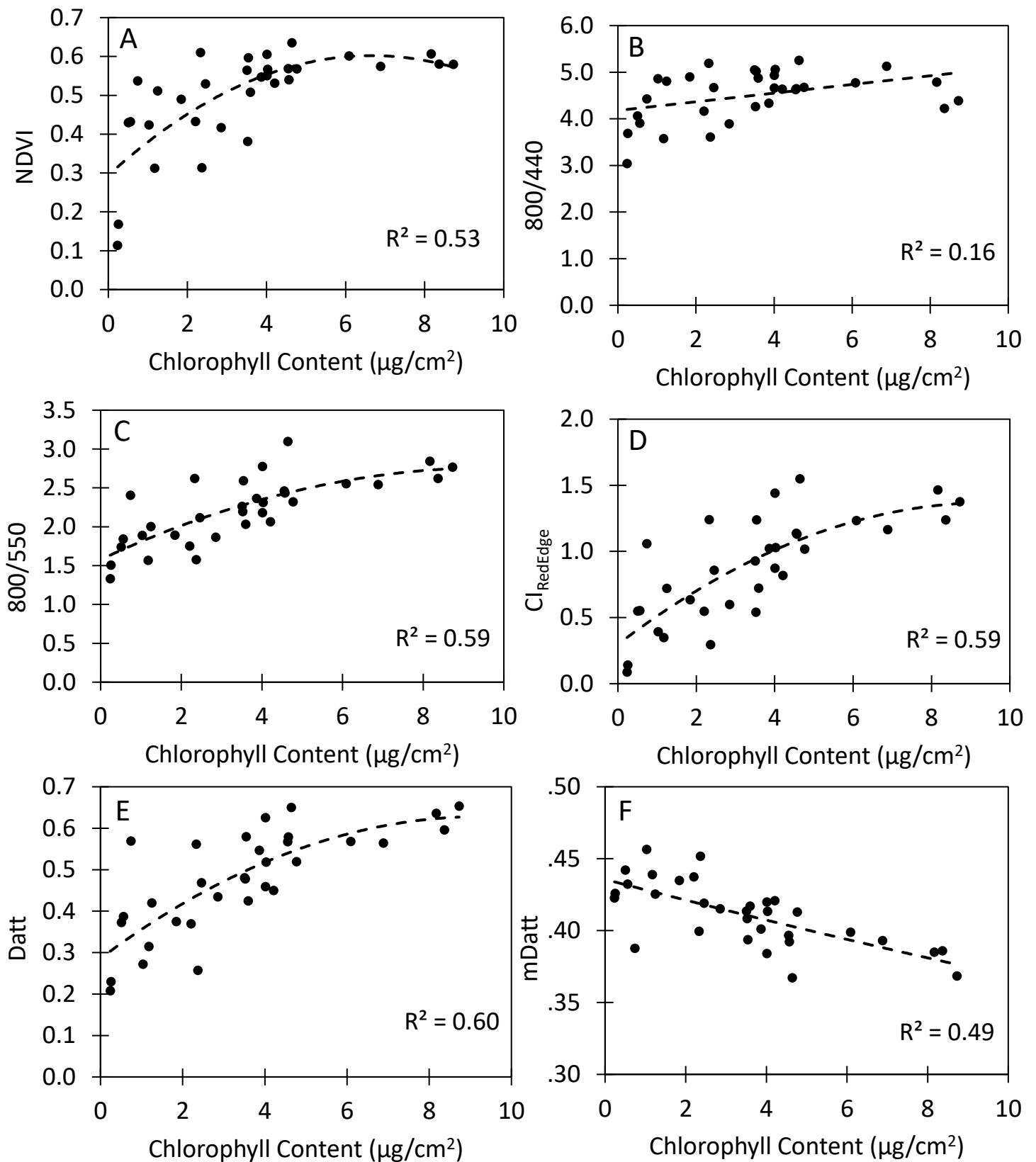
Figure 5.7 The relationship between chlorophyll content and the spectral indices (Table 5.2) of **A)** NDVI **B)** 800nm/440nm **C)** 800nm/550nm **D)** CI$_{RedEdge}$ **E)** Datt **F)** mDatt, statistics as Table 5.4
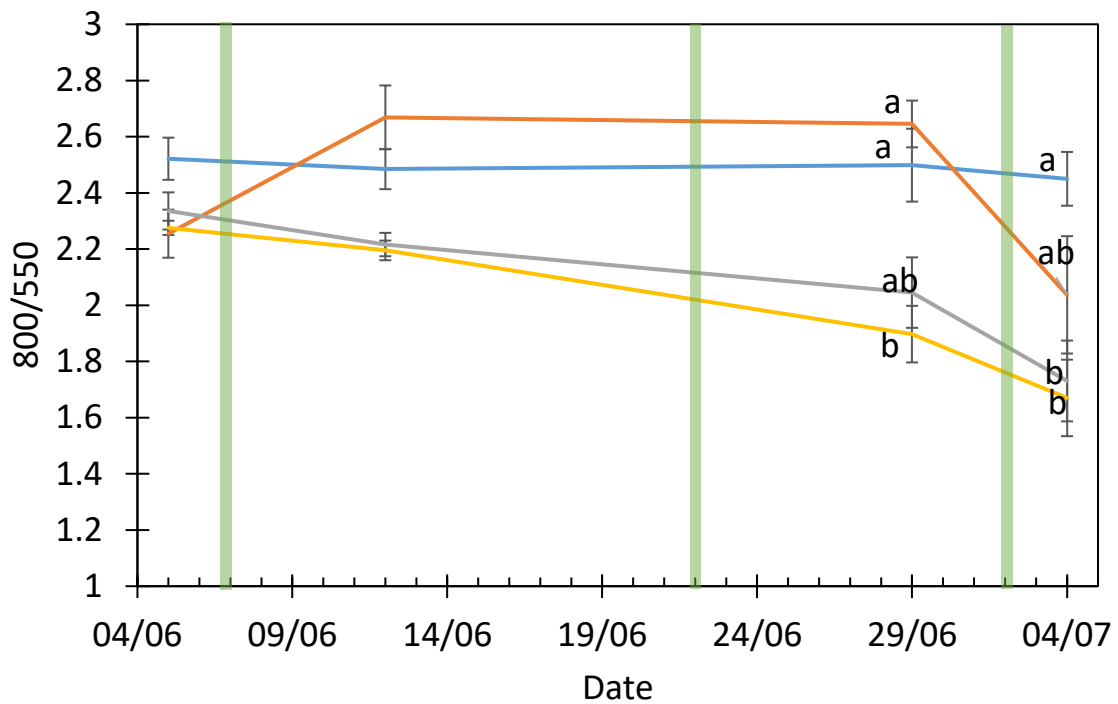
Figure 5.8 Measurements of 800nm/550nm for treatment groups across the timeframe of the experiment. Green bars indicate days in which a nitrogen treatment was applied. ● N ● ND ●H ● HD. Error ± S.E, n=6. Different letters indicate a significant difference between treatments on the same day. June 29th: Significant difference between N and HD (p < 0.05), ND and HD (p < 0.01). July 4th: Significant difference between N and H (p < 0.01), N and HD (p < 0.001).

Table 5.5 Spectral indices and coefficient of determination (R^2) to soil and leaf relative water content (%). * = p<0.05

Index	Soil RWC	Leaf RWC
NDVI	.32	.43
mrNDVI	.2	.26
NDRE	.14	.22
$ND_{Shimada}$	.20	.19
$NDWI_{Green}$	.14	.23
PRI	.47*	.52*
$PRI_{570-515}$	.04	.00
$PRI_{560-510}$	.05	.19
$CI_{RedEdge}$	.15	.24
$CI_{800-720}$	.11	.19
Datt	.16	.18
mDatt	.02	.06
740/800	.00	.04
690/600	.09	.50*
800/550	.10	.20
800/440	.25	.61*
$\frac{(800/665)}{440}$	.25	.52*
617/614	.35*	.55*
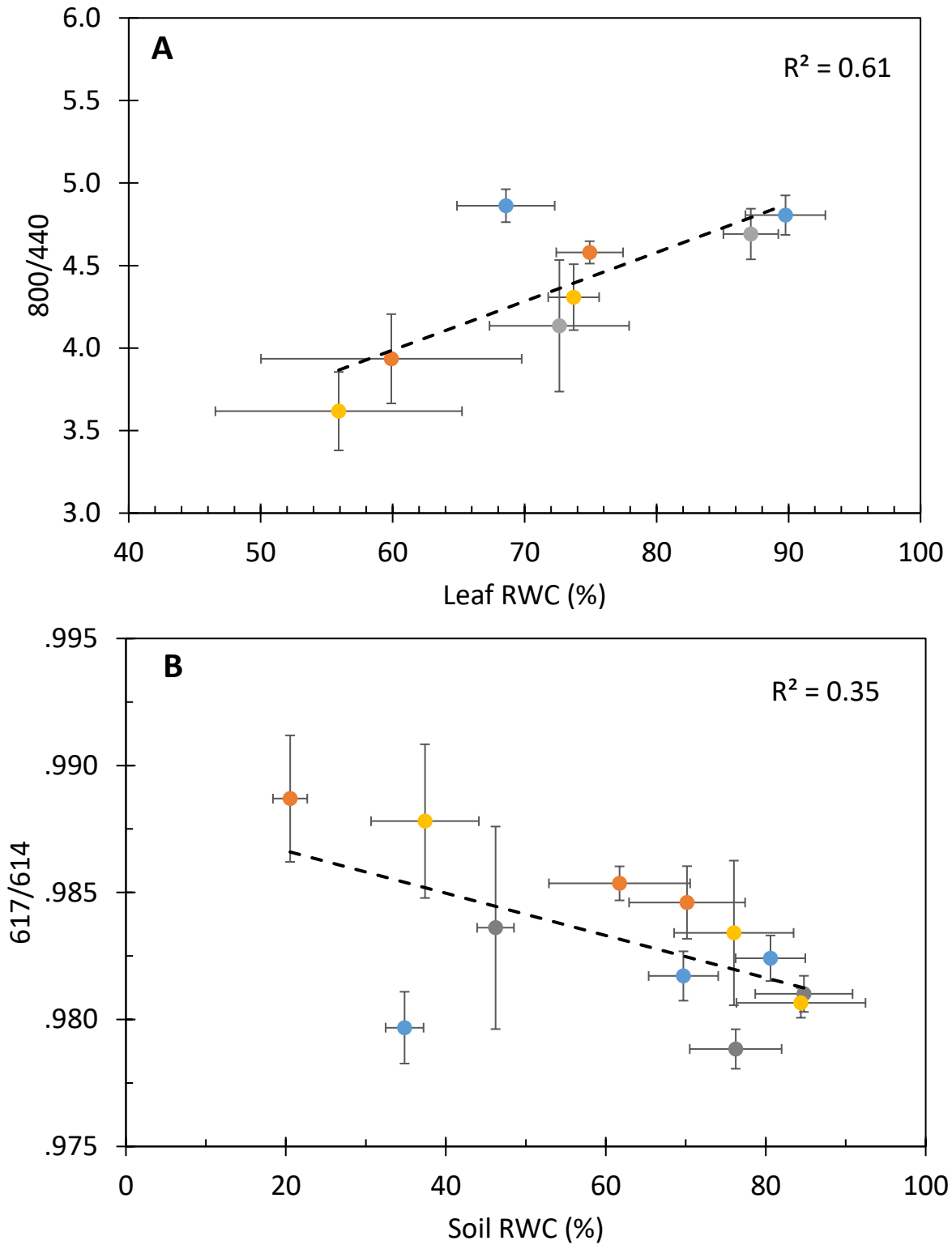
Figure 5.9 The relationship between **A)** 800/440 and leaf relative water content (RWC) (p<0.05), and **B)** 617/614 and leaf relative water content (RWC) (p<0.05). ● N ● ND ● H ● HD. Error ± S.E, n=6.
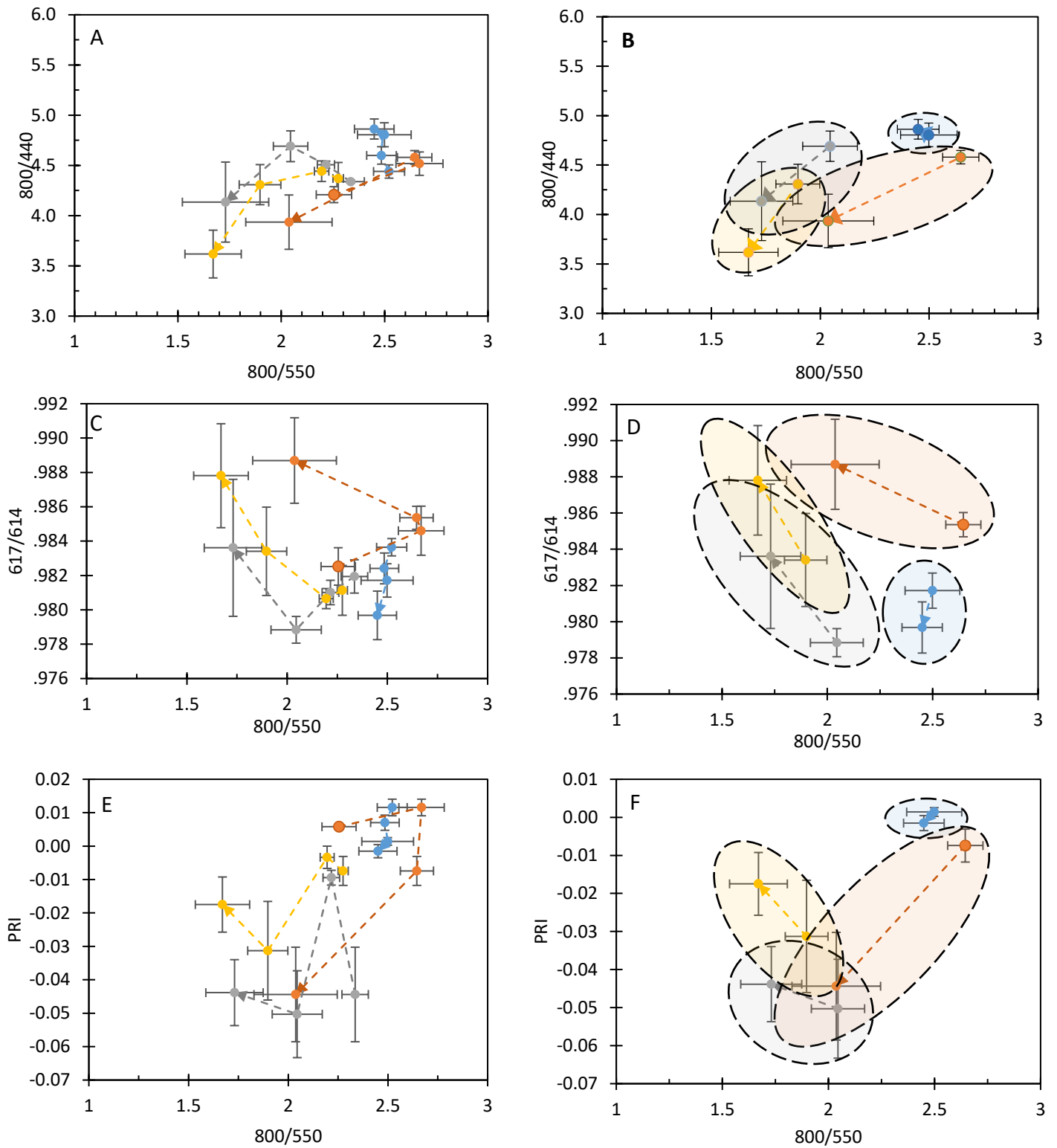
Figure 5.10 The relationship between the 800nm/550nm index, as an indicator of chlorophyll content, and the indices of 800nm/440nm (**A, B**), 617nm/614nm (**C, D**), and PRI (**E, F**), as indicators of water status,. Measurements shown are (**A, C, E**) across the timeframe of the experiment, or (**B, D, F**) data points for the last two measurement days. Shaded ovals indicate the representative region that each treatment group occupied. Dotted line with end arrow indicator change in values over time. ● N ● ND ● H ● HD. Error ± S.E, n=6.

5.3.5 Chlorophyll Fluorescence

There was no significant difference in the theoretical maximum efficiency of PSII (F_v/F_m) between treatments (Fig. 5.11 A). However, there was a trend on the final day of measurements (July 4th) for the *ND* and *H* treatments to decrease in F_v/F_m compared to the *N* and *HD* treatment.

There was also no significant difference between treatments for F_q'/F_m' (Fig. 5.11 B), although there an overall decrease for all treatments between the 12th June and 29th June. The values for NPQ with all treatments having similar values, except for a large spike for the *HD* treatment on the 29th (Fig. 5.11 C). There was also with an overall increase of NPQ for all treatments, mirroring the decrease in F_q'/F_m'.

Overall, there was a positive relationship between F_q'/F_m' and soil RWC (Fig. 5.12), and a weak positive relationship between F_v/F_m and soil RWC, and a weak negative relationship between NPQ and soil RWC. However, there is poor separation between all treatments. Using the 800nm/550nm index as an indicator for chlorophyll content, we see weaker relationships between all fluorescence parameters and the index (Fig. 5.12).
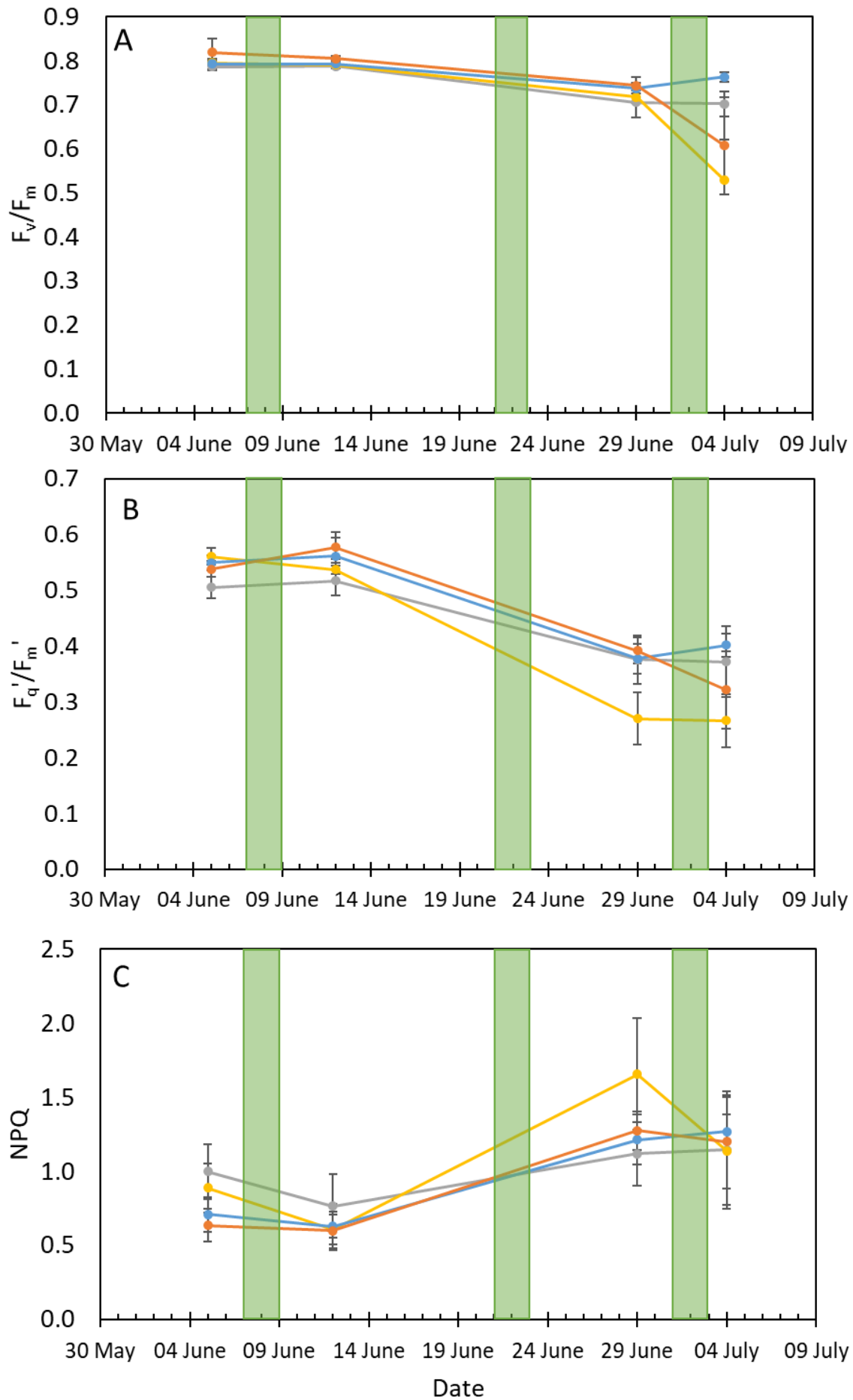
Figure 5.11 Measured **A)** maximum theoretical operating efficiency of photosystem II (PSII) (F_v/F_m) **B)** operating efficiency of PSII (F_q'/F_m') **C)** and non-photochemical quenching (NPQ) over the timeframe of the experiment. Shaded green area indicates days in which a nitrogen treatment was applied to groups N and ND. ● N ● ND ● H ● HD. Error ± S.E, n=6.
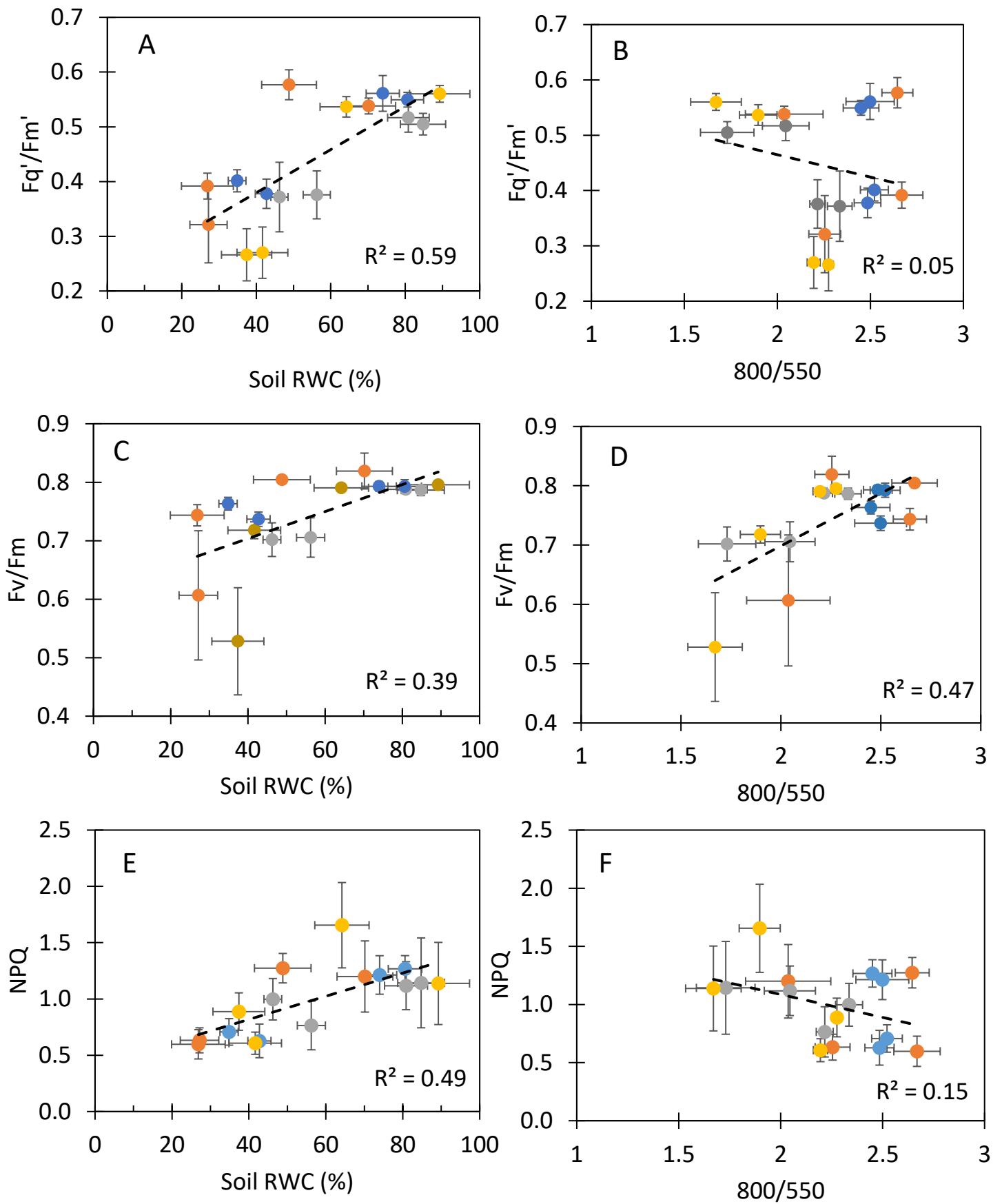
Figure 5.12 Relationship between gravimetric soil relative water content (RWC) and **A)** operating efficiency of PSII (F_q'/F_m'), **C)** maximum theoretical operating efficiency of photosystem II (PSII) (F_v/F_m), **E)** non-photochemical quenching (NPQ), and the 800nm/550nm as an indicator of chlorophyll content and **B)** F_q'/F_m', **D)** F_v/F_m, **F)** and NPQ. ● N ● ND ● H ● HD. Error ± S.E, n=6.

5.3.6 Effect of environment on measurements

As seen in Fig. 5.1, there was variation in daily maximum temperature and lowest relative humidity over the course of the experiment, thus the effect of temperature and relative humidity on measurements was considered (Table 5.6). The measurements of I_g, and all three chlorophyll fluorescence parameters, were significantly influenced by temperature and humidity (Fig. 5.13). The index of stomatal conductance was affected the least out of the four, with moderate effects due to temperature (R^2 = .46) and relative humidity (R^2 = .40). The operative efficiency of PSII (F_q'/F_m') and NPQ showed a strong positive (F_q'/F_m') and negative (NPQ) relationship to temperature (R^2 = .41 for F_q'/F_m', and R^2 = .82 for NPQ) and relative humidity (R^2 = .70 for F_q'/F_m', and R^2 = .76 for NPQ). Spectral reflectance derived indices however, show little to no effect due to temperature or humidity (Table 5.6), except for PRI, which while not a significant relationship, did show a small effect due to humidity and temperature. There is a major effect of PPFD on I_g and fluorescence parameters (Fig. 5.13 C, F, I), with NPQ increasing from 0.6 up to almost 2.0, due to increasing PPFD (Fig 5.13 I), and a similar decrease in F_q'/F_m' from 0.55 down to around 0.35 (Fig. 5.13 F).

Table 5.6 The coefficient of determination (R^2) between environmental variables of temperature, relative humidity and PPFD ($\mu mol\ m^{-2}\ s^{-1}$) on days of measurement, and collected measurements. * = $p<0.05$, ** = $p<0.01$, *** = $p<0.001$

Index	Temperature	Relative Humidity	PAR
I_g	.46**	.40**	--
F_v/F_m	.41**	.32*	.39*
F_q'/F_m'	.82***	.70***	.81***
NPQ	.79***	.78***	.81***
800/550	.13	.11	.14
$CI_{800-720}$	.13	.10	.14
800/440	.00	.00	.01
617/614	.05	.04	.04
PRI	.23	.24	.26*
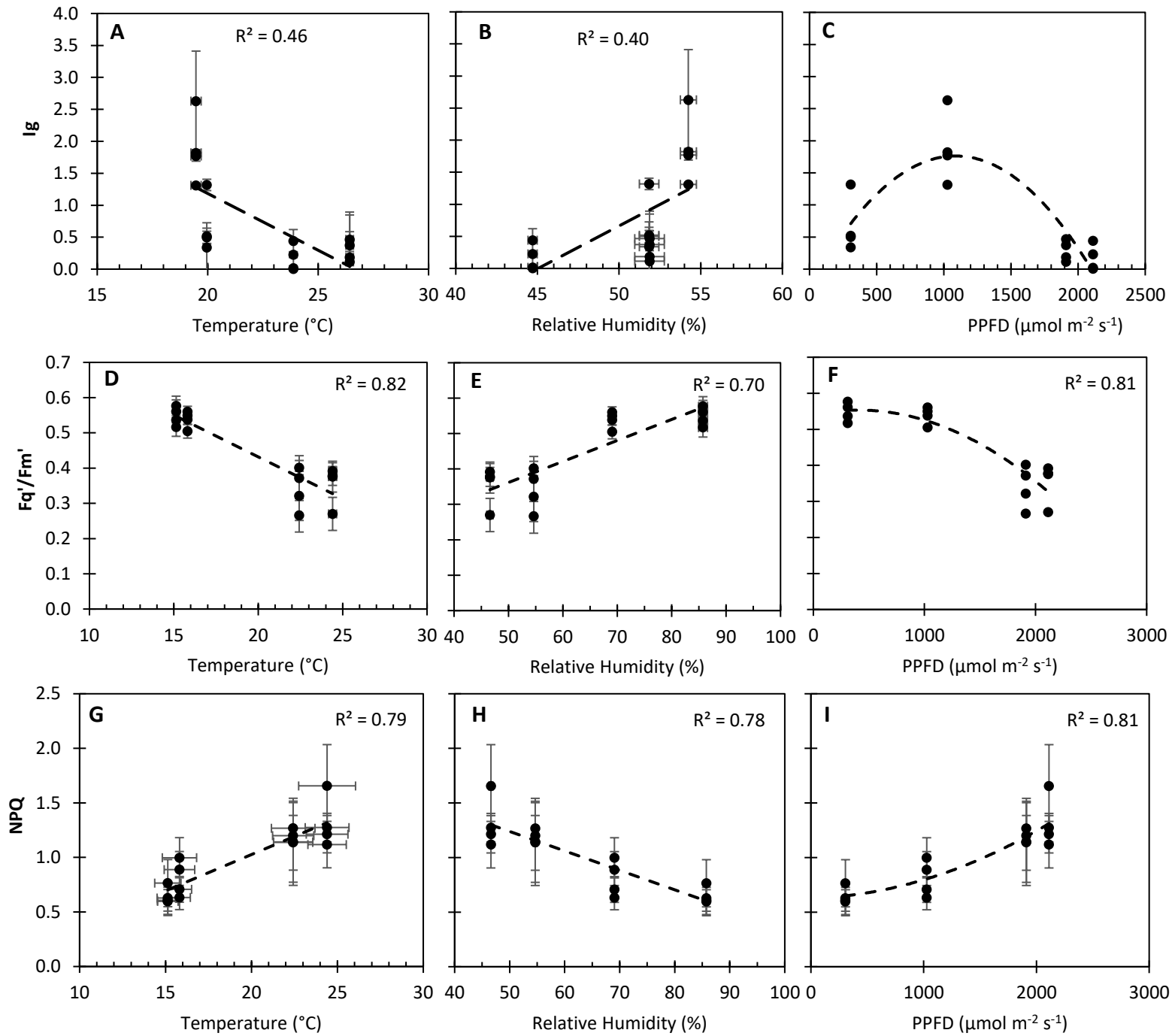
Fïgure 5.13 Relationship of the index of stomatal conductance (**A, B, C**) and chlorophyll fluorescence parameters of the operating efficiency of PSII (F_q'/F_m') (**D, E, F**) and non-photochemical quenching (**G, H, I**), against the environmental factors of ambient temperature (**A,D, G**),relative humidity (**B, E, H**), and PAR as measured at 12pm on each measurements day (**C, F, I**). ● N ● ND ●H ● HD. Error ± S.E, n=6.

5.4 Discussion

5.4.1 Chlorophyll Fluorescence

The trend for a lower F_v/F_m for the two drought treatments (Fig. 5.11) at the end of the experiment indicates photoinhibition of PSII (Murchie & Lawson, 2013). Photoinhibition often occurs when absorbed light energy is in excess of that used in photochemistry. Although there are many photoprotective mechanisms which dissipate excess absorbed light energy (Murchie & Niyogi, 2011), excess absorbed light still results in photodamage, predominantly resulting in the degradation of the D1 protein, a core component of the PSII complex (Gao et al., 2018) located on the reducing side of PSII and vital for electron transport chain through the reduction of plastoquinone (Edelman & Mattoo, 2008; Tyystjärvi, 2013). Damage also occurs to the oxygen-evolving complex of PSII which also affects electron transport, reducing overall photosynthesis (Huang et al. 2018). The cause and effect of photoinhibition aligns with the cause of the decrease in F_v/F_m, which occured during a period of high light (Fig. 5.1, Table. 5.3). The two drought treatments were more susceptible to photoinhibition due to lower g_s, and thus greater reduction in carbon assimilation which reduces the sink for the end products of electron transport (Gollan et al., 2017; Pastenes et al., 2005). However, it should also be noted that the decrease in F_v/F_m may also be the onset of drought induced early senescence (Kooyers, 2015; Sade et al., 2018).

The operating efficiency of PSII (F_q'/F_m') was lower for all treatments in the second half of the experiment, with a parallel increase in NPQ. Non-photochemical quenching increases under high light levels, to dissipate light in excess of what can be used in photochemistry to prevent damage to the photosynthetic machinery, such as through ROS (reactive oxygen species) generation (Guidi et al., 2019). An increase in NPQ due to high light was demonstrated here with the increase in NPQ occurring alongside a high PPFD of PAR (Table 5.3, Fig. 5.13). As NPQ is in competition with photochemistry as a destination for absorbed light when there is an increase in PPFD, and thus a resulting greater fraction of light dissipated through NPQ, there will be a decrease in F_q'/F_m'. Another

factor is the effect of lower g_s for all treatments, which limits carbon assimilation and linear electron transport, and thus the operating efficiency of PSII (Baker, 2008).

All three chlorophyll fluorescence parameters show sensitivity to soil RWC, although F_v/F_m is largely unaffected until soil RWC drops below 60% (Fig. 5.12). Therefore, F_v/F_m can be used as a good indicator of severe water stress, as generally a decrease in F_v/F_m indicates damage to PSII reaction centres, although other factors can affect F_v/F_m, and stress effects on other aspects of a plant will not necessarily manifest into a lower F_v/F_m (Murchie & Lawson, 2013). The parameters of F_q'/F_m' and NPQ have been shown to related to soil water content, although this will depend on the type of soil, and how well the soil drains or retains water (Brutsaert, 2014; Hassan, 2006; Sarlikioti et al., 2010)

Using 800/550 as an indicator of chlorophyll content for the entire time period of the experiment, shows that F_v/F_m appears to be the most sensitive chlorophyll fluorescence parameter to chlorophyll content (Fig 5.12 D). The relationship between chlorophyll content and nitrogen content is closely linked, and photosynthetic capacity is affected by nitrogen content as, in addition to chlorophyll, Calvin cycle proteins constitute the majority of leaf nitrogen (Evans, 1989).

5.4.2 Measuring g_s and water status with the index of stomatal conductance

The index of stomatal conductance (I_g) did not show any significant differences between treatments. A part of why there was no significant difference can be attributed to environmental factors as there was low humidity, and thus increased evaporative demand, towards the end of the experiment, which would have resulted in stomatal closure due to an increased vapour pressure deficit (VPD) between leaf and ambient air (McAdam & Brodribb, 2015; Oren et al., 1999). Despite the effect of environment on g_s, measurements it did show a trend for a higher I_g for the watered treatments of *N* and *H* on the 26th June and 5th July (Fig, 5.5 B), suggesting there was an effect of water status on g_s.

While synthesis of ABA in the roots is a driver of stomatal closure under drought, in the presence of an increase in VPD, stomatal are able to respond and close due to guard cell-autonomous synthesis

of ABA (Bauer et al., 2013). Another factor to consider is the overall decrease in soil RWC for all treatments. While watered treatments were re-watered back up to desired water content, there was still a large amount of soil drying between watering, which would have occurred quicker for well watered soil (Brutsaert, 2014). However, despite this, I_g remains a strong indicator of soil RWC (Fig. 5.6 A), and therefore is a good indicator of water status. The relationship between I_g and leaf RWC would have been linear if not for a small group of *ND* and *HD* with an I_g near zero (Fig. 5.6 B), due to higher temperature, light level, and lower humidity on the day these measurements were collected (26th June), which would have affected drought treatments more than watered treatments.

There are factors aside from low water content or high temperatures and low humidity, that can affect g_s, with the biggest factor not accounted for here being the response of plant defences to disease or pests (Chaerle & Van Der Straeten, 2001), which can have a significant negative effect on measured conductance values. However, overall water status is one of the biggest factors affecting g_s, along with CO_2 concentration, light levels and humidity (Farquhar & Sharkey, 1982)

5.4.3 Spectral indices

A large number of spectral indices demonstrated sensitivity to chlorophyll content, predominantly due to the majority of indices used in the experiment consisting of at least one wavelength between 600nm and 700nm, a spectral region that is highly sensitive to chlorophyll content due to slightly weaker absorption in this region compared with blue (400nm – 500nm). Thus, any change in chlorophyll content will readily alter the amount of light that is absorbed in this spectral region (Sims & Gamon, 2002).

The relationship between indices and chlorophyll content was nonlinear, due to the absorbance of predominantly red light approaching saturation at high chlorophyll contents (Sims & Gamon, 2002). However, two indices which had both a high R^2 and a low RMSE, which were CI$_{RedEdge}$ and 800/550 (Table, 5.4). The index of 800/550 had the lowest RMSE, and was one of the best candidates as an index for tracking chlorophyll content. Indices that used NIR and green light have been shown to

perform strongly for measuring leaf chlorophyll content (Gitelson et al., 2003; Schlemmer et al., 2013; Zhou et al., 2016). Green or red-edge (i.e. approximately 690nm-720nm) regions are ideal as these region do not saturate as ready as blue or red spectral regions (Schlemmer et al., 2013; Ustin et al., 2009).

The spectral index of 800/550 showed significant differences in chlorophyll content between treatments (Fig. 5.8), overall with N and ND having consistently higher values than H and HD treatments. On the final day, the index value for ND was much lower, from 2.6 to 2.1, suggesting that the lower water content in the soil resulted in lower mass flow of water and nutrients to the roots of the plant, and thus reduced the uptake of soil nitrogen and therefore chlorophyll content (McMurtrie & Näsholm, 2018), as well as lower g_s reducing transpiration throughout the plant (Matimati et al., 2014).

The index of 800/440 showed good relationship with leaf RWC (R^2 = .61), indicating a good ability to track leaf RWC. The wavelength at 800nm has been associated with the internal structure of a leaf (Slaton et al., 2001), and thus it is sensitive to changes in the structure of the spongy mesophyll as a result of changes in water content. While the 800/550 index was also proposed previously (*Chapter 3*) as an index of measuring water status, it should also be noted that the strong relationship between 800/550 and chlorophyll content suggests that the very poor relationship seen here between index and leaf RWC (R^2 = .20) and soil RWC (R^2 = .10), is likely due to the effects of chlorophyll content overwhelming any spectral response due to water content. However, the blue spectral region, in which the 440nm wavelength is located, is the region experiencing the least sensitivity to chlorophyll content due to strong, saturating chlorophyll absorption of blue light (Ustin et al., 2009), and thus is not suitable for estimating chlorophyll content (Sims & Gamon, 2002). Therefore, from all indices investigated here, the 800/440 is the best performing index for assessing leaf RWC. The photochemical Reflectance Index (PRI) has a good relationship to both leaf and soil

RWC, and has been extensively utilised to track water status with generally good results (Ballester et al., 2017; Rossini et al., 2013; Sarlikioti, et al., 2010; Suárez et al., 2008).

While the 617/614 index demonstrates the best ability out of the reflectance based spectral indices to soil RWC, (Table 5.5), the performance of the 617/614 index is weak (R^2 = .35). It should be noted that the I_g index outperforms all spectral indices with regards to soil RWC (R^2 = .70). Thus, the I_g index is therefore recommended as the better technique for measurement of soil RWC, however the spectral indices are less affected by environmental factors such as PPFD (Table 5.6), with the low light of cloudy days associated with lower conductance across all plants, which can remove any differences in g_s between watered and droughted plants. A combination of a spectral index to measure leaf RWC and the I_g index to indicate soil RWC would provide a more robust assessment of water content.

There are many spectral indices described in the literature, demonstrating strong relationship between *N* and chlorophyll content. The performance between indices in most cases is broadly similar, however as many indices were developed on one species or variety (e.g. Lu et al., 2015; Schlemmer et al., 2013), there is a tendency for some indices to perform strongly in one instance (e.g. on a particular species), but in other instances has the same performance as other indices. In general, the most reliable performing indices will be very general; NDVI exploits the basic difference between red and NIR light due to chlorophyll absorption of red wavelengths, and similarly the $CI_{RedEdge}$ being initially defined as *(NIR/RedEdge) – 1* (Schlemmer et al., 2013). General spectral regions rather than any specific wavelengths should perform better for most species as the optimal choice of wavelength will vary between species and varieties. This should remain a consideration when using spectral indices for N or chlorophyll content assessment, and optimal indices and wavelengths should be determined prior to measurements.

A simplified spectral toolbox consisting of a combination of two indices; one to assess water content and another for nitrogen and chlorophyll content, can be used to indicate plant health (Fig. 5.10),

showing good separation of the four combinations of water and nitrogen treatments along the *x* and *y* axis, using the spectral indices of 800/440, 617/614 and PRI as indicators of water status.

5.4.4 Environmental Effects

Chlorophyll fluorescence parameters showed sensitivity to environmental factors, presumably due to changes in carboxylation and oxygenation of RuBP and Rubisco which is greatly affected by both temperature and water availability, and thus affecting the rate of photosynthesis (Lorimer, 1981). The overall decrease in leaf RWC due to high temperatures, and subsequent closure of stomata to low humidity is also a factor limiting carbon assimilation and thus photosynthetic efficiency (Baker, 2008). Spectral indices on the other hand appear to be unaffected by environmental factors, with the 800/440 index, which showed sensitivity to leaf RWC, showing no effect due to temperature, humidity or PPFD levels. As the spectral indices are measuring plant pigments or the effects of leaf structure through changes in internal refraction of light affecting the reflectance of NIR, the majority of spectral indices will thus be able to indicate the status of pigment and structural conditions within the leaf while remaining largely unaffected by the measurement environment. However, this is not a suggestion that chlorophyll fluorescence measurements are unsuitable, as the factors measured by both techniques are all crucial components of plant health and performance.

Finally, PRI showed some effect due to the levels of PAR, due to PRI being an indicator of the de-epoxidation state of the xanthophyll cycle, a component of NPQ which aids in heat dissipation of excess absorbed light energy (Baker, 2008), and thus is linked to NPQ measurements which were sensitive to environmental factors. However, it is worth considering that low light levels may reduce the ability of PRI to track water content (Sarlikioti et al., 2010).

5.4.5 Spectral Toolbox

By combining the techniques used in a spectral toolbox, the effects of light, temperature, and chlorophyll and water content, on plant health can be used to identify which effect is presently affecting plant health (Fig. 5.14). The toolbox, in simple terms, works as such; a decrease in the index of stomatal conductance (I_g) may indicate a decrease in plant or soil water content, if in conjunction with a decrease in the 800/440 index. If there is no response by spectral indices, than other factors are affecting g_s such as light, temperature and humidity, or as part of the plant defence mechanism against pests and diseases (Chaerle & Van Der Straeten, 2001)
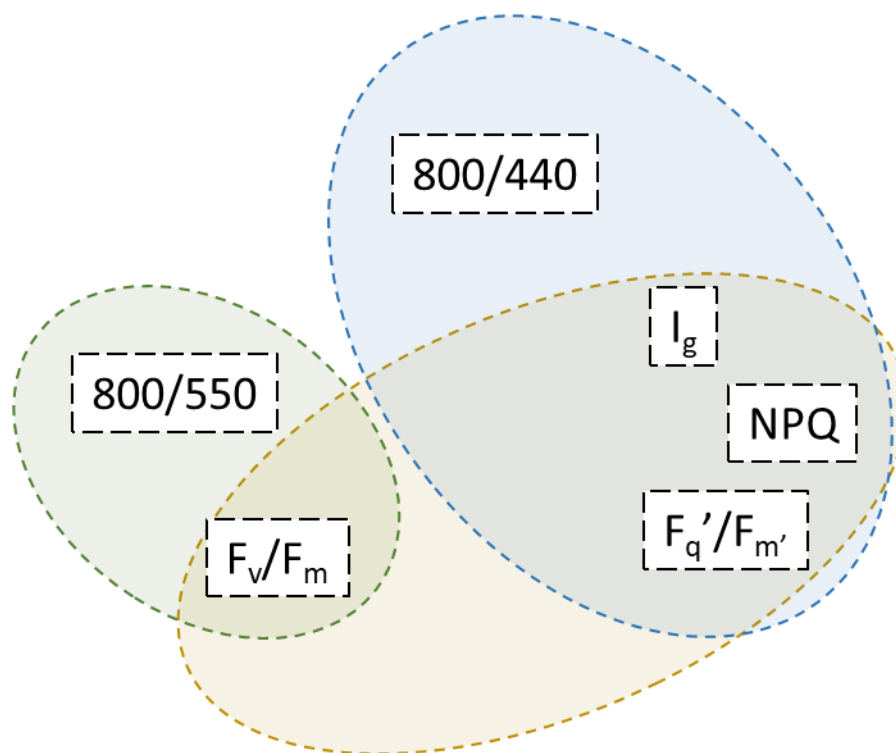
Figure 5.14 Selected indices and measurements, grouped in colours circles representing their ability to indicate (●) water content, (●) nitrogen content, and (●) temperature/humidity/PPFD stress effects

Similarly, decrease in F_q'/F_m' and increase in NPQ can indicate either low water content, or high light and temperature affecting plant performance. If there is a concurrent decrease in the 800/440 index, then there is low water content. If not, plant stress is likely due to high light, or temperature and humidity if there is a decrease I_g.

Finally, if there a decrease in the 800/550 index than there is a decrease in chlorophyll content. There may also be a decrease in F_q'/F_m' (Fig. 5.11 B) (Shangguan et al., 2000). If there is additionally a decline in F_v/F_m, then this indicates severe stress due to nitrogen deficiency.

5.5 Conclusion

A toolbox of spectral techniques can be used to track water and nitrogen of plants, as well as overall plant health and performance. The index of stomatal conductance (I_g), a thermographic technique, can be used to assess water content, predominantly soil relative water content (RWC). The spectral index of 800/550, among others, can be used to assess leaf nitrogen content, while the index of 800/440 can assess leaf water status. Chlorophyll fluorescence can be used to indicate overall plant performance and changes in soil RWC, while F_v/F_m is sensitive to plant nitrogen status. Overall, spectral reflectance indices such as 800/550 and 800/440 show limited effect to environmental factors, and alone can be used as a toolbox to assess plant water and nitrogen content through changes in pigment and leaf structure. However, the addition of thermography and chlorophyll fluorescence to this toolbox enhances the assessment of plant health by incorporating increased physiological measurements, of g_s and photosynthetic performance. The combination of techniques and spectral signatures allows for an overall picture of plant health, and knowledge of the factors driving changes in plant performance. These factors include the impact of high PPFD, high temperatures and low humidity, in addition to plant water and nitrogen status.

Chapter 6 - Discussion

6.1 Low cost NDVI imaging

The *NDVIpi* system provides a foundation for an imaging platform, allowing alternative optical filters to be used calibrated with the same proposed methodology. The benefits of this system over other options, such as commercial offerings, is the ability to customise the system and affordability. The Raspberry Pi is designed to be customisable both physically and in terms of software, and the *NDVIpi* provides a framework in which additional features can be added, or new spectral indices can be implemented for spectral imaging. To date, there is no complete system using low cost devices that can produce calibrated NDVI images, or a system that lends itself to customisation. All current systems require expensive optical filters (Dworak et al., 2013), or lack a comprehensive method of calibration.

The *NDVIpi* system thus fills a niche for low cost imaging devices. With an increased uptake of precision agriculture, especially with the use of unmanned aerial vehicles (Zhang & Kovacs, 2012), most robust and accurate systems commercially available are relatively expensive, ranging from US$4500 for the Micasense RedEdge down to US$1600 for more simpler systems, there is very little option available in the price range of US$400-US$800 that is capable of robust, accurate NDVI measurements.

For research applications this also allows the system to be integrated with other imaging based systems, allowing for more comprehensive imaging and maps of crop performance and health. For instance, thermography, another imaging based technique, is used to measure evapotranspiration and stomatal conductance of plants (Grant et al., 2016; Grant et al., 2006; Guilioni et al., 2008; Leinonen et al., 2006; Maes et al., 2016), and used to indicate water status (Jones et al., 2009; Möller et al., 2007).

Imaging systems for measuring thermography are rapidly decreasing in both size and price, and therefore would be a logical next step in integrating with NDVI imagery. NDVI imaging is regularly used agriculturally as an indicator of chlorophyll and nitrogen content, to optimise fertilizer input and estimating yield. A combined NDVI and thermal imaging system could give an overview of the two primary factors of crop performance, water status and nitrogen content, at an affordable price compared to many multispectral or multi-technique devices, while being more accessible. This can improve yield forecasting, and take precision agriculture to the next step, enabling farms to optimise fertilizer and irrigation inputs to optimise yields and save resources through precise applications of these inputs (Balafoutis et al., 2017; van Evert et al., 2017). For instance, if the NDVI system was employed on a UAV, images could be taken of the entire field. The farmer could then use the subsequent imagery to map NDVI for the entire field, and determine which regions of that field require additional fertilizer application, rather than blanket fertilization of the entire field which will cost more due to the use of more fertilizer, fuel for vehicles, and the cost of any additional labour. Further, reduced fertilizer use can be beneficial to the local environment by preventing the effects of runoff on streams and rivers and other environmental effects (Mulholland et al., 2008; Prasad, 1998). Precision agriculture allows for site-specific inputs (e.g. fertilizer, irrigation) over blanket applications, which not only reduces outgoing costs and therefore increasing profits for farmers, but can reduce greenhouse emissions due to the use of vehicles only when required (Balafoutis et al., 2017; van Evert et al., 2017)

6.2 Spectral signatures and further considerations

The development of spectral indices to measure water content allows farmers and researcher to track water status without the need for destructive assessment of leaf water content, or time consuming assessments of soil water content. However, the proposed indices in *Chapter 4* performed relatively poorly due to the low variability in leaf water content, and thus very little water stress was exhibited. This can be seen by the strong performance of these indices in *Chapter 5*, in

which there was sufficient variation in water status to demonstrate the relationship between these indices and leaf water content. The poor performance of these indices to initially indicate low water content may indicate an insensitivity of visible and NIR based spectral indices to small changes in water status. This is likely due to a combination of factors related to leaf structure that affect the internal refraction of NIR light (Slaton et al., 2001). It is also possible that this effect was species dependant, due to difference in leaf structure between species (Gausman & Allen, 1973), especially as *Chapter 5* investigated water status on wheat rather the *Arabidopsis* plants of *Chapter 4,* and *Chapter 3* worked primarily on *Phaseolus.* It may be that in some species, water content needs to decrease sufficiently for leaf structure to alter and affect the refraction of NIR light across the air/cell interfaces within the spongy mesophyll, whereas in other species (e.g. *Phaselous*) a small change in water content will have a greater effect. At this stage, this is clearly an area that requires further investigation before a conclusion can be made.

Ultimately, some species may be suitable for assessing water status through spectral reflectance in the visible and NIR spectrum, while some may not. Understanding how spectral signatures vary between species is an important aspect of any spectral based toolbox, and understanding the relevant baseline measurements of healthy and stress plants for each species is crucial if spectral techniques are intended to be employed in the field for assessing crop health. This is not exclusive to spectral reflectance based indices, but all techniques. As seen in *Chapter 4*, Col-0 and C24 had vastly different stomatal conductances under normal well-watered conditions (Fig. 4.6, 4.7), with the values for healthy C24 at a similar range as Col-0 with low soil RWC. If a spectral toolbox consisting of thermography was used to measure a crop in the field for instance, and ecotype or variety was not accounted for, this would falsely lead to the assumption that the crops were experiencing low water content, and therefore would be at risk of being over watered. Therefore, it is imperative that baseline data is determined for any species or variety prior to a spectral toolbox being deployed in the field. This may mean that small-scale experiments are performed to 'calibrate' a spectral toolbox to each species and variety that will be monitored.

6.3 Combined Techniques

The combination of the spectral techniques of chlorophyll fluorescence, thermography and spectral reflectance (*Chapter 5*) is a step towards the development of a stress 'catalogue' (Chaerle et al., 2009), detailing the spectral response to biotic and abiotic stressors that negatively affect plant health. While combined techniques have been used before (Calderón et al., 2013; Chaerle et al., 2007; Khanna et al., 2019; Panigada et al., 2014; Suárez et al., 2008), there is no body of work for combining all three spectral techniques. While a framework for assessing plant health has been proposed before, using hyperspectral and other imaging based techniques (Khanna et al., 2019), the addition of thermography and chlorophyll fluorescence allows for a greater understanding of plant performance, with can identify the onset of stress before physical effects of reduced biomass or significant pigment loss can take hold.

Hyperspectral imaging can yield significant information regarding plant health and photosynthetic efficiency, such as the maximum rate of carboxylation (Meacham-Hensold et al., 2019), and should be considered as a useful tool in conjunction with visible and NIR spectrometry, although the high cost of equipment should also be considered. Actively induced chlorophyll fluorescence (i.e. PAM) is a technique that does not necessarily lend itself well to remote sensing applications due to the application of a saturating light pulse, which is not practical at a canopy level, and as such may be one of the biggest bottlenecks regarding the use of a spectral toolbox if the technique is primarily a leaf-level measurement. However, new techniques have been developed that can allow for remote and rapid chlorophyll fluorescence measurements. One of the most common is the use of solar induced fluorescence (SIF) (Meroni et al., 2009), which exploits the absorption of light by atmospheric oxygen at a specific wavelengths, known as Fraunhoffer lines, that also corresponds with chlorophyll fluorescence emission spectra. The reduced intensity of light in the Fraunhoffer lines enable the weak emission of chlorophyll fluorescence to be detected, with the emission spectra adding to the apparent reflectance at these wavelengths (Zarco-Tejada et al., 2000). Thus, variation

in apparent reflectance corresponds to variation in the emission of light through chlorophyll fluorescence. While this technique allows for the measurement of steady state chlorophyll fluorescence, the technique does not actively probe the plant through conventional pulse amplitude-modulated (PAM) measurements (Baker, 2008; Maxwell & Johnson, 2000; Murchie & Lawson, 2013), and so the parameters that can be measured is limited. For instance, $F_{q'}/F_{m'}$, F_v/F_m and NPQ are parameters that can not be measured this way, and are integral to measuring photosynthetic performance and play a large role in the spectral toolbox of *Chapter 4* and *Chapter 5,* with *Chapter 5* especially relying on these parameters for assessing both water and nitrogen content. However, SIF is not necessarily intended as a replacement for other chlorophyll fluorescence parameters, but as an improvement over reflectance based indices for detecting plant stress (Meroni et al., 2009), and there is a body of work using steady-state fluorescence to monitor water stress in plants (Gerhards et al., 2018; Porcar-Castell et al., 2014; Zarco-Tejada et al., 2012) and connecting SIF measurements to other chlorophyll fluorescence parameters (Magney et al., 2017). However, advances in chlorophyll fluorescence technique are enabling the measurement of active chlorophyll fluorescence measurements through remote actively induced measurements using remote pulsed laser based systems (Pieruschka et al., 2012).

Further work on the development of a spectral toolbox needs to expand the stressors investigated beyond water and nitrogen content. While meteorological factors were also investigated, more depth and a larger range of environments needs to be included. Additional stressors, which also have significant impacts on crop yields (Cerda et al., 2017; Oerke, 2006) include pests and disease, which is estimated to be an increasingly import factor under a changing climate (Rosenzweig et al., 2001). Pests and disease affect stomatal conductance, which decreases to prevent further pathogen entry and infection to the rest of the plant (Melotto et al., 2008) and subsequent decreases in nutrient availability and photosynthetic performance. These are, however, all factors that can be detected with spectral signatures, from spectral reflectance (Bauriegel et al., 2011; Calderón et al., 2013; Huang et al., 2015; Rispail & Rubiales, 2015; Saad et al., 2013), to thermography (Chaerle et

al., 1999; Chaerle et al., 2004) and chlorophyll fluorescence (Chaerle et al., 2004) imaging. Logically, building upon this body of work and inclusion of this body of work into the spectral toolbox is clearly also one of the next steps.

Finally, not just assessing the spectral toolbox both across species as previously mentioned, but also assessing the difference between leaf and canopy measurements is required to understand the limitations of the toolbox. Some indices are sensitive to atmospheric effects, or variation in canopy structure, leaf angle, background reflectance and angle of irradiating light (Ballester et al., 2017), and thus there can be a difference in performance between leaf level measurements (i.e. in a laboratory based phenotyping system) and canopy measurement (i.e. UAV or tractor mounted). Similarly, variation in leaf structure and pigment content between species can vary the effectiveness of spectral indices (Ballester et al., 2017), and while it has been reported that this is less of an issues that initially suspected (Sims & Gamon, 2002), understanding baseline measurements of each species is still necessary

6.4 Conclusion

In conclusion, spectral based technique allow for rapid, non-invasive probing of plant and crop health, and have potential to overcome current phenotyping bottlenecks, while enabling farmers to optimise the inputs of fertilizer, water and pesticides on their crops to maximise yields and reduce expenditure. Here we developed a low cost NDVI imaging system based on the Raspberry Pi system, complete with a method for calibrating Raspberry Pi images. Low cost imagery opens up precision agriculture to more researchers and farmers, benefiting yields and phenotyping for future crops, a necessary step in mitigating the effects of a changing climate and global population growth. We developed novel spectral indices that demonstrate potential for the assessment of leaf water content, that are based on visible and near infra-red wavelengths, allowing for these indices to be used with conventional spectrometry equipment, or even incorporated into imaging platforms, rather than the SWIR wavelengths that are conventionally used in remote measurements of water

content. These indices were the incorporated into a spectral toolbox consisting of other reflectance indices, thermography and chlorophyll fluorescence. This spectral toolbox was successfully able to indicate the water and nitrogen status of wheat, and serves as a foundation for future work using spectral toolboxes.

Chapter 7 – References

Ahmad, P., Sarwat, M., & Sharma, S. (2008). Reactive oxygen species, antioxidants and signaling in plants. *Journal of Plant Biology*, *51*(3), 167–173. https://doi.org/10.1007/BF03030694

Afzal, A., Duiker, S. W., & Watson, J. E. (2017). Leaf thickness to predict plant water status. *Biosystems Engineering*, *156*(2011), 148–156. https://doi.org/10.1016/j.biosystemseng.2017.01.011

Ainsworth, E. A., Serbin, S. P., Skoneczka, J. A., & Townsend, P. A. (2014). Using leaf optical properties to detect ozone effects on foliar biochemistry. *Photosynthesis Research*, *119*(1–2), 65–76. https://doi.org/10.1007/s11120-013-9837-y

Anderson, H. B., Nilsen, L., Tømmervik, H., Karlsen, S. R., Nagai, S., & Cooper, E. J. (2016). Using ordinary digital cameras in place of near-infrared sensors to derive vegetation indices for phenology studies of High Arctic vegetation. *Remote Sensing*, *8*(10). http://doi.org/10.3390/rs8100847

Anika, R., Toomey, M., Aubrecht, D. M., & Richardson, A. D. (2018). Monitoring vegetation phenology using an infrared-enabled security camera. *Agricultural and Forest Meteorology 195-196*, *195–196*, 143–151. http://doi.org/10.1016/j.agrformet.2014.05.008

Apan, A., Held, A., Phinn, S., & Markley, J. (2002). Detecting sugarcane 'orange rust' disease using EO-1 Hyperion hyperspectral imagery. *International Journal of Remote Sensing*, *25*(2), 489–498.

Araus, J. L., & Cairns, J. E. (2014). Field high-throughput phenotyping: the new crop breeding frontier. *Trends in Plant Science*, *19*(1), 52–61. https://doi.org/10.1016/j.tplants.2013.09.008

Ashourloo, D., Mobasheri, M. R., & Huete, A. (2014). Developing Two Spectral Disease Indices for Detection of Wheat Leaf Rust (Pucciniatriticina). *Remote Sens*, *6*, 4723–4740. https://doi.org/10.3390/rs6064723

Asner, G. P. (1998). Biophysical and biochemical sources of variability in canopy reflectance. *Remote Sensing of Environment*, *64*(3), 234–253. https://doi.org/10.1016/S0034-4257(98)00014-5

Assmann, S. M., & Shimazaki, K. (1999). The Multisensory Guard Cell. Stomatal Responses to Blue Light and Abscisic Acid. *Plant Physiology*, *119*(3), 809–816. https://doi.org/10.1104/pp.119.3.809

Ayala-Silva, T., & Beyl, C. A. (2005). Changes in spectral reflectance of wheat leaves in response to specific macronutrient deficiency. *Adv Space Res.*, *35*(2), 305–317. Retrieved from http://www.ncbi.nlm.nih.gov/pubmed/15934211

Baker, N. R. (2008). Chlorophyll fluorescence: a probe of photosynthesis in vivo. *Annual Review of Plant Biology*, *59*, 89–113. https://doi.org/10.1146/annurev.arplant.59.032607.092759

Baker, N. R., & Rosenqvist, E. (2004). Applications of chlorophyll fluorescence can improve crop production strategies: An examination of future possibilities. *Journal of Experimental Botany*, *55*(403), 1607–1621. https://doi.org/10.1093/jxb/erh196

Balafoutis, A., Beck, B., Fountas, S., Vangeyte, J., Van Der Wal, T., Soto, I., … Eory, V. (2017). Precision agriculture technologies positively contributing to ghg emissions mitigation, farm productivity and economics. *Sustainability (Switzerland)*, *9*(8), 1–28. https://doi.org/10.3390/su9081339

Ballester, C., Zarco-Tejada, P. J., Nicolás, E., Alarcón, J. J., Fereres, E., Intrigliolo, D. S., & Gonzalez-

Dugo, V. (2017). Evaluating the performance of xanthophyll, chlorophyll and structure-sensitive spectral indices to detect water stress in five fruit tree species. *Precision Agriculture*, *2017*, 1–16. https://doi.org/10.1007/s11119-017-9512-y

Ballottari, M., Girardon, J., Dall'Osto, L., & Bassi, R. (2012). Evolution and functional properties of Photosystem II light harvesting complexes in eukaryotes. *Biochimica et Biophysica Acta - Bioenergetics*, *1817*(1), 143–157. https://doi.org/10.1016/j.bbabio.2011.06.005

Baluja, J., Diago, M. P., Balda, P., Zorer, R., Meggio, F., Morales, F., & Tardaguila, J. (2012). Assessment of vineyard water status variability by thermal and multispectral imagery using an unmanned aerial vehicle (UAV). *Irrigation Science*, *30*(6), 511–522. https://doi.org/10.1007/s00271-012-0382-9

Bannari, A., Morin, D., Bonn, F., & Huete, A. R. (1995). A review of vegetation indices. *Remote Sensing Reviews*, *13*(1), 95–120. https://doi.org/10.1080/02757259509532298

Barati, S., Rayegani, B., Saati, M., Sharifi, A., & Nasri, M. (2011). Comparison the accuracies of different spectral indices for estimation of vegetation cover fraction in sparse vegetated areas The Egyptian Journal of Remote Sensing and Space Sciences. *The Egyptian Journal of Remote Sensing and Space Sciences*, *14*, 49–56. https://doi.org/10.1016/j.ejrs.2011.06.001

Bauer, H., Ache, P., Lautner, S., Fromm, J., Hartung, W., Al-rasheid, K. A. S., … Hedrich, R. (2013). The Stomatal Response to Reduced Relative Humidity Requires Guard Cell-Autonomous ABA Synthesis. *Current Biology*, *23*(1), 53–57. https://doi.org/10.1016/j.cub.2012.11.022

Bauriegel, E., Giebel, A., Geyer, M., Schmidt, U., & Herppich, W. B. (2011). Early detection of Fusarium infection in wheat using hyper-spectral imaging. *Computers and Electronics in Agriculture*, *75*(2), 304–312. https://doi.org/10.1016/j.compag.2010.12.006

Baugh, W. M., & Groeneveld, D. P. (2008). Empirical proof of the empirical line. *International Journal of Remote Sensing*, *29*(3), 665–672. http://doi.org/10.1080/01431160701352162

Bechtold, U., Ferguson, J. N., & Mullineaux, P. M. (2018). To defend or to grow: Lessons from Arabidopsis C24. *Journal of Experimental Botany*, *69*(11), 2809–2821. https://doi.org/10.1093/jxb/ery106

Bechtold, U., Lawson, T., Mejia-Carranza, J., Meyer, R. C., Brown, I. R., Altmann, T., … Mullineaux, P. M. (2010). Constitutive salicylic acid defences do not compromise seed yield, drought tolerance and water productivity in the Arabidopsis accession C24. *Plant, Cell and Environment*, *33*(11), 1959–1973. https://doi.org/10.1111/j.1365-3040.2010.02198.x

Betterle, N., Ballottari, M., Zorzan, S., de Bianchi, S., Cazzaniga, S., Dall'Osto, L., … Bassi, R. (2009). Light-induced dissociation of an antenna hetero-oligomer is needed for non-photochemical quenching induction. *Journal of Biological Chemistry*, *284*(22), 15255–15266. https://doi.org/10.1074/jbc.M808625200

Biehler, K., & Fock, H. (1996). Evidence for the contribution of the Mehler-peroxidase reaction in dissipating excess electrons in drought-stressed wheat. *Plant Physiology*, *112*(1), 265–272. https://doi.org/10.1104/pp.112.1.265

Bilger, W., Bjorkman, O., & Thayer, S. S. (1989). *Light-induced Spectral Absorbance Changes in Relation to Photosynthesis and the Epoxidation State of Xanthophyll Cycle Components in Cotton Leaves1*. 542–551.

Boulord, R., Frisson, T., Ryckewaert, M., & Christophe, A. (2000). PYM : a new , affordable , image-based method using a Raspberry Pi to phenotype plant leaf area in a wide diversity of environments. *Plant Methods*, 1–17. http://doi.org/10.1186/s13007-017-0248-5

Búrquez, A. (1987). Leaf Thickness and Water Deficit in Plants: A Tool for Field Studies. *Journal of Experimental Botany*, *38*(186), 109–114.

Bradbury, M., & Baker, R. N. (1981). Analysis of the slow phases of the in vivo chlorophyll fluorescence induction curve. Changes in the redox state of photosystem II electron acceptors and fluorescence emission from photosystems I and II. *Biochim Biophys Acta.*, *635*(3), 542–551.

Broadley, M. R., Escobar-Gutiérrez, A. J., Burns, A., Burns, I. G. (2010). Nitrogen-limited growth stomatal conductance of lettuce is associated with lower. *New Phytologist*, *152*(1), 97–106.

Brutsaert, W. (2014). Daily evaporation from drying soil: Universal parameterization with similarity. *Water Resources Research*, *50*(4), 3206–3215. https://doi.org/10.1002/2013WR014872

Caemmerer, S. Von. (2000). Biochemical models of leaf photosynthesis. *Techniques in Plant Sciences*, *53*(9), 1689–1699. https://doi.org/10.1017/CBO9781107415324.004

Campbell, P. K. E., Middleton, E. M., Corp, L. A., & Kim, M. S. (2008). Contribution of chlorophyll fluorescence to the apparent vegetation reflectance. *Science of The Total Environment*, *404*(2–3), 433–439. https://doi.org/http://dx.doi.org/10.1016/j.scitotenv.2007.11.004

Carter, G. (1993). Responses of Leaf Spectral Reflectance to Plant Stress. *American Journal of Botany*, *80*(3), 239. https://doi.org/10.2307/2445346

Carter, G. A., & Knapp, A. K. (2001). Leaf optical properties in higher plants: linking spectral characteristics to stress and chlorophyll concentration. *American Journal of Botany*, *88*(4), 677–684. https://doi.org/10.2307/2657068

Calderón, R., Navas-Cortés, J. A., Lucena, C., & Zarco-Tejada, P. J. (2013). High-resolution airborne hyperspectral and thermal imagery for early detection of Verticillium wilt of olive using fluorescence, temperature and narrow-band spectral indices. *Remote Sensing of Environment*, *139*, 231–245. https://doi.org/10.1016/j.rse.2013.07.031

Castro, K. L., & Sanchez-Azofeifa, G. A. (2008). Changes in Spectral Properties, Chlorophyll Content and Internal Mesophyll Structure of Senescing Populus balsamifera and Populus tremuloides Leaves. *Sensors*, *8*, 51–69. https://doi.org/10.3390/s8010051

Ceccato, P., Flasse, S., Tarantola, S., Jacquemoud, S., & Grégoire, J. M. (2001). Detecting vegetation leaf water content using reflectance in the optical domain. *Remote Sensing of Environment*, *77*(1), 22–33. https://doi.org/10.1016/S0034-4257(01)00191-2

Cerda, R., Avelino, J., Gary, C., Tixier, P., Lechevallier, E., & Allinne, C. (2017). Primary and secondary yield losses caused by pests and diseases: Assessment and modeling in coffee. *PLoS ONE*, *12*(1), 1–17. https://doi.org/10.1371/journal.pone.0169133

Chaerle, L, Hagenbeek, D., De Bruyne, E., Valcke, R., & Van Der Straeten, D. (2004). Thermal and chlorophyll-fluorescence imaging distinguish plant-pathogen interactions at an early stage. *Plant and Cell Physiology*, *45*(7), 887–896. https://doi.org/10.1093/pcp/pch097

Chaerle, L, Leinonen, I., Jones, H. G., & Van Der Straeten, D. (2007). Monitoring and screening plant populations with combined thermal and chlorophyll fluorescence imaging. *Journal of Experimental Botany*, *58*(4), 773–784. https://doi.org/10.1093/jxb/erl257

Chaerle, L., Lenk, S., Leinonen, I., Jones, H. G., Van Der Straeten, D., & Buschmann, C. (2009). Multi-sensor plant imaging: Towards the development of a stress-catalogue. *Biotechnology Journal*, *4*(8), 1152–1167. https://doi.org/10.1002/biot.200800242

Chaerle, L, Van Caeneghem, W., Messens, E., Lambers, H., Van Montagu, M., & Van Der Straeten, D. (1999). Presymptomatic visualization of plant-virus interactions by thermography. *Nature*

Biotechnology, *17*(8), 813–816. https://doi.org/10.1038/11765

Chaerle, L, & Van Der Straeten, D. (2001). Seeing is believing: Imaging techniques to monitor plant health. *Biochimica et Biophysica Acta - Gene Structure and Expression*, *1519*(3), 153–166. https://doi.org/10.1016/S0167-4781(01)00238-X

Chang, K. W., Shen, Y., & Lo, J. C. (2005). Predicting rice yield using canopy reflectance measured at booting stage. *Agronomy Journal*, *97*(3), 872–878. https://doi.org/10.2134/agronj2004.0162

Chappelle, E. W., McMurtrey, J. E., Wood, F. M., & Newcomb, W. W. (1984). Laser-induced fluorescence of green plants 2: LIF caused by nutrient deficiencies in corn. *Applied Optics*, *23*(1), 139. https://doi.org/10.1364/ao.23.000139

Chaves, M. M., Pereira, J. S., Maroco, J., Rodrigues, M. L., Ricardo, C. P. P., Osório, M. L., … Pinheiro, C. (2002). How plants cope with water stress in the field. Photosynthesis and growth. *Annals of Botany*, *89*(SPEC. ISS.), 907–916. https://doi.org/10.1093/aob/mcf105

Chutia, J., & Borah, S. P. (2012). Water Stress Effects on Leaf Growth and Chlorophyll Content but Not the Grain Yield in Traditional Rice (Oryza sativa Linn.) Genotypes of Assam, India II. Protein and Proline Status in Seedlings under PEG Induced Water Stress. *American Journal of Plant Sciences*, *3*(July), 971–980. https://doi.org/10.4236/ajps.2012.37115

Clevers, J. G. P. W., & Gitelson, A. A. (2013). Remote estimation of crop and grass chlorophyll and nitrogen content using red-edge bands on sentinel-2 and-3. *International Journal of Applied Earth Observation and Geoinformation*, *23*(1), 344–351. https://doi.org/10.1016/j.jag.2012.10.008

Cook, R. J. (2000). Advances in Plant Health Management in the Twentieth Centure. *Annu. Rev. Phytopathol.*, *38*, 95–116. https://doi.org/10.1177/000312240507000602

Cooper, A. (2005). Heat capacity effects in protein folding and ligand binding: A re-evaluation of the role of water in biomolecular thermodynamics. *Biophysical Chemistry*, *115*(2-3 SPEC. ISS.), 89–97. https://doi.org/10.1016/j.bpc.2004.12.011

Cotelle, V., & Leonhardt, N. (2019). ABA signaling in guard cells. *Advances in Botanical Research*, *92*, 115–170. https://doi.org/10.1016/bs.abr.2019.10.001

Das, A. J., Wahi, A., Kothari, I., & Raskar, R. (2016). Ultra-portable , wireless smartphone spectrometer for rapid , non-destructive testing of fruit ripeness. *Nature Publishing Group*, (April), 1–8. http://doi.org/10.1038/srep32504

Datt, B. (1999). A New Reflectance Index for Remote Sensing of Chlorophyll Content in Higher Plants: Tests using Eucalyptus Leaves. *Journal of Plant Physiology*, *154*, 30–36. https://doi.org/10.1016/S0176-1617(99)80314-9

Daughtry, C. S. T., Walthall, C. L., Kim, M. S., de Colstoun, E. B., & McMurtrey, J. E. (2000). Estimating corn leaf chlorophyll concentration from leaf and canopy reflectance. *Remote Sensing of Environment*, *74*(2), 229–239. https://doi.org/10.1016/s0034-4257(00)00113-9

Davenport, J. R., Perry, E. M., Lang, N. S., & Stevens, R. G. (2005). Leaf spectral reflectance for nondestructive measurement of plant nutrient status. *HortTechnology*, *15*(1), 31–35.

Deglint, J. L., Schoneveld, K., Kazemzadeh, F., & Wong, A. (2016). A Compact Field-portable Computational Multispectral Microscope using Integrated Raspberry Pi. *Journal of Computational Vision and Imaging Systems*, *2*(1). Retrieved from http://openjournals.uwaterloo.ca/index.php/vsl/article/view/91

Demmig-Adams, B, Garab, G., Adams III, W. W., & Govindjee. (2014). *Non-Photochemical Quenching*

and Energy Dissipation in Plants, Algae and Cyanobacteria, (1st ed.). Springer Netherlands.

Demmig-Adams, B., & Adams, W. W. (2006). Photoprotection in an ecological context: The remarkable complexity of thermal energy dissipation. *New Phytologist*, *172*(1), 11–21. https://doi.org/10.1111/j.1469-8137.2006.01835.x

Demmig-Adams, B. (1990). Carotenoids and photoprotection in plants: A role for the xanthophyll zeaxanthin. *BBA - Bioenergetics*, *1020*(1), 1–24. https://doi.org/10.1016/0005-2728(90)90088-L

Demmig, B., Winter, K., Krüger, a, & Czygan, F. C. (1988). Zeaxanthin and the Heat Dissipation of Excess Light Energy in Nerium oleander Exposed to a Combination of High Light and Water Stress. *Plant Physiology*, *87*(1), 17–24. https://doi.org/10.1104/pp.87.1.17

Ding, L., Wang, K. J., Jiang, G. M., Biswas, D. K., Xu, H., Li, L. F., & Li, Y. H. (2005). Effects of nitrogen deficiency on photosynthetic traits of maize hybrids released in different years. *Annals of Botany*, *96*(5), 925–930. https://doi.org/10.1093/aob/mci244

Dobrowski, S. Z., Pushnik, J. C., Zarco-Tejada, P. J., & Ustin, S. L. (2005). Simple reflectance indices track heat and water stress-induced changes in steady-state chlorophyll fluorescence at the canopy scale. *Remote Sensing of Environment*, *97*(3), 403–414. https://doi.org/10.1016/j.rse.2005.05.006

Döring, T. F., Pautasso, M., Finckh, M. R., & Wolfe, M. S. (2012). Concepts of plant health - reviewing and challenging the foundations of plant protection. *Plant Pathology*, *61*(1), 1–15. https://doi.org/10.1111/j.1365-3059.2011.02501.x

Drusch, M., Del Bello, U., Carlier, S., Colin, O., Fernandez, V., Gascon, F., … Bargellini, P. (2012). Sentinel-2: ESA's Optical High-Resolution Mission for GMES Operational Services. *Remote Sensing of Environment*, *120*, 25–36. http://doi.org/10.1016/j.rse.2011.11.026

Dworak, V., Selbeck, J., Dammer, K. H., Hoffmann, M., Zarezadeh, A. A., & Bobda, C. (2013). Strategy for the development of a smart NDVI camera system for outdoor plant detection and agricultural embedded systems. *Sensors (Switzerland)*, *13*(2), 1523–1538. http://doi.org/10.3390/s130201523

Edelman, M., & Mattoo, A. K. (2008). D1-protein dynamics in photosystem II: The lingering enigma. *Photosynthesis Research*, *98*(1–3), 609–620. https://doi.org/10.1007/s11120-008-9342-x

Eitel, J. U. H., Keefe, R. F., Long, D. S., Davis, A. S., & Vierling, L. a. (2010). Active ground optical remote sensing for improved monitoring of seedling stress in nurseries. *Sensors*, *10*(4), 2843–2850. http://doi.org/10.3390/s100402843

Elvanidi, A., Katsoulas, N., Bartzanas, T., Ferentinos, K. P., & Kittas, C. (2017). Crop water status assessment in controlled environment using crop reflectance and temperature measurements. *Precision Agriculture*, 1–18. https://doi.org/10.1007/s11119-016-9492-3

ESA. (2020). Sentinel Online: Technical Guide. Retrieved March 11, 2020, from https://sentinel.esa.int/web/sentinel/sentinel-technical-guides

Evain, S., Flexas, J., & Moya, I. (2004). A new instrument for passive remote sensing: 2. Measurement of leaf and canopy reflectance changes at 531 nm and their relationship with photosynthesis and chlorophyll fluorescence. *Remote Sensing of Environment*, *91*(2), 175–185. https://doi.org/10.1016/j.rse.2004.03.012

Evans, J. R. (1983). Nitrogen and Photosynthesis in the Flag Leaf of Wheat (Triticum aestivum L.). *Plant Physiology*, *72*(2), 297–302. https://doi.org/10.1104/pp.72.2.297

Evans, J. R. (1989). Photosynthesis and nitrogen relationships in leaves of C3 plants. *Oecologia*, *78*,

9–19.

Fageria, N. K., Baligar, V. C., & Li, Y. C. (2008). The role of nutrient efficient plants in improving crop yields in the twenty first century. *Journal of Plant Nutrition*, *31*(6), 1121–1157. https://doi.org/10.1080/01904160802116068

FAO. (2012). *The State of Food Insecurity in the World 2012. Economic growth is necessary but not sufficient to accelerate reduction of hunger and malnutrition*. Rome.

Faralli, M., Cockram, J., Ober, E., Wall, S., Galle, A., Van Rie, J., … Lawson, T. (2019). Genotypic, Developmental and Environmental Effects on the Rapidity of gs in Wheat: Impacts on Carbon Gain and Water-Use Efficiency. *Frontiers in Plant Science*, *10*(April), 1–13. https://doi.org/10.3389/fpls.2019.00492

Farquhar, G. D., & Sharkey, T. D. (1982). Stomatal conductance and photosynthesis. *Ann. Rev. Plant. Physiol.,* 33, 317-345

Fanizza, G., Ricciardi, L., & Bagnulo, C. (1991). Leaf greenness measurements to evaluate water stressed genotypes in Vitis vinifera. *Euphytica*, *55*(1), 27–31. https://doi.org/10.1007/BF00022556

Feret, J. B., François, C., Asner, G. P., Gitelson, A. A., Martin, R. E., Bidel, L. P. R., … Jacquemoud, S. (2008). PROSPECT-4 and 5: Advances in the leaf optical properties model separating photosynthetic pigments. *Remote Sensing of Environment*, *112*(6), 3030–3043. https://doi.org/10.1016/j.rse.2008.02.012

Fernández-Marín, B., Míguez, F., Becerril, J. M., & García-plazaola, J. I. (2011). Activation of violaxanthin cycle in darkness is a common response to different abiotic stresses: a case study in Pelvetia canaliculata. *BMC Plant Biology*, *11*(1), 181. https://doi.org/10.1186/1471-2229-11-181

Ferrier, G. (1995). Evaluation of apparent surface reflectance estimation methodologies. *International Journal of Remote Sensing*, *16*(12), 2291–2297. http://doi.org/10.1080/01431169508954557

Filella, I., & Penuelas, J. (1994). The red edge position and shape as indicators of plant chlorophyll content, biomass and hydric status. *Int. J. Remote Sensing*, Vol. 15, pp. 1459–1470. https://doi.org/10.1080/01431169408954177

Flexas, J., Escalona, J. M., Evain, S., Gulías, J., Moya, I., Osmond, C. B., & Medrano, H. (2002). Steady-state chlorophyll fluorescence (Fs) measurements as a tool to follow variations of net CO2 assimilation and stomatal conductance during water-stress in C3 plants. *European Space Agency, (Special Publication) ESA SP*, (527), 26–29. https://doi.org/doi: 10.1034/j.1399-3054.2002.1140209.x

Flexas, J., Escalona, J. M., & Medrano, H. (1999). Water stress induces different levels of photosynthesis and electron transport rate regulation in grapevines. *Plant, Cell and Environment*, *22*(1), 39–48. https://doi.org/10.1046/j.1365-3040.1999.00371.x

Foley, S., Rivard, B., Sanchez-Azofeifa, G. A., & Calvo, J. (2006). Foliar spectral properties following leaf clipping and implications for handling techniques. *Remote Sensing of Environment*, *103*(3), 265–275. https://doi.org/10.1016/j.rse.2005.06.014

Friedrichs, A., Busch, J. A., Woerd, H. J. Van Der, & Zielinski, O. (2017). *SmartFluo : A Method and Affordable Adapter to Measure Chlorophyll a Fluorescence with Smartphones*. (1), 1–14. https://doi.org/10.3390/s17040678

Fuchs, M. (1990). Infrared measurement of canopy temperature and detection of plant water stress. *Theoretical and Applied Climatology*, *42*(4), 253–261. https://doi.org/10.1007/BF00865986

Furbank, R. T., & Tester, M. (2011). Phenomics - technologies to relieve the phenotyping bottleneck. *Trends in Plant Science*, *16*(12), 635–644. https://doi.org/10.1016/j.tplants.2011.09.005

Gamon, J. A., Field, C. B., Bilger, W., Björkman, O., Fredeen, A. L., & Peñuelas, J. (1990b). Remote sensing of the xanthophyll cycle and chlorophyll fluorescence in sunflower leaves and canopies. *Oecologia*, *85*(1), 1–7. https://doi.org/10.1007/BF00317336

Gamon, J. A., Field, C. B., Goulden, M. L., Griffin, K. L., Hartley, A. E., Joel, G., … Valentini, R. (1995). Relationships between NDVI, canopy structure, and photosynthesis in three Californian vegetation types. *Ecological Applications*, *5*(1), 28–41. https://doi.org/10.2307/1942049

Gamon, J. A., Kovalchuck, O., Wong, C. Y. S., Harris, A., & Garrity, S. R. (2015). Monitoring seasonal and diurnal changes in photosynthetic pigments with automated PRI and NDVI sensors. *Biogeosciences*, *12*(13), 4149–4159. https://doi.org/10.5194/bg-12-4149-2015

Gamon, J.A., Peñuelas, J., & Field, C. B. (1992). A narrow-waveband spectral index that tracks diurnal changes in photosynthetic efficiency. *Remote Sensing of Environment*, *41*(1), 35–44. https://doi.org/10.1016/0034-4257(92)90059-S

Gamon, J A, Field, C. B., Bilger, W., Björkman, O., Fredeen, A. L., & Peñuelas, J. (1990a). Remote sensing of the xanthophyll cycle and chlorophyll fluorescence in sunflower leaves and canopies. *Oecologia*, *85*(1), 1–7.

Gamon, John A, & Bond, B. (2013). Remote Sensing of Environment Effects of irradiance and photosynthetic downregulation on the photochemical re fl ectance index in Douglas- fi r and ponderosa pine. *Remote Sensing of Environment*, *135*, 141–149. https://doi.org/10.1016/j.rse.2013.03.032

Gates, D. M., Keegan, H. J., Schleter, J. C., & Weidner, V. R. (1965). *Spectral Properties of Plants*. *4*(1), 11–20. https://doi.org/10.1364/AO.4.000011

Gao, B. C. (1996). NDWI - A normalized difference water index for remote sensing of vegetation liquid water from space. *Remote Sensing of Environment*, *58*(3), 257–266. https://doi.org/10.1016/S0034-4257(96)00067-3

Gao, J., Wang, H., Yuan, Q., & Feng, Y. (2018). Structure and function of the photosystem supercomplexes. *Frontiers in Plant Science*, *9*(March), 1–7. https://doi.org/10.3389/fpls.2018.00357

García-Tejero, I. F., Costa, J. M., Egipto, R., Durán-Zuazo, V. H., Lima, R. S. N., Lopes, C. M., & Chaves, M. M. (2016). Thermal data to monitor crop-water status in irrigated Mediterranean viticulture. *Agricultural Water Management*, *176*, 80–90. https://doi.org/10.1016/j.agwat.2016.05.008

Gausman, H. W., & Allen, W. A. (1973). Optical Parameters of Leaves of 30 Plant Species. *Plant Physiology*, *52*(1), 57–62. https://doi.org/10.1104/pp.52.1.57

Gerhards, M., Schlerf, M., Rascher, U., Udelhoven, T., Juszczak, R., Alberti, G., … Inoue, Y. (2018). Analysis of airborne optical and thermal imagery for detection of water stress symptoms. *Remote Sensing*, *10*(7). https://doi.org/10.3390/rs10071139

Gilmore, A M. (1997). Mechanistic aspects of xanthophyll cycle-dependent photoprotection in higher plant chloroplasts and leaves. *Physiologia Plantarum*, *99*(1), 197–209. https://doi.org/10.1111/j.1399-3054.1997.tb03449.x

Gitelson, A. A., Peng, Y., Arkebauer, T. J., & Suyker, A. E. (2015). Productivity, absorbed photosynthetically active radiation, and light use efficiency in crops: Implications for remote sensing of crop primary production. *Journal of Plant Physiology*, *177*(February), 100–109. https://doi.org/10.1016/j.jplph.2014.12.015

Gitelson, A, & Merzlyak, M. N. (1994). Spectral Reflectance Changes Associated with Autumn Senescence of Aesculus-hippocastanum L. and Acer-platanoides L. Leaves - Spectral Features and Relation to Chlorophyll Estimation. *Journal of Plant Physiology*, Vol. 143, pp. 286–292. https://doi.org/10.1016/S0176-1617(11)81633-0

Gitelson, A, Gritz, Y., & Merzlyak, M. N. (2003). Relationships between leaf chlorophyll content and spectral reflectance and algorithms for non-destructive chlorophyll assessment in higher plant leaves. *Journal of Plant Physiology*, *160*(3), 271–282. https://doi.org/10.1078/0176-1617-00887

Gollan, P. J., Lima-Melo, Y., Tiwari, A., Tikkanen, M., & Aro, E. M. (2017). Interaction between photosynthetic electron transport and chloroplast sinks triggers protection and signalling important for plant productivity. *Philosophical Transactions of the Royal Society B: Biological Sciences*, *372*(1730). https://doi.org/10.1098/rstb.2016.0390

Gonzalez-Dugo, V., Hernandez, P., Solis, I., & Zarco-Tejada, P. (2015). Using High-Resolution Hyperspectral and Thermal Airborne Imagery to Assess Physiological Condition in the Context of Wheat Phenotyping. *Remote Sensing*, *7*(10), 13586–13605. https://doi.org/10.3390/rs71013586

Goudriaan, J. (1977). *Crop Micrometeorology: A Simulation Study*. Pudoc, Center for Agricultural Publishing and Documentation.

Govender, M., Dye, P. J., Weiersbye, I. M., Witkowski, E. T. F., & Ahmed, F. (2009). Review of commonly used remote sensing and ground-based technologies to measure plant water stress. *Water SA*, *35*(5), 741–752. https://doi.org/10.4314/wsa.v35i5.49201

Govindjee, Shevela, D., & Björn, L. O. (2017). Evolution of the Z-scheme of photosynthesis: a perspective. *Photosynthesis Research*, *133*(1–3), 5–15. https://doi.org/10.1007/s11120-016-0333-z

Gracia-Romero, A., Kefauver, S. C., Fernandez-Gallego, J. A., Vergara-Díaz, O., Nieto-Taladriz, M. T., & Araus, J. L. (2019). UAV and ground image-based phenotyping: A proof of concept with durum wheat. *Remote Sensing*, *11*(10). https://doi.org/10.3390/rs11101244

Grant, O M, Ochagavía, H., Baluja, J., Diago, M. P., Tardáguila, J., Ochagavía, H., … Tardáguila, J. (2016). *Thermal imaging to detect spatial and temporal variation in the water status of grapevine (Vitis vinifera L .)*. *0316*(February). https://doi.org/10.1080/14620316.2015.1110991

Grant, O. M., Tronina, L., Jones, H. G., & Chaves, M. M. (2007). Exploring thermal imaging variables for the detection of stress responses in grapevine under different irrigation regimes. *Journal of Experimental Botany*, *58*(4), 815–825. https://doi.org/10.1093/jxb/erl153

Grant, O. M., Chaves, M. M., & Jones, H. G. (2006). Optimizing thermal imaging as a technique for detecting stomatal closure induced by drought stress under greenhouse conditions. *Physiologia Plantarum*, *127*(3), 507–518. https://doi.org/10.1111/j.1399-3054.2006.00686.x

Gu, Y., Wylie, B. K., Howard, D. M., Phuyal, K. P., & Ji, L. (2013). NDVI saturation adjustment: A new approach for improving cropland performance estimates in the Greater Platte River Basin, USA. *Ecological Indicators*, *30*, 1–6. http://doi.org/10.1016/j.ecolind.2013.01.041

Guo, J., & Trotter, C. M. (2004). Estimating photosynthetic light-use efficiency using the photochemical reflectance index: Variations among species. *Functional Plant Biology*, *31*, 255–

265. https://doi.org/10.1071/FP03185

Guidi, L., Lo Piccolo, E., & Landi, M. (2019). Chlorophyll fluorescence, photoinhibition and abiotic stress: Does it make any difference the fact to be a C3 or C4 species? *Frontiers in Plant Science*, *10*(February), 1–11. https://doi.org/10.3389/fpls.2019.00174

Guilioni, L., Jones, H. G., Leinonen, I., & Lhomme, J. P. (2008). On the relationships between stomatal resistance and leaf temperatures in thermography. *Agricultural and Forest Meteorology*, *148*(11), 1908–1912. https://doi.org/10.1016/j.agrformet.2008.07.009

Haboudane, D., Miller, J. R., Tremblay, N., Zarco-Tejada, P. J., & Dextraze, L. (2002). Integrated narrow-band vegetation indices for prediction of crop chlorophyll content for application to precision agriculture. *Remote Sensing of Environment*, *81*(2–3), 416–426. https://doi.org/10.1016/S0034-4257(02)00018-4

Harris, A., Bryant, R. G., & Baird, A. J. (2006). Mapping the effects of water stress on Sphagnum: Preliminary observations using airborne remote sensing. *Remote Sensing of Environment*, *100*(3), 363–378. https://doi.org/10.1016/j.rse.2005.10.024

Hassan, I. A. (2006). Effects of water stress and high temperature on gas exchange and chlorophyll fluorescence in Triticum aestivum L. *Photosynthetica*, *44*(2), 312–315. https://doi.org/10.1007/s11099-006-0024-7

Hazrati, S., Tahmasebi-Sarvestani, Z., Modarres-Sanavy, S. A. M., Mokhtassi-Bidgoli, A., & Nicola, S. (2016). Effects of water stress and light intensity on chlorophyll fluorescence parameters and pigments of Aloe vera L. *Plant Physiology and Biochemistry*, *106*(May), 141–148. https://doi.org/10.1016/j.plaphy.2016.04.046

Heldt, H.-W., & Piechulla, B. (2011). The Calvin cycle catalyzes photosynthetic CO2 assimilation. *Plant Biochemistry*, 163–191. https://doi.org/10.1016/b978-0-12-384986-1.00006-5

Henrich, V., Krauss, G., Götze, C., & Sandow, C. (2011). Index Database. Retrieved from https://www.indexdatabase.de

Hernandez Clemente, R., Navarro-Cerrillo, R. M., Suárez, L., Morales, F., & Zarco-Tejada, P. J. (2011). Assessing structural effects on PRI for stress detection in conifer forests. *Remote Sensing of Environment*, *115*(9), 2360–2375.

Hoagland, D. R., & Arnon, D. I. (1950). The water-culture method for growing plants without soil. *California Agricultural Experiment Station Circular*, *347*(347), 1–32. http://doi.org/citeulike-article-id:9455435

Hokmalipour, S., & Darbandi, M. H. (2011). Effects of Nitrogen Fertilizer on Chlorophyll Content and Other Leaf Indicate in Three Cultivars of Maize (Zea mays L.). *World Applied Sciences Journal*, *15*(12), 1780–1785.

Horton, P., Ruban, A. V., & Walters, R. G. (1996). Regulation of Light Harvesting in Green Plants. *Annual Review of Plant Physiology and Plant Molecular Biology*, *47*(1), 655–684. https://doi.org/10.1146/annurev.arplant.47.1.655

Huete, A. R. (1988). A soil-adjusted vegetation index (SAVI). *Remote Sensing of Environment*, *25*(3), 295–309. https://doi.org/10.1016/0034-4257(88)90106-X

Huang, L., Ju, S., Zhao, J., Zhang, D., Teng, L., & Yang, F. (2015). *Hyperspectral Measurements for Estimating Vertical Infection of Yellow Rust on Winter Wheat Plant*. 1237–1242. https://doi.org/10.17957/IJAB/15.0034

Huang, W., Zhang, S. B., & Liu, T. (2018). Moderate photoinhibition of photosystem II significantly

affects linear electron flow in the shade-demanding plant Panax notoginseng. *Frontiers in Plant Science*, *9*(May), 1–11. https://doi.org/10.3389/fpls.2018.00637

Huang, Z. A., Jiang, D. A., Y, Y., Sun, J. W., & Jin, S. H. (2004). Effects of nitrogen deficiency on gas exchange, chlorophyll fluorescence, and antioxidant enzymes in leaves of rice plants. *Photosynthetica*, *42*(3), 357–364. https://doi.org/10.1023/B

Idso, S. B., Jackson, R. D., Pinter Jr, P. J., Reginato, R. J., & Hatfield, J. L. (1981). *Normalizing the Stress-Degree-Day Parameter for Environmental Variability*.

Jackson, R. D., Idso, S. B., Reginato, R. J., & Pinter Jr, P. J. (1981). *Canopy Temperature as a Crop Water Stress Indicator*.

Jacquemoud, S., & Baret, F. (1990). PROSPECT: A model of leaf optical properties spectra. *Remote Sensing of Environment*, *34*(2), 75–91. https://doi.org/10.1016/0034-4257(90)90100-Z

Jacquemoud, S., Ustin, S. L., Verdebout, J., Schmuck, G., Andreoli, G., & Hosgood, B. (1996). Estimating leaf biochemistry using the PROSPECT leaf optical properties model. *Remote Sensing of Environment*, *56*(3), 194–202. https://doi.org/10.1016/0034-4257(95)00238-3

Jacquemoud, S., & Ustin, L. S. (2008). Modeling leaf optical properties. http://photobiology.info/Jacq_Ustin.html

Jacquemoud, S., Verhoef, W., Baret, F., Bacour, C., Zarco-Tejada, P. J., Asner, G. P., … Ustin, S. L. (2009). PROSPECT + SAIL models: A review of use for vegetation characterization. *Remote Sensing of Environment*, *113*(SUPPL. 1), S56–S66. https://doi.org/10.1016/j.rse.2008.01.026

Jahns, P., Latowski, D., & Strzalka, K. (2009). Mechanism and regulation of the violaxanthin cycle: The role of antenna proteins and membrane lipids. *Biochimica et Biophysica Acta - Bioenergetics*, *1787*(1), 3–14. https://doi.org/10.1016/j.bbabio.2008.09.013

Järvi, S., Gollan, P. J., & Aro, E.-M. (2013). Understanding the roles of the thylakoid lumen in photosynthesis regulation. *Frontiers in Plant Science*, *4*(October), 1–14. https://doi.org/10.3389/fpls.2013.00434

Jiang, C. D., Gao, H. Y., Zou, Q., & Jiang, G. M. (2004). Inhibition of photosynthesis by shift in the balance of excitation energy distribution between photosystems in dithiothreitol treated soybean leaves. *Photosynthetica*, *42*(3), 409–415. https://doi.org/10.1023/B:PHOT.0000046160.18482.91

Jin, X., Yang, G., Tan, C., & Zhao, C. (2015). Effects of nitrogen stress on the photosynthetic CO2 assimilation, chlorophyll fluorescence, and sugar-nitrogen ratio in corn. *Scientific Reports*, *5*, 9311. https://doi.org/10.1038/srep09311

Jones, H. G. (1999). Use of thermography for quantitative studies of spatial and temporal variation of stomatal conductance over leaf surfaces. *Plant, Cell and Environment*, *22*(9), 1043–1055. https://doi.org/10.1046/j.1365-3040.1999.00468.x

Jones, H. G. (2002). Use of infrared thermography for monitoring stomatal closure in the field: application to grapevine. *Journal of Experimental Botany*, *53*(378), 2249–2260. https://doi.org/10.1093/jxb/erf083

Jones, H. G. (2013). *Plants and Microclimate. A Quantative Approach to Environmental Plant Physiology* (Third Edit). Cambridge University Press.

Jones, H G, & Schofield, P. (2008). Thermal and other remote sensing of plant stress. *General Applied Plant Physiology*, *34*, 19–32.

Jones, Hamlyn G., Serraj, R., Loveys, B. R., Xiong, L., Wheaton, A., & Price, A. H. (2009). Thermal infrared imaging of crop canopies for the remote diagnosis and quantification of plant responses to water stress in the field. *Functional Plant Biology*, *36*(11), 978–989. https://doi.org/10.1071/FP09123

Kaizu, Y., & Imou, K. (2008). A dual-spectral camera system for paddy rice seedling row detection, *Computers and Electronics in Agriculture, 3*, 49–56. http://doi.org/10.1016/j.compag.2008.01.012

Kasahara, M., Kagawa, T., Oikawa, K., Suetsugu, N., Miyao, M., & Wada, M. (2002). Chloroplast avoidance movement reduces photodamage in plants. *Nature*, *420*(December), 829–832. https://doi.org/10.1038/nature01202.1.

Kefauver, S. C., Vicente, R., Vergara-Díaz, O., Fernandez-Gallego, J. A., Kerfal, S., Lopez, A., … Araus, J. L. (2017). Comparative UAV and field phenotyping to assess yield and nitrogen use efficiency in hybrid and conventional barley. *Frontiers in Plant Science*, *8*(October), 1–15. https://doi.org/10.3389/fpls.2017.01733

Khanna, R., Schmid, L., Walter, A., Nieto, J., Siegwart, R., & Liebisch, F. (2019). A spatio temporal spectral framework for plant stress phenotyping. *Plant Methods*, *15*(1), 1–18. https://doi.org/10.1186/s13007-019-0398-8

Kitajima, K., & Hogan, K. P. (2003). *Increases of chlorophyll a/b ratios during acclimation of tropical woody seedlings to nitrogen limitation and high light*. 1–7. https://doi.org/10.1046/j.1365-3040.2003.01017.x

Kiefer, J. (2007). Effects of ultraviolet radiation on DNA. *Chromosomal Alterations: Methods, Results and Importance in Human Health*, *33*, 39–53. https://doi.org/10.1007/978-3-540-71414-9-3

Kolber, Z., Klimov, D., Ananyev, G., Rascher, U., Berry, J., & Osmond, B. (2005). Measuring photosynthetic parameters at a distance: Laser induced fluorescence transient (LIFT) method for remote measurements of photosynthesis in terrestrial vegetation. *Photosynthesis Research*, *84*(1–3), 121–129. https://doi.org/10.1007/s11120-005-5092-1

Kolber, Z. S., Prášil, O., & Falkowski, P. G. (1998). Measurements of variable chlorophyll fluorescence using fast repetition rate techniques: Defining methodology and experimental protocols. *Biochimica et Biophysica Acta - Bioenergetics*, *1367*(1–3), 88–106. https://doi.org/10.1016/S0005-2728(98)00135-2

Kollist, H., Nuhkat, M., & Roelfsema, M. R. G. (2014). Closing gaps: Linking elements that control stomatal movement. *New Phytologist*, *203*(1), 44–62. https://doi.org/10.1111/nph.12832

Kooyers, N. J. (2015). The evolution of drought escape and avoidance in natural herbaceous populations. *Plant Science*, *234*, 155–162. https://doi.org/10.1016/j.plantsci.2015.02.012

Krieger-Liszkay, A. (2005). Singlet oxygen production in photosynthesis. *Journal of Experimental Botany*, *56*(411), 337–346. https://doi.org/10.1093/jxb/erh237

Kromdijk, J., Glowacka, K., Leonelli, L., Gabilly, S. T., Iwai, M., Niyogi, K. K., & Long, S. P. (2016). *Improving photosynthesis and crop productivity by accelerating recovery*. *354*(6314), 857–861.

Kuhlgert, S., Austic, G., Zegarac, R., Osei-Bonsu, I., Hoh, D., Chilvers, M. I., … Kramer, D. M. (2016). MultispeQ Beta: a tool for large-scale plant phenotyping connected to the open PhotosynQ network. *Royal Society Open Science*, *3*(10), 160592. https://doi.org/10.1098/rsos.160592

Lamaoui, M., Jemo, M., Datla, R., & Bekkaoui, F. (2018). Heat and Drought Stresses in Crops and Approaches for Their Mitigation. *Frontiers in Chemistry*, *6*(February), 1–14.

https://doi.org/10.3389/fchem.2018.00026

Lange, O. L., Lösch, R., Schulze, E. D., & Kappen, L. (1971). Responses of stomata to changes in humidity. *Planta*, *100*(1), 76–86. https://doi.org/10.1007/BF00386887

Latowski, D., Kuczyńska, P., & Strzałka, K. (2011). Xanthophyll cycle--a mechanism protecting plants against oxidative stress. *Redox Report : Communications in Free Radical Research*, *16*(2), 78–90. https://doi.org/10.1179/174329211X13020951739938

Lawlor, D. W. (2002). Limitation to photosynthesis in water-stressed leaves: Stomata vs. Metabolism and the role of ATP. *Annals of Botany*, *89*(SPEC. ISS.), 871–885. https://doi.org/10.1093/aob/mcf110

Lawson, T. (2009). Guard cell photosynthesis and stomatal function. *New Phytologist*, *181*(1), 13–34. https://doi.org/10.1111/j.1469-8137.2008.02685.x

Lawson, T., & Vialet-Chabrand, S. (2019). Speedy stomata, photosynthesis and plant water use efficiency. *New Phytologist*, *221*(1), 93–98. https://doi.org/10.1111/nph.15330

Lebourgeois, V., Bégué, A., Labbé, S., Mallavan, B., Prévot, L., & Roux, B. (2007). Can Commercial Digital Cameras Be Used as Multispectral Sensors? A Crop Monitoring Test. *Sensors*, *8*, 7300–7322. http://doi.org/10.3390/s8117300

Leinonen, I., Grant, O. M., Tagliavia, C. P. P., Chaves, M. M., & Jones, H. G. (2006). Estimating stomatal conductance with thermal imagery. *Plant, Cell and Environment*, *29*(8), 1508–1518. https://doi.org/10.1111/j.1365-3040.2006.01528.x

Li, B., Emr, N., Malling, E., & Me, K. (2018). Advances in Non-Destructive Early Assessment of Fruit Ripeness towards Defining Optimal Time of Harvest and Yield Prediction—A Review. *Plants*, *7*(1), 3. http://doi.org/10.3390/plants7010003

Li, F., Miao, Y., Feng, G., Yuan, F., Yue, S., Gao, X., … Chen, X. (2014). Improving estimation of summer maize nitrogen status with red edge-based spectral vegetation indices. *Field Crops Research*, *157*(January), 111–123. https://doi.org/10.1016/j.fcr.2013.12.018

Li, L., Zhang, Q., & Huang, D. (2014). A Review of Imaging Techniques for Plant Phenotyping. *Sensors*, *14*(11), 20078–20111. https://doi.org/10.3390/s141120078

Lichtenthaler, H. K., & Buschmann, C. (2001). Chlorophylls and Carotenoids : Measurement and Characterization by UV-VIS. *Current Protocols in Food Analytical Chemistry*, *F4.3.1-F4.*(Supplement 1), 1–8. https://doi.org/10.1002/0471142913

Liew, O. W., Chong, P. C. J., Li, B., & Asundi, A. K. (2008). Signature Optical Cues: Emerging Technologies for Monitoring Plant Health. In *Sensors* (Vol. 8). https://doi.org/10.3390/s8053205

Lisar, S. Y. S., Motafakkerazad, R., Hossain, M. M., & Rahman, I. M. M. (2012). Water Stress in Plants : Causes , Effects and Responses. *Water Stress*, (February 2016), 1–14. https://doi.org/10.5772/39363

Lodish, H., Berk, A., Zipursky, S. L., Matsudaira, P., Baltimore, D., & Darnell, J. (2000). *Molecular Cell Biology: Section 16.3, Photosynthetic Stages and Light-Absorbing Pigments* (4th Editio). New York: W. H. Freeman.

Lokstein, H., Tian, L., Polle, J. E. W., & DellaPenna, D. (2002). Xanthophyll biosynthetic mutants of Arabidopsis thaliana: Altered nonphotochemical quenching of chlorophyll fluorescence is due to changes in Photosystem II antenna size and stability. *Biochimica et Biophysica Acta - Bioenergetics*, *1553*(3), 309–319. https://doi.org/10.1016/S0005-2728(02)00184-6

Lorimer, G. H. (1981). The Carboxylation and Events in Photosynthesis and Photorespiration. *Ann. Rev. Plant Physiol.*, *32*, 349–283.

Lowe, D. (2004). Distinctive Image Features from Scale-Invariant Keypoints. *International Journal of Computer Vision*, *60*(2), 91–110.

Lu, S., Lu, X., Zhao, W., Liu, Y., Wang, Z., & Omasa, K. (2015). Comparing vegetation indices for remote chlorophyll measurement of white poplar and Chinese elm leaves with different adaxial and abaxial surfaces. *Journal of Experimental Botany*, *66*(18), 1–13. https://doi.org/10.1093/jxb/erv270

Maes, W H, & Steppe, K. (2012). Estimating evapotranspiration and drought stress with ground-based thermal remote sensing in agriculture: a review. *Journal of Experimental Botany*, *63*(2), 4671–4712. https://doi.org/10.1093/jxb/err313

Maes, Wouter H., Baert, A., Huete, A. R., Minchin, P. E. H., Snelgar, W. P., & Steppe, K. (2016). A new wet reference target method for continuous infrared thermography of vegetations. *Agricultural and Forest Meteorology*, *226–227*, 119–131. https://doi.org/10.1016/j.agrformet.2016.05.021

Magney, T. S., Eitel, J. U. H., Huggins, D. R., & Vierling, L. A. (2016). Proximal NDVI derived phenology improves in-season predictions of wheat quantity and quality. *Agricultural and Forest Meteorology*, *217*(January), 46–60. https://doi.org/10.1016/j.agrformet.2015.11.009

Makino, A. (2011). Photosynthesis, Grain Yield, and Nitrogen Utilization in Rice and Wheat. *Plant Physiology*, *155*(1), 125–129. https://doi.org/10.1104/pp.110.165076

Malamy, J., Carr, J. P., Klessig, D. F., & Raskin, I. (1990). Salicylic Acid: a likely endogenous signal in the resistance response of tobacco to viral infection. *Science (New York, N.Y.)*, *250*(4983), 1002–1004. https://doi.org/10.1126/science.250.4983.1002

Malavasi, U. C., & Malavasi, M. M. (2001). Leaf characteristics and chlorophyll concentration of Schyzolobium parahybum and Hymenaea stilbocarpa seedlings grown in different light regimes. *Tree Physiology*, *21*(10), 701–703. https://doi.org/10.1093/treephys/21.10.701

Malenovsky, Z., Mishra, K. B., Zemek, F., Rascher, U., & Nedbal, L. (2009). Scientific and technical challenges in remote sensing of plant canopy reflectance and fluorescence. *Journal of Experimental Botany*, *60*(11), 2987–3004. https://doi.org/10.1093/jxb/erp156

Matimati, I., Verboom, G. A., & Cramer, M. D. (2014). Nitrogen regulation of transpiration controls mass-flow acquisition of nutrients. *Journal of Experimental Botany*, *65*(1), 159–168. https://doi.org/10.1093/jxb/ert367

Maxwell, K., & Johnson, G. N. (2000). Chlorophyll fluorescence--a practical guide. *Journal of Experimental Botany*, *51*(345), 659–668. https://doi.org/10.1093/jexbot/51.345.659

McAdam, S. A. M., & Brodribb, T. J. (2015). The Evolution of Mechanisms Driving the Stomatal Response to Vapor Pressure Deficit, *167*(March), 833–843. https://doi.org/10.1104/pp.114.252940

McAusland, L., Davey, P. A., Kanwal, N., Baker, N. R., & Lawson, T. (2013). A novel system for spatial and temporal imaging of intrinsic plant water use efficiency. *Journal of Experimental Botany*, *64*(16), 4993–5007. https://doi.org/10.1093/jxb/ert288

McMurtrie, R. E., & Näsholm, T. (2018). Quantifying the contribution of mass flow to nitrogen acquisition by an individual plant root. *New Phytologist*, *218*(1), 119–130. https://doi.org/10.1111/nph.14927

Meacham-Hensold, K., Montes, C. M., Wu, J., Guan, K., Fu, P., Ainsworth, E. A., … Bernacchi, C. J.

(2019). High-throughput field phenotyping using hyperspectral reflectance and partial least squares regression (PLSR) reveals genetic modifications to photosynthetic capacity. *Remote Sensing of Environment*, *231*(February), 111176. https://doi.org/10.1016/j.rse.2019.04.029

Medrano, H., Tomás, M., Martorell, S., Flexas, J., Hernández, E., Rosselló, J., … Bota, J. (2015). From leaf to whole-plant water use efficiency (WUE) in complex canopies: Limitations of leaf WUE as a selection target. *Crop Journal*, *3*(3), 220–228. https://doi.org/10.1016/j.cj.2015.04.002

Melotto, M., Underwood, W., & He, S. Y. (2008). Role of Stomata in Plant Innate Immunity and Foliar Bacterial Diseases. *Annu Rev Phytopathol*, *46*, 101–122. https://doi.org/10.1146/annurev.phyto.121107.104959.Role

Merilo, E., Yarmolinsky, D., Jalakas, P., Parik, H., Tulva, I., Rasulov, B., … Kollist, H. (2018). Stomatal VPD Response : There Is More to the Story Than ABA. *Plant Physiology*, *176*(January), 851–864. https://doi.org/10.1104/pp.17.00912

Meroni, M., Rossini, M., Guanter, L., Alonso, L., Rascher, U., Colombo, R., & Moreno, J. (2009). Remote sensing of solar-induced chlorophyll fluorescence: Review of methods and applications. *Remote Sensing of Environment*, *113*(10), 2037–2051. https://doi.org/10.1016/j.rse.2009.05.003

Metz, J., Pakrasi, H. B., Seibert, M., & Arntzen, C. J. (1986). Evidence for a dual function of the herbicide-binding D1 protein in photosystem II. *FEBS Letters*, *205*(2), 269–274.

Minervini, M., Scharr, H., & Tsaftaris, S. A. (2015). Image analysis: The new bottleneck in plant phenotyping [applications corner]. *IEEE Signal Processing Magazine*, *32*(4), 126–131. http://doi.org/10.1109/MSP.2015.2405111

Misra, A. N., Misra, M., & Singh, R. (2012). Chlorophyll Fluorescence in Plant Biology. *Biophysics*, 220. https://doi.org/10.5772/35111

Miyashita, K., Tanakamaru, S., Maitani, T., & Kimura, K. (2005). Recovery responses of photosynthesis, transpiration, and stomatal conductance in kidney bean following drought stress. *Environmental and Experimental Botany*, *53*(2), 205–214. https://doi.org/10.1016/j.envexpbot.2004.03.015

Moran, M. S., Clarke, T. R., Inoue, Y., & Vidal, A. (1994). Estimating crop water deficit using the relation between surface-air temperature and spectral vegetation index. *Remote Sensing of Environment*, Vol. 49, pp. 246–263. https://doi.org/10.1016/0034-4257(94)90020-5

Möller, M., Alchanatis, V., Cohen, Y., Meron, M., Tsipris, J., Naor, A., … Cohen, S. (2006). Use of thermal and visible imagery for estimating crop water status of irrigated grapevine. *Journal of Experimental Botany*, *58*(4), 827–838. https://doi.org/10.1093/jxb/erl115

Mosa, K. A., Ismail, A., & Helmy, M. (2017). Gene Regulation During Cold Stress Acclimation in Plants Viswanathan. *Methods Mol Biol.*, *639*, 39–55. https://doi.org/10.1007/978-3-319-59379-1

Mott, K. A. (1988). Do Stomata Respond to CO2 Concentrations Other than Intercellular. *Plant Physiology*, *86*, 200–203.

Mott, K. A., & Peak, D. (2013). *Testing a vapour-phase model of stomatal responses*. 936–944. https://doi.org/10.1111/pce.12026

Mozzo, M., Dall'Osto, L., Hienerwadel, R., Bassi, R., & Croce, R. (2008). Photoprotection in the antenna complexes of photosystem II: Role of individual xanthophylls in chlorophyll triplet quenching. *Journal of Biological Chemistry*, *283*(10), 6184–6192. https://doi.org/10.1074/jbc.M708961200

Mueller, N. D., Gerber, J. S., Johnston, M., Ray, D. K., Ramankutty, N., & Foley, J. A. (2012). Closing yield gaps through nutrient and water management. *Nature*, *490*(7419), 254–257. https://doi.org/10.1038/nature11420

Mühlbauer, S. K., & Eichacker, L. A. (1998). Light-dependent formation of the photosynthetic proton gradient regulates translation elongation in chloroplasts. *Journal of Biological Chemistry*, *273*(33), 20935–20940. https://doi.org/10.1074/jbc.273.33.20935

Mulholland, P. J., Helton, A. M., Poole, G. C., Hall, R. O., Hamilton, S. K., Peterson, B. J., … Thomas, S. M. (2008). Stream denitrification across biomes and its response to anthropogenic nitrate loading. *Nature*, *452*(7184), 202–205. https://doi.org/10.1038/nature06686

Müller, P., Li, X. P., & Niyogi, K. K. (2001). Non-photochemical quenching. A response to excess light energy. *Plant Physiology*, *125*(4), 1558–1566. https://doi.org/10.1104/pp.125.4.1558

Munné-Bosch, S., & Cela, J. (2006). Effects of water deficit on photosystem II photochemistry and photoprotection during acclimation of lyreleaf sage (Salvia lyrata L.) plants to high light. *Journal of Photochemistry and Photobiology B: Biology*, *85*(3), 191–197. https://doi.org/10.1016/j.jphotobiol.2006.07.007

Munns, R., James, R. A., Sirault, X. R. R., Furbank, R. T., & Jones, H. G. (2010). New phenotyping methods for screening wheat and barley for beneficial responses to water deficit. *Journal of Experimental Botany*, *61*(13), 3499–3507. https://doi.org/10.1093/jxb/erq199

Murchie, E. H., & Lawson, T. (2013). Chlorophyll fluorescence analysis: A guide to good practice and understanding some new applications. *Journal of Experimental Botany*, *64*(13), 3983–3998. https://doi.org/10.1093/jxb/ert208

Murchie, Erik H, & Niyogi, K. K. (2011). Manipulation of photoprotection to improve plant photosynthesis. *Plant Physiology*, *155*(1), 86–92. https://doi.org/10.1104/pp.110.168831

Nelson, N., & Yocum, C. F. (2006). Structure and Function of Photosystems I and II. *Annual Review of Plant Biology*, *57*(1), 521–565. https://doi.org/10.1146/annurev.arplant.57.032905.105350

Neubauer, C. (1993). Multiple Effects of Dithiothreitol on Nonphotochemical Fluorescence Quenching in Intact Chloroplasts (Influence on Violaxanthin De-epoxidase and Ascorbate Peroxidase Activity). *Plant Physiology*, *103*(2), 575–583. Retrieved from http://www.pubmedcentral.nih.gov/articlerender.fcgi?artid=159017&tool=pmcentrez&rendertype=abstract

Ni, Z., Liu, Z., Huo, H., Li, Z.-L., Nerry, F., Wang, Q., & Li, X. (2015). Early Water Stress Detection Using Leaf-Level Measurements of Chlorophyll Fluorescence and Temperature Data. *Remote Sensing*, *7*(3), 3232–3249. https://doi.org/10.3390/rs70303232

Oerke, E. C. (2006). Crop losses to pests. *Journal of Agricultural Science*, *144*(1), 31–43. https://doi.org/10.1017/S0021859605005708

Oren, R., Sperry, J. S., Katul, G. G., Pataki, D. E., Ewers, B. E., Phillips, N., & Schäfer, K. V. R. (1999). Survey and synthesis of intra- and interspecific variation in stomatal sensitivity to vapour pressure deficit, 1515–1526.

Pagnutti, M., Ryan, R. E., Cazenavette, G., Gold, M., Harlan, R., Leggett, E., & Pagnutti, J. (2017). Laying the foundation to use Raspberry Pi 3 V2 camera module imagery for scientific and engineering purposes. *Journal of Electronic Imaging*, *26*(1), 013014. http://doi.org/10.1117/1.JEI.26.1.013014

Panigada, C., Rossini, M., Meroni, M., Cilia, C., Busetto, L., Amaducci, S., … Colombo, R. (2014).

Fluorescence, PRI and canopy temperature for water stress detection in cereal crops. *International Journal of Applied Earth Observation and Geoinformation*, *30*(1), 167–178. https://doi.org/10.1016/j.jag.2014.02.002

Papageorgiou, G. C., & Govindjee. (2004). *Chlorophyll a Fluorescence: A Signature of Photosynthesis*. Dordrecht, The Netherlands: Springer.

Pastenes, C., Pimentel, P., & Lillo, J. (2005). Leaf movements and photoinhibition in relation to water stress in field-grown beans. *Journal of Experimental Botany*, *56*(411), 425–433. https://doi.org/10.1093/jxb/eri061

Peddle, D. R., White, H. P., Soffer, R. J., Miller, J. R., & LeDrew, E. F. (2001). Reflectance processing of remote sensing spectroradiometer data. *Computers and Geosciences*, *27*(2), 203–213. http://doi.org/10.1016/S0098-3004(00)00096-0

Peguero-Pina, J. J., Morales, F., Flexas, J., Gil-Pelegrín, E., & Moya, I. (2008). Photochemistry, remotely sensed physiological reflectance index and de-epoxidation state of the xanthophyll cycle in Quercus coccifera under intense drought. *Oecologia*, *156*(1), 1–11. https://doi.org/10.1007/s00442-007-0957-y

Peng, Y., & Gitelson, A. A. (2011). Application of chlorophyll-related vegetation indices for remote estimation of maize productivity. *Agricultural and Forest Meteorology*, *151*(9), 1267–1276. https://doi.org/10.1016/j.agrformet.2011.05.005

Peñuelas, J., Baret, F., & Filella, I. (1995). Semi-empirical indices to assess caretenoids/chlorophyll a ratio from leaf spectral reflectance. *Photosynthetica*, *32*(2), 221–230.

Peñuelas, J., Filella, I., Biel, C., Serrano, L., & Savé, R. (1993). The reflectance at the 950–970 nm region as an indicator of plant water status. *International Journal of Remote Sensing*, Vol. 14, pp. 1887–1905. https://doi.org/10.1080/01431169308954010

Peñuelas, J., Pinol, J., Ogaya, R., & Filella, I. (1997). Estimation of plant water concentration by the reflectance Water Index WI (R900/R970). *International Journal of Remote Sensing*, *18*(13), 2869–2875. https://doi.org/10.1080/014311697217396

Peterhansel, C., Horst, I., Niessen, M., Blume, C., Kebeish, R., Kürkcüoglu, S., & Kreuzaler, F. (2010). Photorespiration. *Arabidopsis Book*, *8*, 1–24.

Peterman, E. J. G., Gradinaru, C. C., Calkoen, F., Borst, J. C., Van Grondelle, R., & Van Amerongen, H. (1997). Xanthophylls in light-harvesting complex II of higher plants: Light harvesting and triplet quenching. *Biochemistry*, *36*(40), 12208–12215. https://doi.org/10.1021/bi9711689

Pieruschka, R., Klimov, D., Berry, J. A., Osmond, C. B., Rascher, U., & Kolber, Z. S. (2012). *Remote Chlorophyll Fluorescence Measurements with the Laser-Induced Fluorescence Transient Approach*. *918*, 51–59. https://doi.org/10.1007/978-1-61779-995-2

Pieruschka, R., Klimov, D., Berry, J. A., Osmond, C. B., Rascher, U., & Kolber, Z. S. (2012). *Remote Chlorophyll Fluorescence Measurements with the Laser-Induced Fluorescence Transient Approach*. *918*, 51–59. https://doi.org/10.1007/978-1-61779-995-2

Pieruschka, R., & Schurr, U. (2019). Plant Phenotyping: Past, Present, and Future. *Plant Phenomics*, *2019*, 1–6. https://doi.org/10.34133/2019/7507131

Pogson, B. J., Niyogi, K. K., Björkman, O., & DellaPenna, D. (1998). Altered xanthophyll compositions adversely affect chlorophyll accumulation and nonphotochemical quenching in Arabidopsis mutants. *Proceedings of the National Academy of Sciences of the United States of America*, *95*(22), 13324–13329. https://doi.org/10.1073/pnas.95.22.13324

Porcar-Castell, A., Tyystjarvi, E., Atherton, J., van der Tol, C., Flexas, J., Pfundel, E. E., … Berry, J. A. (2014). Linking chlorophyll a fluorescence to photosynthesis for remote sensing applications: mechanisms and challenges. *Journal of Experimental Botany*, *65*(15), 4065–4095. https://doi.org/10.1093/jxb/eru191

Pou, A., Diago, M. P., Medrano, H., Baluja, J., & Tardaguila, J. (2014). Validation of thermal indices for water status identification in grapevine. *Agricultural Water Management*, *134*(MARCH), 60–72. https://doi.org/10.1016/j.agwat.2013.11.010

Prasad, R. (1998). Fertilizer urea, food security, health and the environment. *Current Science*, *75*(7), 677–683.

Prashar, A., & Jones, H. (2014). Infra-Red Thermography as a High-Throughput Tool for Field Phenotyping. *Agronomy*, *4*(3), 397–417. https://doi.org/10.3390/agronomy4030397

R Core Team. (2017). *R: A language and environment for statistical computing*. Retrieved from https://www.r-project.org/

Radin, J. W. (1984). Tomatal Responses To Water Stress and To Abscisic Acid in Phosphorus-Deficient Cotton Plants. *Plant Physiology*, *76*, 392–394. https://doi.org/10.1016/j.jplph.2010.09.020

Rahaman, M. M., Chen, D., Gillani, Z., Klukas, C., & Chen, M. (2015). Advanced phenotyping and phenotype data analysis for the study of plant growth and development. *Frontiers in Plant Science*, *6*(August), 1–15. http://doi.org/10.3389/fpls.2015.00619

Rapaport, T., Hochberg, U., Shoshany, M., Karnieli, A., & Rachmilevitch, S. (2015). Combining leaf physiology, hyperspectral imaging and partial least squares-regression (PLS-R) for grapevine water status assessment. *ISPRS Journal of Photogrammetry and Remote Sensing*, *109*, 88–97. https://doi.org/10.1016/j.isprsjprs.2015.09.003

Ravazi, F., Pollet, B., Steppe, K., & Van Labeke, M. C. (2008). Chlorophyll fluoroescence as a tool for evaluation of drought stress in strawberry. *Photosynthetica*, *46*(4), 631–633. https://doi.org/10.1007/s11099-010-0040-5

Ray, D. K., Mueller, N. D., West, P. C., & Foley, J. A. (2013). Yield Trends Are Insufficient to Double Global Crop Production by 2050. *PLoS ONE*, *8*(6). https://doi.org/10.1371/journal.pone.0066428

Richardson, A. D., Jenkins, Æ. J. P., Braswell, B. H., Hollinger, Æ. D. Y., & Smith, S. V. O. Æ. M. (2007). Use of digital webcam images to track spring green-up in a deciduous broadleaf forest. *Oecologia*, *152*(2), 323–334. http://doi.org/10.1007/s00442-006-0657-z

Rispail, N., & Rubiales, D. (2015). Rapid and Efficient Estimation of Pea Resistance to the Soil-Borne Pathogen Fusarium oxysporum by Infrared Imaging. *Sensors*, *15*(2), 3988–4000. https://doi.org/10.3390/s150203988

Ritchie, G. A. (2006). Chlorophyll Fluorescence : What Is It and What Do the Numbers Mean ? *USDA Forest Service Proceedings*, 34–43.

Ritchie, G. L., Sullivan, D. G., Perry, C. D., Hook, J. E., & Bednarz, C. W. (2008). Preparation of a Low-Cost Digital Camera System for Remote Sensing. *Applied Engineering in Agriculture*, *24*(6), 885–894. http://doi.org/10.13031/2013.25359

Rochaix, J. D. (2011). Regulation of photosynthetic electron transport. *Biochimica et Biophysica Acta - Bioenergetics*, *1807*(3), 375–383. https://doi.org/10.1016/j.bbabio.2010.11.010

Roháček, K., Soukupová, J., & Barták, M. (2008). Chlorophyll fluorescence: a wonderful tool to study plant physiology and plant stress. In *Plant Cell Compartments-Selected Topics* (Vol. 661).

Retrieved from http://www.umbr.cas.cz/~rohacek/Publikace/RevChlFsemifin.pdf

Rosenzweig, C., Iglesias, A., Yang, X. B., Epstein, P., & Chivian, E. (2001). Climate Change and Extreme Weather Events; Implications for Food Production, Plant Diseases, and Pests. *Global Change and Human Health*, *2*(2), 90–104. https://doi.org/10.1023/A:1015086831467

Rossini, M., Fava, F., Cogliati, S., Meroni, M., Marchesi, A., Panigada, C., … Colombo, R. (2013). Assessing canopy PRI from airborne imagery to map water stress in maize. *ISPRS Journal of Photogrammetry and Remote Sensing*, *86*, 168–177. https://doi.org/10.1016/j.isprsjprs.2013.10.002

Rouse, J. W., & Space, G. (1978). Monitoring the vernal advancement of retrogradation of natural vegetation. *Roceedings, 3rd Earth Resource Technology Satellite (ERTS) Symposium*, *1*, 48–62.

Ruban, A. V., Young, A. J., & Horton, P. (1993). Induction of Nonphotochemical Energy Dissipation and Absorbance Changes in Leaves (Evidence for Changes in the State of the Light-Harvesting System of Photosystem II in Vivo). *Plant Physiology*, *102*, 741–750. https://doi.org/10.1104/pp.102.3.741

Ruban, Alexander V., Johnson, M. P., & Duffy, C. D. P. (2012). The photoprotective molecular switch in the photosystem II antenna. *Biochimica et Biophysica Acta - Bioenergetics*, *1817*(1), 167–181. https://doi.org/10.1016/j.bbabio.2011.04.007

Rufelt, H. (1963). Rapid Changes in Transpiration in Plants. *Nature*, *200*(284).

Ryu, Y., Lee, G., Jeon, S., Song, Y., & Kimm, H. (2014). Remote Sensing of Environment Monitoring multi-layer canopy spring phenology of temperate deciduous and evergreen forests using low-cost spectral sensors. *Remote Sensing of Environment*, *149*, 227–238. http://doi.org/10.1016/j.rse.2014.04.015

Saad Gazala, I. F., Sahoo, R. N., Pandey, R., Mandal, B., Gupta, V K, … Sinha, P. (2013). Spectral reflectance pattern in soybean for assessing yellow mosaic disease. *Indian Journal of* Virology, 24(2), 242-249 https://doi.org/10.1007/s13337-013-0161-0

Sade, N., Del Mar Rubio-Wilhelmi, M., Umnajkitikorn, K., & Blumwald, E. (2018). Stress-induced senescence and plant tolerance to abiotic stress. *Journal of Experimental Botany*, *69*(4), 845–853. https://doi.org/10.1093/jxb/erx235

Sadeghi-Tehran, P., Sabermanesh, K., Virlet, N., & Hawkesford, M. J. (2017). Automated method to determine two critical growth stages of wheat: Heading and flowering. *Frontiers in Plant Science*, *8*(February), 1–14. https://doi.org/10.3389/fpls.2017.00252

Sakamoto, T., Gitelson, A. A., Nguy-robertson, A. L., Arkebauer, T. J., Wardlow, B. D., Suyker, A. E., … Shibayama, M. (2012). An alternative method using digital cameras for continuous monitoring of crop status. *Agricultural and Forest Meteorology*, 154-155, 113-126

Sanches, I. D., Souza Filho, C. R., Magalhães, L. a., Quitério, G. C. M., Alves, M. N., & Oliveira, W. J. (2013). Unravelling remote sensing signatures of plants contaminated with gasoline and diesel: An approach using the red edge spectral feature. *Environmental Pollution*, *174*, 16–27. https://doi.org/10.1016/j.envpol.2012.10.029

Sanchez, R. A., Hall, A. J., Trapani, N., & Cohen de Hunau, R. (1983). Effects of water stress on the chlorophyll content, nitrogen level and photosynthesis of leaves of two maize genotypes. *Photosynthesis Research*, *4*(1), 35–47.

Sankaran, S., Mishra, A., Ehsani, R., & Davis, C. (2010). Computers and Electronics in Agriculture A review of advanced techniques for detecting plant diseases. *Computers and Electronics in*

Agriculture, *72*, 1–13. https://doi.org/10.1016/j.compag.2010.02.007

Sarlikioti, V., Driever, S. M., & Marcelis, L. F. M. (2010). Photochemical reflectance index as a mean of monitoring early water stress. *Annals of Applied Biology*, *157*(1), 81–89. https://doi.org/10.1111/j.1744-7348.2010.00411.x

Sayed, O. H. (2003). Chlorophyll fluorescence as a tool in cereal crop research. *Photosynthetica*, *41*(3), 321–330. https://doi.org/10.1023/B:PHOT.0000015454.36367.e2

Schepers, J. S., Blackmer, T. M., Wilhelm, W. W., & Resende, M. (1996). Transmittance and reflectance measurements of corn leaves from plants with different nitrogen and water supply. *Journal of Plant Physiology*, *148*(5), 523–529. https://doi.org/10.1016/S0176-1617(96)80071-X

Schickling, A., Matveeva, M., Damm, A., Schween, J., Wahner, A., Graf, A., … Rascher, U. (2016). Combining Sun-Induced Chlorophyll Fluorescence and Photochemical Reflectance Index Improves Diurnal Modeling of Gross Primary Productivity. *Remote Sensing*, *8*(7), 574. https://doi.org/10.3390/rs8070574

Schindelin, J., Arganda-Carreras, I., Frise, E., Kaynig, V., Longair, M., Pietzsch, T., … A., C. (2012). Fiji: An open source platform for biological image analysis. *Nature Methods*, *9*(7), 676–682. https://doi.org/10.1038/nmeth.2019.Fiji

Schlemmer, M., Gitelson, A., Schepers, J., Ferguson, R., Peng, Y., Shanahan, J., & Rundquist, D. (2013). Remote estimation of nitrogen and chlorophyll contents in maize at leaf and canopy levels. *International Journal of Applied Earth Observation and Geoinformation*, *25*, 47–54. https://doi.org/10.1016/j.jag.2013.04.003

Schlenker, W., & Roberts, M. J. (2009). Nonlinear temperature effects indicate severe damages to U.S. crop yields under climate change. *PNAS*, *106*(37), 15594–15598. https://doi.org/10.1007/BF02365970

Schluter, U., Mascher, M., Colmsee, C., Scholz, U., Brautigam, A., Fahnenstich, H., & Sonnewald, U. (2012). Maize Source Leaf Adaptation to Nitrogen Deficiency Affects Not Only Nitrogen and Carbon Metabolism But Also Control of Phosphate Homeostasis. *Plant Physiology*, *160*(3), 1384–1406. https://doi.org/10.1104/pp.112.204420

Schmidhuber, J., & Tubiello, F. N. (2007). Global food security under climate change. *Sciences-New York*, *2007*.

Schreiber, U., Schliwa, U., & Bilger, W. (1986). Continuous recording of photochemical and non-photochemical chlorophyll fluorescence quenching with a new type of modulation fluorometer. *Photosynthesis Research*, *10*(1), 51–62.

Seelig, H. -D., Hoehn, a., Stodieck, L. S., Klaus, D. M., Adams III, W. W., & Emery, W. J. (2008). The assessment of leaf water content using leaf reflectance ratios in the visible, near-, and short-wave-infrared. *International Journal of Remote Sensing*, *29*(13), 3701–3713. https://doi.org/10.1080/01431160701772500

Serbin, S. P., Dillaway, D. N., Kruger, E. L., & Townsend, P. a. (2012). Leaf optical properties reflect variation in photosynthetic metabolism and its sensitivity to temperature. *Journal of Experimental Botany*, *63*(1), 489–502. https://doi.org/10.1093/jxb/err294

Shackel, K. A, & Brinckmann, E. (1985). In Situ Measurement of Epidermal Cell Turgor, Leaf Water Potential, and Gas Exchange in Tradescantia virginiana L. *Plant Physiology*, *78*(1), 66–70.

Shahenshah, & Isoda, A. (2010). Effects of Water Stress on Leaf Temperature and Chlorophyll Fluorescence Parameters in Cotton and Peanut. *Plant Production Science*, *13*(3), 269–278.

https://doi.org/10.1626/pps.13.269

Shahsafi, A., Roney, P., Zhou, Y., Zhang, Z., Xiao, Y., Wan, C., … Kats, M. A. (2019). Temperature-independent thermal radiation. *Proceedings of the National Academy of Sciences of the United States of America*, *116*(52), 26402–26406. https://doi.org/10.1073/pnas.1911244116

Shanahan, J. (2001). Use of Remote-Sensing Imagery to Estimate Corn Grain Yield Agronomy – Faculty Publications Use of Remote-Sensing Imagery to Estimate Corn Grain Yield. *Agron. J. 93:583–589*, *93*(May), 583–589. https://doi.org/10.2134/agronj2001.933583x

Shangguan, Z. P., Shao, M. A., & Dyckmans, J. (2000). Nitrogen nutrition and water stress effects on leaf photosynthetic gas exchange and water use efficiency in winter wheat, *44*, 141–149.

Sharon, Y., & Bravdo, B. (2001). A fully-automated orchard irrigation system based on continuous monitoring of turgor potential with a leaf sensor. *Acta Horticulturae*, *562*, 55–61.

Sharma, M., Gupta, S. K., Deeba, F., & Pandey, V. (2017). Effects of reactive oxygen species on crop productivity: An overview. In *Reactive Oxygen Species in Plants*. https://doi.org/10.1002/9781119324928.ch6

Sharma, P., Jha, A. B., Dubey, R. S., & Pessarakli, M. (2012). Reactive Oxygen Species, Oxidative Damage, and Antioxidative Defense Mechanism in Plants under Stressful Conditions. *Journal of Botany*, *2012*, 1–26. https://doi.org/10.1155/2012/217037

Shibayama, M., Sakamoto, T., Takada, E., Inoue, A., Takahashi, W., Kimura, A., … Morita, K. (2015). Continuous Monitoring of Visible and Near- Infrared Band Reflectance from a Rice Paddy for Determining Nitrogen Uptake Using Digital Cameras Continuous Monitoring of Visible and Near-Infrared Band Reflectance from a Rice Paddy for Determining Nitrogen Uptake Using Digital Cameras, Crop Physiology & Ecology, 12(3), 293-306. http://doi.org/10.1626/pps.12.293

Shimada, S.; Funatsuka, E.; Ooda, M.; Takyu, M.; Fujikawa, T.; Toyoda, H. (2012). Developing the Monitoring Method for Plant Water Stress Using Spectral Reflectance Measurement. *Journal of Arid Land Studies*, *22*(1), 251–254.

Shrestha, S., Brueck, H., & Asch, F. (2012). Chlorophyll index, photochemical reflectance index and chlorophyll fluorescence measurements of rice leaves supplied with different N levels. *Journal of Photochemistry and Photobiology B: Biology*, *113*(June 2016), 7–13. https://doi.org/10.1016/j.jphotobiol.2012.04.008

Silva-Perez, V., Molero, G., Serbin, S. P., Condon, A. G., Reynolds, M. P., Furbank, R. T., & Evans, J. R. (2018). Hyperspectral reflectance as a tool to measure biochemical and physiological traits in wheat. *Journal of Experimental Botany*, *69*(3), 483–496. https://doi.org/10.1093/jxb/erx421

Simkin, A. J., López-Calcagno, P. E., & Raines, C. A. (2019). Feeding the world: Improving photosynthetic efficiency for sustainable crop production. *Journal of Experimental Botany*, *70*(4), 1119–1140. https://doi.org/10.1093/jxb/ery445

Sims, D. A., & Gamon, J. A. (2003). Estimation of vegetation water content and photosynthetic tissue area from spectral reflectance: A comparison of indices based on liquid water and chlorophyll absorption features. *Remote Sensing of Environment*, *84*(4), 526–537. https://doi.org/10.1016/S0034-4257(02)00151-7

Sims, D., & Gamon, J. A. (2002). Relationships between leaf pigment content and spectral reflectance across a wide range of species, leaf structures and developmental stages. *Remote Sensing of Environment*, *81*(2–3), 337–354. https://doi.org/10.1016/S0034-4257(02)00010-X

Slaton, M. R., Hunt, E. R., & Smith, W. K. (2001). Estimating near-infrared leaf reflectance from leaf

structural characteristics. *American Journal of Botany*, *88*(2), 278–284. https://doi.org/10.2307/2657019

Smith, J. H. C., & French, C. S. (1963). The Major and Accessory Pigments in Photosynthesis. *Annual Review of Plant Physiology*, *14*(1), 181–224. https://doi.org/10.1146/annurev.pp.14.060163.001145

Smith, G. M., & Milton, E. J. (1999). The use of the empirical line method to calibrate remotely sensed data to reflectance. *International Journal of Remote Sensing*, *20*(13), 2653–2662. http://doi.org/10.1080/014311699211994

Souza, R. P., Machado, E. C., Silva, J. A. B., Lagˆ, A. M. M. A., & Silveira, J. A. G. (2004). Photosynthetic gas exchange , chlorophyll fluorescence and some associated metabolic changes in cowpea (Vigna unguiculata) during water stress and recovery. *Environmental and Experimental Botany*, *51*, 45–56. https://doi.org/10.1016/S0098-8472(03)00059-5

Steven, M. D. (1998). The sensitivity of the OSAVI vegetation index to observational parameters. *Remote Sensing of Environment*, *63*(1), 49–60. https://doi.org/10.1016/S0034-4257(97)00114-4

Suárez, L., Zarco-Tejada, P. J., Sepulcre-Cantó, G., Pérez-Priego, O., Miller, J. R., Jiménez-Muñoz, J. C., & Sobrino, J. (2008). Assessing canopy PRI for water stress detection with diurnal airborne imagery. *Remote Sensing of Environment*, *112*, 560–575. https://doi.org/10.1016/j.rse.2007.05.009

Sukhova, E., & Sukhov, V. (2018). *Connection of the Photochemical Reflectance Index (PRI) with the Photosystem II Quantum Yield and Nonphotochemical Quenching Can Be Dependent on Variations of Photosynthetic Parameters among Investigated Plants : A Meta-Analysis*. https://doi.org/10.3390/rs10050771

Tezara, W., Mitchell, V. J., Driscoll, S. D., & Lawlor, D. W. (1999). Water stress inhibits plant photosynthesis by decreasing coupling factor and ATP. *Nature*, *401*(6756), 914–917. https://doi.org/10.1038/44842

Thenkabail, P. S., Smith, R. B., & De Pauw, E. (2000). Hyperspectral vegetation indices and their relationships with agricultural crop characteristics. *Remote Sensing of Environment*, *71*(2), 158–182. https://doi.org/10.1016/S0034-4257(99)00067-X

Thenkabail, P. S., Smith, R. B., & De Pauw, E. (2002). Evaluation of Narrowband and Broadband Vegetation Indices for Determining Optimal Hyperspectral Wavebands for Agricultural Crop Characterization. *Photogrammetric Engineering and Remote Sensing*, *68*(6), 607–621.

Tikhonov, A. N. (2014). The cytochrome b6f complex at the crossroad of photosynthetic electron transport pathways. *Plant Physiology and Biochemistry*, *81*, 163–183. https://doi.org/10.1016/j.plaphy.2013.12.011

Tombesi, S., Nardini, A., Frioni, T., Soccolini, M., Zadra, C., Farinelli, D., … Palliotti, A. (2015). Stomatal closure is induced by hydraulic signals and maintained by ABA in drought-stressed grapevine. *Scientific Reports*, *5*(February), 12449. https://doi.org/10.1038/srep12449

Tóth, V. R., Mészáros, I., Veres, S., & Nagy, J. (2002). Effects of the available nitrogen on the photosynthetic activity and xanthophyll cycle pool of maize in field. *Journal of Plant Physiology*, *159*(6), 627–634. https://doi.org/10.1078/0176-1617-0640

Tovar, J. C., Hoyer, J. S., Lin, A., Tielking, A., Callen, S. T., Elizabeth Castillo, S., … Gehan, M. A. (2018). Raspberry Pi–powered imaging for plant phenotyping. *Applications in Plant Sciences*, *6*(3), 1–12. http://doi.org/10.1002/aps3.1031

Turner, N. C. (2018). Turgor maintenance by osmotic adjustment: 40 years of progress. *Journal of Experimental Botany*, *69*(13), 3223–3233. https://doi.org/10.1093/jxb/ery181

Tuteja, N. (2007). Abscisic acid and abiotic stress signaling. *Plant Signaling and Behavior*, *2*(3), 135–138. https://doi.org/10.4161/psb.2.3.4156

Tyystjärvi, E. (2013). *Photoinhibition of Photosystem II**. *International Review of Cell and Molecular Biology* (Vol. 300). https://doi.org/10.1016/B978-0-12-405210-9.00007-2

Ustin, S. L., Gitelson, A. A., Jacquemoud, S., Schaepman, M., Asner, G. P., Gamon, J. A., & Zarco-Tejada, P. (2009). Retrieval of foliar information about plant pigment systems from high resolution spectroscopy. *Remote Sensing of Environment*, *113*(SUPPL. 1). https://doi.org/10.1016/j.rse.2008.10.019

van Evert, F. K., Gaitán-Cremaschi, D., Fountas, S., & Kempenaar, C. (2017). Can precision agriculture increase the profitability and sustainability of the production of potatoes and olives? *Sustainability (Switzerland)*, *9*(10). https://doi.org/10.3390/su9101863

Vogelmann, T. C. (1993). Plant Tissue Optics. *Annual Review of Plant Physiology and Plant Molecular Biology*, *44*(1), 231–251. https://doi.org/10.1146/annurev.pp.44.060193.001311

Vogelmann, T. C., Bornman, J. F., & Josserand, S. (1989). Photosynthetic Light Gradients and Spectral Regime within Leaves of Medicago sativa. *Philosophical Transactions of the Royal Society B: Biological Sciences*, *323*(1216), 411–421. https://doi.org/10.1098/rstb.1989.0020

Vogelmann, T C., & Björn, L. O. (1984). Measurement of light gradients and spectral regime in plant tissue with a fiber optic probe. *Physiologia Plantarum*, *60*(3), 361–368. https://doi.org/10.1111/j.1399-3054.1984.tb06076.x

Virlet, N., Costes, E., Martinez, S., Kelner, J.-J., & Regnard, J.-L. (2015). Multispectral airborne imagery in the field reveals genetic determinisms of morphological and transpiration traits of an apple tree hybrid population in response to water deficit. *Journal of Experimental Botany*, *66*(18), 5453–5465. https://doi.org/10.1093/jxb/erv355

Virlet, N., Sabermanesh, K., Sadeghi-Tehran, P., & Hawkesford, M. J. (2017). Field Scanalyzer: An automated robotic field phenotyping platform for detailed crop monitoring. *Functional Plant Biology*, *44*(1), 143–153. https://doi.org/10.1071/FP16163

Walter, A., Liebisch, F., & Hund, A. (2015). Plant phenotyping: From bean weighing to image analysis. *Plant Methods*, *11*(1), 1–11. https://doi.org/10.1186/s13007-015-0056-8

Wang, Y., Wang, D., Shi, P., & Omasa, K. (2014). Estimating rice chlorophyll content and leaf nitrogen concentration with a digital still color camera under natural light. *Plant Methods*, *10*(36). https://doi.org/10.1016/S0378-4290(99)00063-5

Wheeler, T., & Von Braun, J. (2013). Climate change impacts on global food security. *Science*, *341*(6145), 508–513. https://doi.org/10.1126/science.1239402

Wong, C. Y. S., & Gamon, J. A. (2015). The photochemical reflectance index provides an optical indicator of spring photosynthetic activation in evergreen conifers. *New Phytologist*, *206*(1), 196–208. https://doi.org/10.1111/nph.13251

Wu, F. Z., Bao, W. K., Li, F. L., & Wu, N. (2008). Effects of water stress and nitrogen supply on leaf gas exchange and fluorescence parameters of Sophora davidii seedlings. *Photosynthetica*, *46*(1), 40–48. https://doi.org/10.1007/s11099-008-0008-x

Xue, J., & Su, B. (2017). Significant Remote Sensing Vegetation Indices : A Review of Developments and Applications, *Journal of Sensors 2017*.

Yendrek, C. R., Tomaz, T., Montes, C. M., Cao, Y., Morse, A. M., Brown, P. J., … Ainsworth, E. A. (2017). High-Throughput Phenotyping of Maize Leaf Physiological and Biochemical Traits Using Hyperspectral Reflectance. *Plant Physiology*, *173*(1), 614–626. https://doi.org/10.1104/PP.16.01447

Zaman-Allah, M., Jenkinson, D. M., & Vadez, V. (2011). A conservative pattern of water use, rather than deep or profuse rooting, is critical for the terminal drought tolerance of chickpea. *Journal of Experimental Botany*, *62*(12), 4239–4252. https://doi.org/10.1093/jxb/err139

Zarco-Tejada, P. J., Berjon, a., & Miller, J. R. (2004). Stress Detection in Crops with Hyperspectral Remote Sensing and Physical Simulation Models. *Airborne Imaging Spectroscopy Workshop*, 1–5. Retrieved from http://digital.csic.es/bitstream/10261/10582/1/40.pdf

Zarco-Tejada, P. J., González-Dugo, V., & Berni, J. A. J. (2012). Fluorescence, temperature and narrow-band indices acquired from a UAV platform for water stress detection using a micro-hyperspectral imager and a thermal camera. *Remote Sensing of Environment*, *117*, 322–337. https://doi.org/10.1016/j.rse.2011.10.007

Zarco-Tejada, P. J., Miller, J. R., Mohammed, G. H., & Noland, T. L. (2000). Chlorophyll fluorescence effects on vegetation apparent reflectance: I. Leaf-level measurements and model simulation. *Remote Sensing of Environment*, *74*(3), 582–595. https://doi.org/10.1016/S0034-4257(00)00148-6

Zarco-Tejada, P. J., Morales, A., Testi, L., & Villalobos, F. J. (2013). Spatio-temporal patterns of chlorophyll fluorescence and physiological and structural indices acquired from hyperspectral imagery as compared with carbon fluxes measured with eddy covariance. *Remote Sensing of Environment*, *133*(November 2015), 102–115. https://doi.org/10.1016/j.rse.2013.02.003

Zhang, C., & Kovacs, J. M. (2012). The application of small unmanned aerial systems for precision agriculture: A review. *Precision Agriculture*, *13*(6), 693–712. https://doi.org/10.1007/s11119-012-9274-5

Zhang, Y., Chen, J. M., Miller, J. R., & Noland, T. L. (2008). Leaf chlorophyll content retrieval from airborne hyperspectral remote sensing imagery. *Remote Sensing of Environment*, *112*(7), 3234–3247. https://doi.org/10.1016/j.rse.2008.04.005

Zhao, D. H., Li, J. L., & Qi, J. G. (2005). Identification of red and NIR spectral regions and vegetative indices for discrimination of cotton nitrogen stress and growth stage. *Computers and Electronics in Agriculture*, *48*(2), 155–169. https://doi.org/10.1016/j.compag.2005.03.003

Zhou, X., Huang, W., Kong, W., Ye, H., Luo, J., & Chen, P. (2016). Remote estimation of canopy nitrogen content in winter wheat using airborne hyperspectral reflectance measurements. *Advances in Space Research*. https://doi.org/10.1016/j.asr.2016.06.034

Živčák, M., Olšovská, K., Slamka, P., Galambošová, J., Rataj, V., Shao, H. B., & Brestič, M. (2014). Application of chlorophyll fluorescence performance indices to assess the wheat photosynthetic functions influenced by nitrogen deficiency. *Plant, Soil and Environment*, *60*(5), 210–215.

Zygielbaum, A. I., Gitelson, A. A., Arkebauer, T. J., & Rundquist, D. C. (2009). Non-destructive detection of water stress and estimation of relative water content in maize. *Geophysical Research Letters*, *36*(12). https://doi.org/10.1029/2009GL038906

Chapter 8 - Appendices

Appendix 1
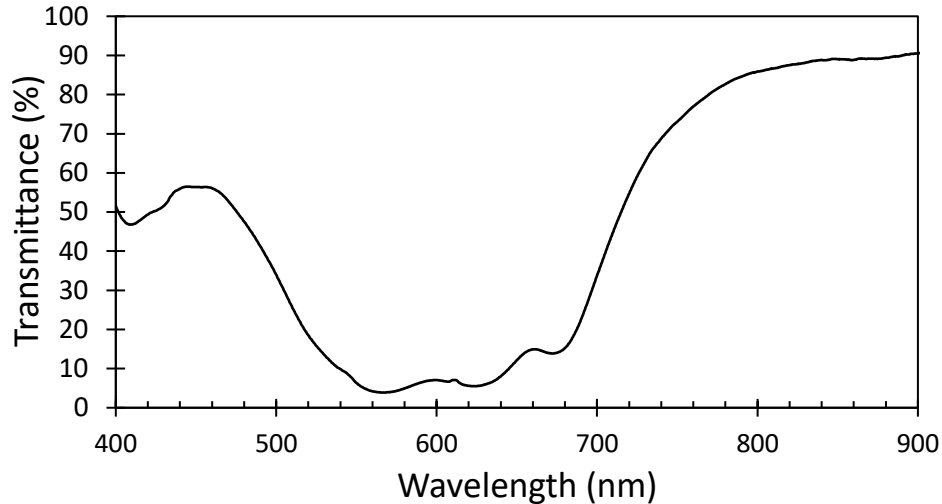
Figure A1 Transmission of light (as a percentage) across the visible spectrum (400nm to 700nm) for the filter Alice Blue 197 (LEE Filters). Strong transmission occurs in the blue regions (from 400nm to 500nm), and weak (<15%) transmission in the red regions. The filter allows NIR (>700nm) to transmit through the filter without much loss (>80% transmittance).

Use of PROSAIL model to simulate reflectance, to calculate the effect of the Alice Blue filter on measured NIR

The Alice Blue filter allows for 90% transmission of NIR light (see Supplementary data S1). However, there is also around 5-15% transmission of visible red light through the filter, depending on wavelength. Therefore, the effect of this 'leakage' of red light was characterised using simulated reflectance data.

Leaf reflectance was modelled using the PROSAIL (Jacquemoud et al., 2009) leaf reflectance model. The model works by using inputs of leaf anatomy, such as leaf thickness and chlorophyll content, and considers the leaf as consisting of multiple 'layers' (e.g. layers representing leaf thickness, water content, pigments, etc.). These layers are treated as semi-transparent plates, and total reflection, refraction and transmission for each plate is calculated. Similarly, scattering and absorption of each plate are also calculated. The sum of all plates yields the total reflection and transmission of light through the modelled leaf.

Increasing or decreasing the layers as defined by the input parameters affects the interaction between irradiance, the absorption of light by pigments, and refraction due to the physical structure of the leaf, thus simulating the total percentage of light which is reflected and transmitted. Simulated reflectance was calculated with varying levels of chlorophyll *a+b* concentration from 0 µg cm^{-3} up to 60 µg cm^{-3}, at 5 µg cm^{-3} intervals (Fig. 5), resulting in an output of 13 simulated leaves. The remaining inputs were set to; Leaf structure, 1.2; Carotenoid content, 10 µg/cm²; Brown pigments,

1.0; Equivalent water thickness, 0.015 cm; Leaf mass per unit area, 0.009 g/cm². The reflectance values that were output by the simulation can be seen in Fig. A2.

We ran a further simulation using the above reflectance values, based on a uniform 800 μmol m^{-1} s^{-2} of irradiating light across all wavelengths. We calculated the irradiating light that was reflected off each simulated leaf. The reflected light from these leaves was passed through the transmission profile of the Alice Blue filter, thus calculating the final amount of light that is theoretically received by the *NDVIpi* camera. NDVI was calculated using NDVI$_{RaspPi}$.
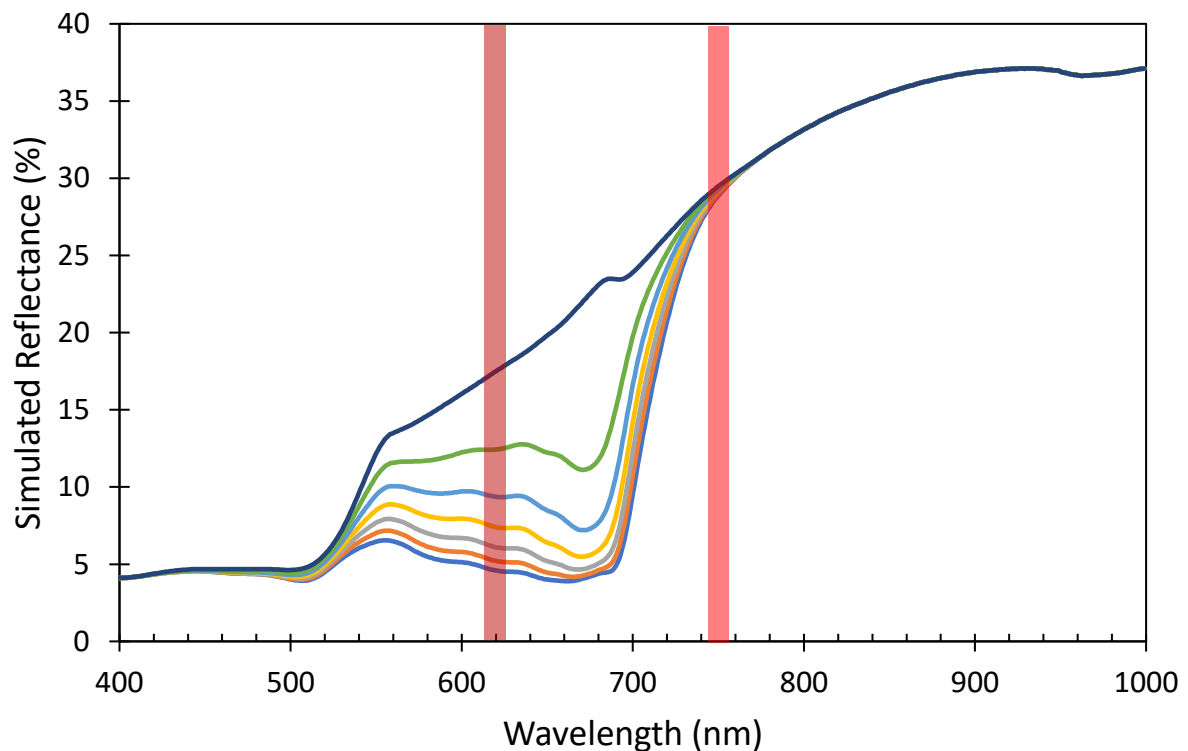

Figure A2 Simulated changes in reflectance due to changes in chlorophyll *a+b*, modelled using the PROSAIL model across simulated chlorophyll *a+b* content from 0 μg cm^{-2} (bottom grey line) up to 60 μg cm^{-2} (top blue line) at 5 μg cm^{-2} intervals. The entire region from 600nm up to 680 shows similar sensitivity to chlorophyll content. Thus, calibration using any region with the red (600nm up to 680nm) spectrum will remain sensitive to chlorophyll content. Highlighted areas correspond to the wavelengths (620nm and 750nm) used by the Raspberry Pi system.
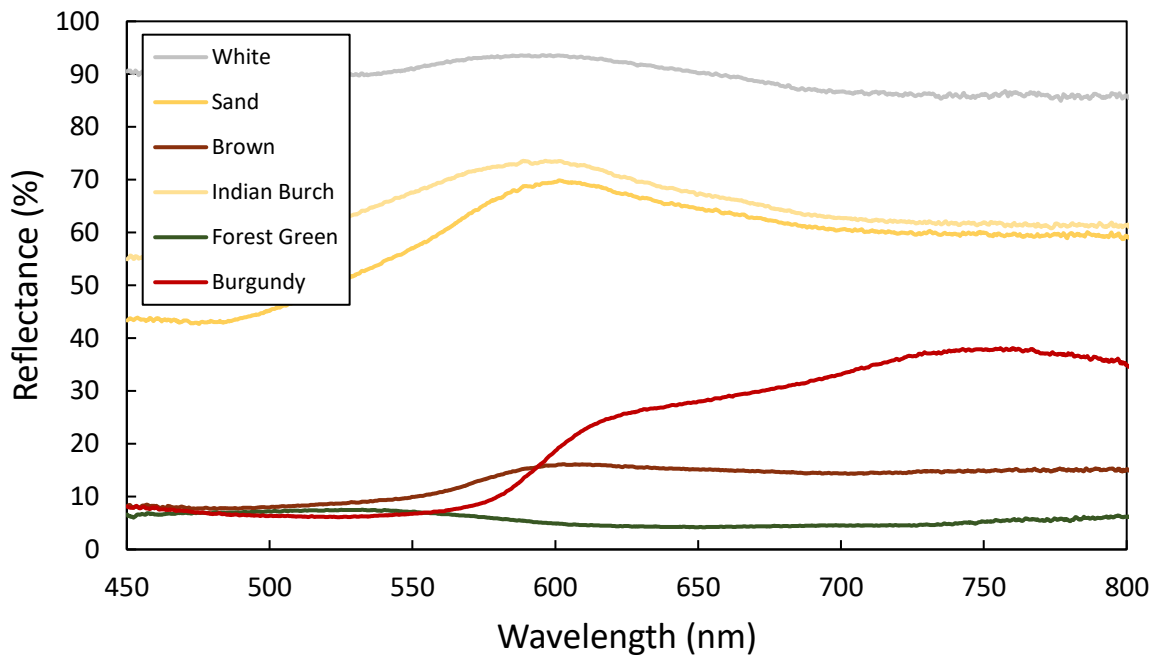
Figure A3 Reflectance of six Kayospruce Odyssey materials selected out of a possible 16 total colours. White (#1), Sand (#2), Brown (#3), Indian Burch (#4), Forest Green (#5), Burgundy (#6), measured with a spectrometer. These materials were chosen for their relative uniformity across the red and near infra-red spectrum, and to ensure a range across reflectance values.
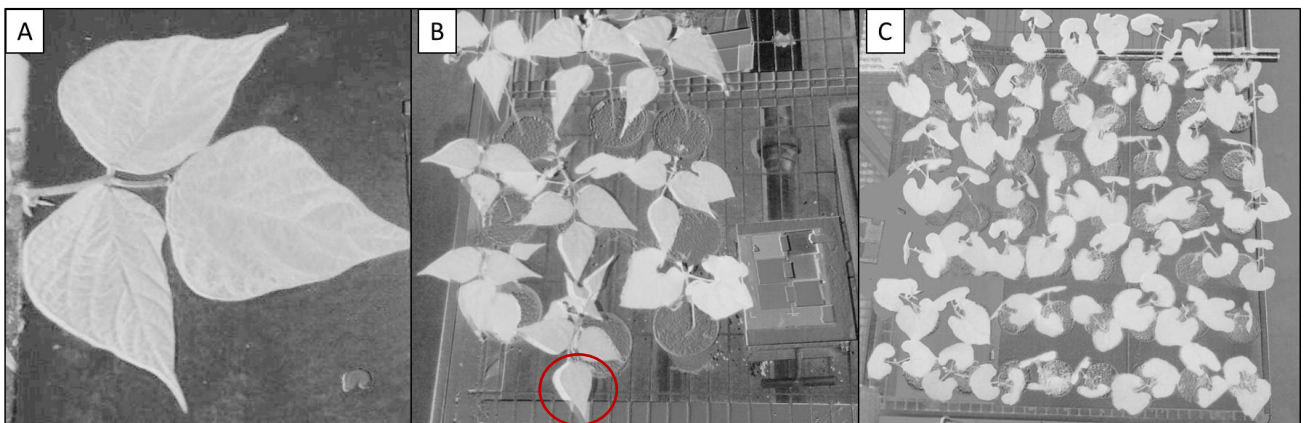
Figure A4 Aligned greyscale NDVI images collected at three different distances from leaves, cropped to show area of interest, demonstrating the accuracy of the SIFT algorithm to align images. The red circle highlights an example of mis-alignment, caused by the leaf not being on a relatively flat plane in relation to the camera. **A)** Image near to leaf (0.60m distance) **B)** Image at a medium distance to leaves (1.00m distance) **C)** Image at a far distance from leaves (1.53m distance).
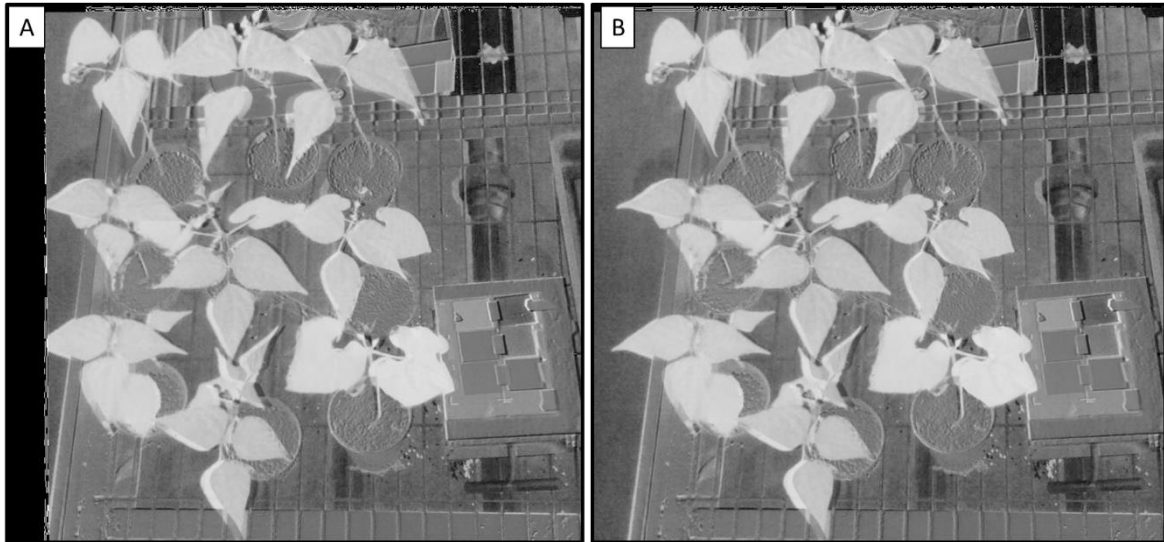
Figure A5 Two greyscale NDVI images from the same source **A)** Resulting NDVI image when the two source images were first cropped to size, then aligned and NDVI image calculated **B)** Resulting NDVI image when the two source images were aligned at full size, then the resulting NDVI image was calculated and cropped to show area of interest
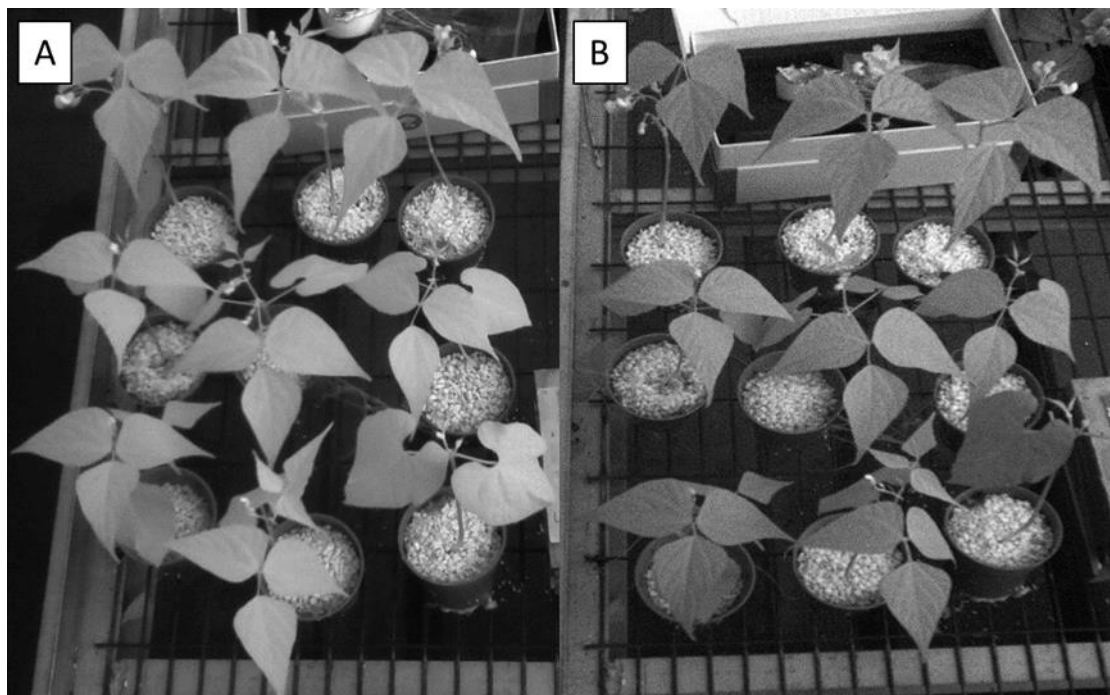
Figure A6 Two greyscale NIR images post-calibration **A)** NIR image captures by the Raspberry Pi NoIR camera **B)** NIR image captured by the Micasense RedEdge camera. The RedEdge has greater definition due to the narrowband filter, whereas the broadband NoIR camera shows a larger uniform intensity across leaves